AN INSIGHT INTO MAGMA SUPPLY TO THE KAROO IGNEOUS PROVINCE: A GEOCHEMICAL INVESTIGATION OF KAROO DYKES ADJACENT TO THE NORTHWESTERN SECTOR OF THE LESOTHO VOLCANIC REMNANT

A THESIS SUBMITTED IN FULFILMENT OF THE REQUIREMENTS FOR THE DEGREE OF

MASTER OF SCIENCE

OF

RHODES UNIVERSITY

BY
VINDINA RAMESH MITHA

JANUARY 2006

ABSTRACT

The emplacement of continental flood basalt provinces is often ascribed to fissure eruption. However, in many provinces the locations of actual vent complexes remains illusive. In southern Africa, the Karoo continental flood basalt province was erupted during the Jurassic between 183 and 179 Ma. The southernmost outcrop of the Karoo continental flood basalt lavas is the Lesotho remnant; and is comprised of the Drakensberg Group which forms the uppermost portion of the Karoo Supergroup. The geochemical stratigraphy for the Drakensberg Group is well established. At the base, there are a number of small volume compositionally diverse units, which form the Barkly East Formation, overlying which, there are larger volume, compositionally less variable units of the Lesotho Formation, which form the bulk of the volcanic sequence. The Lesotho remnant is associated with an abundance of dykes in the adjacent vicinity. This suggests that the lavas were fed from local rather than distal eruption sites.

This study presents whole rock major and trace element data for 94 dykes and three sills from the northern Lesotho - northeastern Free State region and demonstrates that on the basis of geochemistry, all 97 intrusions can be correlated with various units of the northern Barkly East and Lesotho Formations. In addition, the petrographical; characteristics, orientation and distribution of the dykes do not correlate with geochemistry. Geochemical discrimination diagrams have been used to identify five compositionally diverse dykes, which are similar to the northern Barkly East Formation units. Three dykes are characteristic of the Letele unit and two are compositionally similar to the Wonderkop unit.

Although the geochemical characteristics of the Lesotho Formation units are rather well constrained, the composition of these units is typified by considerable overlap in composition. Therefore, since unambiguous classification of dykes with geochemical similarities to the various units of the Lesotho Formation is unachievable using an empirical approach, the multivariate forward-stepwise discriminant function analysis (DFA) technique was used to facilitate the classification of the remaining 89 dykes and three sills. Forward-stepwise DFA classified 23 dykes as having compositional similarities to the Mafika Lisiu unit, 29 as having compositions of the Maloti or Senqu types; and 32 as having the composition of the Mothae type. In addition, eight dykes are compositionally similar to the Oxbow dykes, which intrude the Senqu unit in northern Lesotho. These results suggest that that the Lesotho remnant was fed from local eruption sites and that long distance magma transport for the bulk of the Lesotho remnant basalt lavas is unlikely.

TABLE OF CONTENTS

Table of Contents (cont.)

ACKNOWLEDGEMENTS

MY GRATITUDE NEEDS TO BE EXTENDED TO NUMEROUS PEOPLE…

Luc Chevallier, Michael Cronwright and Janine Cole from the Council for Geoscience;

John Hepple and his staff (Putulo, Bennet, Bongani and Chris) who have so kindly lended assistance during the sample preparation and for the preparation of thin sections;

Sarah Radloff, Emese Bordy, Steffen Buttner, Steve Prevec, Hugh Eales, Ashley Goddard, Jenny Wright, Gillian McGreggor, Glynn Armstrong, Malcolm Roberts, Phyllis Roberts, Aoife Roberts, Mike Earl-Taylor and Sue Abraham for all the ways in which you have helped during this time;

Benni and my *Foibas*; Jamie Pote; Ajay Makan; Emily Hanson; Danica Luac; Louise Lange, Rose Adendorff-Prevec and Ashley Goddard for all the moral support you have given me;

Examiners, Professors Else Ragnhild Neumann and A.R. Duncan;

The NRF for the funding of this project;

The Lord and all my guardian angels who have given me strength and guided me
(! Jai shree Krishna !)

Last, but not least, I would like to extend my sincerest gratitude to my supervisor, "Prof." who has afforded me the chance to grow - not only mentally and academically but also personally and spiritually. My heartfelt appreciation goes to you for your assistance and discussions; for critically reviewing drafts of this thesis; for access to your extensive database and knowledge of the Karoo; and for inspiring and pushing me further than I thought myself capable of. Thank you.

Life should not be a journey to the grave with the intention of arriving safely in an attractive and well-preserved body, but rather to skid in sideways –

Champagne in one hand; strawberries in the other; body thoroughly used up, totally worn out and screaming… "WOO HOO! What a ride!! CAN I DO IT AGAIN?!?"

1 INTRODUCTION

Continental flood basalt provinces are a type of large igneous province which are erupted at a time which is broadly concomitant with continental disintegration and ocean formation (*e.g.* Ernst and Buchan, 2005; Coffin and Edholm, 1992). The provinces are formed as a result of voluminous and rapidly erupted magmas, the majority of which were erupted within 1 m.y., although magmatism may extend for durations of up to 10 m.y. (Courtillot and Renne, 2003; Riley and Knight, 2001). Continental flood basalt provinces are widespread in aerial extent (> 1 Mkm^2) and are typified by lava piles several kilometres thick (Coffin and Edholm, 1992). The nature of magmatism is such, that mantle plumes are often invoked as an emplacement process, since the effusion rate is unlike any current rate of eruption (*e.g.* Ernst *et al.*, 2005; Courtillot *et al.*, 1999; Ernst and Buchan, 1999; Coffin and Edholm, 1992; Kent *et al.*, 1992; Campbell and Griffiths, 1990). In many cases a hotspot tail, forming chains of volcanoes, which show systematic age progressions link a flood basalt to its hotspot and is suggestive of plume processes.

The Karoo and Antarctic Ferrar continental flood basalt provinces (Figure 1) form part of a broader Jurassic Gondwana-wide low-Ti flood basalt province, which parallel the southern margin of Gondwana (Hawkesworth *et al.*, 1999). Portions of these two continental flood basalt provinces were erupted contemporaneously (*e.g.* Encarnacion *et al.*, 1996; Heimann *et al.*, 1994; Harris *et al.*, 1990) in response to the break up of southern Gondwana and the opening of the present southern Atlantic Ocean (Veevers, 2000; Veevers *et al.*, 1994a,b; Hawkesworth *et al.*, 1999). These Gondwanan flood basalt provinces have been ascribed to upwelling mantle beneath Gondwana, but more specifically due to deep-mantle plume processes (Storey *et al.*, 2001; Dalziel *et al.*, 2000; Hawkesworth *et al.*, 1999; Storey and Kyle, 1997; White 1997; Turner, 1999; Storey, 1995; Campbell and Griffiths, 1990; Duncan and Richards, 1991; Richards *et al.*, 1989; White and McKenzie, 1989). However, there are many unknowns with respect to the role of plumes in the origins of continental flood basalt provinces, or whether they play any role at all.

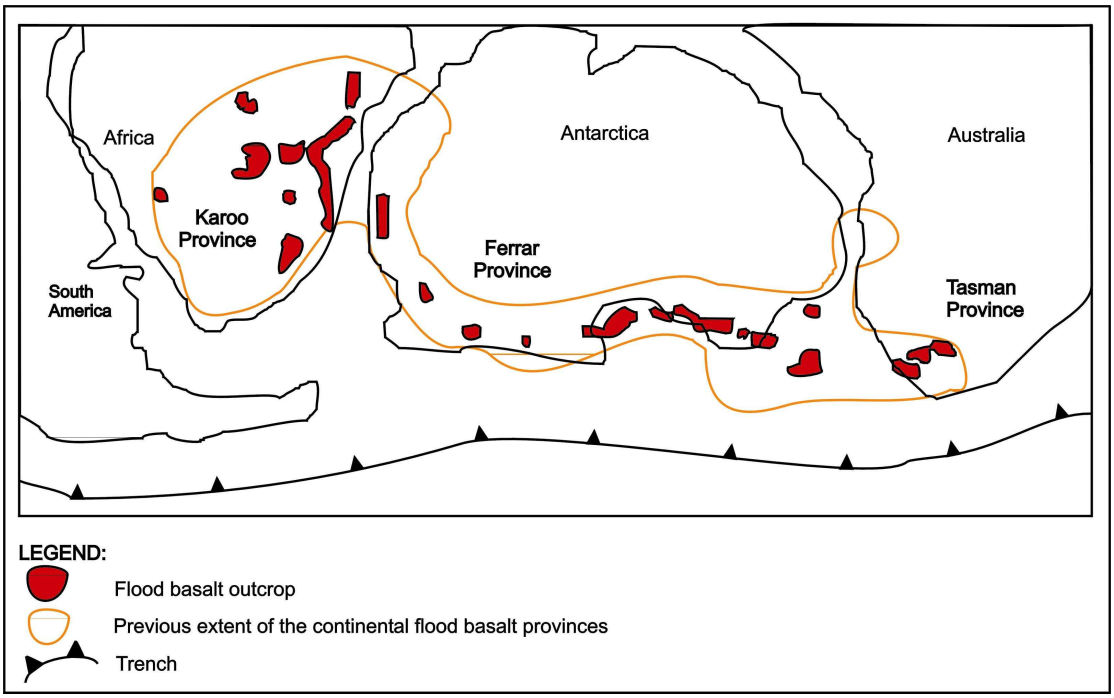

Figure 1. Location of the Jurassic continental flood basalt provinces of Gondwana. The Karoo continental flood basalt province in southern Africa and the Ferrar continental flood basalt province in Antarctica parallel the southern Panthalassic subduction zone along the southern margin of Gondwana. Source: Veevers, 2004, Figure 78, p. 105.

Similarly, shallow level processes in the emplacement of continental flood basalt provinces are also marked by many unknowns. These unknowns relate to the location of eruptive sites of surface flows and long distance surface or shallow intrusive level magma transport. This thesis focuses on examining the relationship between dykes and lavas in the Lesotho remnant in the Karoo continental flood basalt province.

2 OVERVIEW OF THE KAROO CONTINENTAL FLOOD BASALT PROVINCE

The Karoo continental flood basalt province (Figure 2) was emplaced in southern Africa as a thick sequence of voluminous and widespread flood basalt lavas, silicic volcanic rocks and intrusions that extend within an area well in excess of 3 x 10^6 km^2 (Eales *et al*., 1984). These lavas once dominated southern Africa as a continuous carapace but are presently preserved as several erosional remnants that extend north into the African subcontinent (Eales *et al*., 1984). These remnants are the thick basaltic sequences of the Central area, which were emplaced in a cratonic environment (Marsh and Eales, 1984). The majority of these flood basalts are slightly older than the thick rift related sequences in the Lebombo-Save-Mwenezi monocline (Figure 2). The Central area basaltic sequences (Figure 2) incorporate the (a) Springbok Flats and Lesotho remnants, (b) Karoo basin subvolcanic complex, (c) Kalkrand basalts in central Namibia; and (d) remnants in Zimbabwe and Botswana (Marsh and Eales, 1984).

Fitch and Miller (1984) proposed that the Karoo continental flood basalt province was erupted in sporadic pulses within a 50 m.y. period. Major peaks in magmatism at 193 ± 5 Ma and 178 ± 5 Ma were believed to represent magmatism within the Central area and southern Lebombo; and northern Lebombo, respectively (Fitch and Miller, 1984). More recently, Duncan *et al*. (1997) have determined from extensive $^{40}Ar/^{39}Ar$ dating studies that the overwhelming majority of basalts and dolerites in the Central area were emplaced within a geologically brief period at 183 ± 1 Ma. The results from this dating study and from others conducted by Jourdan *et al*. (2004), Rogers *et al*. (2004), Le Gall *et al*. (2002), Jones *et al*. (2001) and Elburg and Goldberg (2000) in northern Botswana and Zimbabwe suggest that the Karoo continental flood basalt province becomes progressively younger towards the north.

Of particular interest in the current study is the southernmost outcrop of the Karoo continental flood basalt province, the Lesotho remnant. The Lesotho remnant was emplaced at 183 ± 1 Ma (Duncan *et al*., 1997) and is a > 1.5 km thick pile of flood basalt lavas that are underlain by the Karoo sedimentary sequence, into which is intruded a myriad of predominantly dolerite intrusions (Eales *et al.*, 1984; Marsh and

Eales, 1984; Marsh *et al.*, 1997). These flood basalt lavas and the spatially related intrusions in the main Karoo basin form the Drakensberg Group. The Drakensberg Group has been the focus of many studies which have essentially been conducted on the geochemistry, petrology and palaeomagnetic reversal stratigraphy of the Drakensberg Group (Marsh, 1998; Marsh and Mndaweni, 1998; Marsh *et al.*, 1997; Hargraves *et al.*, 1997; Mitchell *et al.,* 1996; Sweeney and Watkeys, 1990; Eales *et al.*, 1984; Marsh and Eales, 1984; Marsh, 1984; Mitchell, 1980; Pemberton, 1978; Robey, 1976; Lock *et al.,* 1974; Cox *et al.,* 1967; Cox and Hornung, 1966; Van Zijl *et al.*, 1962 a,b; Graham and Hales, 1957; Lombaard, 1952).

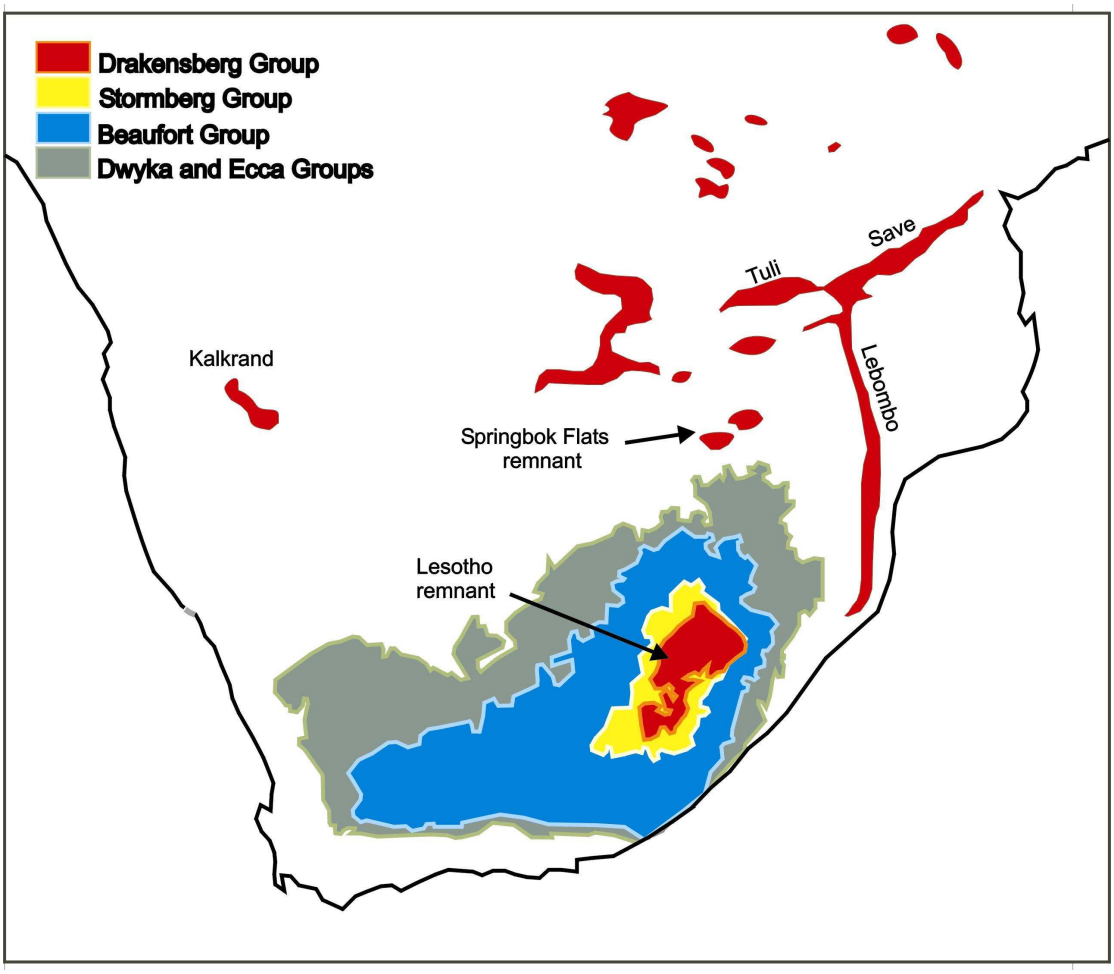

Figure 2. Map of the Karoo continental flood basalt province showing the distribution of the main volcanic remnants (red). The main Karoo basin broadly delineates the major outcrop extent of subvolcanic Karoo intrusions. Sources: volcanic remnants after Marsh *et al.*, 1997, p. 248, Figure 3; Karoo basin stratigraphy after Hancox and Rubidge, 2001, Figure 1, p. 564.

Marsh *et al*. (1997) have produced a comprehensive stratigraphic framework for the Drakensberg Group lavas. The authors geochemically subdivided the Drakensberg Group into a lower Barkly East Formation and an upper Lesotho Formation, which are comprised of lavas that differ in distribution, thickness and overall compositional characteristics. These formations are comprised of a number of stratigraphic units that are defined by a package of geochemically similar lava flows of a single magma type. The Barkly East Formation differs in stratigraphy in northern and southern Lesotho. In northern Lesotho, these units are, from the base up: the Golden Gate, Roma, Letele, Sani and Wonderkop units; and in southern Lesotho these units are, from the base up: the Moshesh's Ford, Roodehoek, Omega, Vaalkop and Kraai River units. The overlying Lesotho Formation is comprised of the Mafika Lisiu, Maloti, Senqu and Mothae units.

Despite the vast volume of literature currently available for the Karoo flood basalt lavas and differentiated intrusions, very few studies have focussed on the subvolcanic complex and its relationship to the lavas. The morphological features of a number of intrusive forms have been described by Chevallier and Woodford (1999), Meyboom and Wallace (1978), Lombaard (1952), Walker and Poldervaart (1949) and Du Toit (1920). In addition, Walker and Poldervaart (1949) and to a lesser extent, Lombaard (1952) focussed on the petrology and petrography of Karoo dolerite. However, in spite of the extreme abundance of outcrops of Karoo dolerite, few geochemical data regarding undifferentiated intrusions have been published. Although Cox and Hornung (1966) determined from major element geochemistry that the basalts and dolerites are similar in composition, Marsh and Eales (1984) - who reported upon a number of unpublished studies such as Robey (1978) - have demonstrated that the majority of intrusions in the Barkly East area are representative of the Mafika Lisiu type (former Lesotho type), and that few dolerites are of the Moshesh's Ford and Kraai River magma types. Following the establishment of the Lesotho Formation stratigraphy by Marsh *et al*. (1997), Marsh and Mndaweni (1998) demonstrated that a ~ 100 km long dyke near Cradock in the central Karoo area has geochemical characteristics of the Maloti or Senqu magma types.

3 CURRENT STUDY

As with other continental flood basalt provinces, the Karoo flood basalt lavas are believed to be the products of fissure eruptions. However, despite the deep dissection of the Karoo basin by post-Gondwana uplift and erosion (Partridge and Maud, 1987), evidence for eruptive fissure vents in the volcanic remnants remain unexposed. Nevertheless, prolific numbers of dykes (*i.e.* the extension of these fissure sites to depth) associated with the flood lavas suggests that they are the likely feeders, which were most probably fed from the highest level storage chambers, now preserved as a multitude of sills in the main Karoo basin. Despite this apparent relationship, studies which focus upon the geochemical relationship between the Lesotho lavas and the spatially related intrusions are few. Provided that the subvolcanic complex was intruded at the same time as the lavas were erupted, the geochemical stratigraphy of Marsh *et al*. (1997) can be extended to include Karoo intrusions, especially those that are not differentiated.

The current study was undertaken in the northern Lesotho - northeastern Free State region (Figure 3) and is aimed at establishing whether a flood basalt – feeder relationship exists between the Drakensberg Group lavas and the immediately adjacent intrusions. This region is well suited to determining whether the lavas were fed from the abundant dykes in its immediate vicinity or whether the lavas may have had remote eruption sites. This is because the geochemical stratigraphy for the Drakensberg Group is well established and the sedimentary sequence below the lavas is host to abundant dykes. The approach taken was that of sampling of as many dykes as possible for geochemical analysis. Dolerite compositions were then compared to that of the main basalt magma types in the Lesotho volcanic sequence established previously by Marsh *et al*. (1997) to determine whether the geochemically defined magma types present in the Lesotho volcanic sequence can be identified within the dolerite suite. In the present study, both the empirical and statistical approaches were utilised in the comparison of dolerite and lava geochemistry.

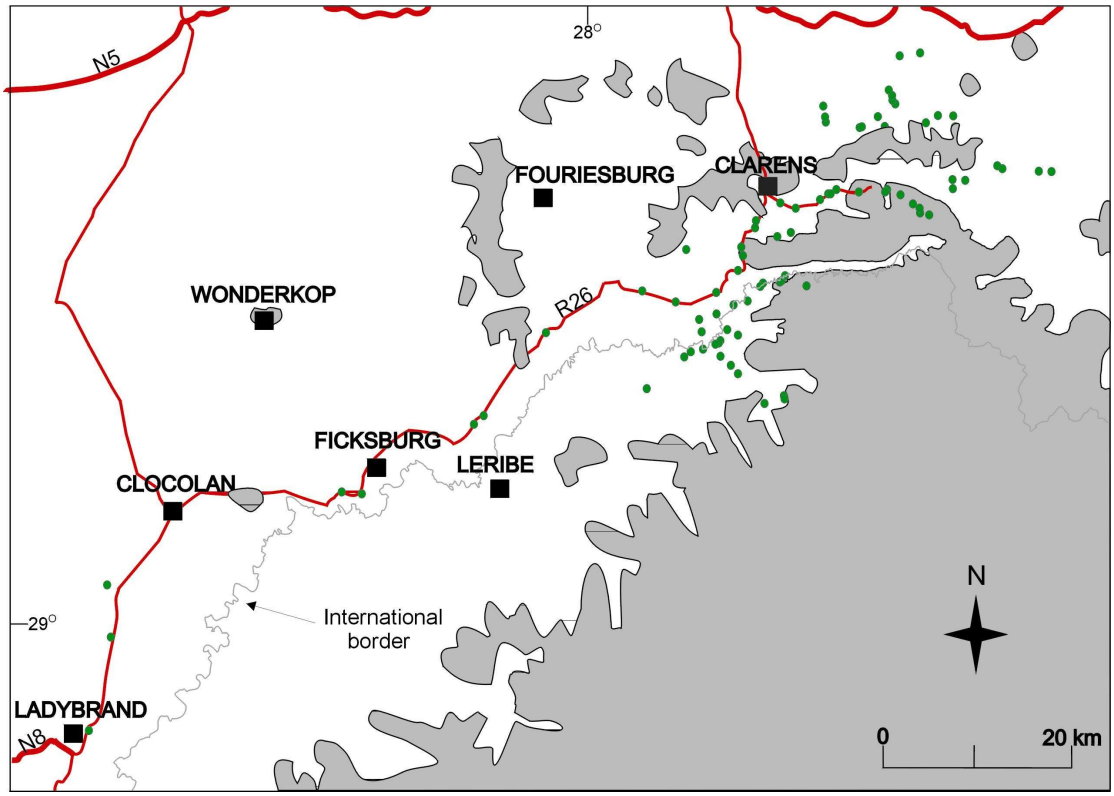

Figure 3. Map of the study area in the northeastern Free State - northern Lesotho region which shows sample localities in relation to the northwestern outcrop border of the Lesotho volcanic remnant (grey). The N5 along the north; and the N8 and R26, which follow the Lesotho – South Africa border are national roads. Data sources: towns and international border from Anon. (2001); Lesotho volcanic remnant from Marsh *et al.* (1997). Map parameters: Datum referenced to WGS84; projection: Albers equal area; standard parallels: - 18; - 32; central meridian: 24; reference latitude: 0.

4 STRATIGRAPHY OF THE KAROO SUPERGROUP

4.1 Introduction

During the Early Palaeozoic, a complex and diachronous series of tectonic events occurred along the subduction-related Panthalassan margin of Gondwana (Figure 1). These included the formation of a Pan-Gondwanide magmatic arc and fold belt, which resulted in the development of a number of sag basins in the hinterland. In southern Africa, these are represented by the Cape Fold Belt and Karoo foreland basin, respectively. The main Karoo basin is bordered along its southern and western margins by the Cape Fold Belt and presently forms a NE – SW trending oval, extending from 25 – 34 ºS and 18 - 32 ºE (Figure 2). Between the Late Carboniferous and Middle Jurassic (circa 300 - 180 Ma) (Catanuneau *et al*., 1998), this basin was filled with sediment derived from the north, south and east. Sedimentary deposition culminated in extensive outpourings of flood basalt lavas. Numerous publications have focussed on the Karoo basin, its sedimentary infilling and its relationship to the Cape Fold Belt (*e.g.* Bordy *et al*., 2004a,b; Veevers, 2004; Hancox and Rubidge, 2001; Bangert *et al*., 1999; Turner, 1999; Johnson *et al*., 1996; Veevers *et al*., 1994a,b; Smith *et al*., 1990; Hälbich *et al*., 1983). This synopsis of the Karoo sedimentary sequence is derived mainly from Catanuneau *et al*. (1998), Veevers (2004) and Veevers *et al*. (1994 a,b); and that of the Karoo volcanic sequence from Marsh and Eales (1984) and Marsh *et al*. (1997).

4.2 Karoo Sedimentary Stratigraphy

The Karoo Supergroup (Figures 2 and 4) is an accumulation of continental Permo-Triassic sediments which record increasing conditions of aridity. At its base is the glaciogenic Dwyka Formation which was succeeded by the deposition of shales, siltstones, greywackes and sandstones of the Ecca Group. The ensuing Beaufort Group, and the overlying Molteno and Elliot Formations accumulated as a range of sandstones, mudstones and siltstones in a fluvial environment. The overlying Clarens Formation consists dominantly of sandstones with minor silty sandstone and mudstone; and formed largely in an aeolian environment. The subsequent

culmination of circa 100 m.y. of sedimentation occurred with the eruption of the volcanic Drakensberg Group in the Middle Jurassic.

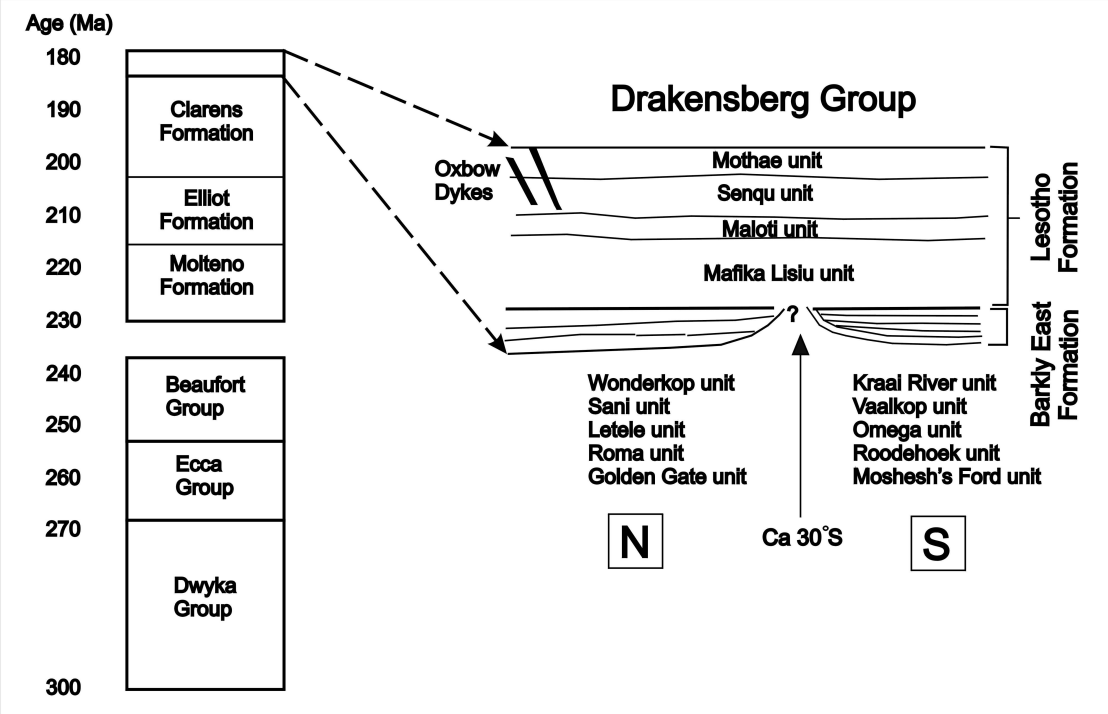

Figure 4. Stratigraphy of the Karoo Supergroup showing the basal sedimentary sequences and the overlying volcanic sequence. Note that only the Barkly East Formation is shown schematically. Sources: volcanic stratigraphy after Marsh *et al.* (1997) and Karoo Supergroup stratigraphy after Catanuneau *et al.*, 1998, Figure 4, p. 421.

4.3 Karoo Volcanic Stratigraphy

4.3.1 Introduction

The Drakensberg Group lavas were erupted onto the sandstone of the Clarens Formation. Evidence provided by Lock *et al.* (1974) suggest that this initial relationship between sedimentation and magmatism was complex and that interlayered sediment-lava sequences within the basal part of the Drakensberg Group are common, particularly in the Barkly East area (Figure 5). This initial interplay progressed very rapidly to profuse magmatism, and is evident especially in the > 1.5 km thick basalt pile preserved in the Lesotho volcanic remnant which, apart from the lower 100 – 200 m, is devoid of any significant sedimentary intercalations. Figures 4 – 8 summarise some important geochemical and stratigraphical relationships of the Barkly East and Lesotho Formations.

Figure 4 shows the detailed schematic stratigraphy of the Drakensberg Group established by Marsh *et al.* (1997). The geochemical stratigraphy is based upon the

recognition of a package of lava flows that share similar geochemical characteristics. These geochemically similar lava flows define a unit, and the combined geochemical characteristics of the flows define a magma type that is distinct from over- and underlying units, which define other magma types. The lower Barkly East Formation is characterised by the limited distribution of thin, compositionally heterogeneous units which differ in stratigraphy north and south of latitude 30 ºS (hereafter, northern- and southern Barkly East Formation). As depicted in Figure 4, these two sets of units are not interlayered. The Barkly East Formation units stand in contrast to the overlying Lesotho Formation units, which are thicker, of limited compositional variability, and extend right across the Lesotho remnant (Figure 6).

4.3.2 The southern Barkly East Formation

The basal lavas in southern Lesotho and the Eastern Cape are the thin Moshesh's Ford lavas which stretch from the Molteno-Jamestown outliers through the Barkly East area to Ongeluksnek (Figure 5). The Moshesh's Ford lavas are characterised by high Ba, Sr, Nb and Zr/Y; and low Ti/Zr and Zr/Nb (Figure 5). Overlying Moshesh's Ford in the Molteno area is a group of lavas with high Ti/Zr and low Zr/Y that form the Roodehoek unit in the Molteno-Jamestown area and Omega unit in the area west of Barkly East. These lavas are characterised by high Cr, Ni, MgO, CaO and Al_2O_3; and low SiO_2, TiO_2, K_2O, P_2O_5, Rb, Zr and Nb abundances. The uppermost unit in the Molteno area is the Vaalkop unit with the Kraai River unit being its stratigraphic equivalent in the Barkly East area. These units share many geochemical characteristics such as similar Nb, Zr, Y, Cr and rare earth element abundances. The Vaalkop lavas (with high Cr/Ni, Rb, Sr, SiO_2, TiO_2, K_2O and P_2O_5; and low Ni and Cu) are, however, distinct from the Kraai River lavas (with distinct Ti/Zr, Ti/P, Zr/Y; low MgO; and high SiO_2).

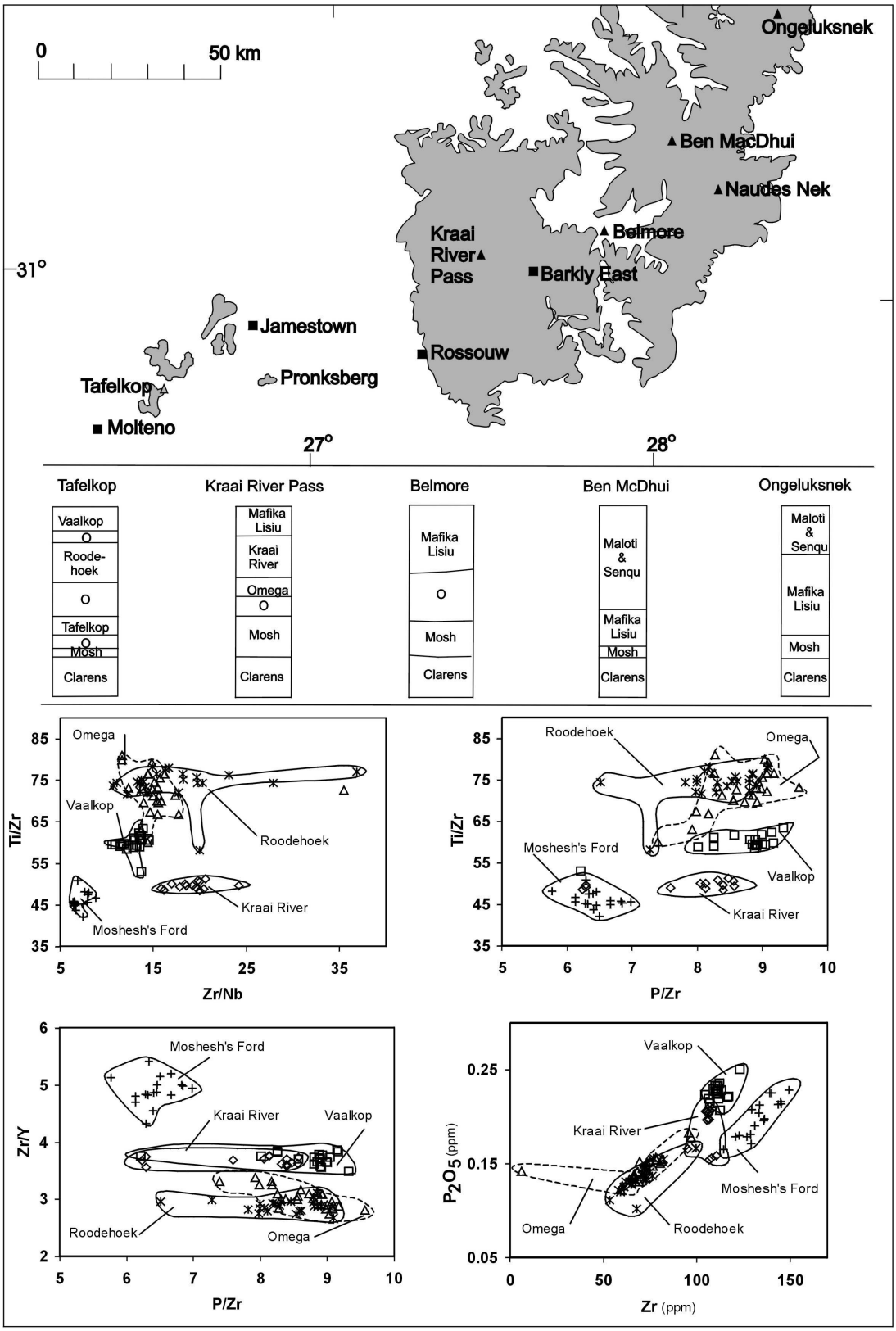

Figure 5. Summary of the southern Barkly East and Lesotho Formations. The map shows the location of stratigraphic sections discussed in the text. Geochemical discrimination diagrams show the compositional variability in the southern Barkly East Formation units. Note that the stratigraphic sections are shown schematically. Symbols are as follows: Kraai River (◇),Vaalkop (□), Omega (△), Roodehoek (✱), Moshesh's Ford (+). Abbreviations: Mosh (Moshesh's Ford), O (other units such as sediments, tephra, unclassified units and dacite). Sources: map from

Caption of Figure 5 cont.

Marsh and Eales, 1984, Figure 1b, p. 29; stratigraphic sections from Marsh and Eales, 1984, Figure 2, p. 30; Tafelkop section from Marsh (2001), Figure 2.5, p. 2-5; geochemical discrimination diagrams from Marsh *et al*. (1997); lava data from Marsh *et al*. (1997) and Marsh (1998).

4.3.3 The northern Barkly East Formation

The basal unit of the Barkly East Formation in northern Lesotho is the Golden Gate (Figures 4 and 6). It is widespread and extends from the Sani Pass northwards into the Free State. This unit is characterised by high Zr/Nb, Zr/Y, and La/Nb; and low Ti/Zr and P/Zr, which reflects enrichments in Zr, La and Th relative to Nb, heavy rare earth elements, P_2O_5, TiO_2 and Y (Figure 7). In the Sani and Bushman's passes, respectively, the Sani and Roma units overlie the Golden Gate unit (Figure 6). The Roma lavas are similar to the Golden Gate lavas in the abundances of incompatible elements, but are distinguished from the latter with high Ti/Zr; and low Zr/Y and P/Zr (Figure 7). Similarly, the Sani lavas are compositionally similar to those of the Roma unit and are distinguished from the latter with high P/Zr and Ti/Zr (Figure 8). The Letele lavas overlie the Golden Gate unit in the Oxbow section (Figure 4) and despite being similar to the Golden Gate and Roma lavas, are distinguished from these with high Ti/Zr; moderate P/Zr and Zr/Nb; and low Zr/Y (Figure 7). The uppermost lava flows form the relatively widespread Wonderkop unit, which stretch from the Sani and Bushman's passes into outliers in the Free State (Figure 6), where they overstep the underlying units, and in places, lie directly upon sandstone of the Clarens Formation (Marsh, 1984). The Wonderkop lavas are characterised by distinctly low Zr/Nb and high Zr/Y (Figure 7).

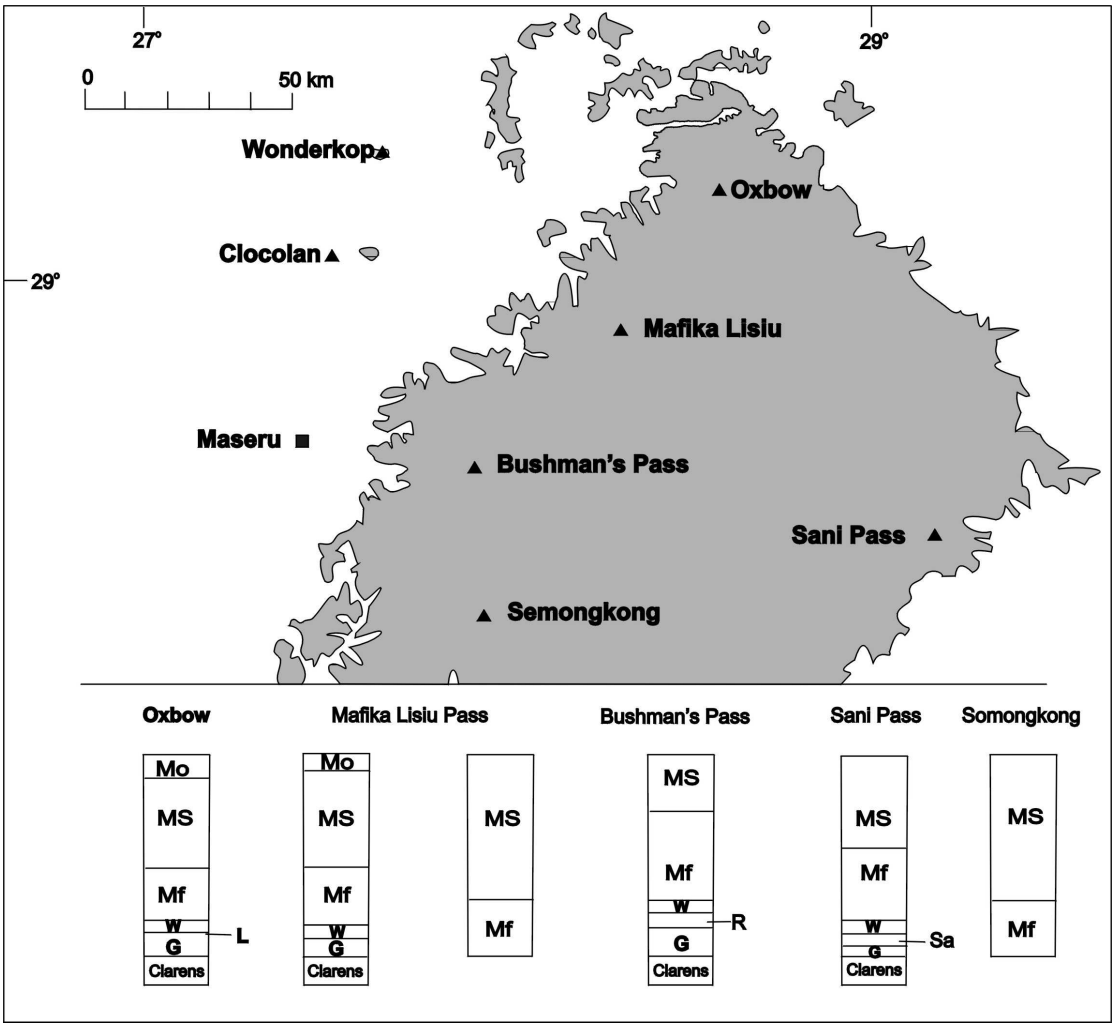

Figure 6. Summary of the northern Barkly East and Lesotho Formations. The map shows the location of the stratigraphic sections as discussed in the text. Abbreviations: G (Golden Gate), R (Roma), L (Letele), S (Sani), W (Wonderkop), Mf (Mafika Lisiu), MS (Maloti & Senqu); Mo (Mothae). Sources: map from Marsh *et al*., 1997, Figure 3, p. 250; stratigraphic sections from Marsh *et al*., 1997, Figure 6, p. 258; geochemical discrimination diagrams and lava data from Marsh *et al*. (1997) and Marsh (1998).

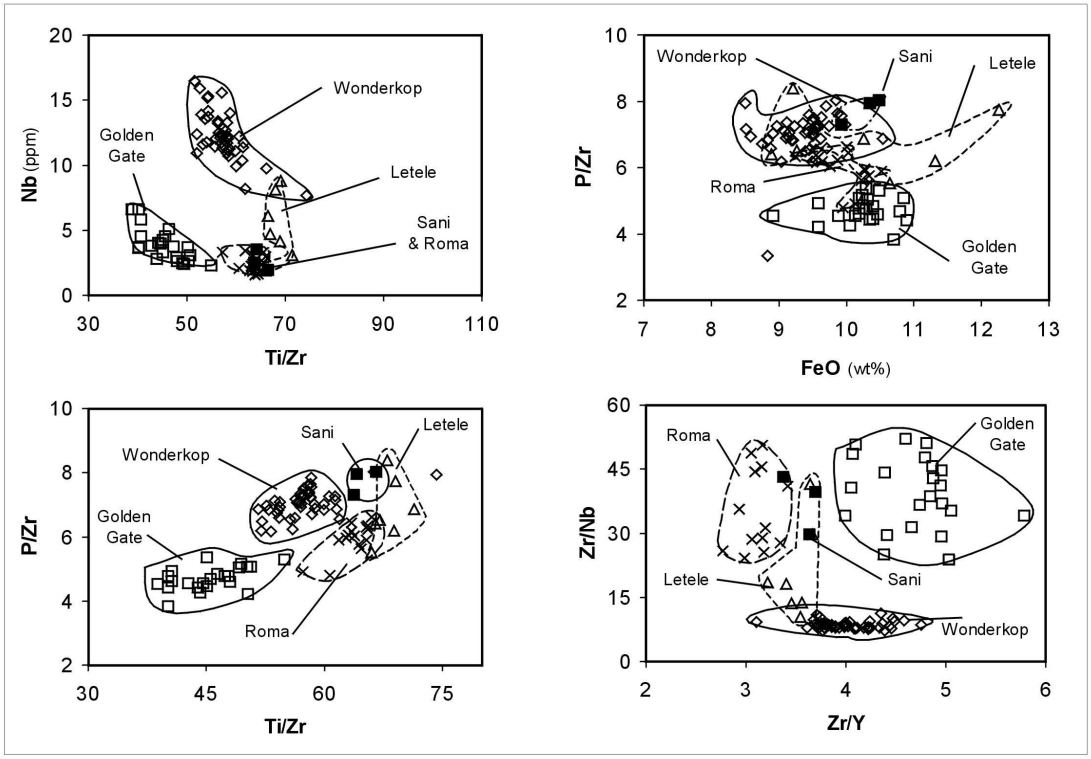

Figure 7. Geochemical discrimination diagrams used to distinguish the northern Barkly East Formation units. Symbols are as follows: Golden Gate (□), Roma (×), Letele (△), Sani (■), Wonderkop (◆). Sources for geochemical discrimination diagrams and lava data are given in the caption of Figure 5.

4.3.4 The Lesotho Formation

The lava sequence which forms the Lesotho Formation contrasts with that of the Barkly East Formation, primarily in the absence of interbedded sedimentary layers. This and the lack of deep weathering horizons and extensive palaeosol development, indicate that the bulk of the Lesotho lava pile was erupted in a geologically short period. In addition, lavas of the Lesotho Formation were erupted onto a virtually planar surface, indicated by the relatively constant thickness of these units (Figures 4 and 6). From Figure 8 it is apparent that the basalts of the Lesotho Formation are characterised by limited compositional variability. From studies of other remnants (*e.g.* Springbok Flats remnant) it appears that the Lesotho Formation dominated the lava carapace, which once covered much of the interior of the African subcontinent.

The basal lavas of the Lesotho Formation are those of the ~ 400 m thick Mafika Lisiu unit (Figures 4 and 6). Although these lavas are of variable composition (*e.g.* in Zr/Nb, P/Zr and Zr/Y), they show the lowest Mg# [1] and Ti/Zr of any other unit of the Lesotho Formation (Figure 8). On the basis of Zr/Nb, a low Zr/Nb Mafika Lisiu subunit (not shown) can be distinguished. The flows of the overlying Maloti unit

[1] Calculated such that all Fe is accounted for as Fe^{2+}

have low Ti/Zr and P/Zr and high Zr/Y relative to the Mafika Lisiu unit (Figure 8) and its base is well defined by sharp decreases in Ti/Zr, P/Zr and Zr/Nb; and a sharp increase in Zr/Y in vertical compositional profiles through the lava sequence. The overlying Senqu unit is more evolved than the underlying units and is characterised by comparatively lower Mg# and higher Zr abundances and, like the Mafika Lisiu unit, is geochemically variable (Figure 8). The uppermost Mothae lavas are more evolved than those of the underlying Senqu unit, and are primarily recognized by low Mg#, Ni, Cr, TiO_2, CaO and Al_2O_3; and high FeO, TiO_2, P_2O_5 and incompatible trace element abundances. In northern Lesotho, the Mothae and Senqu units are intruded by the chemically evolved Oxbow dykes, with low Mg#; and high FeO, Ti/Zr and Zr/Nb; making them quite distinct from other units of the Lesotho Formation. Although these dykes are dissimilar to the lavas into which they intrude, correlative lava flows have been discovered within the Springbok Flats remnant some 400 km north of the Lesotho remnant (Figure 2). The Oxbow dykes and their correlative lavas further north will, in future, be referred to as the Oxbow type. This nomenclature is employed to make the distinction between the 'type succession' lavas and dykes identified by Marsh *et al*. (1997) and the dolerites of possible Oxbow affinity in the current study.

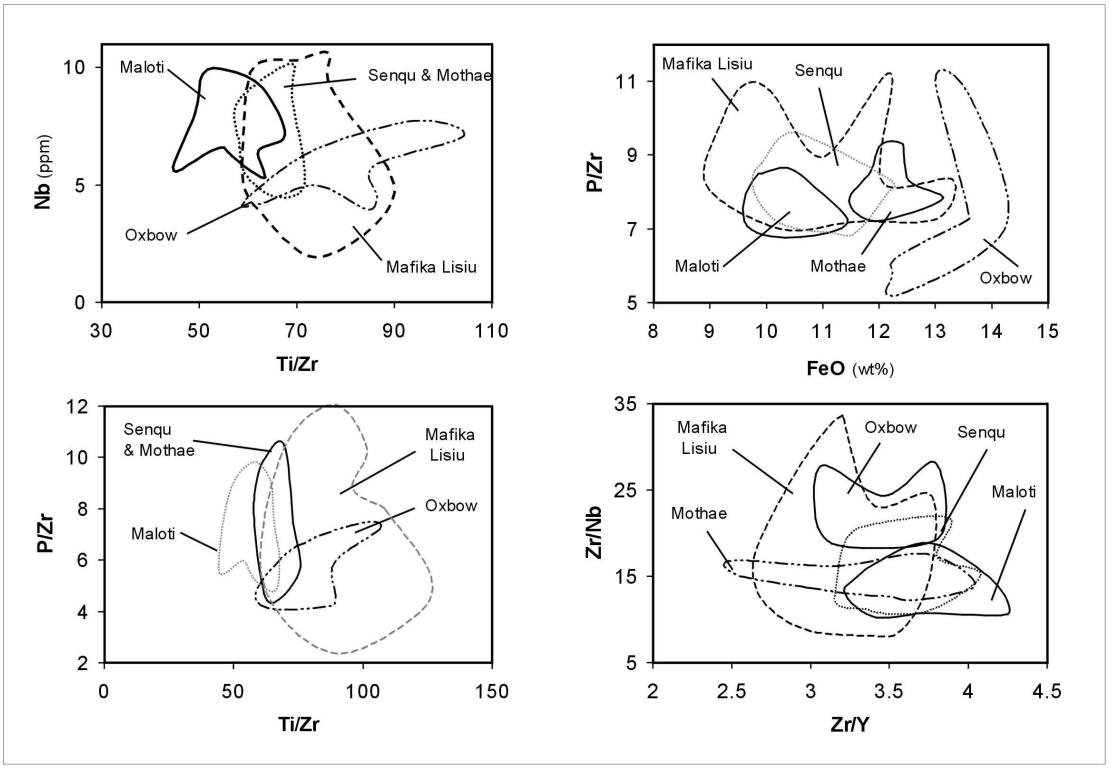

Figure 8. Geochemical discrimination diagrams used to distinguish the Lesotho Formation units. Lava data has been removed and the compositional fields defined by the lavas are shown. Sources for geochemical discrimination diagrams and lava data are given in the caption of Figure 5.

4.4 Intrusions

In addition to extensive outpourings of flood basalt lavas, the Drakensberg Group includes the extensive and perhaps interconnected subvolcanic plumbing system. In South Africa, this network of intrusions is particularly well exposed in the main Karoo basin due to post-Gondwana erosive processes. There are a number of forms of intrusions in the main Karoo basin and these are described by Chevallier and Woodford (1999), Meyboom and Wallace (1978) and Du Toit (1920) from which this review is derived.

Dykes, sills, inclined sheets, sill-ring complexes and other miscellaneous forms such as bell-jar and plug-like intrusions form the intrusive components of the Drakensberg Group. Two primary types of dykes occur in the province. These are (a) narrow (on the scale of metres to tens of metres), vertical intrusions that extend for distances between metres and tens of kilometres; and (b) long penetrative dykes hundreds of kilometres long and tens of metres wide (Mountain, 1943). The former are most abundant in the sequences within and above the Beaufort Group, whereas the latter penetrate throughout the Karoo Supergroup. In the main Karoo basin, dykes

exhibit a range of orientations with no evidence for radiating or oriented dyke swarms. However, widely separated east - west dykes that trend across the main Karoo basin (Chevallier and Woodford, 1999) and other locally oriented swarms trending WNW-ESE in the vicinity of the Lesotho remnant (Du Toit, 1920) and NNW-tending in the Western Cape (Chevallier and Woodford, 1999) have been documented.

Sills in the main Karoo basin vary in thickness between metres and hundreds of metres, and may develop oblique offshoots and undulations. In addition, dyke-like steps are often present where dykes transgress into inclined sheets and sills. Transgression from sill to dyke or vice versa, is dependent on the surrounding lithology – *i.e.* gradual transgression in homogeneous formations and stepped transgression in contrasted strata. Step-like dyke segments are especially prevalent in places where pronounced changes in lithology occur (*e.g.* at the contacts between the Dwyka - Ecca Groups and within the Beaufort Group). Especially prominent within the Karoo Sequence are sill-ring complexes that form basin-like structures, creating in plan view, circular to ovoid outcrops. Fed by local dykes, the rims of these intrusions are likened to inward dipping, linked dyke segments; within which flat sills and horizontal sediments occur. These complexes usually form individual units in the central Karoo, but in the Western Cape, these units coalesce and form interconnected basin-within-basin complexes. Other intrusive forms such as plugs, bell-jar shaped intrusions and laccolites are also present in the main Karoo basin.

5 MAJOR AND TRACE ELEMENT GEOCHEMISTRY

5.1 Introduction and sample preparation

Representative samples of 94 dolerite dykes and 3 sills were collected and analysed for major and trace elements by X-Ray Flourescence Spectrometry (XRF). Major element determinations were performed upon fusion discs, which were prepared according to the method described by Norrish and Hutton (1969). Trace element determinations (for Nb, Zr, Y, Sr, Rb, Cu, Zn, Ni, Co, Cr, V, Ba, Sc, La, Ce, Nd, Pb, Th and U) and Na_2O determinations were performed upon pressed powder pellets, which were prepared according to the method described in Duncan *et al.* (1984a). The unnormalised whole rock major and trace element geochemical data are presented in Table 1 and henceforth only the volatile-free normalised geochemical data are presented in the geochemical variation diagrams.

5.2 Geochemical Classification of the intrusions

All dolerites have between 49.3 and 54.6 wt% normalised SiO_2 (Figure 9). A simple geochemical classification of the lavas and dolerites using the total alkali versus silica diagram (after Le Bas *et al.*, 1986), indicates that the majority of intrusions classify as basaltic or basaltic andesite in composition (Figure 9). Cross, Iddings, Pirsson and Washington (CIPW) norm calculations indicate that these dolerites are hypersthene normative and are therefore tholeiitic.

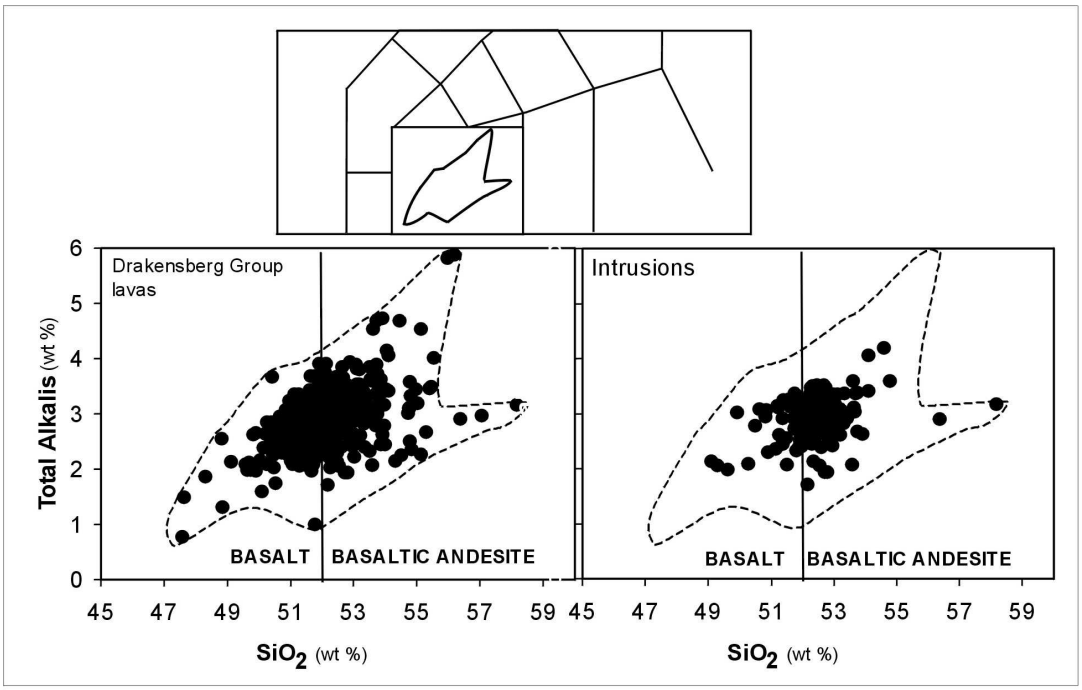

Figure 9. The fields for basalt and basaltic andesite determined from the total alkali versus silica (TAS) diagram (top) after Le Bas *et al.* (1986). All Karoo basalt lavas and dolerites are of basalt or basaltic andesite composition. Basalt lava data sources are given in the caption of Figure 5.

5.3 Major and trace element geochemistry

The major element geochemistry of the dolerites (Figures 10 and 11) suggests that they are differentiated to some degree. In addition, their major element geochemistry overlaps precisely with those of the Drakensberg Group basalt lavas. All the Karoo dolerites are considerably differentiated, with MgO between 4.5 and 9.9 wt%; FeO* [2] between 7.9 and 14 wt%, and Mg numbers (Mg#) between 43.6 and 64.7. The major element data is shown with MgO along the X abscissa in Figures 10 and 11 because MgO shows more variation compared to SiO_2. In addition, because MgO decreases with increasing differentiation in mafic systems it is a useful index of differentiation in mafic rocks.

Figure 10 shows the variation of TiO_2, FeO*, Al_2O_3 and CaO with MgO. TiO_2 varies from 0.9 to 1.7 wt% with decreasing MgO. A similar variation between 9.2 and 10.1 wt% FeO* is also observed as MgO decreases. However, between 6.0 and 5.5 wt% MgO, both FeO* and TiO_2 increase progressively. Al_2O_3 (varying between 13.4 and 18.2 wt%) and CaO (varying between 8.9 and 16 wt%) remain approximately constant between 8.5 and 6.5 wt% MgO, after which they decrease progressively with falling MgO content.

[2] FeO* = total Fe as FeO

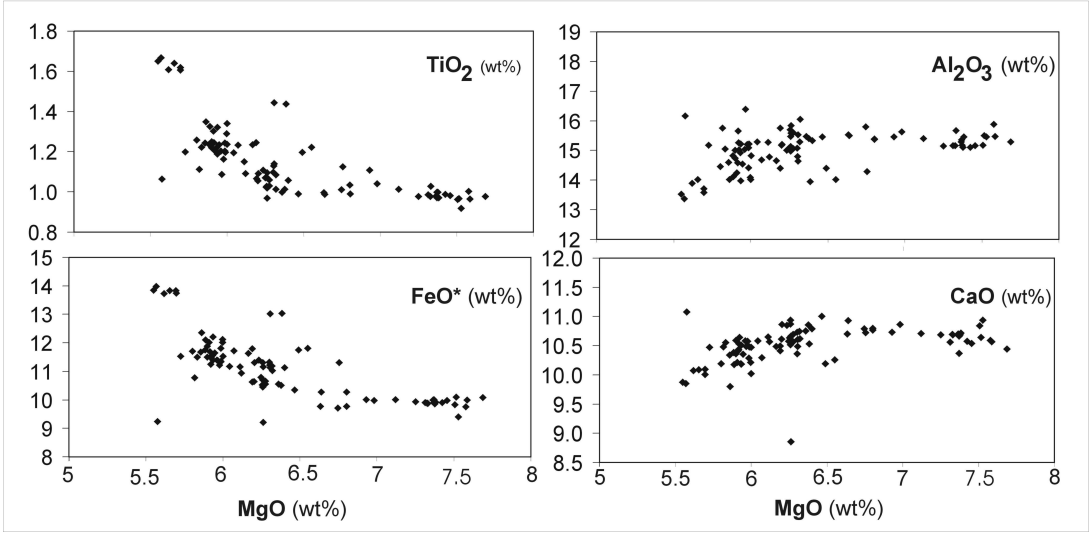

Figure 10. Major element variation diagrams showing the behaviour of TiO_2, Al_2O_3, FeO* and CaO with MgO. Apparent increase in TiO_2 and FeO*; and decrease in Al_2O_3 and CaO are consistent with a broad trend of differentiation suggestive of crystallisation and separation of pyroxene and plagioclase.

The trend for SiO_2 in the dolerites closely matches that described for Al_2O_3 and CaO in that it remains relatively constant between 8.5 and 6 wt% MgO, after which it progressively decreases with decreasing MgO content (Figure 11). Although the abundances of K_2O, Na_2O and P_2O_5 increase with falling MgO content, the trends for these latter elements are typified by considerable scatter. For the total range in MgO, K_2O and P_2O_5 vary between 0.3 and 1.1 wt%; and 0.1 to 0.2 wt%, respectively (Figure 11). Na_2O varies in abundance from 1.7 to 3.1 wt% (Figure 11) and MnO (not shown) varies in abundance between 0.2 and 0.9 wt%.

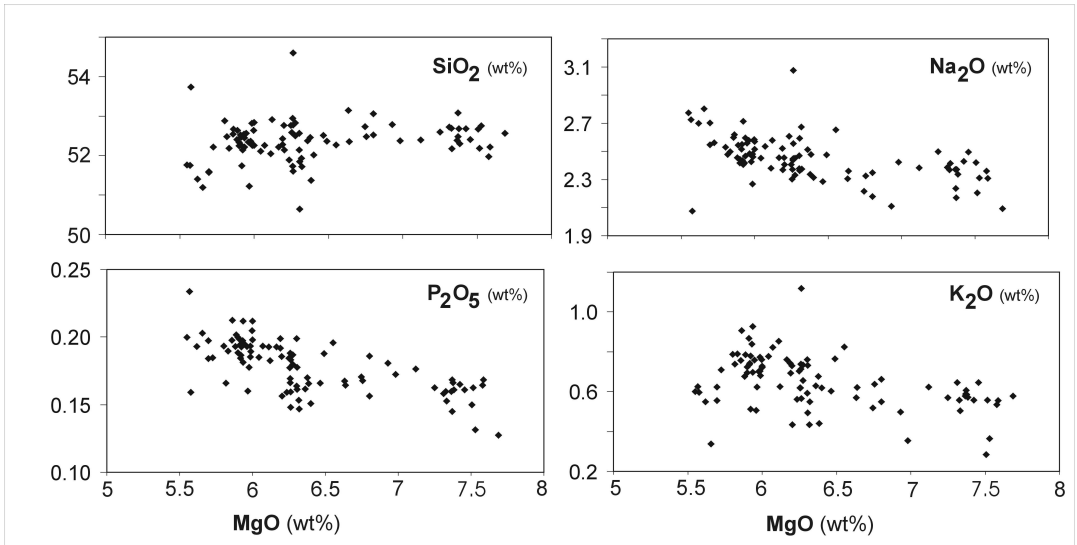

Figure 11. Major element variation diagrams showing the behaviour of SiO_2, K_2O, Na_2O and P_2O_5 with MgO. Apparent increases in K_2O, Na_2O and P_2O_5 with decreasing MgO are characterised by scatter. Despite the scatter in SiO_2, the trend is similar to that of Al_2O_3 and CaO.

Although major elements are important for showing general variations within magmas, trace elements are considered more useful since they can be used to model the chemical evolution of igneous rocks. Trace element partitioning into major basalt mineral phases (namely pyroxene, olivine and plagioclase) is controlled by the size of the lattice site; and the ionic radius and cation charge of the trace elements, which is reflected in mineral-melt partition coefficients (Wood and Blundy, 2003). Compatible trace elements (specifically, with mineral-melt partition coefficients, $D > 1$) substitute to some degree into basalt crystallising minerals, whereas incompatible trace elements (specifically, $D << 1$) are concentrated in the interstitial liquid until the point at which accessory phases which readily incorporate the incompatible trace elements crystallise (*e.g.* zirconium). Incompatible trace elements therefore provide a means with which to gauge the evolution of a mafic magmatic system.

Figures 12 - 14 illustrate the trace element variation in the dolerites in relation to the Drakensberg Group lava samples. Zr is used to illustrate the trace element variation of the lava and dolerite suites, since it is an incompatible high-field-strength (HFS) trace element which is not mobilised during alteration and weathering. In addition, Zr remains incompatible over a lengthy period of crystallisation. This, and the fact that the concentration of Zr is precisely determined by XRF techniques, makes it a useful index of differentiation for trace elements. With the exception of Ba and Sr; and to a lesser extent, Ce and La; complete overlap in the trace element geochemical compositions of the Drakensberg Group lavas and the dolerites is apparent. This suggests that the dolerites are of similar composition to the Drakensberg Group lavas.

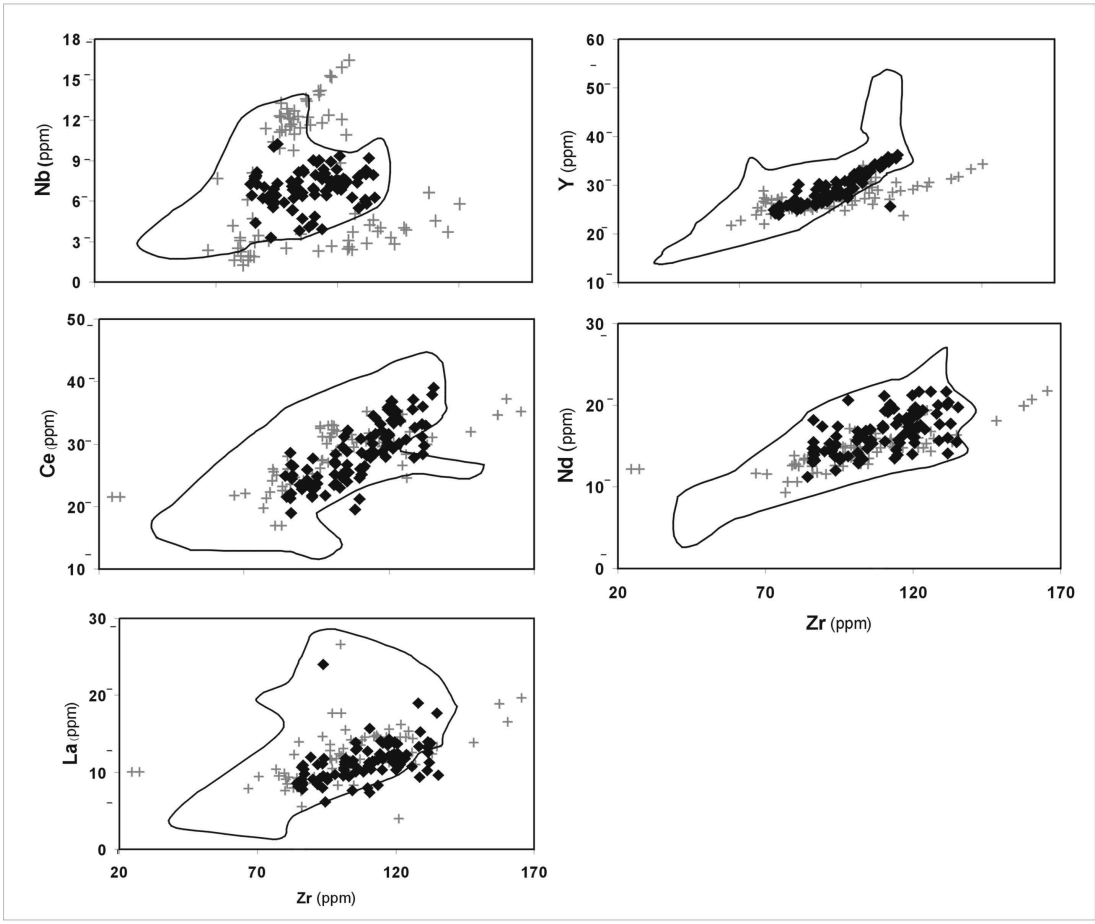

Figure 12. Variation of Nb, Y, Ce, Nd and La with Zr in the dolerites (♦). Shown for comparison are the lavas of the Barkly East Formation (grey crosses) and the compositional fields for the Lesotho Formation lavas (polygons). Basalt lava data sources are given in the caption of Figure 5.

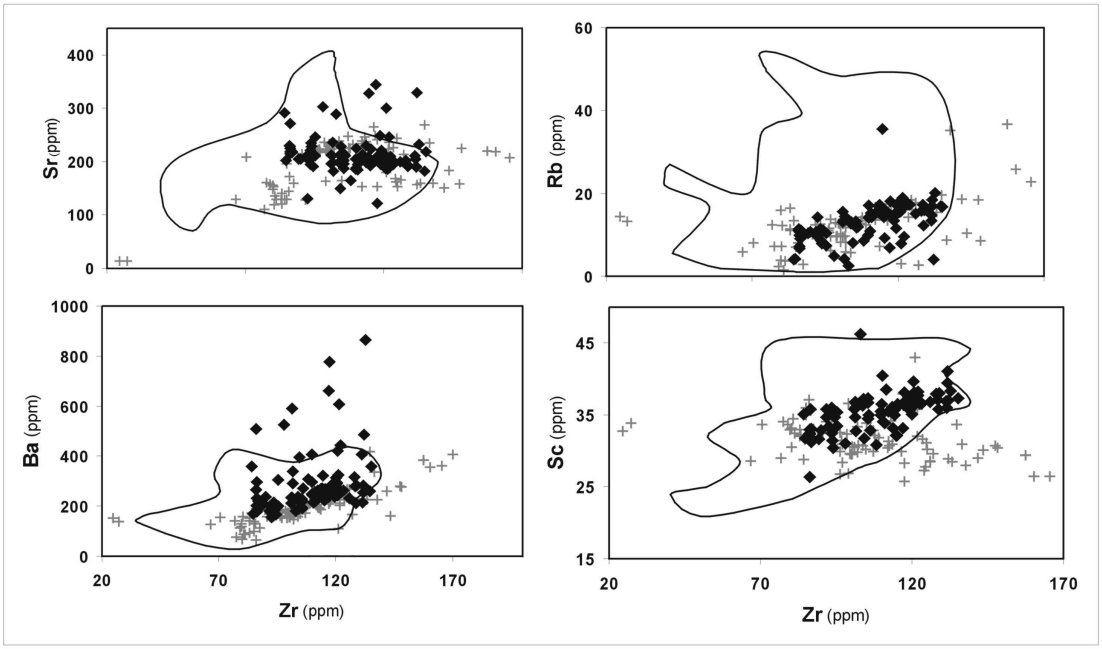

Figure 13. Variation of Sr, Rb, Ba and Sc with Zr in the dolerites (♦). Shown for comparison are the lavas of the Barkly East Formation (grey crosses) and the compositional fields for the Lesotho Formation lavas (polygons). Basalt lava data sources are given in the caption of Figure 5.

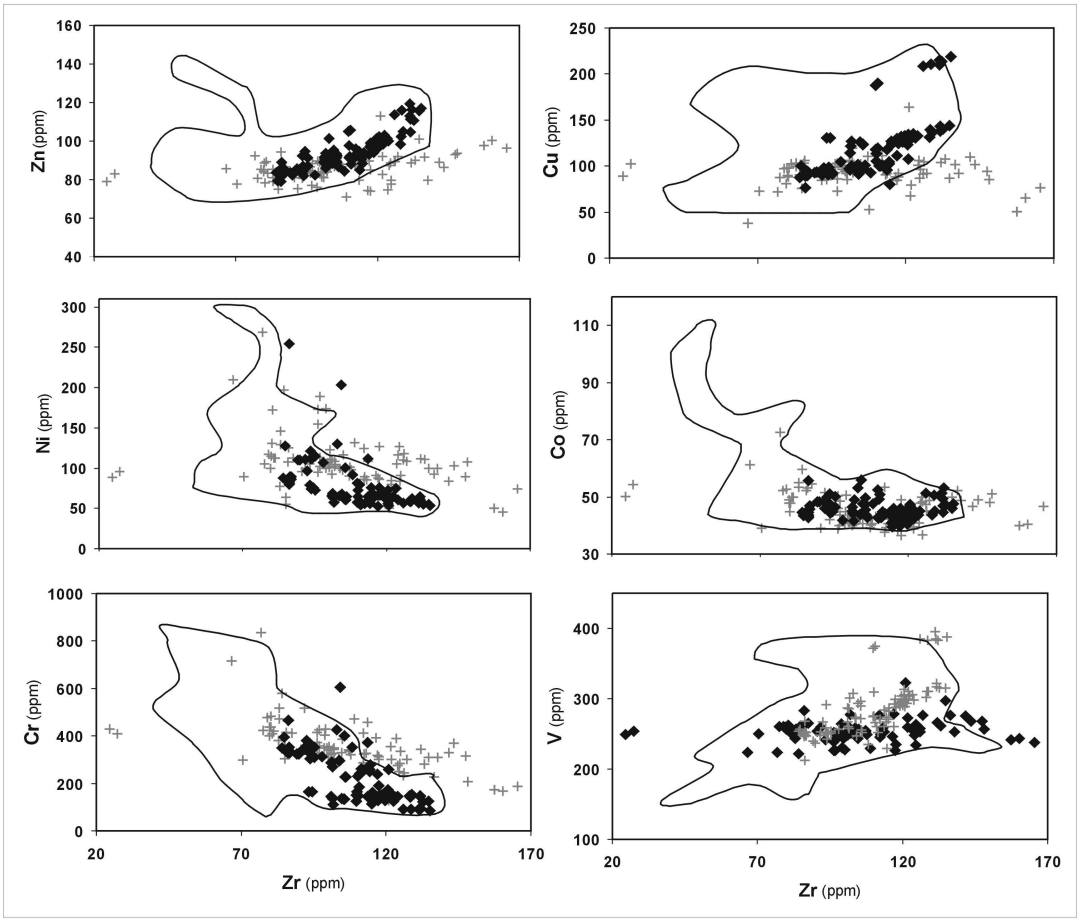

Figure 14. Variation of Zn, Cu, Ni, Co, Cr and V with Zr in the dolerites (♦). Shown for comparison are the lavas of the Barkly East Formation (grey crosses) and the compositional fields for the Lesotho Formation lavas (polygons) are shown. Basalt lava data sources are given in the caption of Figure 5.

Table 1. Unnormalised major and trace element data for the dolerites. GPS coordinates correspond to sample localities in Figure 3.

Sample	VM-01	VM-02	VM-03	VM-04	VM-05	VM-06	VM-07
GPS coordinates	28° 31.762' S; 28° 28.356' E	28° 31.018' S; 28° 30.405' E	28° 31.018' S; 28° 30.403' E	28° 30.715' S; 28° 31.196' E	28° 30.602' 'S; 28° 31.307' E	28° 30.402' S; 28° 32.925' E	28° 30.381' S; 28° 33.794' E
Form of Intrusion	Dyke	Dyke	Dyke	Dyke	Dyke	Dyke	Dyke
Major elements (wt%)							
SiO_2	51.02	51.36	51.30	51.93	51.19	51.16	51.30
TiO_2	1.08	1.29	1.27	1.01	1.01	1.21	1.10
Al_2O_3	14.93	13.68	13.91	15.50	15.37	14.47	13.97
FeO*	11.15	11.95	11.74	10.39	9.69	11.47	11.05
MnO	0.19	0.20	0.20	0.18	0.17	0.20	0.19
MgO	6.17	5.81	5.77	6.18	7.19	5.74	6.60
CaO	10.79	9.97	9.98	10.50	10.48	10.13	10.48
Na_2O	2.41	2.54	2.46	2.27	2.37	2.40	2.27
K_2O	0.73	0.91	0.85	0.61	0.49	0.66	0.62
P_2O_5	0.16	0.21	0.19	0.18	0.15	0.19	0.16
LOI	1.77	1.82	2.04	1.96	1.93	1.79	1.67
H_2O^-	0.13	0.27	0.25	0.14	0.16	0.83	0.26
Total	100.53	100.02	99.95	100.86	100.21	100.25	99.68
Trace elements (ppm)							
Nb	6.3	7.8	7.6	8.2	5.8	7	6.7
Zr	104	129	126	105	92	117	108
Y	30	35	34	27	25	31	29
Sr	200	187	188	211	224	192	184
Rb	13	18	17	12	8	15	14
Zn	90	102	100	88	81	99	90
Cu	121	140	136	96	97	129	111
Ga	17	16.9	18.6	17.7	17.8	18.5	18.2
Th	< 2.4	< 2.5	< 2.4	< 2.3	< 2.3	< 2.4	< 2.4
Pb	< 2.7	< 2.8	3	< 2.6	< 2.6	< 2.7	< 2.7
Ni	61	60	57	60	110	64	71
Ce	26	35	36	32	23	30	30
Nd	16	20	21	17	13	17	15
La	13	14	13	11	12	11	11
Co	45	46	44	43	44	39	48
Cr	130	143	138	224	319	125	226
V	286	310	303	252	246	297	303
Ba	227	277	274	219	180	232	238
Sc	34	39	36	35	30	37	40

Table 1 (cont.)

Sample	VM-08	VM-09	VM-10	VM-11	VM-12	VM-13	VM-14
GPS coordinates	28° 30.386' S; 28° 33.808' E	28° 30.137' S; 28° 36.021' E	28° 30.164' S; 28° 36.143' E	28° 30.164' S; 28° 36.143' E	28° 30.529' S; 28° 37.372' E	28° 30.529' S; 28° 37.372' E	28° 31.196' S; 28° 38286' E
Form of Intrusion	Dyke	Dyke	Dyke	Dyke	Dyke	Dyke	Dyke
Major Elements (wt%)							
SiO_2	50.57	51.91	51.14	51.66	50.62	50.50	51.72
TiO_2	1.11	1.22	1.21	1.32	1.58	1.584	1.04
Al_2O_3	15.15	14.36	14.22	13.75	13.68	13.29	14.88
FeO*	10.85	11.50	11.39	12.12	13.53	13.46	10.43
MnO	0.18	0.20	0.19	0.21	0.22	0.22	0.17
MgO	6.15	5.87	5.76	5.75	5.53	5.58	6.08
CaO	10.34	10.22	10.15	9.61	9.92	9.88	10.40
Na_2O	2.31	2.52	2.49	2.57	2.66	2.64	2.41
K_2O	0.71	0.75	0.72	0.89	0.54	0.54	0.72
P_2O_5	0.17	0.19	0.19	0.21	0.19	0.19	0.18
LOI	1.86	1.85	1.74	2.12	2.10	1.87	1.82
H_2O^-	0.26	0.18	0.26	0.16	0.12	0.23	0.23
Total	99.66	100.77	99.45	100.36	100.69	99.99	100.07
Trace elements (ppm)							
Nb	6.3	7.4	7.2	9	5.4	5.8	8.2
Zr	108	120	121	130	127	129	112
Y	28	31	32	35	34	35	28
Sr	190	183	193	229	188	201	205
Rb	15	17	17	20	12	13	15
Zn	86	100	98	109	114	111	89
Cu	116	128	130	138	207	206	100
Ga	18.7	18.2	18.7	19.2	20.8	20.4	19.2
Th	< 2.4	< 2.4	< 2.4	2.5	2.5	2.7	< 2.4
Pb	< 2.7	2.7	4	3.6	< 2.9	< 2.9	< 2.7
Ni	78	60	59	54	59	61	56
Ce	28	29	33	32	27	31	28
Nd	17	17	17	21	20	21	17
La	15	12	12	14	9	13	12
Co	42	44	44	46	50	49	43
Cr	180	146	142	121	88	93	245
V	259	295	291	309.5	378	377	262
Ba	244	253	nd [3]	848	209	211	239
Sc	33	37	nd	38	35	35	34

[3] Note that nd stands for not determined

Table 1 (cont.)

Sample	VM-15	VM-16	VM-17	VM-18	VM-19	VM-20	VM-21
GPS coordinates	28° 31.525' S; 28° 38.962' E	28° 31.781' S; 28° 39.180' E	28° 28.460' S; 28° 50.196' E	28° 28.460' S; 28° 50.196' E	28° 28.373' S; 28° 49.139' E	28° 28.460' S; 28° 46.016' E	28° 28.281' S; 28° 45.621' E
Form of Intrusion	Dyke	Dyke	Dyke	Dyke	Dyke	Dyke	Dyke
Major Elements (wt%)							
SiO_2	51.24	51.40	50.38	52.00	51.14	51.68	51.59
TiO_2	1.10	1.03	1.57	0.97	1.04	1.23	0.97
Al_2O_3	14.42	14.65	13.40	14.98	15.37	14.24	15.27
FeO*	10.94	10.37	13.51	9.83	10.38	11.67	10.12
MnO	0.19	0.18	0.22	0.17	0.18	0.20	0.18
MgO	6.14	6.11	5.56	7.17	6.04	6.12	6.54
CaO	10.10	10.28	9.77	10.57	10.24	10.29	10.77
Na_2O	2.41	2.39	2.49	2.47	2.31	2.49	2.33
K_2O	0.74	0.72	0.61	0.56	0.68	0.73	0.61
P_2O_5	0.19	0.18	0.18	0.16	0.19	0.20	0.16
LOI	2.14	2.16	1.87	1.79	1.90	1.65	1.65
H_2O^-	0.22	0.21	0.20	0.35	0.23	0.17	0.16
Total	99.84	99.68	99.76	101.02	99.69	100.68	100.36
Trace elements (ppm)							
Nb	9	8.8	6.1	7.7	8.8	7.4	7
Zr	118	109	123	85	107	121	100
Y	30	28	34	24	27	32	25
Sr	204	208	195	213	220	191	208
Rb	15	15	15	11	14	16	13
Zn	96	93	111	81	95	99	87
Cu	105	98	204	90	103	131	94
Ga	18	18.4	22	17	17	19	17.9
Th	< 2.4	< 2.4	< 2.5	< 2.3	< 2.4	< 2.4	< 2.4
Pb	3.5	3.1	2.9	< 2.6	< 2.7	2.9	< 2.7
Ni	52	55	56	79	63	62	66
Ce	36	27	30	22	25	33	27
Nd	20	17	19	13	16	19	14
La	11	11	11	8	11	11	10
Co	41	43	50	43	42	42	44
Cr	252	250	90	328	160	154	285
V	281	264	376	250	269	307	257
Ba	237	255	226	200	396	262	232
Sc	37	35	36	33	36	37	34

Table 1 (cont.)

Sample	VM-22	VM-23	VM-24	VM-25	VM-26	VM-27	VM-28
GPS coordinates	28° 29.564' S; 28° 42.655' E	28° 31.754' S; 28° 40.101' E	28° 31.754' S; 28° 40.101' E	28° 31.310' S; 28° 26.964' E	28° 24.414' S; 28° 30.532' E	28° 25.177' S; 28° 30.711' E	28° 25.621' S; 28° 30.647' E
Form of Intrusion	Dyke	Dyke	Dyke	Dyke	Dyke	Dyke	Dyke
Major Elements (wt%)							
SiO_2	50.51	51.24	51.15	51.26	51.17	51.26	51.64
TiO_2	1.61	1.29	1.20	1.17	1.17	1.18	1.19
Al_2O_3	13.20	13.75	14.75	14.92	15.02	14.73	14.90
FeO*	13.51	11.78	11.27	11.13	10.97	11.16	11.21
MnO	0.21	0.21	0.20	0.18	0.19	0.20	0.19
MgO	5.42	5.73	5.72	5.87	5.93	5.84	5.91
CaO	9.64	9.91	10.34	10.28	10.39	10.36	10.35
Na_2O	2.71	2.48	2.45	2.41	2.41	2.53	2.45
K_2O	0.59	0.76	0.77	0.67	0.76	0.50	0.69
P_2O_5	0.20	0.20	0.19	0.19	0.18	0.19	0.18
LOI	2.10	2.34	1.94	2.14	1.75	1.85	1.80
H_2O^-	0.18	0.18	0.14	0.09	0.27	0.18	0.09
Total	99.86	99.87	100.10	100.32	100.23	99.96	100.60
Trace Elements (ppm)							
Nb	6.1	8.1	7.2	7	7.2	6.8	7.4
Zr	132	128	118	115	117	119	117
Y	35	34	32	31	31	31	31
Sr	214	185	196	120	218	294	193
Rb	16	17	17	15	11	8	15
Zn	114	108	100	96	94	96	96
Cu	214	134	128	123	128	125	124
Ga	19.7	19.5	18	17.5	18.4	17.8	18
Th	< 2.5	< 2.4	< 2.4	< 2.4	< 2.4	< 2.4	< 2.4
Pb	< 2.9	4.2	< 2.7	< 2.7	< 2.7	< 2.7	2.7
Ni	52	63	64	65	63	63	66
Ce	38	28	31	32	29	36	27
Nd	21	17	18	16	17	19	16
La	9	12	10	12	12	12	11
Co	47	44	43	42	44	43	42
Cr	82	144	148	147	146	153	152
V	378	313	285	282	285	293	291
Ba	350	248	307	239	277	317	246
Sc	36	40	37	36	35	37	37

Table 1 (cont.)

Sample	VM-29	VM-30	VM-31	VM-32	VM-33	VM-34	VM-35
GPS coordinates	28° 25.766' S; 28° 33.677' E	28° 25.730' S; 28° 33.862' E	28° 25.083' S; 28° 35.050' E	28° 23.998' S; 28° 36.468' E	28° 23.814' S; 28° 36.264' E	28° 23.610' S; 28° 36.156' E	28° 22.989' S; 28° 35.987' E
Form of Intrusion	Dyke	Dyke	Dyke	Dyke	Dyke	Dyke	Dyke
Major Elements (wt%)							
SiO_2	45.54	51.25	51.84	51.69	52.41	50.78	51.40
TiO_2	1.04	0.98	1.05	1.07	1.06	1.00	0.95
Al_2O_3	16.77	15.35	14.67	14.44	14.99	15.59	14.80
FeO*	7.25	9.45	10.48	10.69	10.61	10.98	9.65
MnO	0.81	0.30	0.19	0.19	0.19	0.18	0.16
MgO	4.14	6.56	6.13	5.98	6.22	6.16	7.15
CaO	14.76	10.49	10.30	10.33	10.48	10.49	10.43
Na_2O	1.60	2.15	2.39	2.52	2.43	2.52	2.31
K_2O	0.31	0.50	0.70	0.61	0.73	0.56	0.54
P_2O_5	0.18	0.17	0.18	0.18	0.18	0.15	0.16
LOI	7.77	2.24	1.99	2.28	1.85	1.54	2.17
H_2O^-	0.61	0.42	0.20	0.28	0.21	0.24	0.23
Total	100.78	99.86	100.11	100.25	101.37	100.20	99.97
Trace Elements (ppm)							
Nb	6.5	7.1	7.9	9.7	7.9	6.3	7.7
Zr	95	93	112	114	110	93	84
Y	28	26	27	29	29	30	25
Sr	267	206	200	336	202	188	213
Rb	2	10	15	7	14	11	7
Zn	94	89	91	91	89	93	84
Cu	91	90	102	109	99	129	88
Ga	19	18	16	19.1	18.1	17.8	16.7
Th	< 2.2	< 2.3	< 2.4	< 2.4	< 2.4	< 2.4	< 2.3
Pb	2.6	< 2.6	< 2.7	3	< 2.7	< 2.7	< 2.6
Ni	120	111	55	51	54	75	84
Ce	21	24	29	nd	26	23	nd
Nd	12	14	16	nd	15	14	nd
La	9	9	12	nd	10	6	nd
Co	49	49	40	39	43	44	44
Cr	393	342	254	235	239	163	321
V	284	247	268	254	258	246	243
Ba	166	195	266	646	257	164	196
Sc	43	34	35	32	34	34	31

Table 1 (cont.)

Sample	VM-36	VM-37	VM-38	VM-39	VM-40	VM-41	VM-42
GPS coordinates	28° 22.877' S; 28° 36.846' E	28° 20.588' S; 28° 36.846' E	28° 20.285' S; 28° 38.647' E	28° 29.931" S; 28° 41.793' E	28° 29.499' S; 28° 41.741' E	28° 29.347' S; 28° 41.715' E	28° 27.745' S; 28° 40.879' E
Form of Intrusion	Dyke	Dyke	Dyke	Sill	Dyke	Dyke	Dyke
Major Elements (wt%)							
SiO_2	51.12	51.65	51.56	51.39	50.91	50.49	51.49
TiO_2	0.89	1.22	0.97	0.96	1.64	1.62	0.96
Al_2O_3	14.98	14.09	14.79	14.87	13.15	13.83	15.03
FeO*	9.12	11.55	9.69	9.79	13.75	13.65	9.82
MnO	0.18	0.20	0.17	0.16	0.23	0.23	0.17
MgO	7.30	5.85	7.27	7.31	5.48	5.58	7.24
CaO	10.60	10.05	10.35	10.33	9.69	9.95	10.52
Na_2O	2.24	2.22	2.38	2.45	2.68	2.76	2.33
K_2O	0.35	0.76	0.55	0.63	0.62	0.33	0.57
P_2O_5	0.13	0.19	0.16	0.16	0.23	0.20	0.18
LOI	2.28	2.31	1.94	1.90	2.04	2.25	1.62
H_2O^-	0.28	0.24	0.21	0.28	0.27	0.21	0.18
Total	99.46	100.33	100.02	100.24	100.68	101.10	100.09
Trace Elements (ppm)							
Nb	6.2	7.1	7.1	7.5	6	5.7	7
Zr	82	82	85	84	129	130	119
Y	23	24	25	25	35	25.3	32
Sr	196	285	214	225	207	325	195
Rb	4	4	11	11	15	4	18
Zn	77	82	81	80	117	115	101
Cu	97	85	92	88	212	211	121
Ga	15.6	15.6	18	16.8	21.4	22.1	18.1
Th	< 2.3	< 2.3	< 2.3	< 2.3	< 2.5	< 2.5	< 2.4
Pb	2.7	< 2.6	< 2.6	2.8	< 2.8	< 2.9	< 2.7
Ni	124	86	84	81	55	57	55
Ce	21	24	24	28	33	29	36
Nd	11	13	13	15	20	19	19
La	8	8	10	11	10	11	12
Co	42	44	46	44	51	53	46
Cr	382	341	329	325	90	92	139
V	249	248	247	241	389	378	308
Ba	165	351	217	261	399	480	286
Sc	31	34	32	31	36	37	39

Table 1 (cont.)

Sample	VM-43	VM-44	VM-45	VM-46	VM-47	VM-48	VM-49
GPS coordinates	28° 27.281' S; 28° 40.900' E	28° 27.026' S; 28° 41.268' E	28° 26.700' S; 28° 41.620' E	28° 25.398' S; 28° 41.704' E	28° 24.781' S; 28° 41.439' E	28° 24.649' S; 28° 40.293' E	28° 25.239' S; 28° 39.362' E
Form of Intrusion	Dyke	Dyke	Dyke	Dyke	Dyke	Sill	Dyke
Major Elements (wt%)							
SiO_2	50.87	50.61	51.37	50.33	50.21	51.45	51.88
TiO_2	1.20	1.18	1.22	0.99	1.07	0.98	0.97
Al_2O_3	14.29	13.57	14.27	15.62	16.06	14.75	15.05
FeO*	11.41	11.44	11.41	10.73	11.16	9.63	9.55
MnO	0.20	0.20	0.19	0.18	0.20	0.16	0.17
MgO	5.91	6.34	5.73	6.15	5.85	7.20	6.65
CaO	10.02	9.93	10.11	10.33	10.28	10.44	10.53
Na_2O	2.47	2.57	2.54	2.31	2.43	2.32	2.30
K_2O	0.80	0.80	0.74	0.53	0.61	0.57	0.54
P_2O_5	0.19	0.19	0.19	0.14	0.16	0.16	0.15
LOI	2.36	2.45	1.87	2.22	1.77	2.05	2.30
H_2O^-	0.28	0.29	0.24	0.21	0.09	0.23	0.25
Total	99.99	99.57	99.88	99.76	99.89	99.93	100.33
Trace Elements (ppm)							
Nb	7.1	7.3	7.4	5.4	6.1	7.7	7.7
Zr	118	117	121	91	100	84	85
Y	31	31	32	28	29	25	25
Sr	187	181	191	190	178	219	214
Rb	17	17	178	11	14	10	9
Zn	96	99	99	90	92	80	85
Cu	131	128	127	127	125	90	88
Ga	19	18.5	17.8	18.2	19.2	17.2	15.7
Th	< 2.4	< 2.4	< 2.4	< 2.4	< 2.4	< 2.3	< 2.6
Pb	< 2.7	< 2.7	5.1	< 2.7	3.4	< 2.6	< 2.6
Ni	63	70	73	76	56	80	87
Ce	33	34	29	21	23	26	24
Nd	17	19	17	13	14	14	14
La	10	13	12	8	12	9	11
Co	42	46	43	50	48	43	42
Cr	144	168	140	161	109	321	345
V	299	296	299	252	295	243	262
Ba	409	284	256	181	286	291	174
Sc	35	37	36	35	36	32	35

Table 1 (cont.)

Sample	VM-50	VM-51	VM-52	VM-53	VM-54	VM-55	VM-56
GPS coordinates	28° 25.719' S; 28° 35.938' E	28° 45.170' S; 28° 16.047' E	28° 42.768' S; 28° 19.183' E	28° 42.484' S; 28° 19.722' E	28° 42.232' S; 28° 20.929' E	28° 43.237' S; 28° 23.232' E	28° 45.430' S; 28° 27.921' E
Form of Intrusion	Dyke	Dyke	Dyke	Dyke	Dyke	Dyke	Dyke
Major Elements (wt%)							
SiO_2	51.79	51.73	51.87	51.19	51.20	51.52	52.25
TiO_2	1.05	1.01	0.98	1.22	1.09	1.20	0.96
Al_2O_3	14.80	15.37	14.83	14.41	14.81	14.62	15.05
FeO*	10.59	10.40	9.69	11.63	11.24	11.33	9.75
MnO	0.18	0.18	0.17	0.19	0.19	0.19	0.17
MgO	6.13	6.18	7.20	5.77	6.15	5.82	7.45
CaO	10.38	10.54	10.13	10.13	10.71	9.99	10.75
Na_2O	2.36	2.30	2.12	2.39	2.57	2.37	2.40
K_2O	0.69	0.65	0.59	0.68	0.55	0.82	0.28
P_2O_5	0.18	0.17	0.14	0.20	0.16	0.19	0.15
LOI	2.05	1.90	2.28	1.94	1.79	1.88	1.59
H_2O^-	0.16	0.22	0.24	0.20	0.18	0.09	0.21
Total	100.37	100.65	100.25	99.96	100.64	100.01	101.01
Trace Elements (ppm)							
Nb	8.7	8	4	7.5	6.5	6.7	7.6
Zr	109	105	99	120	103	119	115
Y	27	26	27	32	29	32	30
Sr	200	208	161	206	226	200	221
Rb	14	12	8	18	8	19	9
Zn	90	85	83	101	94	96	92
Cu	99	99	91	132	124	126	123
Ga	17	19	17.6	17.7	17.7	19.3	18.8
Th	< 2.4	< 2.4	< 2.3	< 2.4	< 2.4	< 2.4	< 2.4
Pb	< 2.6	2.8	3.1	< 2.8	3	3.7	3.6
Ni	55	64	90	63	67	60	63
Ce	26	25	19	34	31	33	34
Nd	15	15	14	18	17	19	17
La	11	13	10	12	11	11	14
Co	44	42	47	43	47	45	44
Cr	257	223	343	123	134	145	151
V	247	248	230	298	290	287	285
Ba	217	268	300	253	389	594	225
Sc	38	32	30	36	36	36	36

Table 1 (cont.)

Sample	VM-57	VM-58	VM-59	VM-60	VM-61	VM-62	VM-63
GPS coordinates	28° 45.562' S; 28° 27.994' E	28° 45.809' S; 28° 26.221' E	28° 43.828' S; 28° 23.775' E	28° 42.581' S; 28° 22.374' E	28° 38.984' S; 28° 23.652' E	28° 38.614' S; 28° 24.471' E	28° 37.366' S; 28° 29.477' E
Form of Intrusion	Dyke	Dyke	Dyke	Dyke	Dyke	Dyke	Dyke
Major Elements (wt%)							
SiO_2	50.99	51.46	50.99	51.04	51.70	51.61	51.13
TiO_2	0.95	1.08	1.19	1.21	0.98	1.26	1.13
Al_2O_3	14.83	15.07	14.69	14.48	15.11	13.82	15.00
FeO*	9.78	9.75	11.23	11.26	9.50	11.79	10.97
MnO	0.16	0.19	0.19	0.19	0.18	0.20	0.19
MgO	7.46	6.76	5.79	5.86	6.45	5.88	6.00
CaO	10.13	10.46	10.40	10.23	10.41	10.01	10.46
Na_2O	2.03	2.06	2.35	2.51	2.24	2.53	2.34
K_2O	0.56	0.48	0.76	0.70	0.55	0.74	0.84
P_2O_5	0.12	0.18	0.19	0.19	0.16	0.20	0.19
LOI	2.28	2.19	2.06	1.68	2.36	1.74	2.09
H_2O^-	0.61	0.40	0.29	0.18	0.34	0.22	0.29
Total	99.90	100.06	100.14	99.53	99.98	100.00	100.63
Trace Elements (ppm)							
Nb	3.2	3.8	7.1	6.9	7.9	7.7	7.5
Zr	90	111	118	119	85	126	112
Y	26	28	31	31	25	33	30
Sr	127	225	207	241	212	189	195
Rb	14	17	15	9	9	16	16
Zn	83	83	95	96	83	103	93
Cu	95	94	126	130	87	134	116
Ga	17	19.8	18.4	18.5	16.2	17.5	17.8
Th	< 2.3	< 2.3	< 2.4	< 2.4	2.3	2.7	2.6
Pb	3.1	< 2.6	3.3	< 2.7	< 2.6	4.1	3.5
Ni	94	108	61	62	87	61	63
Ce	23	27	29	34	26	32	31
Nd	13	17	17	19	14	19	19
La	9	8	12	12	10	15	11
Co	48	43	40	42	45	44	44
Cr	368	362	150	145	321	150	142
V	259	254	288	292	240	305	279
Ba	151	263	258	433	185	276	244
Sc	33	32	36	37	30	37	36

Table 1 (cont.)

Sample	VM-64	VM-65	VM-66	VM-67	VM-68	VM-69	VM-70
GPS coordinates	28° 36.769' S; 28° 27.477' E	28° 36.883' S; 28° 27.378' E	28° 36.969' S; 28° 27.382' E	28° 37.270' S; 28° 25.717' E	28° 37.570' S; 28° 25.377' E	28° 41.045' S; 28° 23.743' E	Approximately 28° 40' S; 28° 23' E
Form of Intrusion	Dyke	Dyke	Dyke	Dyke	Dyke	Dyke	Dyke
Major Elements (wt%)							
SiO_2	51.90	51.53	50.77	53.56	51.03	49.31	51.41
TiO_2	1.24	1.14	1.19	0.95	1.17	1.41	1.01
Al_2O_3	14.18	14.96	14.59	15.29	14.03	14.25	15.05
FeO*	11.49	11.04	11.18	9.04	11.45	12.69	10.05
MnO	0.20	0.19	0.19	0.15	0.19	0.21	0.17
MgO	5.69	5.88	5.73	6.14	6.33	6.14	6.66
CaO	10.00	10.40	10.29	8.68	9.93	10.21	10.57
Na_2O	2.48	2.39	2.35	3.02	2.41	2.52	2.13
K_2O	0.77	0.69	0.70	1.10	0.75	0.48	0.65
P_2O_5	0.19	0.18	0.18	0.16	0.18	0.16	0.18
LOI	1.78	1.90	2.49	1.77	1.89	2.32	2.08
H_2O^-	0.33	0.39	0.35	0.18	0.16	0.26	0.39
Total	100.25	100.68	100.02	100.05	99.52	99.96	100.35
Trace Elements (ppm)							
Nb	7.2	6.3	6.7	7.9	7.3	4.7	10
Zr	126	114	117	113	115	108	93
Y	33	31	31	27	32	29	25
Sr	199	196	205	322	203	180	242
Rb	15	16	15	35	18	11	7
Zn	96	92	95	9	97	103	85
Cu	129	123	127	79	122	185	89
Ga	19.2	18.2	20.5	17	18.2	21.8	16.1
Th	< 2.4	< 2.4	< 2.4	3	< 2.4	< 2.5	< 2.3
Pb	< 2.7	3.4	< 2.7	6.1	< 2.7	< 2.8	< 2.6
Ni	58	67	63	74	74	77	71
Ce	35	31	31	34	28	25	23
Nd	18	16	18	17	15	17	15
La	19	12	11	14	14	7	9
Co	43	40	43	39	45	49	45
Cr	145	160	143	274	184	143	303
V	296	277	285	225	292	364	246
Ba	311	264	245	317	755	210	298
Sc	37	36	34	32	37	33	33

Table 1 (cont.)

Sample	VM-71	VM-72	VM-73	VM-74	VM-75	VM-76	VM-77
GPS coordinates	28° 41.487' S; 28° 22.240' E	28° 41.726' S; 28° 22.075' E	28° 41.790' S; 28° 21.951' E	28° 32.229' S; 28° 25.425' E	28° 32.678' S; 28° 25.129' E	28° 31.459' S; 28° 25.088' E	28° 33.252' S; 28° 25.004' E
Form of Intrusion	Dyke	Dyke	Dyke	Dyke	Dyke	Dyke	Dyke
Major Elements (wt%)							
SiO_2	51.14	51.54	51.21	51.47	51.47	50.72	51.15
TiO_2	0.95	1.02	0.99	0.96	0.99	1.18	1.21
Al_2O_3	15.15	15.51	15.06	15.21	15.11	15.34	14.36
FeO*	9.78	8.86	9.79	9.77	10.32	11.27	11.39
MnO	0.17	0.29	0.16	0.18	0.19	0.19	0.20
MgO	7.43	5.35	6.96	7.27	6.26	5.80	6.04
CaO	10.35	10.63	10.47	10.54	10.65	10.23	10.27
Na_2O	2.26	1.99	2.33	2.30	2.29	2.39	2.40
K_2O	0.54	0.57	0.61	0.56	0.66	0.73	0.74
P_2O_5	0.17	0.15	0.17	0.16	0.17	0.18	0.19
LOI	1.91	3.24	1.83	1.80	1.68	1.73	1.84
H_2O^-	0.35	0.53	0.20	0.16	0.15	0.26	0.16
Total	100.20	99.69	99.78	100.37	99.93	100.04	99.95
Trace Elements (ppm)							
Nb	6.1	4.5	9.8	5.9	8	8.2	7.4
Zr	87	101	92	90	102	117	117
Y	25	27	24	26	26	32	32
Sr	200	180	230	205	208	194	196
Rb	10	12	10	11	13	15	17
Zn	82	89	83	84	87	98	94
Cu	91	93	88	89	100	127	128
Ga	16.7	16.9	16.5	16.8	17.7	18.3	18.5
Th	< 2.3	< 2.3	< 2.3	< 2.3	< 2.4	< 2.4	< 2.4
Pb	2.6	3.5	< 2.6	< 2.6	3.3	3.2	< 2.7
Ni	108	96	72	109	65	65	65
Ce	23	28	27	24	29	35	35
Nd	15	17	15	15	16	21	18
La	12	13	24	11	11	14	14
Co	47	48	43	45	43	45	41
Cr	317	385	296	338	289	148	153
V	234	261	237	249	267	290	293
Ba	205	184	199	198	234	249	270
Sc	31	36	31	35	37	35	36

Table 1 (cont.)

Sample	VM-78	VM-79	VM-80	VM-81	VM-82	VM-83	VM-84
GPS coordinates	28° 34.526' S; 28° 23.950' E	28° 34.951' S; 28° 23.965' E	28° 36.518' S; 28° 23.325' E	28° 38.209' S; 28° 21.809' E	28° 40.964' S; 28° 20.597' E	28° 40.078' S; 28° 20.387' E	28° 39.615' S; 28° 21.895' E
Form of Intrusion	Dyke	Dyke	Dyke	Dyke	Dyke	Dyke	Dyke
Major Elements (wt%)							
SiO_2	50.66	50.76	51.28	51.21	50.97	51.39	50.27
TiO_2	0.98	1.17	1.30	0.95	1.07	0.97	1.41
Al_2O_3	15.47	14.82	13.60	14.99	14.74	15.13	13.65
FeO*	9.51	10.93	11.77	9.76	11.07	10.12	12.75
MnO	0.16	0.18	0.20	0.16	0.19	0.18	0.21
MgO	7.39	5.75	5.82	7.19	6.16	6.33	6.25
CaO	10.32	10.23	9.72	10.40	10.49	10.77	10.30
Na_2O	2.30	2.64	2.44	2.18	2.32	2.24	2.43
K_2O	0.52	0.50	0.71	0.57	0.58	0.59	0.43
P_2O_5	0.16	0.18	0.21	0.16	0.16	0.16	0.16
LOI	2.23	2.33	2.51	1.93	1.98	1.96	1.79
H_2O^-	0.23	0.22	0.29	0.39	0.19	0.14	0.26
Total	99.94	99.73	99.86	99.92	99.93	99.96	99.90
Trace Elements (ppm)							
Nb	5.6	7.2	7.7	6.7	6.5	6.9	4.2
Zr	91	115	131	91	103	88	107
Y	25	31	35	26	29	25	30
Sr	215	241	177	201	191	201	182
Rb	8	13	17	11	13	11	10
Zn	81	92	112	85	91	81	103
Cu	93	128	140	90	121	91	184
Ga	16.2	18.5	18.6	16.5	17.8	16.6	20.4
Th	< 2.3	< 2.4	< 2.4	< 2.3	< 2.4	< 2.3	< 2.5
Pb	< 2.6	< 2.7	3.3	< 2.6	2.9	2.9	< 2.8
Ni	118	67	53	109	63	108	80
Ce	21	30	37	23	24	22	21
Nd	12	17	20	14	16	14	16
La	11	12	17	9	10	9	8
Co	45	43	45	46	46	47	51
Cr	359	145	121	339	131	318	147
V	246	285	306	284	290	232	363
Ba	165	280	253	209	222	234	290
Sc	31.6	35.6	38	34	36	32	34

Table 1 (cont.)

Sample	VM-85	VM-86	VM-87	VM-88	VM-89	VM-90	VM-91
GPS coordinates	28° 38.908' S; 28° 18.355' E	28° 38.096' S; 28° 15.478' E	28° 35.067' S; 28° 19.125' E	28° 33.891' S; 28° 26.765' E	Approximately 28° 33.5' S; 28° 28' E	28° 53.279' S; 27° 50.053' E	29° 00.495' S; 27° 30.006' E
Form of Intrusion	Dyke	Dyke	Dyke	Dyke	Dyke	Dyke	Dyke
Major Elements (wt%)							
SiO_2	51.29	51.53	51.40	51.49	50.91	51.96	51.18
TiO_2	1.17	1.08	1.09	1.01	0.94	0.97	1.07
Al_2O_3	14.95	15.17	15.43	15.16	15.13	14.94	14.92
FeO*	11.20	11.10	10.56	10.24	9.85	9.76	11.10
MnO	0.19	0.18	0.18	0.19	0.17	0.17	0.19
MgO	5.83	6.27	5.70	6.13	7.33	7.21	6.09
CaO	10.32	10.66	10.27	10.65	10.38	10.41	10.66
Na_2O	2.42	2.65	2.43	2.32	2.15	2.35	2.36
K_2O	0.68	0.43	0.72	0.61	0.54	0.64	0.43
P_2O_5	0.18	0.15	0.16	0.17	0.16	0.16	0.15
LOI	2.07	1.93	1.86	1.89	2.20	1.77	1.63
H_2O^-	0.22	0.11	0.30	0.19	0.27	0.29	0.20
Total	100.52	101.26	100.09	100.05	100.03	100.62	99.99
Trace Elements (ppm)							
Nb	7	5.3	6.8	7.3	6.2	7.7	7.3
Zr	115	101	108	102	90	85	100
Y	31	28	28	27	25	25	26
Sr	201	235	201	195	203	227	209
Rb	15	4	17	12	10	11	13
Zn	95	90	90	89	84	78	87
Cu	127	121	115	98	88	91	95
Ga	17.9	18.2	17.7	18	17.3	17.8	17.6
Th	< 2.4	< 2.4	< 2.4	< 2.4	< 2.3	< 2.3	< 2.4
Pb	< 2.7	< 2.7	< 2.7	< 2.7	< 2.6	< 2.6	2.7
Ni	65	63	56	64	108	83	65
Ce	33	28	24	24	25	21	23
Nd	17	16	15	13	14	14	14
La	13	11	13	11	8	9	9
Co	44	44	42	43	47	43	44
Cr	126	134	124	289	339	327	283
V	287	284	269	268	242	246	262
Ba	233	587	245	223	177	501	229
Sc	36	36	35	36	34	32	35

Table 1 (cont.)

Sample	VM-92	VM-93	KMK100	KMK101	GRT102	AGG
GPS coordinates	29° 04.274' S; 27° 30.468' E	29° 11.082' S; 27° 28.749' E	Approximately 28° 48' S; 28° 01' E	Approximately 29° 015' S; 28° 47.5' E	Approximately 28° 41' S; 27° 07.5' E	Approximately 28° 52' S; 27° 53.5' E
Form of intrusion	Dyke	Dyke	Dyke	Dyke	Dyke	Sill
Major Elements (wt%)						
SiO_2	50.60	50.86	48.74	51.29	51.32	50.21
TiO_2	1.01	1.03	1.26	0.98	1.18	1.00
Al_2O_3	15.10	14.99	15.25	15.15	14.91	13.64
FeO*	9.64	10.88	10.04	10.33	11.33	10.18
MnO	0.18	0.18	0.16	0.18	0.23	0.17
MgO	6.75	6.26	9.08	6.23	5.63	9.61
CaO	10.50	10.55	9.93	10.53	10.29	9.39
Na_2O	2.34	2.26	2.47	2.46	2.52	2.08
K_2O	0.34	0.61	0.48	0.62	0.70	0.58
P_2O_5	0.17	0.15	0.23	0.16	0.18	0.16
LOI	3.02	1.96	2.04	1.82	2.21	2.11
H_2O^-	0.30	0.21	0.25	0.29	0.06	0.31
Total	99.95	99.93	99.92	100.03	100.56	99.45
Trace Elements (ppm)						
Nb	5.7	5.2	4.3	6.7	6.6	3.7
Zr	95	98.9	84	100	113	101
Y	25	27	23	26	30	26
Sr	293	192	266	194	189	145
Rb	5	15	7	13	14	12
Zn	80	90	87	84	93	88
Cu	101	111	74	98	124	88
Ga	17.3	17.9	18	17.8	18	16.5
Th	2.3	< 2.3	< 2.3	< 2.3	< 2.4	< 2.3
Pb	< 2.6	< 2.7	< 2.6	< 2.6	< 2.7	< 2.6
Ni	103	67	248	66	67	197
Ce	21	25	19	26	28	25
Nd	15	15	13	14	15	14
La	9	10	8	11	10	7
Co	41	46	54	41	45	54
Cr	303	141	456	265	113	587
V	248	280	207	252	266	239
Ba	507	207	225	332	219	182
Sc	30	36	26	32	32	31

6 GEOCHEMICAL COMPARISON OF DOLERITES WITH LAVAS OF THE DRAKENSBERG GROUP

6.1 Introduction

Ten geochemically diverse volcanic units of the basal Barkly East Formation and four geochemically homogenous units of the overlying Lesotho Formation form the bulk of the Drakensberg Group (Figure 4). In addition, the Oxbow dykes, which intrude into the upper portions of the Lesotho Formation are recognised as another geochemically distinct magma type. Using incompatible trace element signatures and incompatible trace element ratios, Marsh *et al.* (1997) have demonstrated that it is possible to discriminate most effectively amongst the more geochemically diverse units (*i.e.* those of the Barkly East Formation and the Oxbow type). However, with lavas of Lesotho Formation compositions, geochemical discrimination diagrams used without additional stratigraphic information may not be able to supply an unambiguous identification, since the magma types are characterised by subtle variation typified by considerable overlap in composition. Nevertheless, based upon geochemical characteristics of the magma types, Marsh *et al.* (1997) have provided a number of geochemical parameters with which to 'fingerprint' samples (*e.g.* lavas and dolerites) of unknown magma type.

The process of characterisation of unknowns is inherently dependant upon adequate initial definition (s) of the magma type. In this respect, from the data of Marsh *et al.* (1997), the compositional variation in the Mafika Lisiu, Maloti, Senqu and Mothae units of the Lesotho Formation is rather well constrained, since their geochemical characteristics are determined from large sample sets (typically > 16 samples). The same could be said for some of the units of the Barkly East Formation (*i.e.* Golden Gate and Wonderkop units). However, for others such as the Roma, Letele and Sani units, the number of samples are few, being only two lavas each for the Roma and Letele units; and three for the Sani unit. Thus, the data of Marsh *et al.* (1997) for the Roma, Golden Gate, Wonderkop and Letele units have been augmented by an additional 10, 2, 21 and 3 samples, respectively obtained from Marsh (1998) and Rehácek (1995).

From Marsh *et al.* (1997), it is apparent that the lavas of the Lesotho Formation are more compositionally homogeneous and define a limited compositional space

around which the magma types of the northern- and southern Barkly East Formations scatter (see Marsh *et al*., 1997, Figure 15, p. 264). This allows for the possibility that any dolerites which did not fall within the field defined by the Lesotho Formation lavas are of the northern Barkly East Formation compositions. Two dolerites plotted consistently in the vicinity of the Wonderkop lavas, three plotted consistently near the Letele lavas; and eight dolerites plotted consistently with the Oxbow type.

6.2 Characterisation of dolerites with geochemical similarities to the northern Barkly East Formation

Figure 15 compares the compositions of dykes with the lavas from the northern Barkly East Formation. The four interelement geochemical plots illustrate the diversity in composition between the Wonderkop and Golden Gate magma types; and the similarities amongst those of the Sani, Roma and Letele magma types. From Figure 15, three dolerites (VM-57, VM-58 and VM-72) are classified as having a compositional affinity to the Letele type on the basis of moderate P/Zr, Zr/Nb and Zr/Y, despite having slightly lower Ti/Zr; and higher MgO relative to the lavas. The identification of these dolerites as Letele type is further reinforced by very similar patterns on a primitive mantle normalised multielement plot (Figure 16A) on which a slight negative slope for Letele lavas (bold polygons) and dolerites with affinity to the Letele magma type is evident. In addition, Letele dolerites are characterised by elevated Rb, Ba, Nb , Nd, Ce and to a lesser extent, La; and are depleted in K relative to the lavas (Figure 16A). The restricted range for Ce, Nd and La in the Letele type is based upon a single lava for which REE concentrations are available.

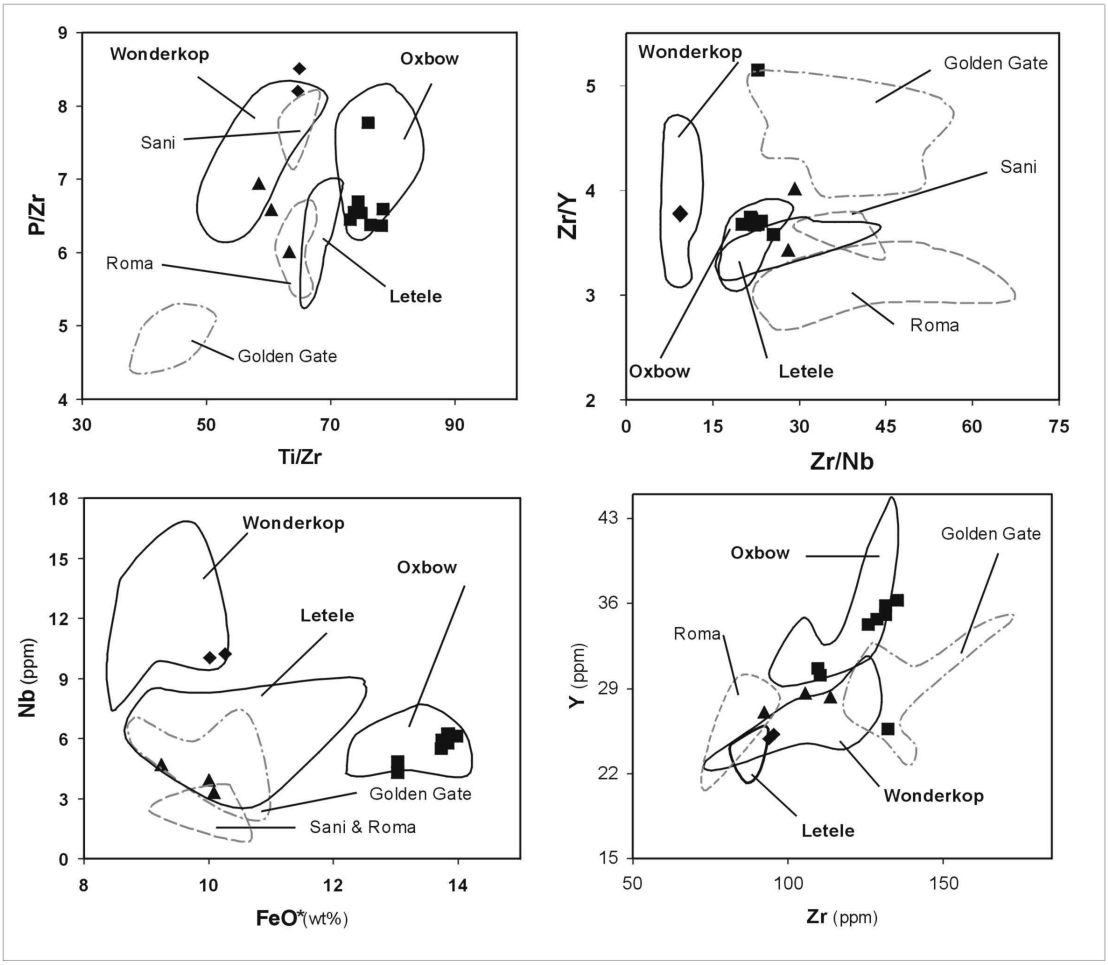

Figure 15. Geochemical discrimination diagrams for the northern Barkly East Formation units (polygons) and dolerites (black, filled symbols) with affinity to the Wonderkop and Letele types. Also shown is the Oxbow type and dolerites with compositional similarities to the Oxbow type identified in this study. Symbols for the respective dyke magma types are as follows: Wonderkop (◆), Letele (▲), Oxbow (■). Basalt lava data sources are given in the caption of Figure 5; some data for the Letele unit is from Rehácek (1995).

Two ratios that are the most useful in distinguishing Wonderkop basalts from other Barkly East Formation basalts are Zr/Nb and Zr/Y (Figure 15). In addition, the majority of Wonderkop basalts (bold polygon) are characterised by enrichments in the highly incompatible LIL trace elements relative to the moderately incompatible HFS trace elements (Figure 16B). The exceptions are aberrant lavas (grey, dashed lines) which are enriched in La (M54); excessively enriched in Ce and to a lesser extent, Nd, Nb and Zr; with excessive depletions in Sr (M115). Two dolerites (VM-70 and VM-73) have the characteristic Zr/Nb and Zr/Y of Wonderkop lavas and are classified as being of Wonderkop type (Figure 15). The dolerites bear similarities to the lavas in the abundances of all elements (Figure 16B), but are slightly enriched in Ba.

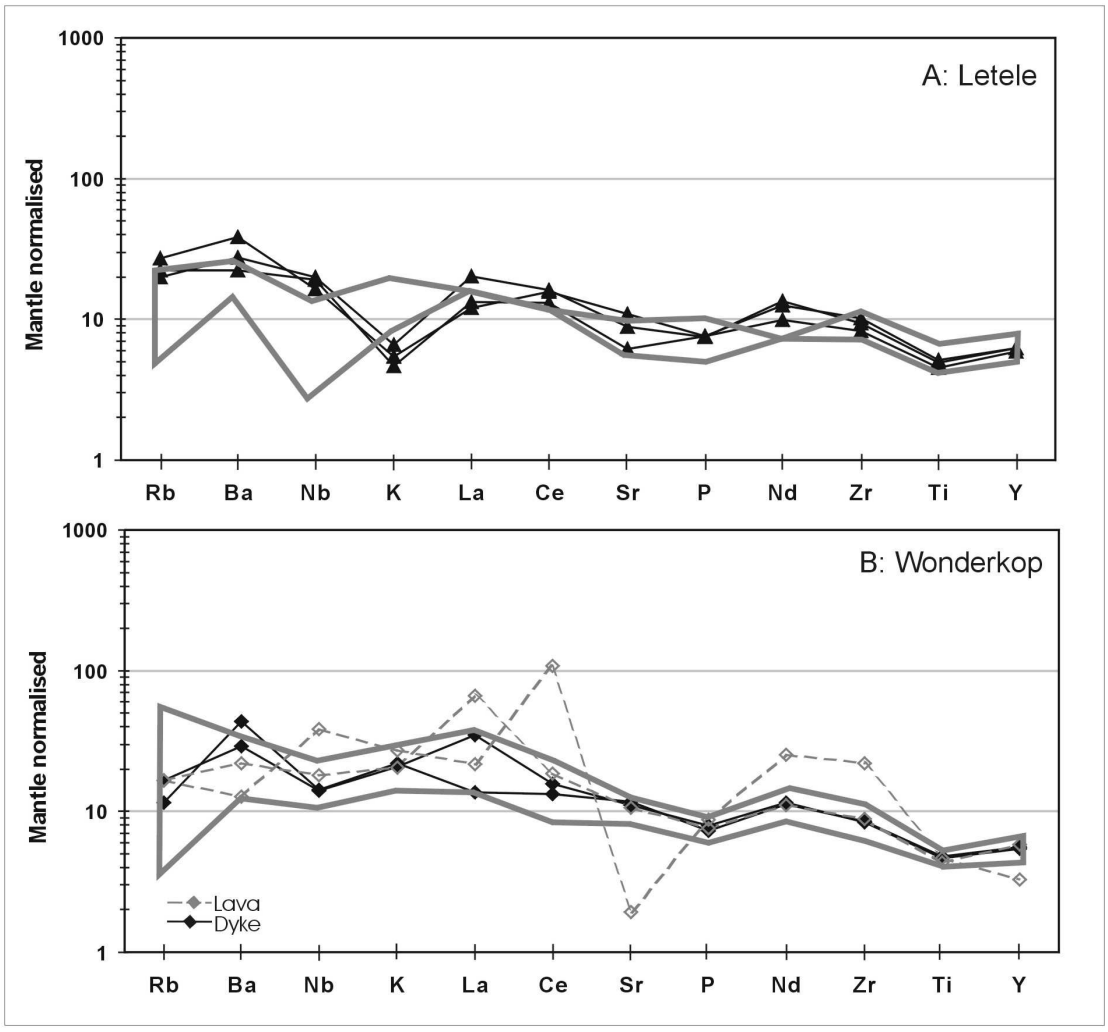

Figure 16. Primitive mantle normalised multi element diagram for the dolerites with compositional affinity to the Wonderkop and Letele types (heavy polygons). Also shown (withunfilled diamonds and dashed lines) are Wonderkop lavas which deviate from the generalised pattern (see text for lava numbers). Data Sources: mantle normalisation values from Sun and McDonough (1989); basalt lava data sources given in the captions of Figures 5 and 17.

6.3 Geochemical characterisation of dolerites with compositional similarities to the Oxbow type

The more homogeneous compositions of the Lesotho Formation types make the empirical approach used for the Barkly East Formation less reliable. The exception is the Oxbow type, which is geochemically quite distinctive as previously discussed. In addition to its distinct geochemistry (low Mg#; high FeO*, Ti/Zr and Zr/Nb), the Oxbow type is typified by a restricted compositional range (Figures 15 and 17). The generalised pattern for the Oxbow type is characterised by enrichments of the highly incompatible LIL trace elements relative to the moderately incompatible HFS trace elements.

Figure 15 includes eight dolerites (VM-12, VM-13, VM-17, VM-22, VM-40, VM-41, VM-69 and VM-84) that show geochemical signatures consistent with the evolved Oxbow type. These geochemical features are high TiO_2, FeO*, MgO, Ti/Zr, Zr/Nb and P/Zr. The dolerites show a restricted compositional range for La, Ce, Sr, P, Nd, Zr and Y, but are relatively variable in the abundances of the LIL trace elements (Figure 17). In addition, the dolerites are enriched in Ba relative to that in the lavas. VM-41 is the only dyke which is aberrant to other dolerites and the Oxbow type, in that it shows higher Ba and Sr; and lower Rb and K contents (Figure 17). Despite the elevated Ba contents in the dolerites classified here as Oxbow, the incompatible and other trace elements indicate that the similarities between the Oxbow dolerites and the Oxbow type is valid.

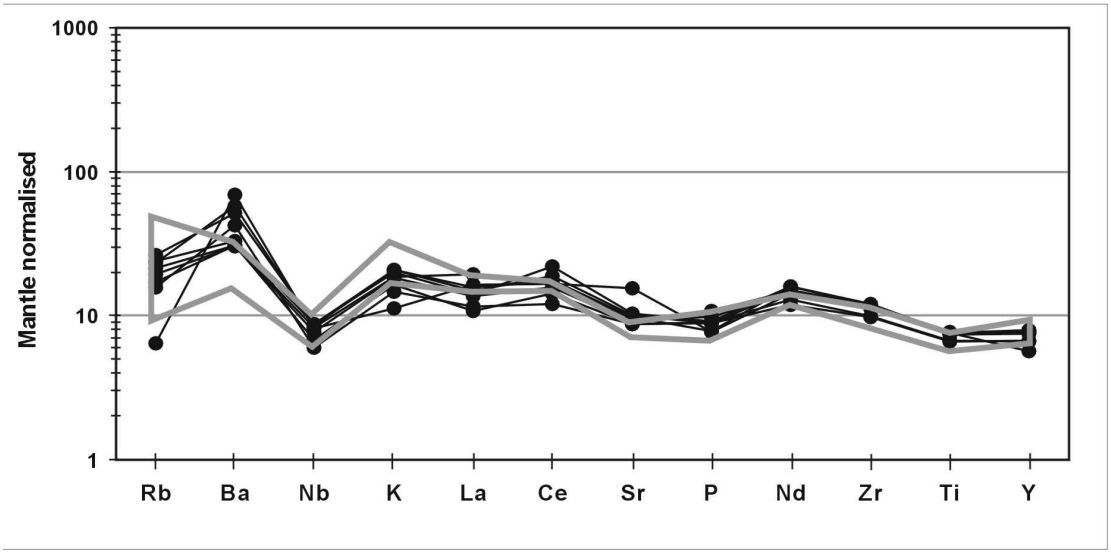

Figure 17. Primitive mantle normalised multielement diagram for the Oxbow type shown in comparison to dolerites with compositional affinity to the Oxbow type. Data sources given in the caption of Figures 5 and 17.

6.4 Distribution and orientation of Letele, Wonderkop and Oxbow dykes

Figure 18 summarises the orientation and distribution of dykes of the Wonderkop, Letele and Oxbow types. Both Letele and Wonderkop dykes are located close to the present basalt outcrop in northern Lesotho. Letele dykes are oriented NW - SE (VM-57), E - W (VM-58) and N - S (VM-72), whereas Wonderkop dykes are oriented N – S (VM-73) and NE – SW (VM-70). In contrast, the majority of Oxbow dykes are longer and occur over a wider area, the majority of which trend NW – SE. In addition, dykes VM-22 and VM-40 are samples from the same dyke and VM-69 and

VM-84 are apparent *en echelon* dyke segments. However, the sample size for each magma type is too small to establish a link between the composition of the dolerite and the orientation of the dyke.

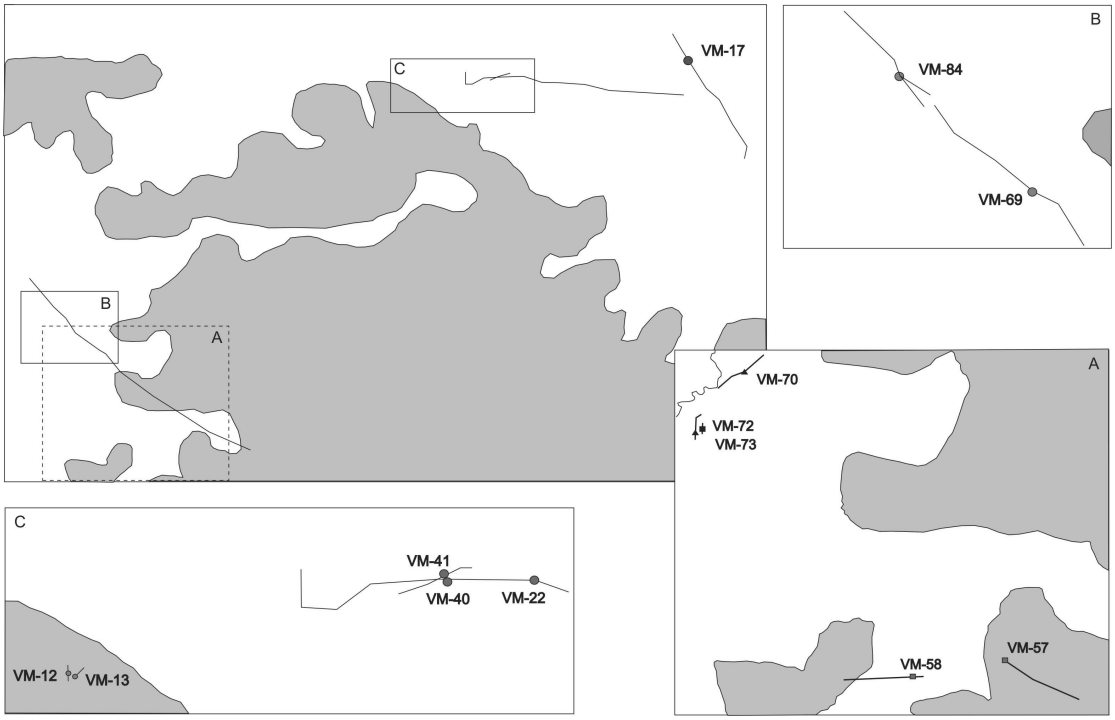

Figure 18. Spatial distribution of dykes with affinity to Letele, Wonderkop and Oxbow types. Points represent sample localities of Letele dykes (■), Wonderkop dykes (▲) and Oxbow dykes (●). Map parameters and data sources are detailed in the caption of Figure 3.

7 DISCRIMINANT FUNCTION ANALYSIS

7.1 Introduction

Multivariate analysis is a statistical technique which examines concurrently the relationships amongst several variables. A type of multivariate analysis is discriminant function analysis (DFA), which is the study of linear representations of relationships among variables that tends to maximise the variance between naturally occurring populations relative to the variance within them. It is a statistical technique that is able to analyse numerous variables concurrently and identify patterns within them provided that the variables show a multivariate normal distribution. Correlations between the variables may be imposed because geological data, specifically geochemical data is represented as parts of a whole - i.e. in percentages or parts per million (Ahrens, 1965).

However, numerous applications of DFA in the Earth sciences in which successful results are produced demonstrate that DFA is a robust technique. The successful application of DFA has been demonstrated in classifying sedimentary samples into known depositional environments (Hart and Ferrell, no date); in discriminating amongst raw and silica standardised values for different arc segments in Luzon in the Philippines (Ragland and Defant, 1983); and one of the most extensively debated applications - discriminating amongst basaltic lavas from different tectonic environments (Pearce and Cann, 1973). In addition, DFA has use in stratigraphical classification - for example, Bowen *et al*. (1986) have successfully used DFA to test the validity of their volcanic stratigraphy of the Witwatersrand triad; and with some success, Mahoney *et al*. (2000) and Seth *et al*. (2004) have used DFA to discriminate amongst numerous Formations of the Deccan Traps in India.

Furthermore, DFA has been successfully used to discriminate amongst numerous subsets of geochemical data of Karoo igneous rocks. In this respect, Duncan *et al*. (1984b) have used DFA to compare (a) basaltic and silicic rocks in different areas (*e.g.* northern Lebombo and Central area low-Ti rocks), (b) compositional differences within a Formation (*e.g.* Letaba Formation in different geographical areas); and (c) compositional differences amongst the basaltic lava units of the Barkly East Formation.

The current chapter deals with determining the provenance of dykes with compositional similarities to the units of the Lesotho Formation. As demonstrated in Chapter 4, the geochemical differences amongst the units of the Lesotho Formation are slight; and interelement and incompatible trace element ratio plots are ineffective in classifying dykes, for which there is no additional stratigraphic information. Forward stepwise discriminant function analysis (FS-DFA) is chosen to facilitate the classification of dykes with compositional similarities to the units of the Lesotho Formation. In particular, FS-DFA is used to discriminate amongst the *a priori* compositional populations (*i.e.* lava units) of the Lesotho Formation established previously by Marsh *et al*. (1997). The results of the lava classification are then extended to the dyke population. FS-DFA has been accessed as part of the *STATISTICA 7* computer package and the following summary has been extensively derived from the electronic help manual (StatSoft, Inc., 2002).

7.2 Forward stepwise discriminant function analysis

7.2.1 Introduction

In this application of FS-DFA, the technique is employed to determine whether the *a priori,* geochemically defined stratigraphic lava units of the Lesotho Formation differ with regard to the mean of a combination of compositional variables (*i.e.* concentration of elements). From these predefined units, FS-DFA formulates a Model by detecting which elements (*e.g.* SiO_2, Zr) discriminate best amongst the Lesotho Formation units. The results of the Model are then extended to dykes with compositional similarities to the units of the Lesotho Formation. FS-DFA is chosen to facilitate the classification of dykes with compositional similarities to the Lesotho Formation because it provides a classification of lavas or dykes into different units, with a better than chance accuracy.

FS-DFA identifies discriminating elements by building a step-by-step Model where each step is representative of the addition of one element. Therefore, the number of steps and elements is exactly equal. At each step, *STATISTICA 7* evaluates and reviews all the elements by calculating their significance with respect to the amount of discrimination afforded. Only those elements that are capable of producing the maximum discrimination between units are retained in the Model. Thus, an

element that has been selected as discriminatory in an earlier step may be excluded in later steps.

FS-DFA computes a number of statistical parameters which are used to determine whether the statistical Model is valid. The Wilks' *Lambda* (which symbolises the statistical significance of the discriminatory power of an element); and the Partial *Lambda* (which describes how well a element contributes to the discrimination), are the most important parameters. The Wilks' *Lambda* ranges from 0.0 (excellent discriminatory power) to 1.0 (no discriminatory power); and similarly, elements with the lowest Partial *Lambdas* possess the greatest discrimination power, whereas those with successively less discriminatory power have successively larger values. From the Partial *Lambda*, an *F*-statistic is calculated for each element at each step. The *F*-statistic, which relates the number of units, lava samples and elements, defines the degree to which any element contributes to the overall discrimination. This parameter is user-defined as both *F*-to-enter and *F*-to-remove values, specified at the beginning of each Model. If the *F*-statistic for an element is greater than the *F*-to-enter, the element is included in the Model whereas if the *F*-statistic is less than the *F*-to-remove, the element is excluded from the Model.

The *p*-level denotes the statistical significance of an element and refers to the probability of error in accepting the result of a Model or the discriminatory power of an element. Acceptable (0.05) and highly acceptable (< 0.01) *p*-levels indicate a < 5 % probability that the relation between elements is by chance. Besides being a measure of the reliability of the contribution of an element to a Model, the *p*-level is also a measure of the reliability of the Model itself. The tolerance, which is also used to evaluate the discriminatory elements, is a measure of the redundancy of an element. The lower the tolerance level, the more redundant an element - for example, an element with a 0.01 tolerance, indicates that it is 99 % redundant.

Two primary modes of FS-DFA are particularly useful in the current application - discrimination and classification. Discrimination is essentially summarised in the form of a graphical non-orthogonal two-dimensional X-Y plot of the lavas; and classification, which indicates to what degree of success the lavas are classified by the Model. In the current application, both modes are equally important and the latter is extended to classify dykes of unknown provenance.

7.2.2 Forward stepwise discriminant function analysis as a discrimination tool – a review of canonical correlation analysis

Discrimination is achieved in the form of a canonical correlation analysis, which expresses the relationship between two or more elements, and is based on the maximal correlation between the discriminant function coefficients. The discriminant function coefficients - *W* in equation (1) - are calculated by FS-DFA for each element in each canonical root. The coefficients represent the partial correlations of the elements with the respective canonical root. The discriminant function scores are calculated for the dataset using equation (1), which is the sum of the product of a raw coefficient and the concentrations for all elements in the Model, together with that of the computed constant for that unit. In this formula, the subscript ***I*** denotes the discriminant (or classification) function; the subscripts ***1***, ***2***, ***M*** denote the ***M*** elements; ***C*** is a constant; W_I is the weight of the discriminant function (or classification function) for an element; ***X*** is the concentration of that element; and ***S*** is the resultant discriminant (or classification) function score. The discriminant functions are used to formulate a two-dimensional scatterplot.

$$S_I = C_I + W_{I1}*X_1 + W_{I2}*X_2 + ... + W_{IM}*X_M \quad (1)$$

In order to understand the nature of each root, the discriminant function coefficients are standardised – *i.e.* they are recalculated to mean of zero and a standard deviation of one and are now the standardised discriminant function coefficients. These standardised coefficients pertain to the standardised elements. In addition to allowing for an understanding of the nature of each canonical root, the standardised discriminant function coefficients indicate the relative contributions of each element to its structure and are used for interpretation because the values are of comparable scales. The factor structure is representative of correlations between the elements in the Model and the discriminant functions and these are also used in the interpretative process.

Eigenvalues are fundamental to canonical analysis and describe the proportion of variates (weighted means of the elements) accounted for by the correlation between the respective canonical variates. Successively lesser eigenvalues are representative of successively lesser correlation. From the resultant correlation coefficients (square root of an eigenvalue), FS-DFA extracts non-orthogonal canonical roots, which each

represent weighted sums of the elements. The number of canonical roots will always be the lesser of either one less than the number of units or equal to the minimum number of elements. The first root will always account for the greatest variability (since it retains the significance of all roots combined); and subsequent roots will always account for successively less variability.

7.2.3 Forward stepwise discriminant function analysis as a classification tool

The Model developed under discrimination can now be used to classify unknown samples (*e.g.* dykes and other lavas) and a summary of which is computed in the form of a classification matrix. The matrix indicates (a) to what degree of success the Model predicts unit membership; and (b) details the number of correctly classified and misclassified samples. The classification uses classification function scores in equation (1) to compute classification functions. For the dataset used to compute the Model, FS-DFA uses these scores and tabulates the results (classification of lavas). Since this process is devoted to classifying samples, the number of units in a Model will determine the number of classification functions for that Model, the results of which are prioritised – the first column shows the best possible classification and that in the third column is the least.

Mahalanobis distances (measure of a distance between a sample and its unit centroid) are an adjunct to the classification process. Proportional to the Mahalanobis distance from a population centroid, posterior probabilities (the probability that a lava belongs to a particular unit) also assist in classification. Every sample should belong to the unit for which it shows the smallest Mahalanobis distance and for which it displays the largest posterior probability.

7.2.4 Extending the discrimination and classification process to unknown samples

The discrimination and classification process can also be extended to samples of unknown provenance (*e.g.* dykes and lavas with compositional affinity to the Lesotho Formation). This latter process of classifying unknowns can only be accomplished once a Model has been finalised. Once this has been accomplished, equation (1) is used to compute classification and discriminant function scores for each unknown.

7.2.5 Summary

In summary, FS-DFA is a useful technique which, when used as a confirmatory procedure, allows for the use of large databases such as that now available for the Drakensberg Group lavas. The technique also forms an independent verification of empirical classification such as the stratigraphical subdivision of the Lesotho Formation lavas by Marsh *et al.* (1997). Most importantly, it can be used to classify a substantial number of dykes from the same population to any one of the specified units. If it is demonstrated that a dyke is compositionally similar to a particular unit, it can be inferred that the dyke may well have been a feeder to the lavas of that unit.

Evidently, the classification and discrimination process will be subject to those considerations outlined in Chapter 6 – *i.e.* that the correct classification of an unknown is highly dependant upon initial definition of the unit to which it is compared. Finally, not negating FS-DFA's effective discrimination and classification potential, a note must be made regarding one of its drawbacks. In its current application, the statistical technique is *only* able to determine to which unit a dyke is most likely to belong- *i.e.* it is only able to classify dykes into *specified* units. Thus, the technique is unable to determine whether a dyke belongs to a unit that has not been recognised or defined, nor is it able to separate or define units which have not been initially identified (*e.g.* an unrecognised magma type or a magma type for which only a few samples are recognised).

7.3 Using DFA to verify the geochemical stratigraphy of the Lesotho Formation of Marsh *et al.* (1997)

7.3.1 Introduction

In the current application of FS-DFA and following the rationale of previous applications (*e.g.* Mahoney *et al.*, 2000; Seth *et al.*, 2004), only the whole rock geochemical analyses are used - that is the unnormalised major and trace element data - excluding data relating to stratigraphic height and other derived values such as Mg# and ratios of elements. Th and Pb are excluded from all Models due to the fact that in many samples, the concentrations of these elements is below the detection limit of XRF techniques. In addition, Ga, Ba and Sc are excluded from all Models because of inconsistencies amongst the lava and dyke data sets. Furthermore, incomplete geochemical data sets for Mafika Lisiu lavas are compensated for by calculating the average Nb and Rb abundances and assigning this average to samples for which such data is unavailable. These samples are BMC-12 and OXB-59 for which the Rb average is calculated as 11.46; and SOM-90 for which the Nb average is calculated as 6.26.

For all the discriminant function Models, a user-specified tolerance value of 0.01 excludes from the Models all variables that are 99% redundant in the discrimination. The *F*-statistic is specified as per Duncan *et al.* (1984) - that is an *F*-to-enter of four and an *F*-to-remove of three. In addition, the *a priori* classification probability is set as being equal for each population since the disproportionate number of lavas in each population may be a product of sampling.

7.3.2 Model 1: the discrimination of the lower Lesotho Formation, the upper Lesotho Formation and the Oxbow dykes including stratigraphic height as a variable

Because the geochemically defined magma types occur at specific stratigraphic intervals in the volcanic sequence, the stratigraphic height [4] of a lava sample assists greatly in determining to which unit it belongs. Such data are non-existent for the dykes. Therefore, to explore whether the exclusion of stratigraphic height fundamentally influences the ability to discriminate between units in the Lesotho Formation, two Models are computed. Models 1 and 2, for which the results are

presented in Tables 2 and 3, respectively. For both of these Models the data was grouped as follows. The lower Lesotho Formation (*i.e.* the Mafika Lisiu as well as the low Zr/Nb Mafika Lisiu subunit - collectively, Mafika Lisiu$_T$) is sufficiently different in terms of Mg#, Ti/Zr and Zr/Y compared to the overlying units of the Lesotho Formation (Marsh *et al.*, 1997, Figure 11, p. 261). It is therefore considered as a single unit. Secondly, since the Maloti unit divides the Lesotho Formation into two parts, the lavas of the upper Lesotho Formation (that is the Maloti, Senqu and Mothae units - collectively, MSM) are considered as a single population. The Oxbow type is included as the third population because it is sufficiently different (lower Mg#, higher TiO_2) to be singled from lavas of the upper portions of the Lesotho Formation (Marsh *et al.*, 1997, Figure 11, p. 261).

Table 2. Summary of stepwise analysis for Model 1 showing the effect of stratigraphic height (Height) as a variable, elements included in the Model and the computed statistical parameters used to evaluate an element's contribution to the discrimination. Stratigraphic height has the highest *F*-to-remove, and the lowest Partial and Wilks' *Lambdas* which signifies its discriminatory power.

N = 473	Wilks' *Lambda*	Partial *Lambda*	*F*-remove	*p*-level	Tolerance	R-square
Height	0.106020	0.627698	136.7146	0.000000	0.769328	0.230673
Cu	0.071673	0.928507	17.7480	0.000000	0.769206	0.230794
Zr	0.094018	0.707826	95.1450	0.000000	0.190828	0.809172
TiO_2	0.106018	0.627708	136.7088	0.000000	0.123963	0.876037
P_2O_5	0.086554	0.768869	69.2909	0.000000	0.181364	0.818636
Cr	0.084542	0.787162	62.3240	0.000000	0.446244	0.553756
Y	0.074117	0.897889	26.2132	0.000000	0.235521	0.764479
SiO_2	0.074341	0.895179	26.9905	0.000000	0.773222	0.226778
Al_2O_3	0.072466	0.918343	20.4956	0.000000	0.668405	0.331595
V	0.071128	0.935618	15.8613	0.000000	0.481043	0.518957

Table 2 is a summary of Model 1 and demonstrates the discriminatory power of stratigraphic height - highest *F*-to-remove at 136.7 and lowest Partial and Wilks' *Lambdas* (0.6 and 0.1, respectively) - which signifies its large contribution to the discrimination. The contribution of stratigraphic height to the discrimination in root 1 (Table 3A) is only fourth in rank, but it is the variable that shows the greatest correlation with the elements in the Model (Table 3B) despite a very low weighting in both roots (Table 3C). However, stratigraphic height is still considered as being discriminatory and its contribution in a Model is demonstrated. In this case, both the

classification and discriminant functions would not be correctly computed since the stratigraphic height for the dykes are not available.

Overall, there is a 98 % success rate in classification of the lava population (Table 4) when stratigraphic height is included as a variable. When compared to Model 2 (Table 6), it is evident that with (Model 1) or without (Model 2) stratigraphic height, the classification success rate is about equal, with numerous common elements (Tables 3 and 5). However, the exclusion of stratigraphic height as a variable (Table 5) results in additional steps whereas inclusion of this variable (Table 3) results in fewer steps - that is, fewer elements in the Model.

Table 3. The coefficients which are used for interpreting the discriminant functions in Model 1. (A) Standardised coefficients for canonical variables which show the relative contribution of each element to the canonical roots. (B) Factor structure matrix which shows the correlations between the elements and the discriminant functions. (C) Raw coefficients for canonical variables showing the weighting structure used to calculate discriminant functions.

Standardised coefficients for canonical variables			**Factor structure matrix**			**Raw coefficients for canonical variables**		
	Root 1	**Root 2**		**Root 1**	**Root 2**		**Root 1**	**Root 2**
Height	-0.57317	-0.58781	**Height**	-0.646341	-0.121266	**Height**	-0.0024	-0.0025
Cu	-0.14761	0.34943	**Cu**	-0.274245	0.441078	**Cu**	-0.0087	0.0207
Zr	-1.35412	0.14637	**Zr**	-0.491650	0.078842	**Zr**	-0.1395	0.0151
TiO_2	0.87385	1.96596	**TiO_2**	-0.328885	0.368691	**TiO_2**	9.0566	20.3754
P_2O_5	0.41020	-1.36025	**P_2O_5**	-0.220987	0.003923	**P_2O_5**	21.1858	-70.2532
Cr	0.74525	-0.16735	**Cr**	0.373839	-0.067339	**Cr**	0.0100	-0.0022
Y	0.38943	-0.70856	**Y**	-0.323037	0.065184	**Y**	0.1468	-0.2671
SiO_2	0.35458	-0.22655	**SiO_2**	0.020411	-0.058063	**SiO_2**	0.4808	-0.3072
Al_2O_3	0.26110	-0.32733	**Al_2O_3**	0.057164	-0.170464	**Al_2O_3**	0.3947	-0.4948
V	-0.40131	0.02906	**V**	-0.314916	0.327755	**V**	-0.0195	0.0014
						Constant	-26.1629	25.3672
Eigenvalue	**4.80804**	**1.58721**				**Eigenvalue**	**4.8080**	**1.5872**
Cumulative Proportion	**0.75181**	**1.00000**				**Cumulative Proportion**	**0.7518**	**1.0000**

Thus, although stratigraphic height is one of the most effective variables for discrimination within the lava sequence, it is excluded from the Models because stratigraphic height is not a variable within the dyke data set. As has been demonstrated, its exclusion produces very little difference in the classification success rate. In the following section, Model 2 is reviewed in order to facilitate the classification of unknown dykes.

Table 4. Classification matrix for Model 1 which indicates a > 98 % overall success rate in classification when discriminating Mafika Lisiu$_T$ from Maloti-Senqu-Mothae from Oxbow. One Mafika Lisiu$_T$ lava sample and six Maloti-Senqu-Mothae (MSM) lava samples are misclassified.

N=473	Number of samples (Marsh *et al*., 1997)	Mafika Lisiu$_T$	MSM	Oxbow	Percent Correct
Mafika Lisiu$_T$	235	**229**	6	0	97.4
MSM	234	1	**233**	0	99.6
Oxbow	4	0	0	**4**	100.0

7.3.3 Model 2: the discrimination of the lower Lesotho Formation, the upper Lesotho Formation and the Oxbow dykes

As discussed above, the broad compositional units in Model 2 are Mafika Lisiu$_T$, Maloti-Senqu-Mothae and Oxbow. Model 2 consists of 18 steps (Table 5), in which the overall discrimination amongst the specified groups is highly significant (Wilks' *Lambda* = 0.09; F = 58.326 and $p < 0.000$). The independent contributions of each element to the overall prediction are highly significant ($p < 0.01$), which indicates that all elements are significant contributors, except Ni, La and Rb ($0.2 > p > 0.5$). The Wilks' *Lambda* indicates that K_2O, FeO* and Sr followed by Nb, Na_2O, V and MgO are statistically significant in the discrimination process. However, the Partial *Lambda* indicates that Zr, TiO_2, Cr and P_2O_5, respectively, contribute the greatest to the discrimination since they possess a Partial *Lambda* of < 0.85.

Despite the fact that the F-to-remove for La, Rb and to a lesser extent, Ni, are less than the user-specified F-to-remove of 3, the Wilks' *Lambda* for these elements indicates that these elements are statistically significant in the discrimination process (Table 5). Results of the classification are given in detail in Appendix A (Tables A and B).

Table 6 summarises the classification of the three lava groups. Of 473 lavas, 465 were classified correctly (along the diagonal) and there are only six lavas which are misclassified by FS-DFA. The results of the discrimination are shown graphically in Figure 19. The Oxbow dykes are clearly different to the lavas of the Lesotho Formation and root 1 provides some discrimination between Mafika Lisiu$_T$ and Maloti-Senqu-Mothae samples. Altogether, even though the lavas of the Lesotho Formation show limited range in composition, FS-DFA demonstrates that it is possible to discriminate lavas of the lower Lesotho Formation from those of the upper Lesotho Formation with an overall success rate > 98 %.

Table 5. Summary of stepwise analysis for Model 2 showing the elements included in the Model and the computed statistical parameters used to evaluate an element's contribution to the discrimination. All elements except Ni, La and Rb ($0.2 > p > 0.5$) are significant contributors to the discrimination.

N = 473	Step	Wilks' *Lambda*	Partial *Lambda*	*F*-remove	*p*-level	Tolerance	R-square
Zr	1	0.132814	0.684091	104.5963	0.000000	0.163327	0.836673
TiO_2	2	0.128428	0.707454	93.6620	0.000000	0.113013	0.886987
P_2O_5	3	0.107434	0.845700	41.3254	0.000000	0.141400	0.858600
Cr	4	0.116393	0.780602	63.6608	0.000000	0.352396	0.647604
FeO*	5	0.092427	0.982508	4.0324	0.018373	0.519518	0.480482
Y	6	0.098929	0.918408	20.1225	0.000000	0.202862	0.797138
Cu	7	0.096045	0.945985	12.9329	0.000003	0.726770	0.273230
SiO_2	8	0.102231	0.888745	28.3537	0.000139	0.233924	0.766076
V	9	0.094490	0.961551	9.0570	0.000000	0.392831	0.607170
Al_2O_3	10	0.098826	0.919367	19.8653	0.002047	0.169678	0.830322
Nb	11	0.093375	0.973036	6.2767	0.000007	0.408878	0.591122
MgO	12	0.095772	0.948681	12.2526	0.000278	0.04582	0.954178
Na_2O	13	0.094201	0.964497	8.3375	0.031536	0.583879	0.416121
K_2O	14	0.092254	0.984855	3.4831	0.016289	0.369978	0.630022
Sr	15	0.092524	0.981986	4.1549	0.052697	0.733082	0.266918
Ni	16	0.092045	0.987090	2.9624	0.052697	0.110053	0.889947
La	17	0.091786	0.989882	2.3151	0.099920	0.813349	0.186651
Rb	18	0.091447	0.993550	1.4705	0.230906	0.394797	0.605203

Table 6. Classification matrix for Model 2 which indicates a > 98 % overall success rate in classification when discriminating Mafika $Lisiu_T$ from Maloti-Senqu-Mothae from Oxbow. Four each of Mafika $Lisiu_T$ and Maloti-Senqu-Mothae lava samples are misclassified.

N=473	Number of samples (Marsh *et al.*, 1997)	Mafika $Lisiu_T$	MSM	Oxbow	Percent Correct
Mafika $Lisiu_T$	235	**231**	4	0	98.3
MSM	233	4	**229**	0	98.3
Oxbow	4	0	0	**4**	100.0

Table 7. The coefficients which are used for interpreting the discriminant functions in Model 2. (A) Standardised coefficients for canonical variables which show the relative contribution of each element to the canonical roots. (B) Factor structure matrix which shows the correlations between the elements and the discriminant functions.

Standardised coefficients for canonical variables			Factor structure matrix		
	Root 1	**Root 2**		**Root 1**	**Root 2**
Zr	1.42939	0.73264	**Zr**	0.519254	0.148855
TiO_2	-0.53429	-2.11958	**TiO_2**	0.394678	-0.267780
P_2O_5	-0.85493	0.97616	**P_2O_5**	0.229393	0.103886
Cr	-0.86250	-0.19964	**Cr**	-0.395254	-0.104113
FeO*	0.17672	0.12659	**FeO***	0.365560	-0.192806
Y	-0.57395	0.50864	**Y**	0.343808	0.082563
Cu	0.17047	-0.31118	**Cu**	0.347656	-0.379216
SiO_2	-0.76493	0.06704	**SiO_2**	-0.031664	0.055834
V	0.34786	-0.00380	**V**	0.375149	-0.226610
Al_2O_3	-0.75441	0.16850	**Al_2O_3**	-0.081866	0.172082
Nb	-0.15979	-0.29379	**Nb**	0.040101	0.114921
MgO	-1.17501	-0.07917	**MgO**	-0.216094	-0.044096
Na_2O	-0.24462	-0.15377	**Na_2O**	0.052419	-0.070072
K_2O	0.19398	0.14146	**K_2O**	0.080297	0.136213
Sr	0.05156	-0.20670	**Sr**	-0.077430	-0.037512
Ni	0.37171	-0.10290	**Ni**	-0.170661	-0.090458
La	0.00402	0.15388	**La**	0.176178	0.136912
Rb	-0.03923	-0.16959	**Rb**	0.068602	0.034949
Eigenvalue	**4.23023**	**1.10437**			
Cumulative Proportion	**0.79298**	**1.00000**			

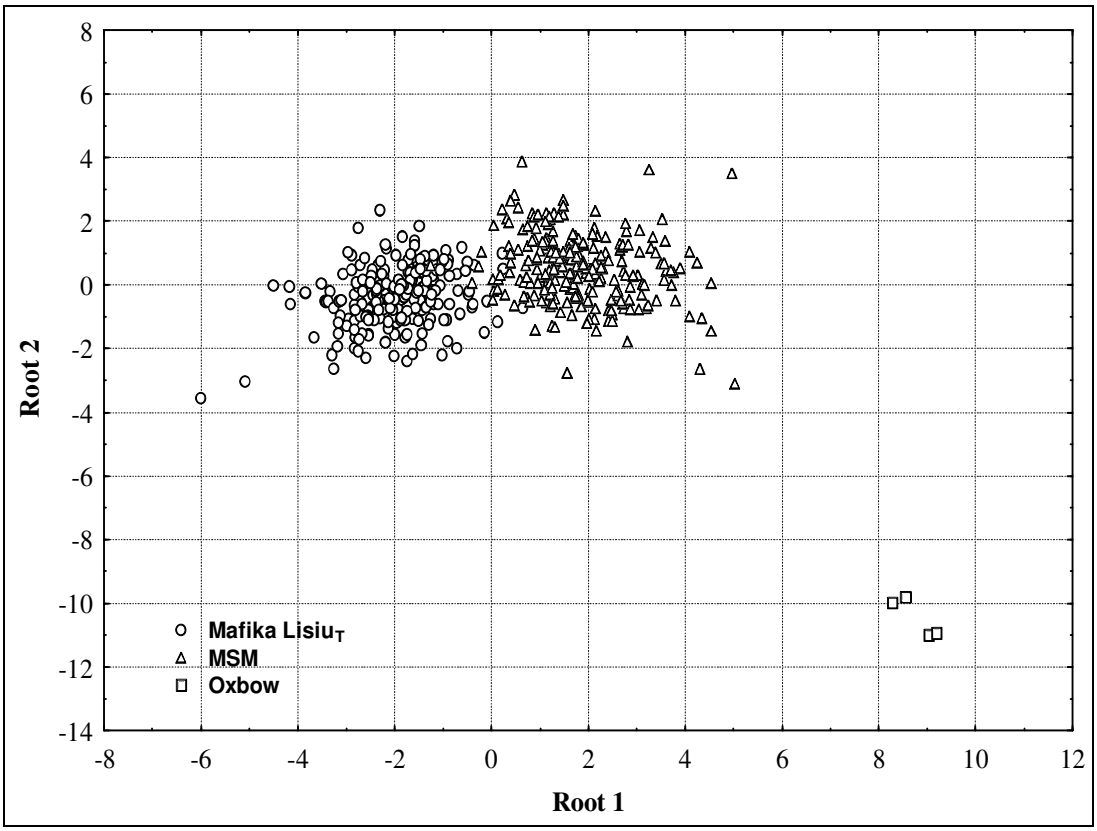

Figure 19. Plot of canonical root 1 vs. root 2 for Model 2 in which the discrimination of Mafika Lisiu$_T$, MSM (Maloti-Senqu-Mothae) and Oxbow is achieved. Root 2 primarily discriminates Oxbow from the other Lesotho Formation lava samples, whereas root 1 separates Mafika Lisiu$_T$ from Maloti-Senqu-Mothae. Formation centroids (not shown) have the following function scores – Oxbow: 8.77236 - 10.4199; Maloti-Senqu-Mothae: - 1.82869, 0.5072; Mafika Lisiu: 1.95413, - 0.3242. Root 1 = 79.7665 + 0.1470Zr – 5.5411TiO_2 – 44.1494P_2O_5 – 0.0116Cr + 0.2604FeO* – 0.2163Y + 0.0101Cu - 1.0374SiO_2 + 0.0169V -1.1400Al_2O_3 - 0.0846Nb - 0.9146MgO – 0.7954Na_2O + 0.9741K_2O + 0.0020Sr + 0.0076Ni + 0.0012La - 0.0067Rb. **Root** 2 = - 2.8458 + 0.0753Zr - 21.9822TiO_2 + 50.4097P_2O_5 – 0.0027Cr + 0.1866FeO* – 0.1917Y - 0.0184Cu + 0.0909SiO_2 – 0.0002V + 0.2546Al_2O_3 - 0.1555Nb - 0.0616MgO - 0.5Na_2O + 0.7103K_2O - 0.0080Sr - 0.0021Ni + 0.0465La - 0.0291Rb.

7.3.4 Extending the discrimination and classification of Model 2 to dykes with compositional affinity to the Lesotho Formation

The Model developed from the lava database can now be applied to the dyke dataset to determine to which geochemically defined lava units the dykes might belong. The classification results are given in Table C (Appendix A) and are summarised in Figure 20. Figure 20 compares the lava and dyke classification in Model 2. The majority of dykes classified as being of Mafika Lisiu$_T$ composition plot within the Mafika Lisiu$_T$ lava field although several of the dykes plot within the overlap of the Mafika Lisiu$_T$ and Maloti-Senqu-Mothae lava fields. There are, however, two dykes (VM-37 and KMK100) with large negative root 2 values which

plot outside the field defined by the lavas. The majority of dykes with compositional similarities to the Maloti-Senqu-Mothae lavas plot outside of the field defined by the lavas. In addition, several Maloti-Senqu-Mothae dykes plot within the overlap between the Mafika Lisiu$_T$ and Maloti-Senqu-Mothae lava fields and numerous dykes plot within the Maloti-Senqu-Mothae lava field.

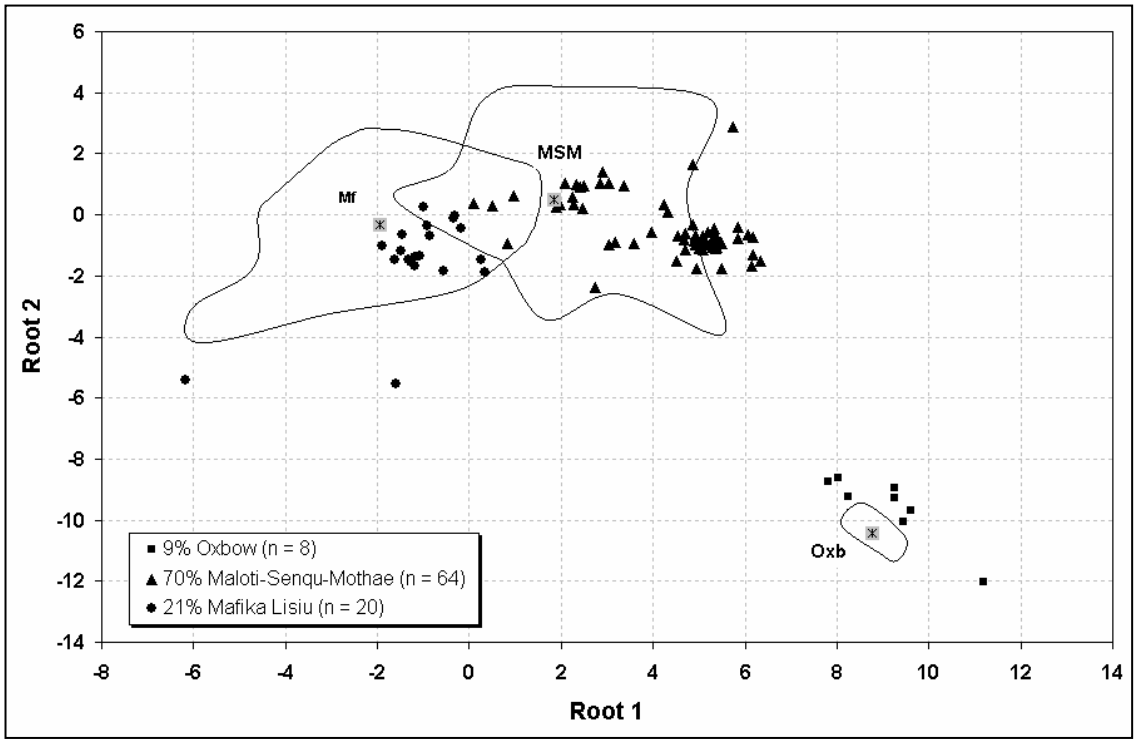

Figure 20. Plot of canonical root 1 vs. root 2 using the discriminant functions and raw coefficients of Model 2 to classify the dyke population. For comparison, the fields for Mafika Lisiu$_T$, Maloti-Senqu-Mothae and Oxbow are shown. Discriminant function equations are given in the caption of Figure 19. Classification function equations are given at the base of Table C (Appendix A). Formation centroids (stars backed with grey squares), correspond to the means in Figure 19 and have the following abbreviations: Oxbow (Oxb); Maloti-Senqu-Mothae (MSM); Mafika Lisiu$_T$ (Mf).

The Oxbow dykes are clearly different to the lavas of the Lesotho Formation despite plotting outside of the field defined by the Oxbow type (Figure 20). However, this is an artefact of adequate definition of the Oxbow magma type of four dolerite samples from the Lesotho remnant which were used to formulate Model 2, despite the fact that an additional five lava samples from the Springbok Flats remnant are used to illustrate the geochemical extent of the Oxbow type in the geochemical discrimination diagrams. However, the contrast of the Oxbow population from the rest of the Lesotho Formation is evident (Figure 20).

In addition, two dykes (VM-32 and VM-35) for which La concentrations are not available are not included in the current classification. Of the 84 dykes and 3 sills, 8 dykes classify as Oxbow; 62 dykes and one sill classify as Maloti-Senqu-Mothae; and 17 dykes and 2 sills classify as Mafika Lisiu$_T$.

7.3.5 Model 3: the discrimination of Mafika Lisiu$_T$, Maloti-Senqu (MS) from Mothae

Marsh *et al.* (1997) have shown that the Mothae lavas are distinctly evolved than the underlying Senqu lavas with lower Mg# and higher TiO_2. In this section, a Model is developed to discriminate between Mafika Lisiu$_T$; Maloti and Senqu (collectively, MS); and Mothae lavas with the Oxbow samples being excluded from the lava dataset. Model 3 consists of 13 steps (Table 8) in which the *F*-to-remove is larger than the user-specified *F*-to-enter of four.

Table 8. Summary of stepwise analysis for Model 3 showing the elements included in the Model and the statistical parameters used to evaluate an element's contribution to the discrimination. All elements are highly statistically significant ($p < 0.01$).

N = 469	Step	Wilks' *Lambda*	Partial *Lambda*	*F*-remove	*p*-level	Tolerance	R-square
Zr	1	0.203931	0.691998	101.0357	0.000000	0.224395	0.775605
P_2O_5	2	0.158209	0.891984	24.4888	0.000000	0.220022	0.779978
Cr	3	0.191863	0.735522	81.6244	0.000000	0.373932	0.626068
FeO*	4	0.145090	0.972635	6.3865	0.001839	0.612819	0.387181
TiO_2	5	0.156855	0.899681	25.3117	0.000000	0.147826	0.852174
SiO_2	6	0.157154	0.897969	25.7926	0.000000	0.244535	0.755465
Al_2O_3	7	0.158725	0.889083	28.3193	0.000000	0.18962	0.810038
V	8	0.147176	0.958853	9.7412	0.000072	0.433823	0.566178
Y	9	0.146334	0.964367	8.3875	0.000265	0.286050	0.713949
Na_2O	10	0.149431	0.944379	13.3695	0.000002	0.593767	0.406233
MgO	11	0.151260	0.932961	16.3113	0.000000	0.047786	0.952214
Ni	12	0.144292	0.978013	5.1032	0.006431	0.120337	0.879663
K_2O	13	0.143610	0.982658	4.0060	0.018853	0.802830	0.197170

Overall, the statistical discrimination is highly significant (Wilks' *Lambda* = 0.141; $F = 58.042$ and $p < 0.000$). All 13 variables in Model 3 are highly statistically significant, which is indicated by the highest *p*-level of 0.01 for K_2O. The Wilks' *Lambda* suggests that K_2O, Ni, FeO*, Y, V and Na_2O are statistically significant in the discrimination. However, the Partial *Lambda* (< 0.89) indicates that Zr, Al_2O_3,

P_2O_5, SiO_2 and TiO_2 contribute the most to the discrimination. The tolerance values of the variables indicate that K_2O, FeO*, Na_2O and V are all < 78 % redundant in the Model and the R-square values of MgO, Ni, TiO_2; followed by Al_2O_3; P_2O_5, Cr, Zr and SiO_2, respectively account for almost all of the variability within Model 3.

Table 9. Classification matrix for Model 3 which indicates a > 95 % overall success rate in classification when discriminating Mafika Lisiu$_T$ from Maloti-Senqu and Mothae.

N=469	Number of Samples (Marsh *et al.*, 1997)	Mafika Lisiu$_T$	MS	Mothae	Percent correct
Mafika Lisiu$_T$	**236**	**232**	4	0	98.3
MS	218	6	**204**	8	93.6
Mothae	15	0	1	**14**	93.3

Detailed classification is presented in Tables D and E in Appendix A. Table 9 summarises the classification of 469 lava samples which have an overall success rate > 95 % with samples from all three groups being individually classified to a success rate > 93 %. Figure 21 summarises these results in a plot of the two canonical roots for Model 3. Mothae lavas plot with a large negative root 1 and large positive root 2 in an area that overlaps only slightly with the Maloti-Senqu lavas. As expected from the results of Model 2, the relative positions of the Mafika Lisiu$_T$ and Maloti-Senqu compositional fields are very similar to those shown in Figure 19.

Table 10. The coefficients which are used for interpreting the discriminant functions in Model 3. (A) Standardised coefficients for canonical variables which show the relative contribution of each element to the canonical roots. (B) Factor structure matrix which shows the correlations between the elements and the discriminant functions.

Standardised coefficients for canonical variables			Factor structure matrix		
	Root 1	**Root 2**		**Root 1**	**Root 2**
Zr	-1.21025	-0.830917	**Zr**	-0.599468	0.356062
P_2O_5	0.78032	0.090277	**P_2O_5**	-0.283868	0.435708
Cr	0.90102	0.442101	**Cr**	0.395105	0.095403
FeO*	-0.23463	0.040959	**FeO***	-0.357012	0.417097
TiO_2	0.54369	1.242980	**TiO_2**	-0.398776	0.602310
SiO_2	0.70372	0.263624	**SiO_2**	0.006407	0.203198
Al_2O_3	0.82064	-0.390172	**Al_2O_3**	0.069817	-0.429399
V	-0.27122	-0.354071	**V**	-0.334798	0.220459
Y	0.22029	0.547443	**Y**	-0.417206	0.533577
Na_2O	0.32493	-0.177051	**Na_2O**	-0.036831	0.023618
MgO	1.31558	-0.222126	**MgO**	0.218427	-0.029017
Ni	-0.45606	0.235247	**Ni**	0.179838	0.037495
K_2O	-0.16382	0.015262	**K_2O**	-0.115809	0.155022
Eigenvalue	**4.06152**	**0.400010**			
Cumulative Proportion	**0.91034**	**1.000000**			

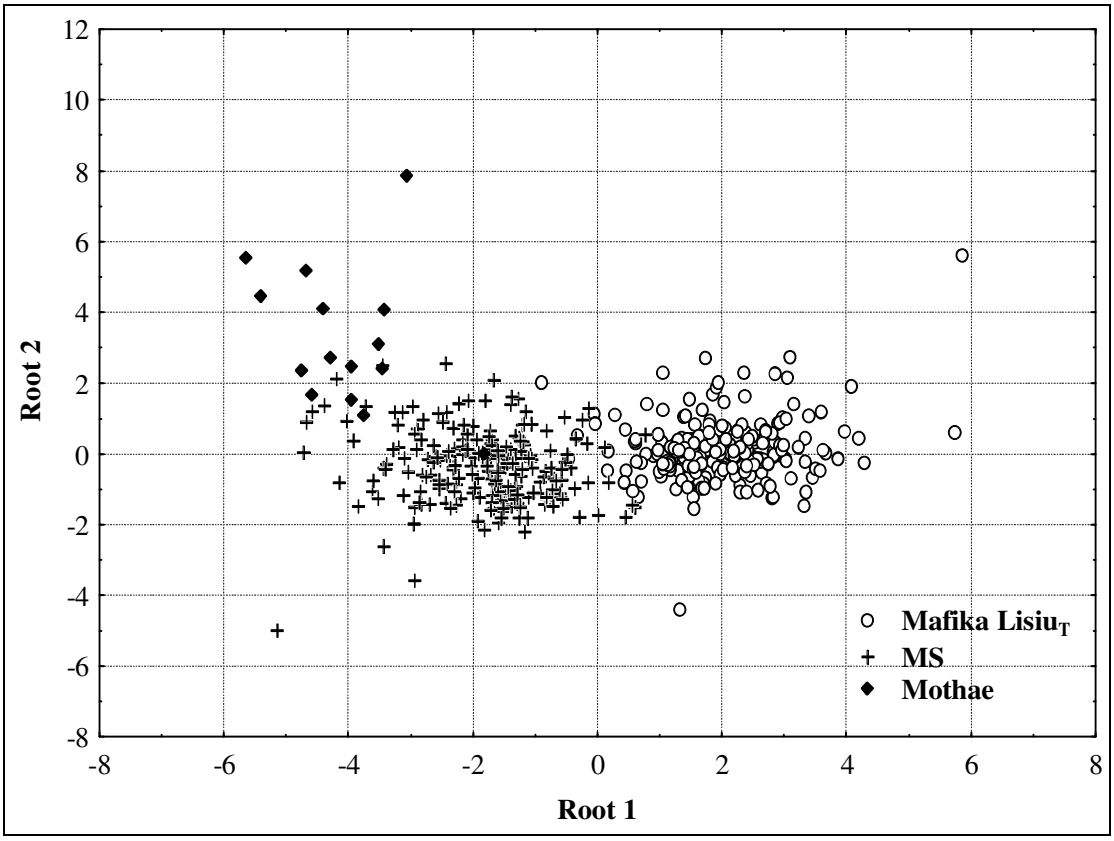

Figure 21. Plot of canonical root 1 vs. root 2 for Model 3 in which the discrimination of Mafika Lisiu$_T$, Maloti-Senqu (MS) and Mothae is achieved. Root 2 primarily discriminates Mothae from the underlying Lesotho Formation units, although discrimination amongst the three specified populations is achieved. Formation centroids (not shown) have the following function scores – Mothae: -4.04035, 3.228278; Maloti-Senqu: - 1.84386, -0.350394; Mafika Lisiu$_T$: 1.96003, 0.118482. Root 1 = - 78.254 - 0.1359Zr + 42.911P_2O_5 + 0.0121Cr – 0.3702FeO* + 6.3456TiO_2 + 0.9593 SiO_2 + 1.2880Al_2O_3 - 0.0136V – 0.0921Y + 1.0539Na_2O + 1.0249MgO - 0.0093Ni - 0.8284K_2O. **Root 2 =** - 17.8669 - 0.0933Zr + 4.9645P_2O_5 + 0.0059Cr + 0.0646 FeO* + 14.5073TiO_2 + 0.3594SiO_2 - 0.6124Al_2O_3 + 0.0177V + 0.2288Y - 0.5742Na_2O - 0.173MgO - 0.0048Ni + 0.0772K_2O.

7.3.6 Extending the discrimination and classification of Model 3 to dykes with compositional affinity to the Lesotho Formation

As with Model 2, Model 3 is now applied to classify the unknown dykes to determine which dykes are of Mothae composition. The classification results are given in Table F (Appendix A) and are summarised in Figure 22 which compares the lava and dyke datasets. In this regard, three dykes (VM-29, VM-81 and KMK101) classified by Model 3 as Maloti-Senqu-Mothae are reclassified by the current Model as Mafika Lisiu$_T$. The dolerites with compositional affinity to the Mafika Lisiu$_T$ type plot in an area that overlaps only slightly with the Maloti-Senqu lavas. Twenty-three dykes are classified as Mafika Lisiu$_T$, the majority of which show small positive discrimination in root 1 and small negative and small to large positive discrimination

in root 2; and are consistent with the field defined by Mafika $Lisiu_T$ lavas. Unchanged and identical to the dyke classification in Model 2, are the two dykes (VM-37 and KMK100) with large positive discrimination for root 2 which plot far beyond the field defined by the Mafika $Lisiu_T$ lavas. These dykes, along with VM-37, all have root 2 values > 2.

Twenty-nine dykes classified as Maloti-Senqu show moderate negative discrimination in root 1 and small positive and negative discrimination in root 2, the majority of which plot within the Maloti-Senqu lava field, along the lower left edge of the Mothae lava field. Eight Maloti-Senqu dykes, which show the lowest root 1 scores, plot outside the field defined by the Maloti-Senqu lavas. The most aberrant of these dolerites are VM-42 and VM-56 which have root 2 values < -2. In addition, VM-21 and VM-52 differ from the remainder of the dykes in that they plot within the compositional field defined by the Mafika $Lisiu_T$ lavas.

Mothae lavas plot with large negative root 1 and large positive root 2 in an area that overlaps only slightly with the Maloti-Senqu lavas (Figure 22). These lavas define a relatively large field, most of which is displaced to moderately high values of root 2. Nevertheless, the 32 Mothae dykes show moderate negative (root 1) and moderate to large positive (root 2) discrimination. Although all of the dykes classified as Mothae plot outside of the field defined by the Mothae lavas and largely within that defined by Maloti-Senqu, the dykes form a trend that parallels the outer left edge of the Mothae lava field. Relatively few Maloti-Senqu and no Mothae dykes plot within the overlap of the Mothae and Maloti-Senqu lava fields. VM-87 is the only dolerite which is aberrant to other Mothae dolerites in that it has a root 2 value < 0. Table 11 shows the resultant dyke classification as per Model 3.

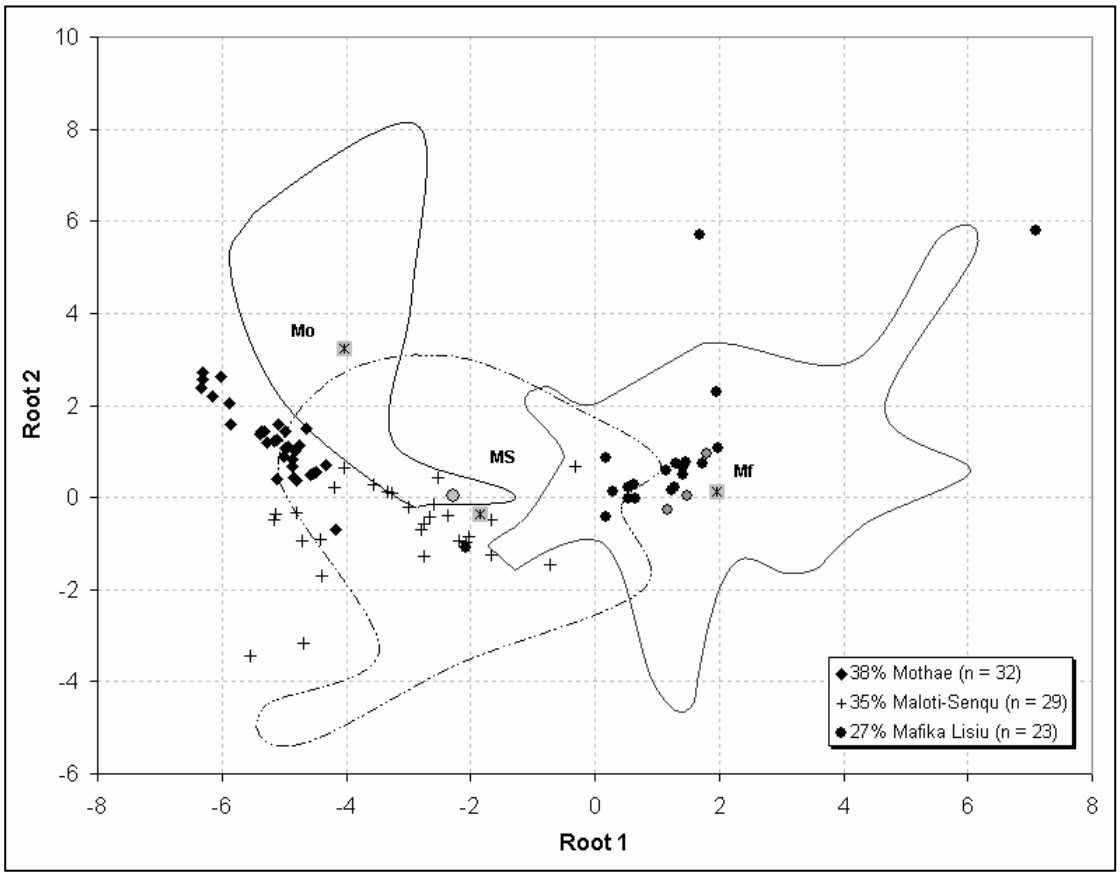

Figure 22. Plot of canonical root 1 vs. root 2 using the discriminant functions and raw coefficients of Model 3 to classify the dyke population. For comparison, the fields for Mafika Lisiu$_T$, Maloti-Senqu and Mothae are shown. Discriminant function equations are detailed in the caption of Figure 21. Classification function equations are given at the base of Table F (Appendix A). Formation centroids (stars backed by grey squares) correspond to the means in Figure 21 and have the following abbreviations: Mothae (Mo); Maloti-Senqu (MS); Mafika Lisiu$_T$ (Mf).

Table 11. Resultant classification of dykes as per Model 3.

Mafika Lisiu$_T$	Maloti-Senqu	Mothae
VM-05	VM-01	VM-02
VM-18	VM-04	VM-03
VM-29	VM-08	VM-06
VM-30	VM-14	VM-07
VM-35	VM-15	VM-09
VM-36	VM-16	VM-10
VM-37	VM-19	VM-11
VM-38	VM-21	VM-20
VM-39	VM-31	VM-23
VM-48	VM-32	VM-24
VM-49	VM-33	VM-25
VM-61	VM-34	VM-26
VM-71	VM-42	VM-27
VM-74	VM-46	VM-28
VM-78	VM-47	VM-43
VM-83	VM-50	VM-44
VM-89	VM-51	VM-45
VM-90	VM-52	VM-53

Table 11 (cont.)

Mafika Lisiu$_T$	Maloti-Senqu	Mothae
VM-92	VM-54	VM-55
KMK100	VM-56	VM-59
KMK101	VM-63	VM-60
AGG	VM-67	VM-62
	VM-75	VM-64
	VM-79	VM-65
	VM-81	VM-66
	VM-82	VM-68
	VM-86	VM-76
	VM-88	VM-77
	VM-91	VM-80
	VM-93	VM-85
		VM-87
		GRT102

7.3.7 Models 4 and 5: the discrimination of Maloti lavas from Senqu lavas

The lavas of the Maloti and Senqu units, respectively overlie the Mafika Lisiu unit. These two units, which are of limited compositional variability (Figure 8), form the majority of the upper Lesotho Formation. Due to the similarity in composition between the Maloti and Senqu types, FS-DFA is not able to provide a distinct discrimination between these two types as demonstrated in Models 4 and 5 (Tables 12 and 13, respectively). Model 4 was developed to discriminate amongst Mafika Lisiu$_T$, Maloti and Senqu, but resulted in excessive misclassification of lava samples (n = 41) (Table 12). In addition to the high misclassification rate, Model 4 produces a relatively low overall success rate in comparison to Models 1 – 3 and is therefore rejected. Model 5 was developed to discriminate amongst the Maloti, Senqu and Mothae types; and was also discarded because the overall success rate was too low in comparison to that of Model 3, despite a similar misclassification rate to that in the latter Model (Table 13).

Table 12. Classification matrix for Model 4 which discriminates Mafika Lisiu$_T$, Maloti and Senqu. The misclassification of 41 lava samples renders this model ineffective in discriminating between the specified populations in spite of the > 91 % success classification rate.

	Number of samples (Marsh *et al.*, 1997)	Mafika Lisiu$_T$	Maloti	Senqu	Percent correct
Mafika Lisiu$_T$	235	**224**	4	7	95.3
Maloti	47	2	**40**	5	85.1
Senqu	172	3	18	**151**	87.8

Table 13. Classification matrix for Model 5 which discriminates amongst the Maloti, Senqu and Mothae types. Although only 18 lava samples are misclassified, the success rate in classification is > 93 % which is less than that for Models 2 and 3.

	Number of samples (Marsh *et al.*, 1997)	Maloti	Senqu	Mothae	Percent Correct
Maloti	47	**40**	7	0	85.1
Senqu	172	4	**165**	3	95.9
Mothae	15	0	2	**13**	86.7

7.4 Summary

FS-DFA was chosen to facilitate the classification of dykes with compositional similarities to the Lesotho Formation. Because the technique requires a number of *a priori*, empirically classified populations, it was considered appropriate to use FS-DFA since the multivariate technique provides a direct comparison of dyke geochemistry with that of the stratigraphic units of Marsh *et al.* (1997). Primarily, two Models have been formed and the results of the classification and discrimination for each are extended to the dykes, for which classification is then possible.

In this respect, FS-DFA has proven to be successful when classifying lavas of Mafika Lisiu$_T$, Mothae and Oxbow types. When used to discriminate the Mafika Lisiu$_T$ from the Oxbow magma type, FS-DFA produced an overall > 98 % success rate in classification and demonstrates that FS-DFA effectively discriminates amongst the *a priori* classified lavas of Marsh *et al.* (1997). The results of Model 2 have allowed for the classification of 19 dykes as Mafika Lisiu type, 8 as Oxbow type and the remaining 63 dykes as Maloti-Senqu-Mothae. In addition, the overall success rate in classification was obtained when FS-DFA was used to discriminate the Maloti-Senqu from the Mothae type in Model 3 is > 95 %. As in Model 2, the results of the lava classification are extended to the dyke population. To a large extent, the dyke classification results of Model 3 are consistent with those from Model 2. The important difference between the two Models are (a) the classification of dykes VM-32 as Maloti-Senqu and VM-35 as Mafika Lisiu$_T$, for which the concentrations of La are unavailable and (b) the reclassification of three Maloti-Senqu-Mothae dykes to Mafika Lisiu$_T$ in Model 3. In total, the number of Mafika Lisiu$_T$ dykes amounts to 23. Sixty-three dykes were initially classified in Model 2 as being of Maloti-Senqu-Mothae composition, three of which are accounted for as discussed above. Thirty-two of these dykes are determined to be representative of Mothae type and 28 are of

Maloti-Senqu composition. The total number of dykes compositionally similar to the Maloti-Senqu type is 29.

FS-DFA is thus an effective technique when used to discriminate amongst units of the Lesotho Formation and produced an overall success rate in classification > 95 % when used to discriminate amongst the Mafika Lisiu$_T$, Mothae and Oxbow types. FS-DFA therefore provides an independent verification of the stratigraphy developed by Marsh *et al*. (1997). In addition, the majority of elements used to develop the model are largely comprised of the incompatible trace elements, similar to those employed by Marsh *et al*. (1997) to empirically define the Lesotho Formation units. Furthermore, FS-DFA provides a means of classifying dykes with compositional similarities to the Lesotho Formation units. Moreover, the current application of the lava dataset in two models with slightly different modification to the manner in which the data is grouped produces similar results for the resultant dyke classification.

8 PETROGRAPHY

8.1 Introduction

The purpose of thin section examination is to determine whether dolerites with compositional affinity to the Drakensberg Group are petrographically distinct in texture and mineralogy. Macroscopically, the fresh dolerites surfaces are light to dark grey in colour and dominantly fine-grained although there are medium-grained dolerites. The dolerites are characterised by plagioclase, pyroxene and in many specimens, minor olivine.

8.2 Dolerites of the Barkly East Formation magma types

8.2.1 Dolerites of the Letele magma type

Table 14 shows the main petrographic characteristics of Letele dolerites. These hypocrystalline dolerites range from aphyric fine-grained to porphyritic medium-grained with subhedral phenocrysts of (a) plagioclase up to 1.5 mm in length (frequently in glomeroporphyritic aggregates), (b) euhedral augite < 2 mm in diameter and (c) elongate euhedral olivine < 1.5 mm in diameter. The groundmass textures range from ophitic to subophitic (Figure 23) intergrowths of plagioclase and pyroxene; and intergranular (with discrete pyroxene grains between the plagioclase grains). Euhedral groundmass plagioclase < 1.5 mm in diameter is randomly oriented in all dolerites; however, there are local arrangements of radiate and crude fan-like plagioclase in VM-72. Groundmass olivines < 0.5 mm in diameter occur as euhedral to subhedral grains, often in clusters. Some olivine grains are host to small euhedral opaque minerals. Alteration products of calcite, chlorite and iddingsite form pseudomorphs after olivine grains, which are included in clinopyroxene. Devitrified glassy areas enclose skeletal and elongate plagioclase (VM-72); and intrafasiculate intergrowths of pyroxene within plagioclase (VM-58).

Table 14. Petrographic characteristics of dolerites of the Letele magma type.

	Crystallinity	Grain size	Relationship	Phenocryst phases	Size	Habit	Groundmass Texture
VM-57	hypocrystalline	medium-grained	inequigranular, porphyritic	plagioclase	< 1.5 mm	subhedral	subophitic
				augite	< 2 mm	subhedral	
				olivine	< 1.5 mm	elongate and subhedral	
VM-58	hypocrystalline	fine-grained	inequigranular, porphyritic	olivine	< 0.75 mm	elongate and euhedral	subophitic
VM-72	hypocrystalline	medium-grained	inequigranular, porphyritic	olivine	< 1.5 mm	elongate and euhedral	intersertal
				plagioclase	< 2 mm	subhedral	
				augite	< 2 mm	euhedral	

Groundmass minerals

Minerals	Size	Habit
Plagioclase	Fine-grained: 1 – 0.08 mm Medium-grained: < 1.5 mm	euhedral
Pyroxene	Fine-grained: 0.5 – 0.06 mm Medium-grained: < 1.5 mm	subhedral to anhedral
Olivine	Fine-grained: 0.5 – 0.25 mm Medium-grained: < 1 mm	euhedral to subhedral

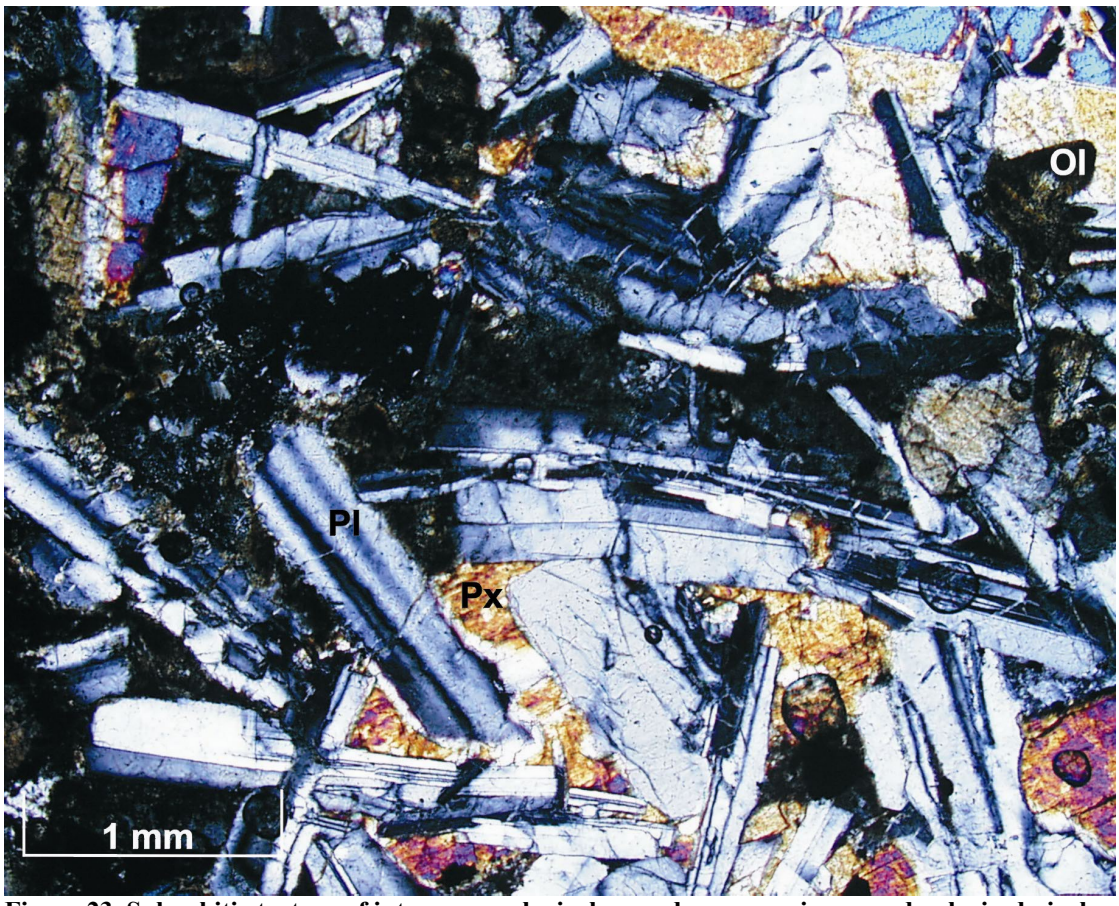

Figure 23. Subophitic texture of intergrown plagioclase and pyroxene in crossed polarised nicols (XPL) (VM-57). Abbreviations: Pl (plagioclase), Px (pyroxene), Ol (olivine).

8.2.2 Dolerites of the Wonderkop magma type

Table 15 details the petrographic characteristics of Wonderkop dolerites, which are equigranular fine- to medium-grained and are characterised by ophitic and subophitic textures of plagioclase and pyroxene intergrowths as shown in Letele dolerites. The dolerites are characterised by pigeonite, augite, plagioclase and olivine. Abundant pigeonite and augite in discrete grains < 1.4 mm in diameter commonly show undulose extinction. Plagioclase is commonly < 0.75 mm in length and is randomly oriented, but is occasionally observed in a crude variolitic texture. Clusters of subhedral olivine < 0.75 mm in diameter are altered to iddingsite. Small opaque minerals range in habit from anhedral blebs to skeletal crystals, especially common in devitrified glassy areas, which also enclose subparallel clinopyroxene microlites.

Table 15. Petrographic characteristics of dolerites of the Wonderkop magma type.

	Crystallinity	Granularity	Relationship	Groundmass texture
VM-70	hypocrystalline	fine-grained	equigranular, aphyric	ophitic
VM-73	holocrystalline	medium-grained	equigranular, aphyric	subophitic

Groundmass minerals

Minerals	Size	Habit
Plagioclase	Fine-grained: 0.75 – 0.06 mm Medium-grained: < 1.5 mm	subhedral to euhedral
Pyroxene	Fine-grained: 1.4 – 0.8 mm Medium-grained: < 1.2 mm	subhedral to anhedral
Olivine	Fine-grained: 0.75 – 0.25 mm Medium-grained: < 1 mm	subhedral

8.3 Dolerites of the Lesotho Formation magma types

8.3.1 Dolerites of the Mafika Lisiu magma type

Dolerites of the Mafika Lisiu magma type are largely hypocrystalline, fine-grained, equigranular and aphyric (Table 16). The phenocrysts in the inequigranular dolerites are (a) 2 to 0.25 mm euhedral to subhedral plagioclase within glomeroporphyritic aggregates; (b) elongate subhedral olivine < 3 mm in length (Figure 24); and (c) euhedral augite phenocrysts < 2 mm in diameter (Figure 25).

Euhedral to subhedral plagioclase (< 0.75 mm in the fine-grained dolerites; < 3 mm in the medium-grained dolerites) and subhedral to euhedral pigeonite and augite in discrete grains (< 0.75 mm in the fine-grained dolerites; < 3.5 mm in the medium-grained dolerites) are present within the groundmass and form ophitic to subophitic intergrowths or intergranular to intersertal textures (Figures 24 and 25). 0.75 – 0.25 mm-sized olivine is scattered within the groundmass and is characterised by alteration as described for dolerites of the Letele and Wonderkop magma types. Euhedral to subhedral opaque oxide minerals are common within the groundmass, whereas skeletal habits are most common within devitrified glassy areas.

Figure 24. Subophitic textures of intergrown plagioclase and pyroxene in VM-05 (A) and AGG (B), respectively. Altered groundmass olivine (A) and elongate subhedral phenocrysts of olivine (B) are also shown. Photomicrographs are in XPL. Abbreviations are given in the caption of Figure 23.

Table 16. Petrographic characteristics of dolerites of the Mafika Lisiu᷑ magma type.

	Crystallinity	Granularity	Relationship	Phenocryst phases	Size	Habit	Groundmass texture
VM-05	hypocrystalline	medium-grained	inequigranular, porphyritic	plagioclase	< 2.5 mm	subhedral to anhedral	subophitic
				olivine	< 3 mm	elongate and subhedral	
VM-18	hypocrystalline	medium-grained	inequigranular, porphyritic	plagioclase	< 3 mm	euhedral to subhedral	ophitic
VM-29	hypocrystalline	fine-grained	equigranular, aphyric				variolitic
VM-30	hypocrystalline	fine-grained	equigranular, aphyric				intergranular
VM-35	hypocrystalline	fine-grained	equigranular, aphyric				subophitic
VM-36	holocrystalline	fine-grained	inequigranular, porphyritic	augite	< 2.5 mm	euhedral	intersertal
				olivine	< 3 mm	elongate and subhedral	
VM-37	hypocrystalline	fine-grained	equigranular, aphyric				subophitic
VM-38	hypocrystalline	medium-grained	equigranular, aphyric				ophitic
VM-39	hypocrystalline	fine-grained	equigranular, aphyric				subophitic
VM-48	holocrystalline	medium-grained	equigranular, aphyric				ophitic
VM-49	holocrystalline	medium-grained	equigranular, aphyric				ophitic
VM-61	holocrystalline	fine-grained	inequigranular, porphyritic	augite	< 2 mm	euhedral	subophitic
				olivine	< 3 mm	elongate and subhedral	
VM-71	hypocrystalline	fine-grained	equigranular, aphyric				subophitic
VM-74	hypocrystalline	fine-grained	inequigranular, porphyritic	plagioclase	< 2 mm	subhedral	intergranular
				olivine	< 3 mm	elongate and subhedral	
VM-78	hypocrystalline	fine-grained	inequigranular, porphyritic	olivine	< 3 mm	elongate and subhedral	intergranular
				plagioclase	< 1.5 mm	euhedral to subhedral	
VM-83	hypocrystalline	fine-grained	equigranular, aphyric				subophitic
VM-89	hypocrystalline	fine-grained	equigranular, aphyric				intersertal
VM-90	hypocrystalline	medium-grained	equigranular, aphyric				ophitic
VM-92	hypocrystalline	fine-grained	inequigranular, porphyritic	plagioclase	< 2 mm	euhedral to subhedral	intergranular
KMK100	hypocrystalline	fine-grained	inequigranular, porphyritic	olivine	< 3 mm	elongate and subhedral	ophitic
KMK101	hypocrystalline	fine-grained	inequigranular, porphyritic	olivine plagioclase	< 3 mm < 2 mm	elongate and subhedral euhedral to subhedral	ophitic

Table 16 (cont.)

	Crystallinity	Granularity	Relationship	Phenocryst phases	Size	Habit	Groundmass texture
AGG	hypocrystalline	fine-grained	inequigranular, porphyritic	olivine	< 3 mm	elongate and subhedral	subophitic

Groundmass minerals

	Size	Habit
Olivine	Fine-grained: 0.75 – 0.25 mm Medium-grained: < 3 mm	euhedral to subhedral
Augite and pigeonite	Fine-grained: 0.75 – 0.13 mm Medium-grained: < 3 mm	euhedral to subhedral
Plagioclase	Fine-grained: 0.75 – 0.08 mm Medium-grained: < 3.5 mm	subhedral to euhedral

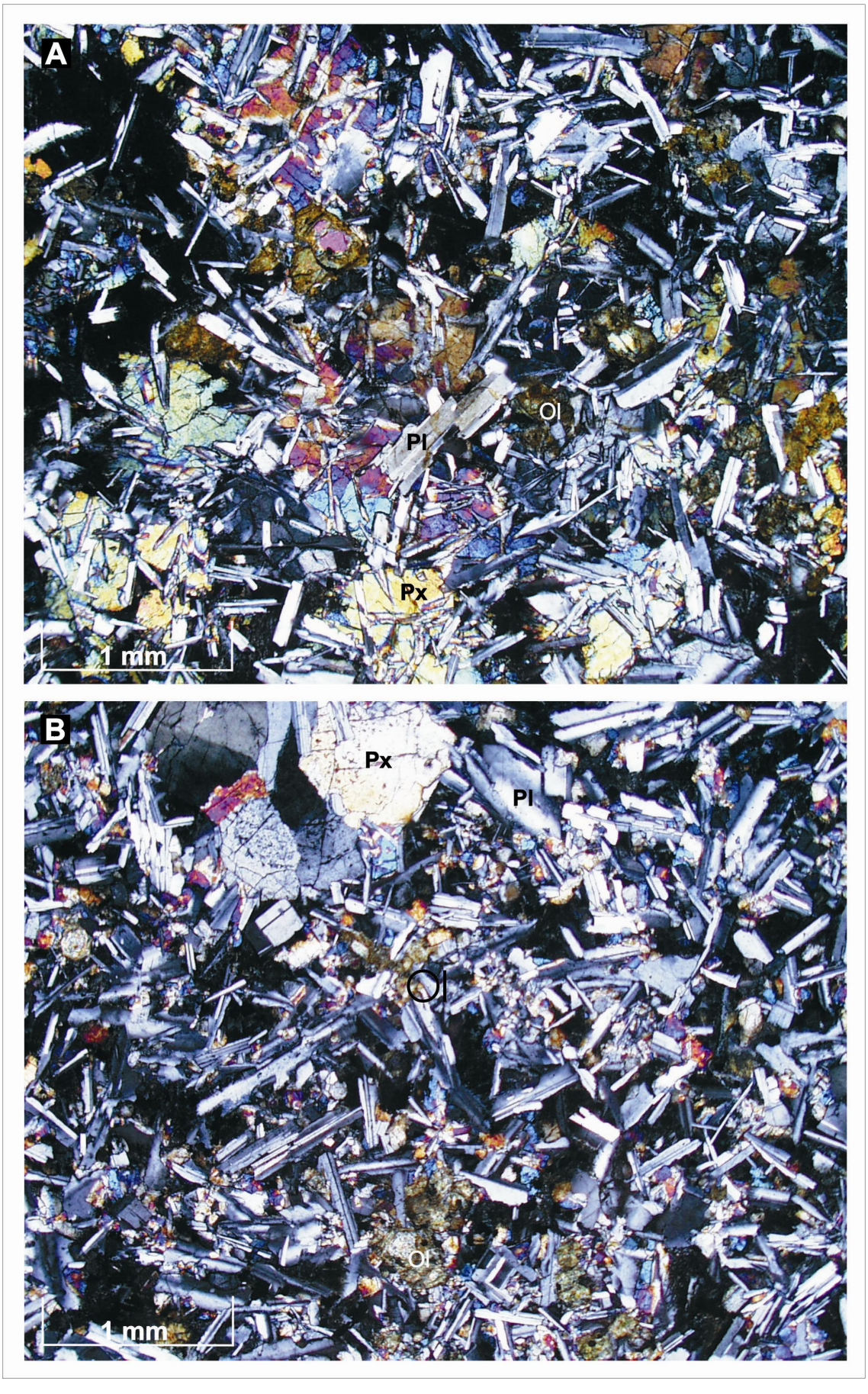

Figure 25. Subophitic integrowth of plagioclase and pyroxene (A); and intersertal texture with glass and minor pyroxene grains between plagioclase (B) in VM-35 and VM-36, respectively. Shown within the intergranular groundmass texture are euhedral pyroxene phenocrysts. Photomicrographs shown in XPL. Abbreviations given in caption of Figure 23.

8.3.2 Dolerites of the Maloti-Senqu magma types

Dolerites of the Maloti and Senqu magma types are mainly plagioclase glomeroporphyritic, with three (VM-16, VM-19 and VM-86) being olivine phyric plagioclase glomeroporphyritic dolerites (Table 17). The plagioclase within the glomeroporphyritic aggregates is euhedral to subhedral in habit; 3.5 to 2 mm in length and is commonly zoned. As shown for Mafika Lisiut dolerites, elongate subhedral olivine phenocrysts up to 1.5 m in length are also scattered in the groundmass in the three above mentioned dolerites.

The groundmass in these dolerites is comprised of euhedral grains of pigeonite and augite; and zoned euhedral to subhedral plagioclase in subophitic intergrowths or form an intergranular texture (Figures 26 and 27). Euhedral to subhedral and altered olivine < 0.5 mm in diameter often occurs in clusters which are scattered within the groundmass. Skeletal, euhedral and dendritic opaque oxide minerals are abundant in some but not all dolerites.

Figure 26. Intergranular texture of discrete pyroxene grains between the plagioclase in VM-88. Photomicrograph is in XPL. Abbreviations given in the caption of Figure 23.

Figure 27. Intergranular texture of pyroxene and plagioclase with minor glass (A); and subophitic intergrowth of plagioclase and pyroxene (B) in VM-34 and VM-91, respectively. Glomeroporphyritic aggregates of plagioclase are shown within the intergranular groundmass of VM-34. Photomicrograph is in XPL. Abbreviations given in the caption of Figure 23.

Table 17. Petrographic characteristics of dolerites of the Maloti-Senqu magma types.

	Crystallinity	Granularity	Relationship	Phenocryst phases	Size	Habit	Groundmass texture
VM-01	holocrystalline	medium-grained	inequigranular, porphyritic	plagioclase	< 2.5 mm	subhedral to euhedral	subophitic
VM-04	hypocrystalline	fine-grained	inequigranular, porphyritic	plagioclase	< 2 mm	euhedral to subhedral	intergranular
VM-08	holocrystalline	medium-grained	inequigranular, porphyritic	plagioclase	< 2.5 mm	euhedral to subhedral	subophitic
VM-14	hypocrystalline	fine-grained	equigranular, aphyric			euhedral to subhedral	intergranular
VM-15	holocrystalline	fine-grained	equigranular, aphyric				intergranular
VM-16	holocrystalline	fine-grained	inequigranular, porphyritic	plagioclase	< 1.5 mm	subhedral to euhedral	intergranular
				olivine	< 1.5 mm	elongate and subhedral	
VM-19	holocrystalline	fine-grained	inequigranular, porphyritic	plagioclase	< 1.5 mm	subhedral to euhedral	intergranular
				olivine	< 1.5 mm	elongate and subhedral	
VM-21	holocrystalline	fine-grained	inequigranular, porphyritic	plagioclase	< 1 mm	euhedral to subhedral	subophitic
VM-31	hypocrystalline	medium-grained	inequigranular, porphyritic	plagioclase	< 2 mm	subhedral to euhedral	subophitic
VM-32	hypocrystalline	fine-grained	equigranular, aphyric				intergranular
VM-33	hypocrystalline	fine-grained	inequigranular, porphyritic	plagioclase	< 1.5 mm	euhedral to subhedral	subophitic
VM-34	hypocrystalline	fine-grained	inequigranular, porphyritic	plagioclase	< 3.5 mm	euhedral to subhedral	intergranular
VM-42	hypocrystalline	fine-grained	equigranular, aphyric				intergranular
VM-46	holocrystalline	fine-grained	inequigranular, porphyritic	plagioclase	< 3 mm	euhedral to subhedral	intergranular
				olivine	< 1.5 mm	elongate and subhedral	
VM-47	holocrystalline	fine-grained	inequigranular, porphyritic	plagioclase		euhedral to subhedral	intergranular
VM-50	hypocrystalline	fine-grained	inequigranular, porphyritic	plagioclase	< 3 mm	euhedral to subhedral	intergranular
VM-51	hypocrystalline	fine-grained	inequigranular, porphyritic	plagioclase	< 2 mm		subophitic
VM-52	hypocrystalline	fine-grained	equigranular, aphyric				Intersertal
VM-54	hypocrystalline	fine-grained	inequigranular, porphyritic	plagioclase	< 2 mm	subhedral to euhedral	subophitic
VM-56	hypocrystalline	medium-grained	inequigranular, porphyritic	plagioclase	< 3 mm	subhedral to euhedral	intergranular
VM-63	holocrystalline	medium-grained	inequigranular, porphyritic	plagioclase	< 2.5 mm	euhedral to subhedral	subophitic
VM-67	hypocrystalline	medium-grained	equigranular, aphyric				ophitic
VM-75	hypocrystalline	fine-grained	inequigranular, porphyritic	plagioclase	< 1.5 mm	subhedral to euhedral	subophitic
VM-79	holocrystalline	medium-grained	inequigranular, porphyritic	plagioclase	< 2 mm	subhedral to euhedral	subophitic

Table 17 (cont.)

	Crystallinity	Granularity	Relationship	Phenocryst phases	Size	Habit	Groundmass texture
VM-81	hypocrystalline	medium-grained	equigranular, aphyric			subhedral to euhedral	ophitic
VM-82	hypocrystalline	fine-grained	inequigranular, porphyritic	plagioclase	< 2 mm	euhedral to subhedral	subophitic
VM-86	hypocrystalline	fine-grained	inequigranular, porphyritic	plagioclase	< 2 mm	euhedral to subhedral	subophitic
				olivine	< 2 mm	elongate and subhedral	
VM-88	hypocrystalline	fine-grained	inequigranular, porphyritic	plagioclase	< 1.5 mm	euhedral to subhedral	intergranular
VM-91	hypocrystalline	fine-grained	inequigranular, porphyritic	plagioclase	< 2.5 mm	euhedral to subhedral	subophitic
VM-93	hypocrystalline	fine-grained	inequigranular, porphyritic	plagioclase	< 2 mm	euhedral to subhedral	intergranular

Groundmass minerals

Minerals	Size	Habit
Plagioclase	Fine-grained: 0.75 – 0.13 mm Medium-grained: < 2 mm	euhedral to subhedral
Olivine	Fine-grained: 0.5 – 0.13 mm Medium-grained: < 1 mm	euhedral to subhedral
Pigeonite and augite	Fine-grained: 0.5 – 0.13 mm Medium-grained: < 2 mm	subhedral to euhedral

8.3.3 Dolerites of the Mothae magma type

Dolerites of the Mothae magma type are holocrystalline to hypocrystalline, the majority of which are plagioclase glomeroporphyritic. In addition, four dolerites (VM-11, VM-20, VM-23 and VM-68) are equigranular aphyric; and (VM-02, VM-07; VM-23 and VM-25) contain phenocrysts of olivine or clinopyroxene. The plagioclase within the glomeroporphyritic aggregates are comprised of zoned euhedral to subhedral laths 2.5 to 0.13 mm in length. The olivine phenocrysts are euhedral to subhedral and are up to 1.5 mm in length. These, and the < 2.5 mm-sized subhedral clinopyroxene phenocrysts are scattered within the groundmass.

The groundmass is comprised of abundant < 1 mm-sized euhedral plagioclase; and subhedral grains of pigeonite and augite < 1 mm in diameter, which are intergrown in subophitic, intergranular or intersertal textures (Figures 28 and 29). 0.75 mm-sized euhedral to subhedral groundmass olivine is wholly altered to iddingsite, with lesser amounts of serpentine, bowlingite and calcite. Opaque oxide minerals are present with skeletal habits within glassy interstitial areas and with subhedral to euhedral habits within the groundmass.

Figure 28. Intersertal texture of discrete pyroxene grains and some devitrified glass between the plagioclase grains in VM-23. Photomicrograph in XPL. Abbreviations given in the caption of Figure 23.

Table 18. Petrographic characteristics of dolerites of the Mothae magma type

	Crystallinity	Granularity	Relationship	Phenocryst phases	Size	Habit	Groundmass texture
VM-02	holocrystalline	fine-grained	inequigranular, porphyritic	olivine	< 1.5 mm	euhedral	intergranular
				plagioclase	< 2 mm	euhedral	
VM-03	hypocrystalline	medium-grained	inequigranular, glomeroporphyritic	plagioclase	< 2 mm	euhedral to subhedral	intergranular
VM-06	hypocrystalline	fine-grained	inequigranular, glomeroporphyritic	plagioclase	< 2 mm	euhedral	subophitic
VM-07	hypocrystalline	medium-grained	inequigranular, porphyritic	olivine	< 2 mm	euhedral	porphyritic
VM-09	holocrystalline	fine-grained	equigranular, aphyric				
VM-10	holocrystalline	fine-grained	inequigranular, glomeroporphyritic	plagioclase	< 2 mm	euhedral to subhedral	subophitic
VM-11	holocrystalline	fine-grained	equigranular, aphyric				intergranular
VM-20	hypocrystalline	fine-grained	equigranular, aphyric				intergranular
VM-23	hypocrystalline	fine-grained	inequigranular, porphyritic	plagioclase	< 0.8 mm	euhedral	intersertal
				augite	< 0.8 mm	euhedral	
				olivine	< 0.4 mm	subhedral	
VM-24	holocrystalline	fine-grained	inequigranular, glomeroporphyritic	plagioclase	< 1.5 mm	euhedral	intergranular
VM-25	hypocrystalline	fine-grained	inequigranular, porphyritic	plagioclase	< 1.7 mm	subhedral to euhedral	subophitic
				augite	< 2 mm	subhedral	
VM-26	hypocrystalline	fine-grained	inequigranular, glomeroporphyritic	plagioclase	< 1.5 mm	euhedral to subhedral	intergranular
VM-27	hypocrystalline	fine-grained	inequigranular, glomeroporphyritic	plagioclase	< 4 mm	euhedral to subhedral	intergranular
VM-28	holocrystalline	fine-grained	inequigranular, glomeroporphyritic	plagioclase	< 2 mm	euhedral to subhedral	intergranular
VM-43	holocrystalline	fine-grained	inequigranular, glomeroporphyritic	plagioclase	< 1.5 mm	euhedral to subhedral	intergranular
VM-44	hypocrystalline	fine-grained	equigranular, aphyric				intergranular
VM-45	hypocrystalline	fine-grained	inequigranular, glomeroporphyritic	plagioclase	< 2 mm	euhedral to subhedral	intergranular
VM-53	hypocrystalline	fine-grained	equigranular, aphyric				intergranular
VM-55	hypocrystalline	fine-grained	inequigranular, glomeroporphyritic	plagioclase	< 2 mm	euhedral to subhedral	intergranular
VM-59	hypocrystalline	fine-grained	inequigranular, glomeroporphyritic	plagioclase	< 4 mm	euhedral to subhedral	intergranular
VM-60	holocrystalline	fine-grained	inequigranular, glomeroporphyritic	plagioclase	< 2 mm	euhedral to subhedral	intergranular
VM-62	holocrystalline	fine-grained	equigranular, aphyric				subophitic
VM-64	hypocrystalline	fine-grained	inequigranular, glomeroporphyritic	plagioclase	< 2 mm	euhedral to subhedral	

Table 18 (cont.)

	Crystallinity	Granularity	Relationship	Phenocryst phases	Size	Habit	Groundmass texture
VM-65	hypocrystalline	fine-grained	equigranular, aphyric				subophitic
VM-66	holocrystalline	fine-grained	inequigranular, glomeroporphyritic	plagioclase	< 2 mm	euhedral to subhedral	intergranular
VM-68	hypocrystalline	medium-grained	equigranular, aphyric				intergranular
VM-76	hypocrystalline	fine-grained	inequigranular, glomeroporphyritic	plagioclase	< 2 mm	euhedral	intergranular
VM-77	hypocrystalline	medium-grained	inequigranular, glomeroporphyritic	plagioclase	< 2 mm	euhedral	subophitic
VM-80	hypocrystalline	fine-grained	inequigranular, glomeroporphyritic	plagioclase	< 2 mm	subhedral	intergranular
VM-85	holocrystalline	medium-grained	inequigranular, glomeroporphyritic	plagioclase	< 3 mm	subhedral	subophitic
VM-87	hypocrystalline	medium-grained	equigranular, aphyric				intergranular
GRT102	hypocrystalline	fine-grained	inequigranular, glomeroporphyritic	plagioclase	< 4 mm	euhedral to subhedral	subophitic

Groundmass minerals

Minerals	Size	Habit
Olivine	Fine-grained: 0.75 – 0.25 mm Medium-grained: < 1 mm	euhedral to subhedral
Plagioclase	Fine-grained: 1 – 0.12 mm Medium-grained: < 3 mm	subhedral to anhedral
Augite and pigeonite	Fine-grained: 1 – 0.13 mm Medium-grained: < 3 mm	euhedral to subhedral

Figure 29. Intersertal texture of plagioclase enclosed in a glassy groundmass in VM-23. Microphenocrysts of plagioclase, pyroxene and altered olivine are scattered within the groundmass. Photomicrograph is in XPL. Abbreviations are given in the caption of Figure 23.

8.3.4 Dolerites of the Oxbow magma type

Oxbow dolerites are holocrystalline to hypocrystalline and aphyric to porphyritic in texture (Table 18). The phenocrysts in these dolerites are olivine and plagioclase (Table 19), which are often in glomeroporphyritic aggregates. The aggregates of plagioclase are monomineralic and consist of subhedral to anhedral grains of plagioclase ranging from 4 to 0.12 mm in length (most commonly from 1 to 0.25 mm). Isolated subhedral olivine phenocrysts scattered within the groundmass can reach up to 2 mm in length.

The groundmass is characterised by subophitic or intergranular textures of randomly oriented plagioclase and abundant augite and pigeonite (Table 19) as shown for dolerites of the Lesotho Formation. The pyroxene may be twinned (e.g. VM-13 and VM-17), although the majority is untwinned. Altered euhedral to subhedral grains of olivine within the groundmass occur in clusters of 3 or 4 grains. Alteration products are serpentine, iddingsite, bowlingite and chlorophaeite. Opaque oxide minerals showing skeletal, cubic anhedral habits

are usually small (< 0.25 mm), in all dolerites but in VM-17, the opaque oxide minerals reach up to 1 mm in diameter. In addition, the hypocrystalline dolerites (Table 19) contain an abundance of devitrified glass within which are enclosed clinopyroxene microlites.

8.4 Summary

Two previous studies have commented on the petrology and petrography of Karoo dolerites. In their study of dolerites from the main Karoo basin, Walker and Poldervaart (1949) noted that 12 distinct dolerite types could be recognised. However, a subsequent study of Karoo dolerites in the Eastern Cape by Robey (1976) demonstrated that the petrographic types of Walker and Poldervaart (1949) do not correlate with geochemistry. This study extends the work of Robey (1976) to dolerites of both the Barkly East and Lesotho Formations. These dolerites are holocrystalline or hypocrystalline and aphyric to dominantly plagioclase glomeroporphyritic. In addition, a minor proportion of dolerites are olivine- and augite-phyric. The dolerites are characterised by a limited variety of textures – these are ophitic, subophitic, intergranular and intersertal which are largely formed by plagioclase and pyroxene; and minor olivine and opaque oxide minerals. All magma types display a range of textural features. The results of this study agree with the findings of Robey (1976) and demonstrates that petrography does not, in general, correlate with geochemistry. In addition, the petrographic types of Walker and Poldervaart (1949) could not be identified within the dolerite suite.

Table 19. Resultant classification of dykes as per Model 3.

	Crystallinity	Granularity	Relationship	Phenocryst phases	Size	Habit	Groundmass texture
VM-12	hypocrystalline	fine-grained	inequigranular, glomeroporphyritic	plagioclase	< 1 mm	euhedral to subhedral	subophitic
VM-13	hypocrystalline	fine-grained	inequigranular, glomeroporphyritic	plagioclase	< 2 mm	subhedral to anhedral	intergranular
VM-17	hypocrystalline	fine-grained	inequigranular, glomeroporphyritic	plagioclase	< 4 mm	subhedral to anhedral	intergranular
VM-22	hypocrystalline	fine-grained	equigranular, aphyric				subophitic
VM-40	hypocrystalline	fine-grained	equigranular, aphyric				subophitic
VM-41	hypocrystalline	fine-grained	Inequigranular, glomeroporphyritic	plagioclase	< 2 mm	euhedral to subhedral	intergranular
VM-69	hypocrystalline	fine-grained	Inequigranular, porphyritic	olivine	< 2 mm	euhedral to subhedral	intergranular
VM-84	hypocrystalline	fine-grained	Inequigranular, porphyritic	olivine	< 2 mm	euhedral to subhedral	subophitic

Groundmass Minerals

Minerals	Size	Habit
Olivine	Fine-grained: 1 – 0.25 mm	euhedral to subhedral
Plagioclase	Fine-grained: 0.75 – 0.25 mm	subhedral
Pigeonite and augite	Fine-grained: 0.5 – 0.33 mm	anhedral to subhedral

9 GEOCHEMICAL COMPARISON OF DOLERITES WITH LAVAS OF THE LESOTHO FORMATION

9.1 Introduction

DFA is a classification scheme that is reasonably different to those usually employed by igneous petrologists and treats the analyses in a highly complex manner. This section deals with the presentation of comparisons using normal variation diagrams of the magma type classification of dolerites (as derived from Model 3) with the compositional fields defined by the lava data (Figures 30 – 35). Because DFA utilised the lava composition to define the classifying parameters, a high degree of correspondence between dolerite compositions and lava unit is expected. However, some samples are characterised by scatter away from the compositional fields defined by the respective lava units. These diagrams also include the Oxbow type. However, because the geochemical characteristics of the Oxbow dolerites have been discussed and the number of Oxbow dykes identified empirically in Chapter 6 coincide exactly with those classified by Model 2, the Oxbow dolerites will not be discussed further in this section and are only shown for comparison.

9.2 The geochemistry of Mafika Lisiu dolerites

The Mafika Lisiu unit and the low Zr/Nb Mafika Lisiu subunit form the lower part of the Lesotho Formation. These basal units directly overlie the Wonderkop unit in northern Lesotho and are comprised of a sequence of basalt flows that are compositionally variable (Figure 31). Although the composition of the Mafika $Lisiu_T$ type is very similar to that of the upper Lesotho Formation, the former is characterised by the highest Mg# and Ti/Zr; and lowest Zr/Y in the entire Lesotho Formation basalt sequence, despite some minor overlap between the Mafika $Lisiu_T$ and Maloti-Senqu types as demonstrated in Figures 31 and 32. The Mafika $Lisiu_T$ type has variable P/Nb, Ti/P, P/Zr, Zr/Nb and Nb/La; low FeO*, TiO_2 and to a lesser extent, P_2O_5 and Zr relative to overlying lavas of the Lesotho Formation (Figures 31 and 32).

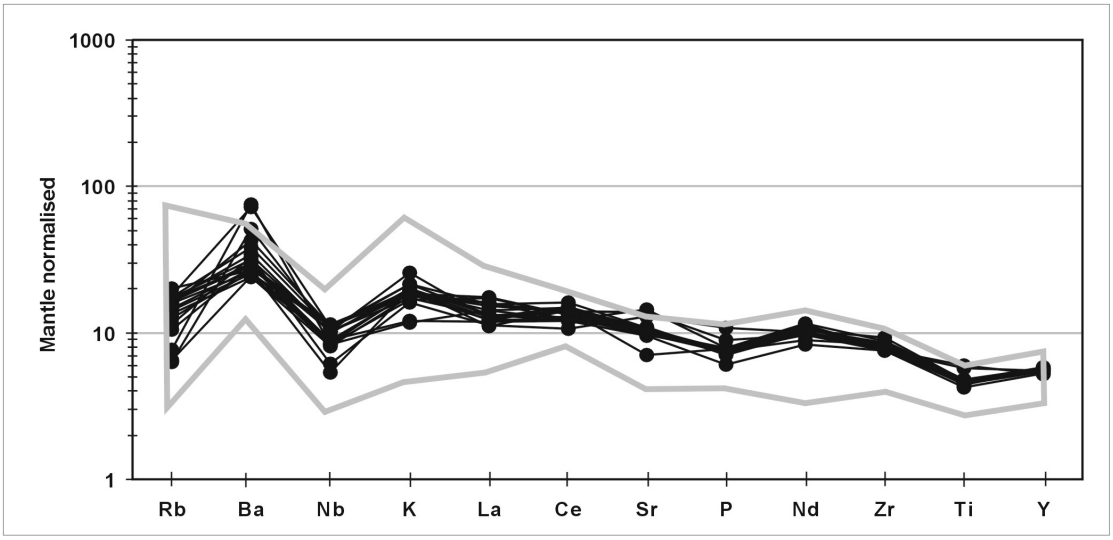

Figure 30. Primitive mantle normalised multi element diagram for the Mafika Lisiu lavas (heavy polygon) relative to the primitive mantle normalised dolerites of Mafika Lisiu affinity. Data sources are given in the caption of Figures 5 and 18.

Figures 31 and 32 summarise some geochemical characteristics of the Mafika Lisiu$_T$ dolerites, the majority of which (filled dots) plot within the overlap between the compositional fields of the Mafika Lisiu$_T$ and Maloti-Senqu lavas. These dolerites show strong compositional affinity to the Mafika Lisiu$_T$ type in having similar Mg#, Zr/Y and Ti/Zr. The dolerites are also characterised by a narrow range in Zr, TiO_2 and FeO*; high Ti/Zr and Mg#; low Zr/Nb and P/Z; and moderate Zr/Y (Figures 31 and 32).

There are four intrusions (dots with grey fill) - VM-29, VM-37, KMK100 and AGG - which are distinctly different to other Mafika Lisiu$_T$ dolerites (Figures 31 and 32). KMK100 is characterised by high TiO_2, Zr/Y, P/Zr and P/Nb but is similar to AGG with high MgO, Ni, Co, Cr, FeO*, Zr/Nb, Zr/Y, P/Nb and to a lesser extent, P_2O_5; and low Zr, Y and Cu. These geochemical characteristics are broadly consistent with up to 3 mm olivine phenocryst accumulation in both dolerites. VM-37 exhibits high P_2O_5 and TiO_2, P/Zr and P/Nb; and low Mg#, Zr/Y and Zr/Nb, relative to other Mafika Lisiu$_T$ dolerites. High TiO_2 and to a lesser extent, Cr and V contents are consistent with the abundance of opaque oxide minerals in VM-37. Elevated abundances of incompatible trace elements (such as Zr, TiO_2, Y, P_2O_5 and Sr) and moderate Ce, Nd, La coupled with low MgO and FeO* suggest that VM-29 is an evolved dolerite with affinity to the Mafika Lisiu$_T$ type. VM-29 is also enriched in CaO, TiO_2, P_2O_5, MnO, V and Cr; and displays low Mg#, FeO*, Zr and Ti/P. The

elevated CaO; and TiO_2, MnO, V and Cr abundances are respectively consistent with the extensive calcite replacement and abundance of opaque oxide minerals in this dolerite.

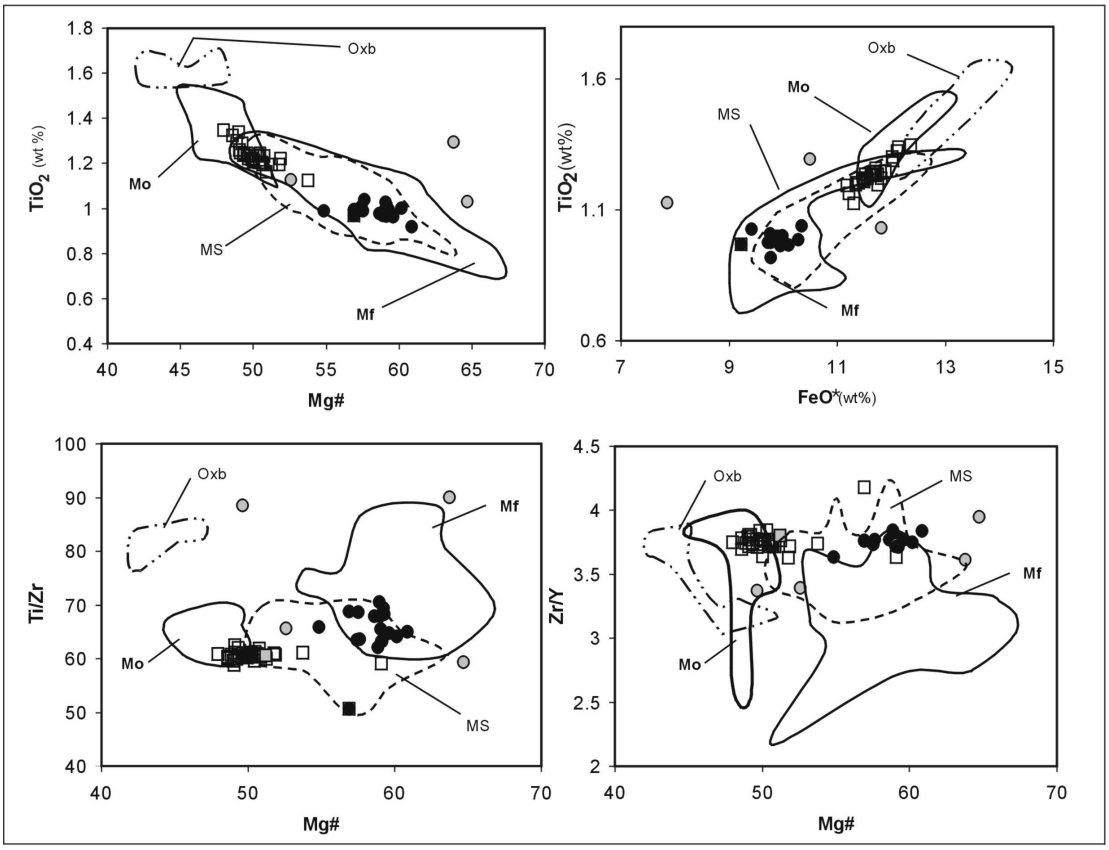

Figure 31. Geochemical discrimination diagrams which show Mafika Lisiu$_T$ (dots) and Mothae dolerites (squares) relative to the respective magma types as defined by the lava samples. Labelled polygons represent the extent of the Mafika Lisiu$_T$ (Mf), Maloti or Senqu (MS), Mothae (Mo) and Oxbow (Oxb) compositional fields. Grey fill of respective dolerites show compositionally variable dolerites whereas black fill for Mafika Lisiu$_T$ and open squares for Maloti dolerites show dolerites with restricted compositional variability. Basalt lava data sources are detailed in the caption of Figure 5.

As noted in Chapter 7, VM-37, KMK100 and AGG have root 2 values that are greater than other Mafika Lisiu$_T$ dolerites – i.e. root 2 > 2 (Figure 20). These differences for VM-29 are, however, not reflected upon the canonical plot in Figure 22. The relative displacements of VM-37 and KMK100 upon the root 2 axis; and the relative displacement of KMK100 upon both root axes are clarified by the standardised coefficients (Table 10A). VM-37, and to a lesser extent, AGG, are similar to other dolerites and the Mafika Lisiu$_T$ lavas in root 1, but differ in root 2 values. The standardised coefficients for root 1 show that Zr and MgO account for most of the variation, whereas in root 2, TiO_2 accounts for the majority of the

variation. VM-29 shows high Zr and low MgO relative to other Mafika Lisiu dolerites, whereas VM-37 has low Zr and MgO. KMK100 has high Zr and MgO; and AGG has low Zr and high MgO. FS-DFA is therefore able to exploit differences in the concentrations of Zr and MgO and this is evidenced by the relative positions of VM-29, VM-37, KMK100 and AGG upon the canonical plot (Figure 22).

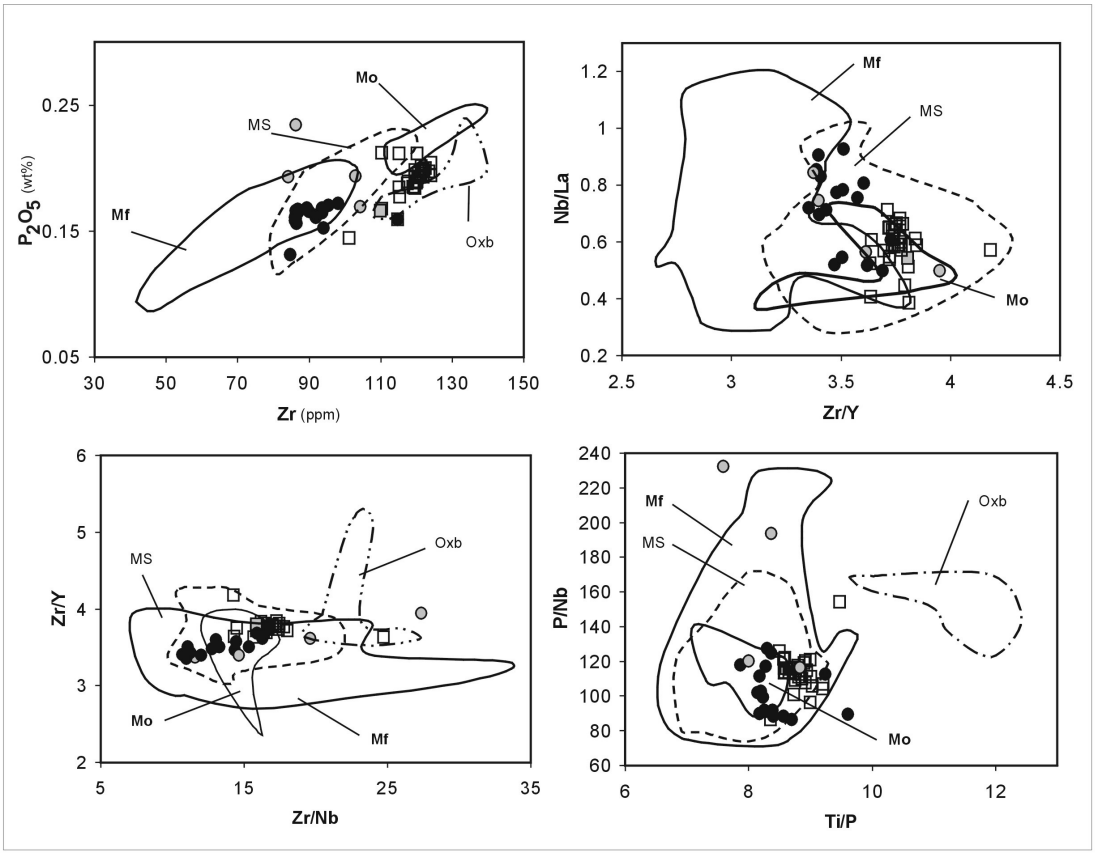

Figure 32. Geochemical discrimination diagrams which show Mafika Lisiu$_T$ (dots) and Mothae dolerites (squares) relative to the respective magma types as defined by the lava samples. Labelled polygons represent the extent of the Mafika Lisiu$_T$ (Mf), Maloti or Senqu (MS), Mothae (Mo) and Oxbow (Oxb) compositional fields. Grey fill of respective dolerites show compositionally variable dolerites, whereas black fill for Mafika Lisiu$_T$ and open squares for Maloti dolerites show dolerites with restricted compositional variability. Basalt lava data sources are detailed in the caption of Figure 5.

9.3 Geochemistry of Maloti-Senqu dolerites

Lavas of the Maloti and Senqu units overlie those of the Mafika Lisiu$_T$ unit and form magma types that are typified to some extent by overlap in FeO*, TiO_2, P_2O_5, P/Zr, Zr/Nb, Nb/La, Zr/Y; and to a lesser extent, Mg# and Ti/Zr when compared with the Mothae and Mafika Lisiu$_T$ magma types. These differences are reflected in the interelement plots shown in Figure 34, which summarises some important

geochemical characteristics of Maloti-Senqu dolerites. The majority of Maloti-Senqu dolerites plot within the field defined by the Maloti-Senqu lavas although there is some overlap with the Mafika Lisiu$_T$ and Mothae types in regard to FeO*, TiO_2, Mg# and Zr/Y (Figure 33).

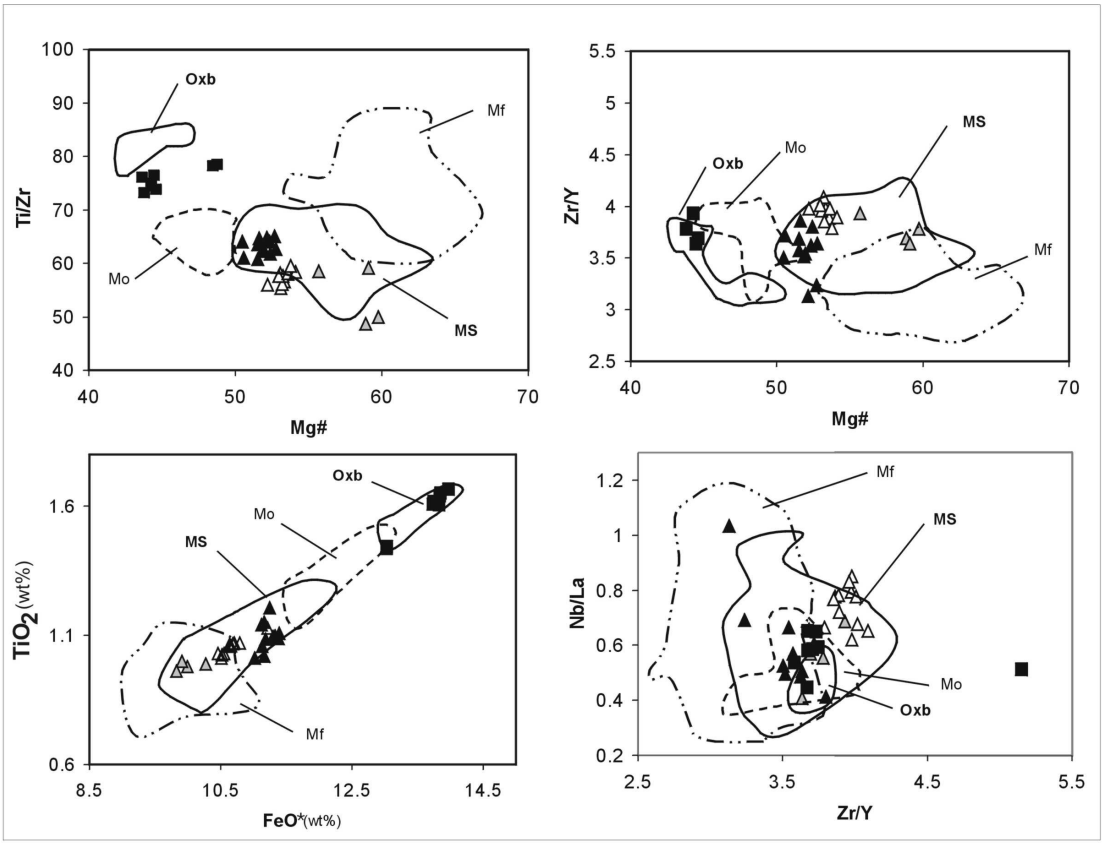

Figure 33. Geochemical discrimination diagrams which show Maloti-Senqu (triangles) and Oxbow dolerites (squares) relative to the respective magma types as defined by the lava samples. Labelled polygons represent the extent of the Mafika Lisiu$_T$ (Mf), Maloti or Senqu (MS), Mothae (Mo) and Oxbow (Oxb) compositional fields. Black fill of respective dolerites show compositionally variable dolerites whereas grey and no fill for Maloti-Senqu dolerites show those with restricted compositional variability. Basalt lava data sources are detailed in the caption of Figure 5.

Two primary sets of Maloti-Senqu dolerites are recognised – one which clusters at the low Mg# end of the lava field and a smaller group of 4 dolerites (VM-21, VM-42, VM-52 and VM-56) that scatter to higher Mg# (Figure 33). The high Mg#, compositionally variable Maloti-Senqu dolerites (triangles with black fill) are distinct from other Maloti-Senqu dolerites (triangles with no fill) with relatively lower FeO*, TiO_2, Mg#, despite being similar in Zr/Y and Nb/La (Figure 34). The differences amongst these two sets of Maloti-Senqu dolerites are reflected in the primitive mantle normalised multielement diagrams in Figure 35. The low Mg# dolerites are

characterised by a narrow compositional range of the HFS trace elements relative to the marginally elevated HFS trace element contents in the dolerites with high Mg#.

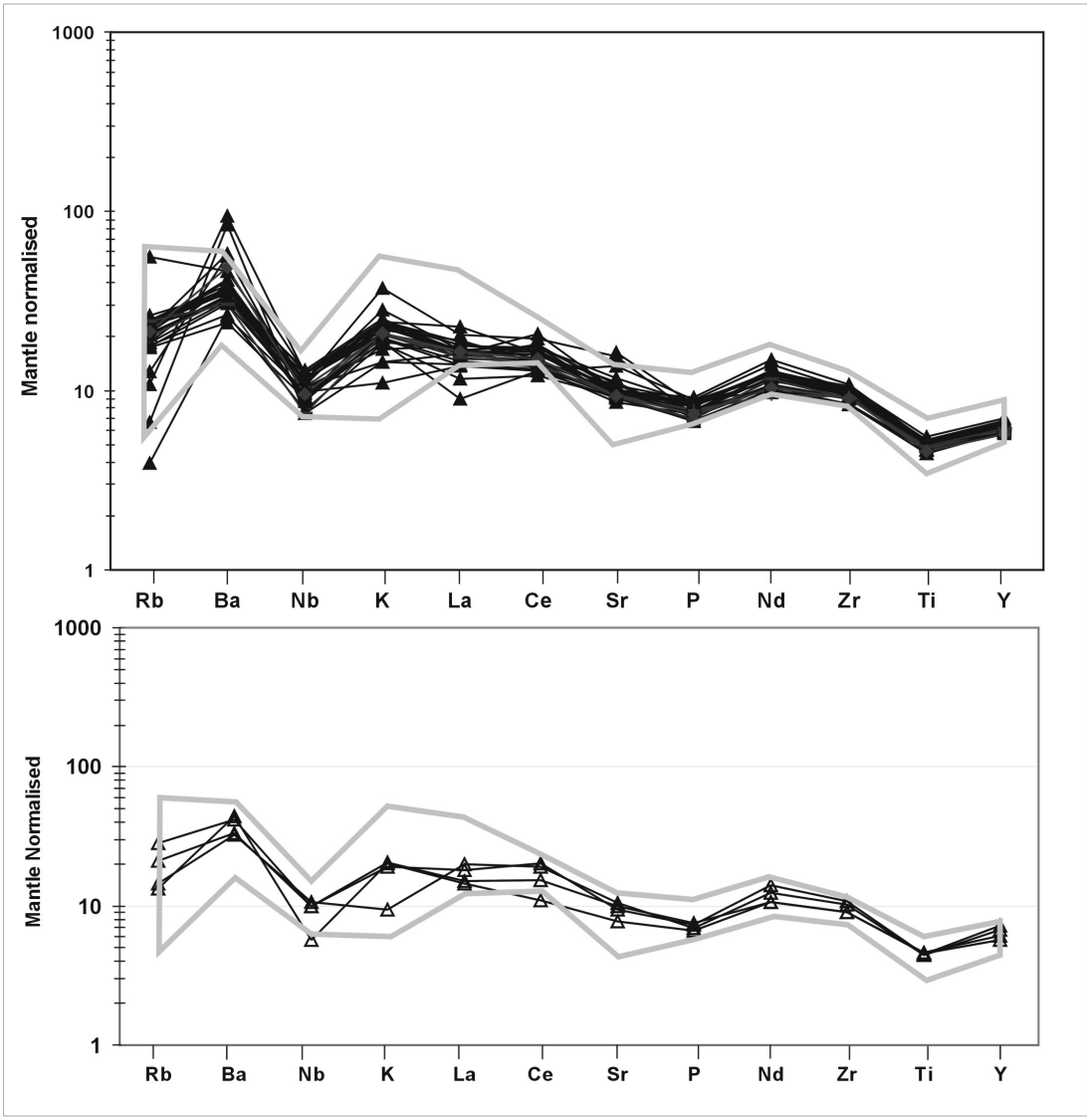

Figure 34. Primitive mantle normalised multi element diagrams for the Maloti-Senqu lavas (heavy grey polygons) relative to the primitive mantle normalised dolerites of Maloti-Senqu affinity. Top multielement pattern shows low Mg# dolerites and the bottom multielement pattern shows high Mg# dolerites. Data sources are detailed in the caption of Figures 5 and 18.

As discussed in Chapter 7, VM-42 and VM-56 are characterised by the lowest root 2 values in Maloti-Senqu dolerites, with root 2 being < - 2. VM-42 shows high Zr, Al_2O_3, V, Y, Na_2O and MgO - all of which are negative in root 2 (Table 10A) and thus control the vertical displacement of the dyke samples. FS-DFA is therefore able to exploit differences in the concentrations of the above mentioned elements and this is evidenced by the fact that VM-42 and VM-56 show large and negative root 2

values. VM-21 and VM-52 have similar root 2 values to other Maloti-Senqu dolerites, but have root 1 values > - 2 and plot within the field defined by the Mafika Lisiu$_T$ lavas (Figure 22). VM-21 has high P_2O_5, FeO*, Al_2O_3 and K_2O - all of which have negative standardised coefficients in root 1, whereas VM-52 shows high Cr, TiO_2, SiO_2 and Ni. However, both VM-21 and VM-42 have low Zr and MgO and it is the latter elements which influences the position of VM-21 and VM-42 on the canonical plot (Figure 22).

9.4 Geochemistry of Mothae dolerites

Lavas of the Mothae type form the uppermost unit in the Lesotho volcanic remnant and are distinctly more evolved relative to all underlying units of the Lesotho Formation. Although the Mothae type bears similarities to the underlying Senqu unit in the abundances of incompatible trace elements, the Mothae type is distinguished from the latter by higher TiO_2 and lower Mg#, as shown in Figure 31. The majority of Mothae dolerites show a narrow range in composition, especially in Ti/Zr, Zr/Nb, P/Zr and Zr/Y and are compared with the field for Mothae lavas in Figures 31 and 32. The overlap is good but the dolerites have marginally higher Ba, Zr/Nb and Ti/P; and marginally lower P/Zr, TiO_2 and P_2O_5 (Figures 31 – 33). One sample (VM-87) plots away from the other samples and exhibits a root 2 value < 0 (Figure 22). VM-87 exhibits lower TiO_2, FeO*, and P_2O_5 than any other Mothae dolerite or lava of the Mothae unit. These differences are magnified by the coefficients used to calculate the discriminant functions. VM-87 has low abundances of the major and trace elements compared to other dolerites, but especially in Zr, V and MgO (Table 10A) which are the negative coefficients that influence the position of VM-87 on the canonical diagram in Figure 22.

The dolerites of the Mothae type depart from the pattern shown by other dolerites of the Lesotho Formation in that the majority of dolerites plot outside of the field defined by the Mothae lavas. These differences are apparent in the (a) canonical plot (Figure 22) and (b) the variation diagrams in Figure 32 and to a lesser extent, Figure 31. The restricted compositional field for the Mothae type is undoubtedly a product of the small sample size (n = 15 in the original lava dataset) although this could also reflect the possible restricted compositional character of the Mothae type. If this is the case, then the classification of these dolerites as being of the Mothae type extends

the Mothae lava field. However, in the canonical plot (Figure 22), the non-orthogonal X-Y compositional space for the Mothae lavas is well defined, the majority of which is removed from the Maloti-Senqu lava field. This suggests that there is a possibility that the dolerites are not an exact match to the Mothae type and may well represent another magma type that is presently unrecognised within the lava suite.

It is apparent that lavas of the Mothae type consistently occur at the top of all sampled sections and is more differentiated than any of the underlying magma types in the Lesotho Formation (higher contents of the incompatible elements and lower Mg#). Despite the fact that a magma composition similar to the Mothae type could be mimicked by evolved fractional crystallisation of the Mafika Lisiu, Maloti or Senqu magma types, Marsh and Mndaweni (1998) have shown that even long dykes (up to 100 km) are compositionally homogeneous. For these reasons, these dolerites are considered as being of Mothae type.

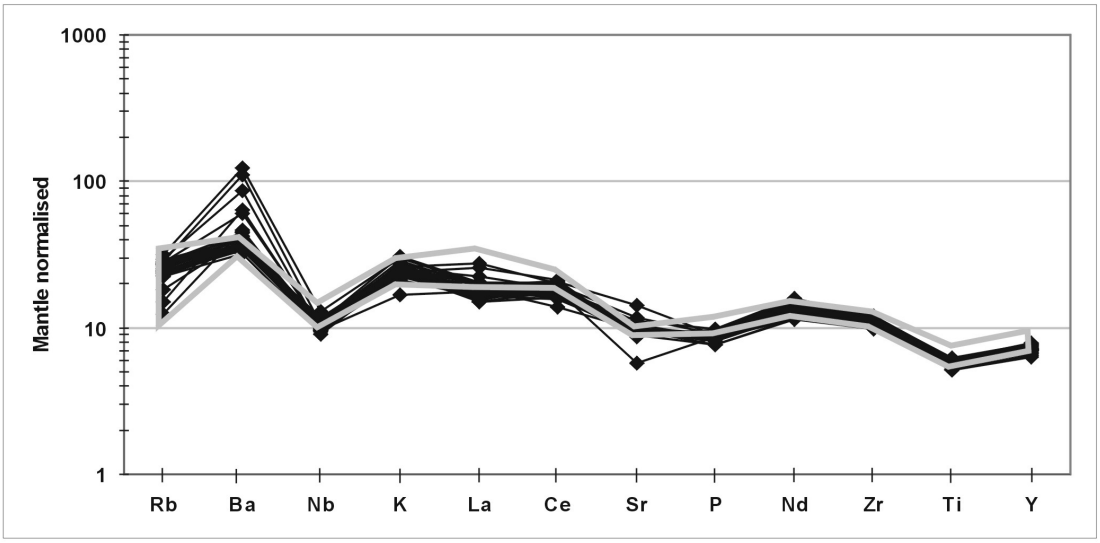

Figure 35. Primitive mantle normalised multi element diagram for the Mothae lavas (heavy grey polygon) relative to the primitive mantle normalised dolerites of Mothae affinity. Also shown (with unfilled diamonds and dashed lines) are number of Mothae lavas which deviate from the generalised pattern (see text). Data sources are detailed in the captions of Figures 5 and 18.

9.5 Spatial location and distribution and orientation of dykes with compositional similarities to the Lesotho Formation

Figures 36 – 38 show the spatial distribution and orientation of dykes of the Lesotho Formation. These dykes are scattered throughout northern Lesotho and the northeastern Free State and show no specific orientation. Mothae dykes are, however, clustered close to the Oxbow section and the Mafika Lisiu pass within which the Mothae unit lavas are located. In addition, the majority of Mothae dykes are short in length and show no specific orientation.

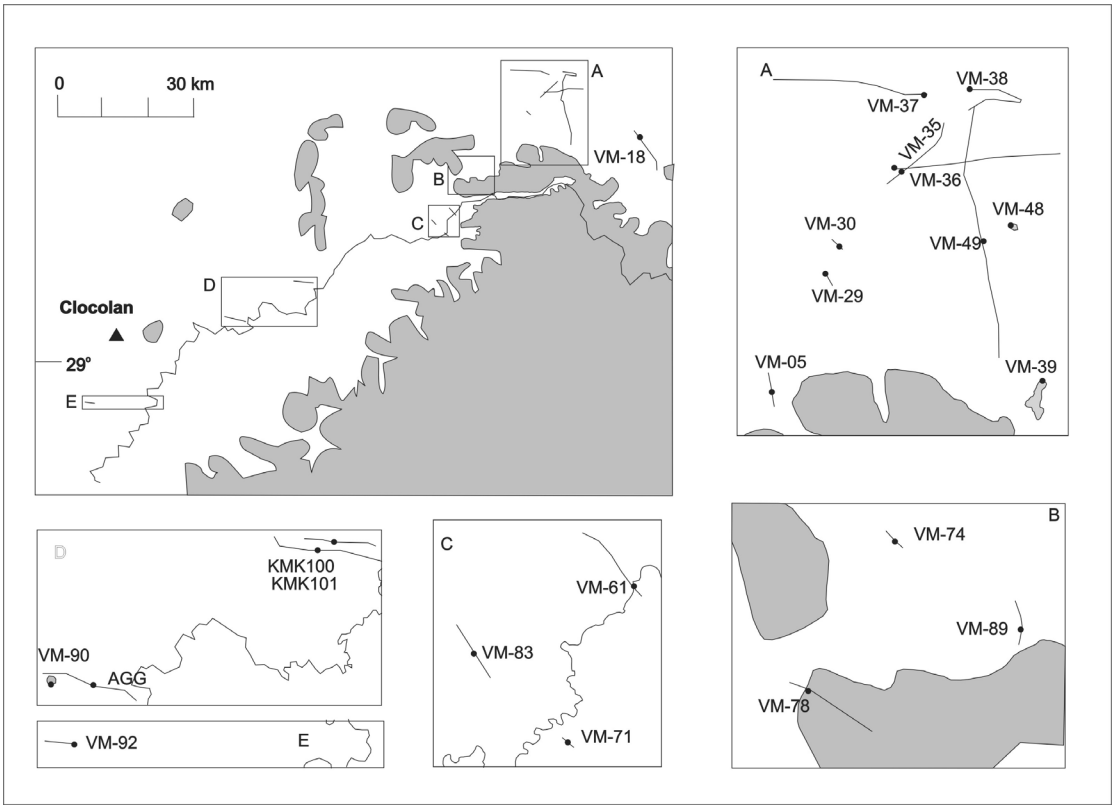

Figure 36. Spatial distribution of Mafika Lisiu$_T$ dykes and sills (top left). Labelled inset maps (A - E) show demarcated areas in detail. Points represent sample localities. Map parameters and data sources detailed in the caption of Figure 3.

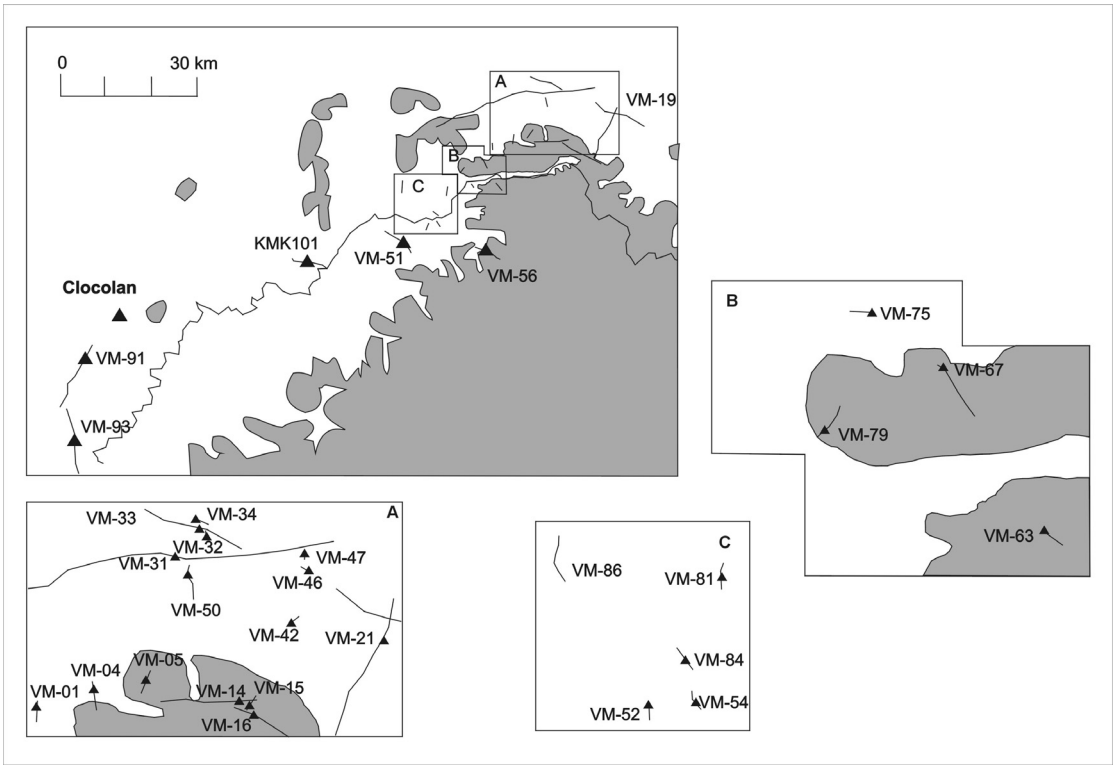

Figure 37. Spatial distribution of Maloti-Senqu dykes (top left). Labelled inset maps (A - C) show demarcated areas in detail. Points represent sample localities. Map parameters and data sources detailed in the caption of Figure 3.

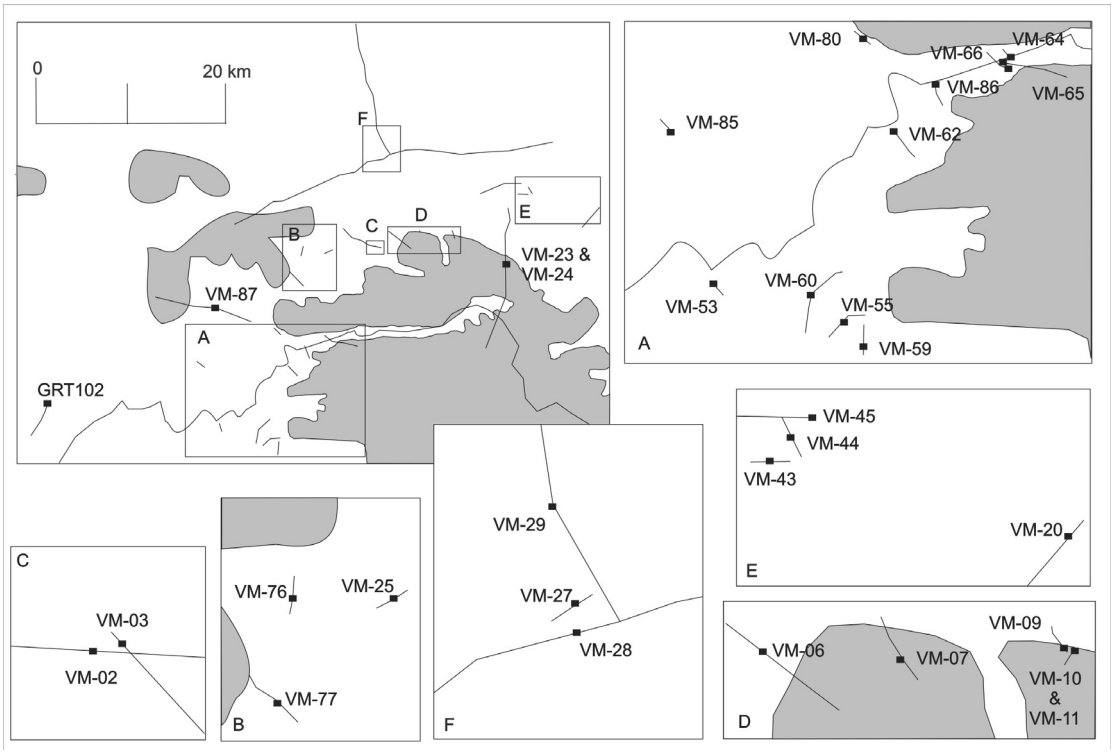

Figure 38. Spatial distribution of Mothae dykes (top left). Labelled inset maps (A - F) show demarcated areas in detail. Points represent sample localities. Map parameters and data sources detailed in caption of Figure 3.

10 DISCUSSION

10.1 General considerations with respect to the emplacement of the Lesotho remnant

As with other continental flood basalt provinces, it is generally assumed (*e.g.* Eales *et al*., 1984) that the lavas of the Karoo continental flood basalt province result from fissure-fed lava eruption. However, in spite of the abundance of dykes spatially related to the Lesotho basalt lava sequence, there is a paucity of evidence (such as spatter cones, tuff cones and pumice deposits) relating to actual vent complexes (Self *et al*., 1997; Reidel and Tolan, 1992; Swanson *et al*., 1975) that shows surface eruptive sites within it. Post-Gondwanan erosion has resulted in deep dissection of the Karoo lava sequence and has most probably removed the surface expression of actual eruption sites. However, the deeper levels of the magma supply system - the extension of the eruptive vent to depth (*i.e.* the dykes) – exist as a plethora of dykes spatially related to the Lesotho volcanic remnant. These vents were most likely fed from the multitude of sills in the main Karoo basin.

This relationship between the Lesotho flood basalts and its feeders can be investigated is by comparing the compositions of dykes with the characteristic magma types of the Drakensberg Group units defined previously by Marsh *et al*. (1997). If a dyke can be unequivocally paired with a unit of lavas, then it is probable that the dyke represents a feeder to that unit and would suggest that long distance transport for those lavas from distal eruption sites is unlikely. The current study has demonstrated that the empirical geochemical plots of Marsh *et al*. (1997) are most useful when matching dyke to lava composition. In this regard, simple interelement and ratio plots have proven useful when characterising dykes of diverse geochemistry. In this manner, potential feeders have been identified for (a) the Letele and Wonderkop units of the Barkly East Formation; and (b) all the units of the Lesotho Formation (*i.e.* Mafika Lisiu, Maloti or Senqu and Mothae).

10.2 Implications for the geochemical stratigraphy of the Lesotho Formation

FS-DFA provides a direct means of comparison between the geochemically defined stratigraphic units building the Lesotho volcanic remnant and the dykes in its immediate vicinity. FS-DFA may prove to be a useful tool in such stratigraphic studies and is used in the current study to test the validity of the Lesotho Formation stratigraphy developed by Marsh *et al*. (1997). In this respect, it is important to review the lavas which are misclassified. Table 20 lists the misclassified lavas from Models 1 – 3 and Figure 39 shows these misclassified lavas within their respective stratigraphic contexts. Note that Model 1 includes stratigraphic height as a variable, whereas in Models 2 and 3, stratigraphic height is excluded.

From Table 20 it is apparent that ON31-2 and MLP-15A are misclassifications common to all models. Similarly, lavas M101, M102, ON31-2, SOM-40, BMC13-1 and BMC-14 are misclassifications which are common to Models 2 and 3 (Table 20). In Model 1, all the misclassified lava samples are located at the boundary between units, although this is the case with only some of the misclassified samples from Models 2 and 3 (Figure 39). The samples that are located at the boundary between units are OXB-09, MLP-15A, SOM-40, SP-28, SP-29, SP-30, SP-32, ON31-2, ON30-2, BMC13-1 and BMC14-1, whereas samples MLP-34 – MLP-37, MLP-21, MLP-124 – MLP-126, SOM-10, SOM-11 and SOM-25 are not (Figure 39). Samples that are located at the boundary of two lava units may represent genuine misclassifications by Marsh *et al*. (1997) and most probably indicate that a slight modification to the boundary between lava units is required. However, the latter set of samples are located well within their respective units for this inference to be entirely true. Rather, the latter group of samples is inferred to represent an intercalation of lava types near the boundary of a unit – possibly representing the contemporaneity of two magma types. In this manner, the stratigraphy defined by Marsh *et al*. (1997) could be revised because the contemporaneity of two magma types was not considered in the approach adopted by the authors.

In addition, M101 and M102 are not shown within the respective stratigraphic context but occur near the base of the Mafika Lisiu unit, close to the contact with the underling Wonderkop unit. A plausible explanation for the misclassification is unclear. Possible reasons for the difference in misclassified lava samples between

Model 1; and Models 2 and 3 could be because each model is different with respect to (a) the elements included in the model; and (b) the significance and contribution of the elements to the discrimination. Thus, the misclassification of lava samples will be slightly different. In addition, Marsh *et al*. (1997) have used a limited number of immobile elements, whereas DFA uses all the data including elements which are mobile. Therefore, if the mobile elements are included in the DFA then the variably altered nature of the samples may also contribute to the misclassification.

The difference between misclassified lavas by Model 1 on the one hand and Models 2 and 3 on the other could be because stratigraphic height was taken as height above sea level. Since the base of each stratigraphic section is not at the same elevation above sea level, absolute height above sea level does not correlate with height in the stratigraphic sequence. Furthermore, all units may not be of uniform thickness and it would therefore stand to reason that this could result in misclassifications by Model 1, which differ from those resulting from Models 2 and 3. Therefore, although stratigraphic height was taken as height above sea level, it appears as though FS-DFA accounts for the fact that lavas of the same unit from different stratigraphic sections occur at different heights.

Table 20. A comparison of misclassified lavas from Models 1 – 3. ON31-2 and MLP-15A are misclassified lava samples common to all Models. In addition, 6 other lavas are common to Models 2 and 3. Lavas marked with asterisks (*) may represent genuine empirical misclassifications by Marsh *et al.* (1997) as discussed in the text. Other misclassified lava samples may represent the contemporaneity of two magma types.

Model 1	Actual	DFA		Model 2	Actual	DFA		Model 3	Actual	DFA		Model 3	Actual	DFA
				M101	Mf	MSM		M101	Mf	MS		*MLP-21	MS	Mf
				M102	Mf	MSM		M102	Mf	MS		MLP-35	MS	Mo
*ON30-2	Mf	MSM										MLP-36	MS	Mo
*ON31-2	Mf	MSM		*ON31-2	Mf	MSM		*ON31-2	Mf	MS		MLP-37	MS	Mo
				*SOM-40	Mf	MSM		*SOM-40	Mf	MS		SOM-25	MS	Mf
				*BMC13-1	MSM	Mf		*BMC13-1	MS	Mf		SOM-10	MS	Mo
				*BMC-14	MSM	Mf		*BMC-14	MS	Mf		SOM-11	MS	Mo
SP-28	Mf	MSM										OXB-09	Mo	MS
SP-29	Mf	MSM												
SP-30	Mf	MSM												
SP-32	Mf	MSM												
								MLP-154	MS	Mf				
*MLP-15A	MSM	Mf		*MLP-15A	MSM	Mf		*MLP-15A	MS	Mf				
				MLP-34	MSM	Mf								
								MLP-124	MS	Mo				
								MLP-125	MS	Mo				
								MLP-126	MS	Mo				

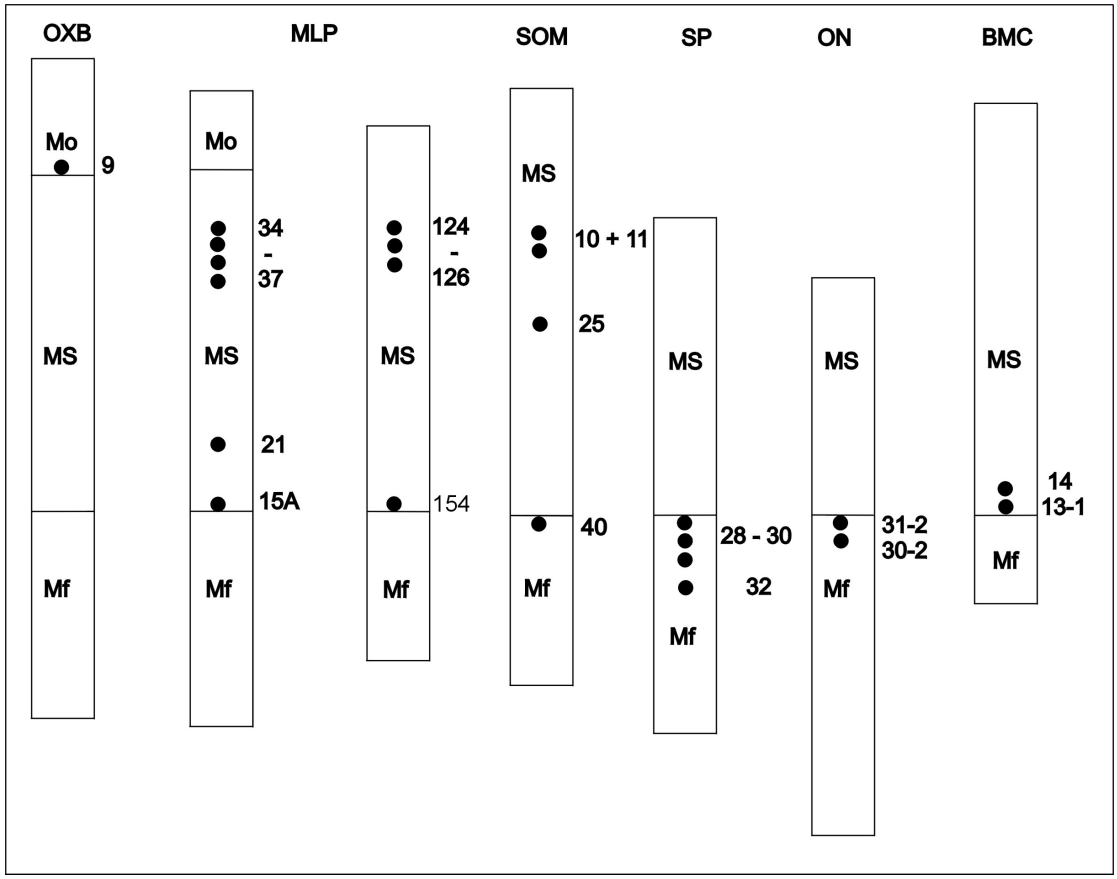

Figure 39. Pertinent stratigraphic sections from Marsh *et al.* (1997) showing the approximate positions of misclassified lava samples from Models 1 – 3 as discussed in the text. Stratigraphic units are labelled as in Chapter 7. Numbers to the right of stratigraphic sections represent specific lava samples represented by dots within the column. Sample numbers are listed in Table 15. Abbreviations: OXB – Oxbow, MLP – Mafika Lisiu Pass, SOM - Semongkong, SP – Sani Pass, ON – Ongeluksnek Pass. Source: Marsh *et al.*, 1997, Figure 6, p. 258.

10.3 Implications for the emplacement of and magma supply to the Lesotho volcanic sequence

Several previous studies have commented on the comparison between the compositions of Karoo lavas of Lesotho and the Karoo dolerites. In their study of the basalts of Lesotho (then Basotholand), Cox and Hornung (1966) noted that the compositions of the lavas and dolerites are similar. This view was supported by Marsh and Eales (1984) on the basis of comparisons of major element composition of a substantial set of basalts from the Barkly East area and Karoo dolerites. In addition, they noted the occurrence of dykes of Moshesh's Ford and Kraai River. Subsequent to the establishment of the detailed geochemical stratigraphy by Marsh *et al*. (1997), Marsh and Mndaweni (1998) showed that the composition of a single, long homogeneous dyke near Cradock correlates with the Mafika Lisiu magma type.

However, none of these studies were focussed on a detailed and systematic study of comparison between the composition of lavas and dolerites. In addition, the earlier studies are also inadequate in clarifying whether dykes and basalt flows of the same magma type have a close spatial relationship or whether the lavas have flowed in from distal vents. The research presented in this thesis is the first such study which demonstrates that dykes and basalt flows of the same magma type in the Karoo continental flood basalt province have a close spatial relationship.

In the current study, three dykes are of the Letele and two of the Wonderkop types of the northern Barkly East Formation. A further 81 dykes and three sills are shown to be compositionally similar to the Mafika Lisiu, Maloti-Senqu and Mothae units of the Lesotho Formation. Furthermore, eight dykes have compositional similarities to the Oxbow magma type. Based upon the similarity in composition between the Lesotho remnant lavas and the intrusions located adjacent to the northern and north western portion of the lava pile, this study demonstrates that it is most likely that the bulk of the Lesotho remnant was erupted from vents located in its immediate vicinity. Thus, it is most unlikely that the lavas of the Lesotho remnant were emplaced from distal eruptive vents as speculated by White (1997). The possibility does remain that many of these dykes, which are short, may not have fed a surface fissure eruption or have erupted over a small fraction of their total length (Mège and Korme, 2004).

No dolerites collected in the study area (Figure 3) have compositional characteristics similar to the Sani, Roma and Golden Gate types of the northern Barkly East Formation, which are small volume types of the this Formation. As demonstrated for lava flows in other continental flood basalt provinces (*e.g.* Elliot *et al*., 1999; Self *et al.* 1997; Storey and Kyle, 1997; White, 1992) these could have been fed from distal sources removed from the area which was covered in the sampling programme. Alternatively, there may be very few dykes of these compositions and these could have been missed during sampling. In this regard, Elliot and Fleming (2004) have suggested long distance magma transport for the Golden Gate type and the results of the current study are consistent with these observations.

11 CONCLUSIONS

94 dykes and three sills were collected and analysed for major and trace elements. On the basis of composition the dykes can be subdivided into a number of geochemically distinct groups on empirical grounds and the results of DFA can be correlated with several of the stratigraphic units in the Lesotho volcanic sequence.

Geochemical discrimination diagrams from Marsh *et al*. (1997) have been used to classify dykes of diverse composition that correlate with the Barkly East Formation. Three dykes have broad geochemical affinities with the Letele type and two are identified to be representative of the Wonderkop type. This suggests that the lavas in these two units were fed from local eruption fissures.

The multivariate technique, FS-DFA, has been used to facilitate the identification of dykes with similarities to the different stratigraphic units of the Lesotho Formation. FS-DFA produces a > 95 % success rate in classification when used to discriminate amongst the Mafika $Lisiu_T$, Maloti-Senqu, Mothae and Oxbow types. 23 dykes have been identified as Mafika $Lisiu_T$ type, 31 as Maloti or Senqu, 32 as Mothae and eight as the Oxbow type. This suggests that the bulk of the > 1.5 km thick Lesotho volcanic remnant was also fed from local eruption fissures now represented by a diffuse plexus of dykes and that long distance transport of lavas from remote eruption sites is unlikely. The same could be said for the Wonderkop and Letele units of the underlying Barkly East Formation, although it appears as if these units were erupted from fissures located in close proximity to the present outcrop pattern of these lavas.

No intrusions of the Sani, Roma and Golden Gate units of the northern Barkly East Formation have been found. This implies that either intrusions of such composition were missed during sampling or that these lavas were emplaced from distal sources removed from the area which was covered in the sampling programme.

Table A: CLASSIFICATION OF CASES (Model 2)															
Misclassified cases are marked (*) and highlighted															
Abbreviations: Mf (Mafika Lisiu), MSM (Maloti, Senqu and Mothae), Oxb (Oxbow)															
Actual classification		**1**	**2**	**3**		**Actual classification**		**1**	**2**	**3**		**Actual classification**		**1**	**2**	**3**
BMC-10	Mf	Mf	MSM	Oxb		**M23**	Mf	Mf	MSM	Oxb		**M76**	Mf	Mf	MSM	Oxb
BMC-11	Mf	Mf	MSM	Oxb		**M24**	Mf	Mf	MSM	Oxb		**M77**	Mf	Mf	MSM	Oxb
BMC-12	Mf	Mf	MSM	Oxb		**M25**	Mf	Mf	MSM	Oxb		**M78**	Mf	Mf	MSM	Oxb
BUS-10	Mf	Mf	MSM	Oxb		**M26**	Mf	Mf	MSM	Oxb		**M8**	Mf	Mf	MSM	Oxb
BUS-11	Mf	Mf	MSM	Oxb		**M27**	Mf	Mf	MSM	Oxb		**M80**	Mf	Mf	MSM	Oxb
BUS-13	Mf	Mf	MSM	Oxb		**M28**	Mf	Mf	MSM	Oxb		**M81**	Mf	Mf	MSM	Oxb
BUS-14	Mf	Mf	MSM	Oxb		**M29**	Mf	Mf	MSM	Oxb		**M82**	Mf	Mf	MSM	Oxb
BUS-15	Mf	Mf	MSM	Oxb		**M3**	Mf	Mf	MSM	Oxb		**M83**	Mf	Mf	MSM	Oxb
BUS-16	Mf	Mf	MSM	Oxb		**M30**	Mf	Mf	MSM	Oxb		**M84**	Mf	Mf	MSM	Oxb
BUS-17	Mf	Mf	MSM	Oxb		**M31**	Mf	Mf	MSM	Oxb		**M85**	Mf	Mf	MSM	Oxb
BUS-19	Mf	Mf	MSM	Oxb		**M32**	Mf	Mf	MSM	Oxb		**M86**	Mf	Mf	MSM	Oxb
BUS-20	Mf	Mf	MSM	Oxb		**M33**	Mf	Mf	MSM	Oxb		**M87**	Mf	Mf	MSM	Oxb
BUS-21	Mf	Mf	MSM	Oxb		**M34**	Mf	Mf	MSM	Oxb		**M88**	Mf	Mf	MSM	Oxb
BUS-24	Mf	Mf	MSM	Oxb		**M35**	Mf	Mf	MSM	Oxb		**M89**	Mf	Mf	MSM	Oxb
BUS-25	Mf	Mf	MSM	Oxb		**M36**	Mf	Mf	MSM	Oxb		**M9**	Mf	Mf	MSM	Oxb
BUS-26	Mf	Mf	MSM	Oxb		**M37**	Mf	Mf	MSM	Oxb		**M91**	Mf	Mf	MSM	Oxb
BUS-27	Mf	Mf	MSM	Oxb		**M38**	Mf	Mf	MSM	Oxb		**M92**	Mf	Mf	MSM	Oxb
BUS-28	Mf	Mf	MSM	Oxb		**M39**	Mf	Mf	MSM	Oxb		**M93**	Mf	Mf	MSM	Oxb
M1	Mf	Mf	MSM	Oxb		**M4**	Mf	Mf	MSM	Oxb		**M94**	Mf	Mf	MSM	Oxb
M100	Mf	Mf	MSM	Oxb		**M40**	Mf	Mf	MSM	Oxb		**M95**	Mf	Mf	MSM	Oxb
***M101**	Mf	MSM	Mf	Oxb		**M41**	Mf	Mf	MSM	Oxb		**M96**	Mf	Mf	MSM	Oxb

Table A cont.

Actual classification		1	2	3		Actual classification		1	2	3		Actual classification		1	2	3
***M102**	Mf	MSM	Mf	Oxb		**M42**	Mf	Mf	MSM	Oxb		**M97**	Mf	Mf	MSM	Oxb
M103	Mf	Mf	MSM	Oxb		**M45**	Mf	Mf	MSM	Oxb		**M98**	Mf	Mf	MSM	Oxb
M104	Mf	Mf	MSM	Oxb		**M46**	Mf	Mf	MSM	Oxb		**M99**	Mf	Mf	MSM	Oxb
M128	Mf	Mf	MSM	Oxb		**M47**	Mf	Mf	MSM	Oxb		**MLP-07**	Mf	Mf	MSM	Oxb
M129	Mf	Mf	MSM	Oxb		**M48**	Mf	Mf	MSM	Oxb		**MLP-08**	Mf	Mf	MSM	Oxb
M136	Mf	Mf	MSM	Oxb		**M5**	Mf	Mf	MSM	Oxb		**MLP-09**	Mf	Mf	MSM	Oxb
M137	Mf	Mf	MSM	Oxb		**M59**	Mf	Mf	MSM	Oxb		**MLP-11**	Mf	Mf	MSM	Oxb
M138	Mf	Mf	MSM	Oxb		**M6**	Mf	Mf	MSM	Oxb		**MLP-12**	Mf	Mf	MSM	Oxb
M139	Mf	Mf	MSM	Oxb		**M60**	Mf	Mf	MSM	Oxb		**MLP-13**	Mf	Mf	MSM	Oxb
M140	Mf	Mf	MSM	Oxb		**M7**	Mf	Mf	MSM	Oxb		**MLP-14**	Mf	Mf	MSM	Oxb
M141	Mf	Mf	MSM	Oxb		**M70**	Mf	Mf	MSM	Oxb		**MLP-155**	Mf	Mf	MSM	Oxb
M142	Mf	Mf	MSM	Oxb		**M71**	Mf	Mf	MSM	Oxb		**MLP-156**	Mf	Mf	MSM	Oxb
M143	Mf	Mf	MSM	Oxb		**M72**	Mf	Mf	MSM	Oxb		**MLP-157**	Mf	Mf	MSM	Oxb
M2	Mf	Mf	MSM	Oxb		**M73**	Mf	Mf	MSM	Oxb		**MLP-158**	Mf	Mf	MSM	Oxb
M21	Mf	Mf	MSM	Oxb		**M74**	Mf	Mf	MSM	Oxb		**MLP-159**	Mf	Mf	MSM	Oxb
M22	Mf	Mf	MSM	Oxb		**M75**	Mf	Mf	MSM	Oxb		**MLP-160**	Mf	Mf	MSM	Oxb
MLP-161	Mf	Mf	MSM	Oxb		**OXB-57**	Mf	Mf	MSM	Oxb		**M132**	Mf	Mf	MSM	Oxb
MLP-162	Mf	Mf	MSM	Oxb		**OXB-58**	Mf	Mf	MSM	Oxb		**M133**	Mf	Mf	MSM	Oxb
MLP-164	Mf	Mf	MSM	Oxb		**OXB-59**	Mf	Mf	MSM	Oxb		**M134**	Mf	Mf	MSM	Oxb
MLP-165	Mf	Mf	MSM	Oxb		**SOM-100**	Mf	Mf	MSM	Oxb		**M135**	Mf	Mf	MSM	Oxb
MLP-169	Mf	Mf	MSM	Oxb		***SOM-40**	Mf	MSM	Mf	Oxb		**M14**	Mf	Mf	MSM	Oxb
MLP-170	Mf	Mf	MSM	Oxb		**SOM-82**	Mf	Mf	MSM	Oxb		**M15**	Mf	Mf	MSM	Oxb
MLP-171	Mf	Mf	MSM	Oxb		**SOM-83**	Mf	Mf	MSM	Oxb		**M16**	Mf	Mf	MSM	Oxb
MLP-172	Mf	Mf	MSM	Oxb		**SOM-84**	Mf	Mf	MSM	Oxb		**M17**	Mf	Mf	MSM	Oxb
MLP-174	Mf	Mf	MSM	Oxb		**SOM-86**	Mf	Mf	MSM	Oxb		**M18**	Mf	Mf	MSM	Oxb

Table A cont.

Actual classification		1	2	3		Actual classification		1	2	3		Actual classification		1	2	3
MLP-175	Mf	Mf	MSM	Oxb		**SOM-87**	Mf	Mf	MSM	Oxb		**M19**	Mf	Mf	MSM	Oxb
MLP-176	Mf	Mf	MSM	Oxb		**SOM-91**	Mf	Mf	MSM	Oxb		**M20**	Mf	Mf	MSM	Oxb
MLP-177	Mf	Mf	MSM	Oxb		**SOM-92**	Mf	Mf	MSM	Oxb		**M61**	Mf	Mf	MSM	Oxb
MLP-178	Mf	Mf	MSM	Oxb		**SOM-94**	Mf	Mf	MSM	Oxb		**M62**	Mf	Mf	MSM	Oxb
MLP-180	Mf	Mf	MSM	Oxb		**SOM-95**	Mf	Mf	MSM	Oxb		**M63**	Mf	Mf	MSM	Oxb
ON19-2	Mf	Mf	MSM	Oxb		**SOM-96**	Mf	Mf	MSM	Oxb		**M64**	Mf	Mf	MSM	Oxb
ON20-2	Mf	Mf	MSM	Oxb		**SOM-97**	Mf	Mf	MSM	Oxb		**M65**	Mf	Mf	MSM	Oxb
ON-21	Mf	Mf	MSM	Oxb		**SOM-98**	Mf	Mf	MSM	Oxb		**M66**	Mf	Mf	MSM	Oxb
ON22-2	Mf	Mf	MSM	Oxb		**SOM-99**	Mf	Mf	MSM	Oxb		**M67**	Mf	Mf	MSM	Oxb
ON-23	Mf	Mf	MSM	Oxb		**SP-28**	Mf	Mf	MSM	Oxb		**M68**	Mf	Mf	MSM	Oxb
ON-24	Mf	Mf	MSM	Oxb		**SP-29**	Mf	Mf	MSM	Oxb		**M69**	Mf	Mf	MSM	Oxb
ON-25	Mf	Mf	MSM	Oxb		**SP-30**	Mf	Mf	MSM	Oxb		**MLP-01**	Mf	Mf	MSM	Oxb
ON28-2	Mf	Mf	MSM	Oxb		**SP-31**	Mf	Mf	MSM	Oxb		**MLP-02**	Mf	Mf	MSM	Oxb
ON-29	Mf	Mf	MSM	Oxb		**SP-38**	Mf	Mf	MSM	Oxb		**MLP-03**	Mf	Mf	MSM	Oxb
ON30-2	Mf	Mf	MSM	Oxb		**SP-39**	Mf	Mf	MSM	Oxb		**MLP-04**	Mf	Mf	MSM	Oxb
***ON31-2**	Mf	MSM	Mf	Oxb		**SP-40**	Mf	Mf	MSM	Oxb		**MLP-05**	Mf	Mf	MSM	Oxb
ON-35	Mf	Mf	MSM	Oxb		**SP-41**	Mf	Mf	MSM	Oxb		**MLP-166**	Mf	Mf	MSM	Oxb
ON36-1	Mf	Mf	MSM	Oxb		**SP-42**	Mf	Mf	MSM	Oxb		**MLP-167**	Mf	Mf	MSM	Oxb
ON-37	Mf	Mf	MSM	Oxb		**SP-43**	Mf	Mf	MSM	Oxb		**MLP-168**	Mf	Mf	MSM	Oxb
ON38-3	Mf	Mf	MSM	Oxb		**SP-44B**	Mf	Mf	MSM	Oxb		**ON-39**	Mf	Mf	MSM	Oxb
ON41-2	Mf	Mf	MSM	Oxb		**BMC-02**	Mf	Mf	MSM	Oxb		**ON40-2**	Mf	Mf	MSM	Oxb
ON-42	Mf	Mf	MSM	Oxb		**BMC-04**	Mf	Mf	MSM	Oxb		**ON-47**	Mf	Mf	MSM	Oxb
ON-43	Mf	Mf	MSM	Oxb		**BMC-05**	Mf	Mf	MSM	Oxb		**OXB-46**	Mf	Mf	MSM	Oxb
ON44-2	Mf	Mf	MSM	Oxb		**BMC-06**	Mf	Mf	MSM	Oxb		**OXB-47**	Mf	Mf	MSM	Oxb
ON-45	Mf	Mf	MSM	Oxb		**BMC-07**	Mf	Mf	MSM	Oxb		**OXB-48**	Mf	Mf	MSM	Oxb

Table A cont.

Actual classification		1	2	3		Actual classification		1	2	3		Actual classification		1	2	3
OXB-42	Mf	Mf	MSM	Oxb		**BUS-22**	Mf	Mf	MSM	Oxb		**OXB-49**	Mf	Mf	MSM	Oxb
OXB-43	Mf	Mf	MSM	Oxb		**M10**	Mf	Mf	MSM	Oxb		**OXB-52**	Mf	Mf	MSM	Oxb
OXB-44	Mf	Mf	MSM	Oxb		**M11**	Mf	Mf	MSM	Oxb		**OXB-54**	Mf	Mf	MSM	Oxb
OXB-45	Mf	Mf	MSM	Oxb		**M12**	Mf	Mf	MSM	Oxb		**SP-32**	Mf	Mf	MSM	Oxb
OXB-50	Mf	Mf	MSM	Oxb		**M13**	Mf	Mf	MSM	Oxb		**SP-33**	Mf	Mf	MSM	Oxb
OXB-55	Mf	Mf	MSM	Oxb		**M130**	Mf	Mf	MSM	Oxb		**SP-34**	Mf	Mf	MSM	Oxb
OXB-56	Mf	Mf	MSM	Oxb		**M131**	Mf	Mf	MSM	Oxb		**SP-35**	Mf	Mf	MSM	Oxb
SP-36	Mf	Mf	MSM	Oxb		**SOM-38A**	MSM	MSM	Mf	Oxb		**MLP-127**	MSM	MSM	Mf	Oxb
SP-37	Mf	Mf	MSM	Oxb		**SOM-39**	MSM	MSM	Mf	Oxb		**MLP-128**	MSM	MSM	Mf	Oxb
***BMC13-1**	MSM	Mf	MSM	Oxb		**SP-21**	MSM	MSM	Mf	Oxb		**MLP-129**	MSM	MSM	Mf	Oxb
***BMC-14**	MSM	Mf	MSM	Oxb		**SP23-2**	MSM	MSM	Mf	Oxb		**MLP-130**	MSM	MSM	Mf	Oxb
BMC15-3	MSM	MSM	Mf	Oxb		**SP-24**	MSM	MSM	Mf	Oxb		**MLP-131**	MSM	MSM	Mf	Oxb
BMC-16	MSM	MSM	Mf	Oxb		**SP-25**	MSM	MSM	Mf	Oxb		**MLP-132**	MSM	MSM	Mf	Oxb
BMC-17	MSM	MSM	Mf	Oxb		**SP-26**	MSM	MSM	Mf	Oxb		**MLP-133**	MSM	MSM	Mf	Oxb
BMC-18	MSM	MSM	Mf	Oxb		**SP-27**	MSM	MSM	Mf	Oxb		**MLP-134**	MSM	MSM	Mf	Oxb
BUS-29	MSM	MSM	Mf	Oxb		**BMC19-2**	MSM	MSM	Mf	Oxb		**MLP-136**	MSM	MSM	Mf	Oxb
BUS-30	MSM	MSM	Mf	Oxb		**BMC-20**	MSM	MSM	Mf	Oxb		**MLP-137**	MSM	MSM	Mf	Oxb
BUS-31	MSM	MSM	Mf	Oxb		**BMC25-2**	MSM	MSM	Mf	Oxb		**MLP-138**	MSM	MSM	Mf	Oxb
BUS-32	MSM	MSM	Mf	Oxb		**BMC-28**	MSM	MSM	Mf	Oxb		**MLP-139**	MSM	MSM	Mf	Oxb
BUS-33	MSM	MSM	Mf	Oxb		**BMC-29**	MSM	MSM	Mf	Oxb		**MLP-140**	MSM	MSM	Mf	Oxb
MLP-146	MSM	MSM	Mf	Oxb		**BMC32-2**	MSM	MSM	Mf	Oxb		**MLP-141**	MSM	MSM	Mf	Oxb
MLP-147	MSM	MSM	Mf	Oxb		**BUS-34**	MSM	MSM	Mf	Oxb		**MLP-142**	MSM	MSM	Mf	Oxb
MLP-148	MSM	MSM	Mf	Oxb		**BUS-35**	MSM	MSM	Mf	Oxb		**MLP-143**	MSM	MSM	Mf	Oxb
MLP-149	MSM	MSM	Mf	Oxb		**BUS-36**	MSM	MSM	Mf	Oxb		**MLP-144**	MSM	MSM	Mf	Oxb
MLP-150	MSM	MSM	Mf	Oxb		**BUS-37**	MSM	MSM	Mf	Oxb		**MLP-145**	MSM	MSM	Mf	Oxb

Table A cont.

Actual classification		1	2	3	Actual classification		1	2	3	Actual classification		1	2	3
MLP-151	MSM	MSM	Mf	Oxb	**BUS-38**	MSM	MSM	Mf	Oxb	**MLP-20**	MSM	MSM	Mf	Oxb
MLP-152	MSM	MSM	Mf	Oxb	**BUS-39**	MSM	MSM	Mf	Oxb	**MLP-21**	MSM	MSM	Mf	Oxb
MLP-153	MSM	MSM	Mf	Oxb	**BUS-40**	MSM	MSM	Mf	Oxb	**MLP-22**	MSM	MSM	Mf	Oxb
MLP-154	MSM	MSM	Mf	Oxb	**MLM-01**	MSM	MSM	Mf	Oxb	**MLP-23**	MSM	MSM	Mf	Oxb
***MLP-15A**	MSM	Mf	MSM	Oxb	**MLM-02**	MSM	MSM	Mf	Oxb	**MLP-24**	MSM	MSM	Mf	Oxb
MLP-15B	MSM	MSM	Mf	Oxb	**MLM-03**	MSM	MSM	Mf	Oxb	**MLP-25**	MSM	MSM	Mf	Oxb
MLP-16	MSM	MSM	Mf	Oxb	**MLM-04**	MSM	MSM	Mf	Oxb	**MLP-26**	MSM	MSM	Mf	Oxb
MLP-17	MSM	MSM	Mf	Oxb	**MLM-05**	MSM	MSM	Mf	Oxb	**MLP-27**	MSM	MSM	Mf	Oxb
MLP-18	MSM	MSM	Mf	Oxb	**MLM-06**	MSM	MSM	Mf	Oxb	**MLP-28**	MSM	MSM	Mf	Oxb
MLP-19	MSM	MSM	Mf	Oxb	**MLM-07**	MSM	MSM	Mf	Oxb	**MLP-30**	MSM	MSM	Mf	Oxb
ON-04	MSM	MSM	Mf	Oxb	**MLM-08**	MSM	MSM	Mf	Oxb	**MLP-31**	MSM	MSM	Mf	Oxb
ON33-2	MSM	MSM	Mf	Oxb	**MLM-09**	MSM	MSM	Mf	Oxb	**MLP-32**	MSM	MSM	Mf	Oxb
ON34-3	MSM	MSM	Mf	Oxb	**MLM-10**	MSM	MSM	Mf	Oxb	**MLP-33**	MSM	MSM	Mf	Oxb
OXB-37	MSM	MSM	Mf	Oxb	**MLM-11**	MSM	MSM	Mf	Oxb	***MLP-34**	MSM	Mf	MSM	Oxb
OXB-38	MSM	MSM	Mf	Oxb	**MLM-12**	MSM	MSM	Mf	Oxb	**MLP-35**	MSM	MSM	Mf	Oxb
OXB-39	MSM	MSM	Mf	Oxb	**MLM-13**	MSM	MSM	Mf	Oxb	**MLP-36**	MSM	MSM	Mf	Oxb
OXB-40	MSM	MSM	Mf	Oxb	**MLM-14**	MSM	MSM	Mf	Oxb	**MLP-37**	MSM	MSM	Mf	Oxb
OXB-41	MSM	MSM	Mf	Oxb	**MLM-15**	MSM	MSM	Mf	Oxb	**ON-05**	MSM	MSM	Mf	Oxb
SOM-33	MSM	MSM	Mf	Oxb	**MLM-16**	MSM	MSM	Mf	Oxb	**ON-07**	MSM	MSM	Mf	Oxb
SOM-34	MSM	MSM	Mf	Oxb	**MLM-17**	MSM	MSM	Mf	Oxb	**ON-10-2**	MSM	MSM	Mf	Oxb
SOM-35	MSM	MSM	Mf	Oxb	**MLP-124**	MSM	MSM	Mf	Oxb	**ON-11**	MSM	MSM	Mf	Oxb
SOM-36	MSM	MSM	Mf	Oxb	**MLP-125**	MSM	MSM	Mf	Oxb	**ON-16**	MSM	MSM	Mf	Oxb
SOM-37	MSM	MSM	Mf	Oxb	**MLP-126**	MSM	MSM	Mf	Oxb	**ON-17**	MSM	MSM	Mf	Oxb
ON-18	MSM	MSM	Mf	Oxb	**BMC-36**	MSM	MSM	Mf	Oxb	**SOM-11**	MSM	MSM	Mf	Oxb
OXB-14	MSM	MSM	Mf	Oxb	**BMC-37**	MSM	MSM	Mf	Oxb	**SOM-12**	MSM	MSM	Mf	Oxb

Table A cont.															
Actual classification		**1**	**2**	**3**		**Actual classification**		**1**	**2**	**3**		**Actual classification**		**1**	**2**	**3**
OXB-15	MSM	MSM	Mf	Oxb		**MLP-111**	MSM	MSM	Mf	Oxb		**SOM-13**	MSM	MSM	Mf	Oxb
OXB-16	MSM	MSM	Mf	Oxb		**MLP-112**	MSM	MSM	Mf	Oxb		**SOM-14**	MSM	MSM	Mf	Oxb
OXB-18	MSM	MSM	Mf	Oxb		**MLP-113**	MSM	MSM	Mf	Oxb		**SOM-16**	MSM	MSM	Mf	Oxb
OXB-19	MSM	MSM	Mf	Oxb		**MLP-114**	MSM	MSM	Mf	Oxb		**SOM-18**	MSM	MSM	Mf	Oxb
OXB-20	MSM	MSM	Mf	Oxb		**MLP-115**	MSM	MSM	Mf	Oxb		**SP-01**	MSM	MSM	Mf	Oxb
OXB-21	MSM	MSM	Mf	Oxb		**MLP-116**	MSM	MSM	Mf	Oxb		**SP-02**	MSM	MSM	Mf	Oxb
OXB-26	MSM	MSM	Mf	Oxb		**MLP-117**	MSM	MSM	Mf	Oxb		**SP-03**	MSM	MSM	Mf	Oxb
OXB-27	MSM	MSM	Mf	Oxb		**MLP-118**	MSM	MSM	Mf	Oxb		**SP-04**	MSM	MSM	Mf	Oxb
OXB-28	MSM	MSM	Mf	Oxb		**MLP-119**	MSM	MSM	Mf	Oxb		**SP-05**	MSM	MSM	Mf	Oxb
OXB-30	MSM	MSM	Mf	Oxb		**MLP-120**	MSM	MSM	Mf	Oxb		**SP06-1**	MSM	MSM	Mf	Oxb
OXB-31	MSM	MSM	Mf	Oxb		**MLP-121**	MSM	MSM	Mf	Oxb		**SP06-2**	MSM	MSM	Mf	Oxb
OXB-32	MSM	MSM	Mf	Oxb		**MLP-122**	MSM	MSM	Mf	Oxb		**SP07-2**	MSM	MSM	Mf	Oxb
OXB-33	MSM	MSM	Mf	Oxb		**MLP-123**	MSM	MSM	Mf	Oxb		**SP-08**	MSM	MSM	Mf	Oxb
OXB-34	MSM	MSM	Mf	Oxb		**MLP-38**	MSM	MSM	Mf	Oxb		**MLP-60**	MSM	MSM	Mf	Oxb
OXB-35	MSM	MSM	Mf	Oxb		**MLP-39**	MSM	MSM	Mf	Oxb		**MLP-61**	MSM	MSM	Mf	Oxb
SOM-19	MSM	MSM	Mf	Oxb		**MLP-40**	MSM	MSM	Mf	Oxb		**MLP-62**	MSM	MSM	Mf	Oxb
SOM-20	MSM	MSM	Mf	Oxb		**MLP-41**	MSM	MSM	Mf	Oxb		**MLP-63**	MSM	MSM	Mf	Oxb
SOM-21	MSM	MSM	Mf	Oxb		**MLP-42**	MSM	MSM	Mf	Oxb		**MLP-64**	MSM	MSM	Mf	Oxb
SOM-22	MSM	MSM	Mf	Oxb		**MLP-43**	MSM	MSM	Mf	Oxb		**MLP-65**	MSM	MSM	Mf	Oxb
SOM-23	MSM	MSM	Mf	Oxb		**MLP-44**	MSM	MSM	Mf	Oxb		**OXB-01**	MSM	MSM	Mf	Oxb
SOM-25	MSM	MSM	Mf	Oxb		**MLP-45**	MSM	MSM	Mf	Oxb		**OXB-02**	MSM	MSM	Mf	Oxb
SOM-26	MSM	MSM	Mf	Oxb		**MLP-46**	MSM	MSM	Mf	Oxb		**OXB-03**	MSM	MSM	Mf	Oxb
SOM-27	MSM	MSM	Mf	Oxb		**MLP-47**	MSM	MSM	Mf	Oxb		**OXB-04**	MSM	MSM	Mf	Oxb
SOM-28	MSM	MSM	Mf	Oxb		**MLP-48**	MSM	MSM	Mf	Oxb		**OXB-05**	MSM	MSM	Mf	Oxb
SOM-29	MSM	MSM	Mf	Oxb		**MLP-50**	MSM	MSM	Mf	Oxb		**OXB-06**	MSM	MSM	Mf	Oxb

Table A cont.

Actual classification		1	2	3		Actual classification		1	2	3		Actual classification		1	2	3
SOM-30	MSM	MSM	Mf	Oxb		**OXB-10**	MSM	MSM	Mf	Oxb		**OXB-07**	MSM	MSM	Mf	Oxb
SOM-31	MSM	MSM	Mf	Oxb		**OXB-11**	MSM	MSM	Mf	Oxb		**OXB-08**	MSM	MSM	Mf	Oxb
SOM-32	MSM	MSM	Mf	Oxb		**OXB-12**	MSM	MSM	Mf	Oxb		**OXB-09**	MSM	MSM	Mf	Oxb
SP10-2	MSM	MSM	Mf	Oxb		**OXB-13**	MSM	MSM	Mf	Oxb		**OXB-14A**	Oxb	Oxb	Mf	MSM
SP11-2	MSM	MSM	Mf	Oxb		**SOM-01**	MSM	MSM	Mf	Oxb		**OXB-22**	Oxb	Oxb	Mf	MSM
SP-12	MSM	MSM	Mf	Oxb		**SOM-02**	MSM	MSM	Mf	Oxb		**OXB-23**	Oxb	Oxb	Mf	MSM
SP13-3	MSM	MSM	Mf	Oxb		**SOM-03**	MSM	MSM	Mf	Oxb		**OXB-24**	Oxb	Oxb	Mf	MSM
SP14-3	MSM	MSM	Mf	Oxb		**SOM-04**	MSM	MSM	Mf	Oxb						
SP16-1	MSM	MSM	Mf	Oxb		**SOM-05**	MSM	MSM	Mf	Oxb						
SP-17	MSM	MSM	Mf	Oxb		**SOM-06**	MSM	MSM	Mf	Oxb						
SP18-2	MSM	MSM	Mf	Oxb		**SOM-07**	MSM	MSM	Mf	Oxb						
SP20-2	MSM	MSM	Mf	Oxb		**SOM-08**	MSM	MSM	Mf	Oxb						
SP-22	MSM	MSM	Mf	Oxb		**SOM-09**	MSM	MSM	Mf	Oxb						
BMC-35	MSM	MSM	Mf	Oxb		**SOM-10**	MSM	MSM	Mf	Oxb						

Table B1. Squared Mahalanobis Distances from Group Centroids for each lava (Model 2)						Table B2. Posterior Probabilities for each lava (Model 2)				
Actual classification		**Mf**	**MSM**	**Oxb**		**Actual classification**		**Mf**	**MSM**	**Oxb**
BMC-10	Mf	48.8143	54.8912	225.7382		**BMC-1 0**	Mf	0.954281	0.045719	0.000000
BMC-11	Mf	25.2077	26.3266	197.8303		**BMC-11**	Mf	0.636334	0.363666	0.000000
BMC-12	Mf	15.0381	31.6612	219.9140		**BMC-12**	Mf	0.999754	0.000246	0.000000
BUS-10	Mf	23.8911	35.4400	213.9531		**BUS-10**	Mf	0.996904	0.003096	0.000000
BUS-11	Mf	20.0996	27.7271	224.1265		**BUS-11**	Mf	0.978410	0.021590	0.000000
BUS-13	Mf	19.5249	32.4000	210.5010		**BUS-13**	Mf	0.998402	0.001598	0.000000
BUS-14	Mf	13.6968	20.9026	201.3473		**BUS-14**	Mf	0.973478	0.026522	0.000000
BUS-15	Mf	10.0600	27.7908	239.2865		**BUS-15**	Mf	0.999859	0.000141	0.000000
BUS-16	Mf	18.5211	43.9550	255.2852		**BUS-16**	Mf	0.999997	0.000003	0.000000
BUS-17	Mf	13.3102	35.3839	242.9909		**BUS-17**	Mf	0.999984	0.000016	0.000000
BUS-19	Mf	8.4375	30.1776	228.4110		**BUS-19**	Mf	0.999981	0.000019	0.000000
BUS-20	Mf	4.5473	18.6624	206.4337		**BUS-20**	Mf	0.999140	0.000860	0.000000
BUS-21	Mf	6.6351	25.2512	228.5490		**BUS-21**	Mf	0.999909	0.000091	0.000000
BUS-24	Mf	7.0324	20.5201	227.2767		**BUS-24**	Mf	0.998823	0.001177	0.000000
BUS-25	Mf	9.7138	13.4090	195.0572		**BUS-25**	Mf	0.863846	0.136154	0.000000
BUS-26	Mf	9.9225	26.3133	226.4442		**BUS-26**	Mf	0.999724	0.000276	0.000000
BUS-27	Mf	8.8132	15.6900	222.3821		**BUS-27**	Mf	0.968883	0.031117	0.000000
BUS-28	Mf	10.9124	21.4838	247.5146		**BUS-28**	Mf	0.994962	0.005038	0.000000
M1	Mf	14.2697	24.8448	224.8626		**M1**	Mf	0.994971	0.005029	0.000000
M100	Mf	3.4087	18.9266	241.8420		**M100**	Mf	0.999573	0.000427	0.000000
***M101**	Mf	30.6261	26.5709	183.6142		***M101**	Mf	0.116338	0.883662	0.000000
***M102**	Mf	20.5045	9.8151	201.2171		***M102**	Mf	0.004751	0.995249	0.000000
M103	Mf	23.4284	42.6218	215.4351		**M103**	Mf	0.999932	0.000068	0.000000
M104	Mf	14.9781	32.3232	208.1987		**M104**	Mf	0.999829	0.000171	0.000000
M128	Mf	1.0146	17.7097	212.7194		**M128**	Mf	0.999763	0.000237	0.000000
M129	Mf	9.5933	10.9505	211.6052		**M129**	Mf	0.663424	0.336576	0.000000
M136	Mf	14.3633	31.8497	291.2781		**M136**	Mf	0.999840	0.000160	0.000000
M137	Mf	9.9876	27.1431	229.3074		**M137**	Mf	0.999812	0.000188	0.000000
M138	Mf	5.9481	25.8560	244.1312		**M138**	Mf	0.999952	0.000048	0.000000
M139	Mf	13.1656	33.8207	230.3359		**M139**	Mf	0.999967	0.000033	0.000000
M140	Mf	16.1340	35.8412	227.3052		**M140**	Mf	0.999947	0.000053	0.000000
M141	Mf	9.0257	27.6322	236.0781		**M141**	Mf	0.999909	0.000091	0.000000
M142	Mf	6.6680	23.0074	215.8690		**M142**	Mf	0.999717	0.000283	0.000000
M143	Mf	9.6422	32.6088	229.0715		**M143**	Mf	0.999990	0.000010	0.000000
M2	Mf	10.2329	20.7716	232.9920		**M2**	Mf	0.994879	0.005121	0.000000
M21	Mf	7.6966	24.8194	238.1680		**M21**	Mf	0.999809	0.000191	0.000000
M22	Mf	9.9042	22.6486	210.3801		**M22**	Mf	0.998295	0.001705	0.000000
M23	Mf	6.2961	18.3807	226.3523		**M23**	Mf	0.997629	0.002371	0.000000
M24	Mf	5.8303	17.9457	226.1526		**M24**	Mf	0.997666	0.002334	0.000000

Table B1 cont.

Actual classification		Mf	MSM	Oxb
M25	Mf	10.7465	26.7373	239.3792
M26	Mf	9.4814	19.5166	220.0757
M27	Mf	7.8354	19.6112	217.5867
M28	Mf	5.0839	14.8251	208.1886
M29	Mf	6.7387	17.1747	214.6641
M3	Mf	7.7339	18.4987	230.6819
M30	Mf	5.4307	16.7252	215.7967
M31	Mf	11.5028	20.3135	191.8267
M32	Mf	8.0824	23.7670	208.1031
M33	Mf	8.1319	30.3672	233.9754
M34	Mf	11.4796	37.0547	237.1900
M35	Mf	16.0145	48.0256	274.3674
M36	Mf	107.5321	123.1341	280.0256
M37	Mf	9.2184	26.9938	239.0574
M38	Mf	28.4638	36.8876	257.4717
M39	Mf	17.0779	26.4144	246.3030
M4	Mf	8.7310	17.8655	228.4674
M40	Mf	9.5979	25.8315	228.0807
M41	Mf	14.8864	29.0669	234.2454
M42	Mf	307.4897	315.3249	558.7113
M45	Mf	21.2096	37.5787	220.7272
M46	Mf	24.5009	40.3092	210.7136
M47	Mf	17.3689	35.0520	231.1618
M48	Mf	10.6620	28.7217	231.7651
M5	Mf	7.5862	12.9726	221.4405
M59	Mf	7.2046	17.9422	231.0879
M6	Mf	5.7282	19.3595	227.3821
M60	Mf	3.7858	13.6715	227.1929
M7	Mf	141.3845	152.3586	300.5247
M70	Mf	11.3904	31.3831	246.4171
M71	Mf	3.7897	17.7543	215.9208
M72	Mf	5.7295	19.6700	231.5742
M73	Mf	6.7540	25.1637	243.0645
M74	Mf	12.3786	29.8072	256.3885
M75	Mf	11.3200	21.2903	219.2728
M76	Mf	11.1025	20.6416	223.8760
M77	Mf	10.3645	25.6174	208.9001
M78	Mf	7.3464	25.1089	211.1982
M8	Mf	16.9179	37.3416	283.1062
M80	Mf	8.9360	24.3417	209.2192
M81	Mf	9.9260	24.9450	233.6705
M82	Mf	8.4012	27.1421	218.0140
M83	Mf	11.2288	40.2947	269.9206

Table B2 cont.

Actual classification		Mf	MSM	Oxb
M25	Mf	0.999663	0.000337	0.000000
M26	Mf	0.993423	0.006577	0.000000
M27	Mf	0.997235	0.002765	0.000000
M28	Mf	0.992390	0.007610	0.000000
M29	Mf	0.994611	0.005389	0.000000
M3	Mf	0.995424	0.004576	0.000000
M30	Mf	0.996485	0.003515	0.000000
M31	Mf	0.987935	0.012065	0.000000
M32	Mf	0.999607	0.000393	0.000000
M33	Mf	0.999985	0.000015	0.000000
M34	Mf	0.999997	0.000003	0.000000
M35	Mf	1.000000	0.000000	0.000000
M36	Mf	0.999591	0.000409	0.000000
M37	Mf	0.999862	0.000138	0.000000
M38	Mf	0.985398	0.014602	0.000000
M39	Mf	0.990699	0.009301	0.000000
M4	Mf	0.989721	0.010279	0.000000
M40	Mf	0.999702	0.000298	0.000000
M41	Mf	0.999168	0.000832	0.000000
M42	Mf	0.980499	0.019501	0.000000
M45	Mf	0.999721	0.000279	0.000000
M46	Mf	0.999631	0.000369	0.000000
M47	Mf	0.999855	0.000145	0.000000
M48	Mf	0.999880	0.000120	0.000000
M5	Mf	0.936623	0.063377	0.000000
M59	Mf	0.995362	0.004638	0.000000
M6	Mf	0.998905	0.001095	0.000000
M60	Mf	0.992916	0.007084	0.000000
M7	Mf	0.995877	0.004123	0.000000
M70	Mf	0.999954	0.000046	0.000000
M71	Mf	0.999073	0.000927	0.000000
M72	Mf	0.999061	0.000939	0.000000
M73	Mf	0.999899	0.000101	0.000000
M74	Mf	0.999836	0.000164	0.000000
M75	Mf	0.993208	0.006792	0.000000
M76	Mf	0.991587	0.008413	0.000000
M77	Mf	0.999513	0.000487	0.000000
M78	Mf	0.999861	0.000139	0.000000
M8	Mf	0.999963	0.000037	0.000000
M80	Mf	0.999549	0.000451	0.000000
M81	Mf	0.999452	0.000548	0.000000
M82	Mf	0.999915	0.000085	0.000000
M83	Mf	1.000000	0.000000	0.000000

Table B1 cont.

Actual classification		Mf	MSM	Oxb
M84	Mf	13.1307	39.1756	270.9067
M85	Mf	9.6663	27.5759	238.5988
M86	Mf	6.3095	26.8910	245.7204
M87	Mf	13.7971	25.8207	240.6420
M88	Mf	8.1885	26.2698	208.1276
M89	Mf	8.3807	29.2192	235.3087
M9	Mf	8.2583	23.7240	216.2937
M91	Mf	31.2373	45.3507	285.4250
M92	Mf	14.4462	30.4396	249.9213
M93	Mf	5.8971	17.8851	211.8123
M94	Mf	12.0331	36.9244	241.1805
M95	Mf	9.9191	29.2862	230.4410
M96	Mf	13.3454	37.6046	251.5723
M97	Mf	10.4226	41.6933	280.5893
M98	Mf	6.4075	27.2903	230.2418
M99	Mf	7.1061	28.5901	243.0194
MLP-07	Mf	12.4540	22.4161	241.2774
MLP-08	Mf	9.7412	21.0693	244.0154
MLP-09	Mf	10.3740	17.4323	236.6081
MLP-11	Mf	27.1769	33.4171	245.2238
MLP-12	Mf	63.8172	66.0200	270.5800
MLP-13	Mf	58.3341	63.4082	274.7317
MLP-14	Mf	12.3750	21.3706	205.4349
MLP-155	Mf	18.6914	28.3200	220.7972
MLP-156	Mf	11.2508	21.8798	244.7616
MLP-157	Mf	14.3590	26.1762	234.1499
MLP-158	Mf	11.5400	32.1470	264.7198
MLP-159	Mf	8.3987	26.3260	249.3279
MLP-160	Mf	9.7116	14.7044	233.8168
MLP-161	Mf	10.4359	19.8349	239.7423
MLP-162	Mf	11.0611	19.4777	224.4178
MLP-164	Mf	10.3266	27.1442	224.5383
MLP-165	Mf	4.4063	16.9349	211.1010
MLP-169	Mf	20.8694	37.5938	191.2959
MLP-170	Mf	18.1496	36.7018	255.1909
MLP-171	Mf	8.3882	32.3860	206.9026
MLP-172	Mf	7.4928	26.0282	187.3727
MLP-174	Mf	13.0060	30.9622	238.8022
MLP-175	Mf	9.9428	21.6318	218.7265
MLP-176	Mf	11.6800	32.2323	226.4823
MLP-177	Mf	100.2693	121.3784	329.7103
MLP-178	Mf	19.6686	43.3042	242.9267
MLP-180	Mf	14.8234	38.5003	223.7479

Table B2 cont.

Actual classification		Mf	MSM	Oxb
M84	Mf	0.999998	0.000002	0.000000
M85	Mf	0.999871	0.000129	0.000000
M86	Mf	0.999966	0.000034	0.000000
M87	Mf	0.997556	0.002444	0.000000
M88	Mf	0.999882	0.000118	0.000000
M89	Mf	0.999970	0.000030	0.000000
M9	Mf	0.999562	0.000438	0.000000
M91	Mf	0.999139	0.000861	0.000000
M92	Mf	0.999664	0.000336	0.000000
M93	Mf	0.997512	0.002488	0.000000
M94	Mf	0.999996	0.000004	0.000000
M95	Mf	0.999938	0.000062	0.000000
M96	Mf	0.999995	0.000005	0.000000
M97	Mf	1.000000	0.000000	0.000000
M98	Mf	0.999971	0.000029	0.000000
M99	Mf	0.999978	0.000022	0.000000
MLP-07	Mf	0.993180	0.006820	0.000000
MLP-08	Mf	0.996544	0.003456	0.000000
MLP-09	Mf	0.971506	0.028494	0.000000
MLP-11	Mf	0.957716	0.042284	0.000000
MLP-12	Mf	0.750517	0.249483	0.000000
MLP-13	Mf	0.926698	0.073302	0.000000
MLP-14	Mf	0.988989	0.011011	0.000000
MLP-155	Mf	0.991953	0.008047	0.000000
MLP-156	Mf	0.995104	0.004896	0.000000
MLP-157	Mf	0.997291	0.002709	0.000000
MLP-158	Mf	0.999966	0.000034	0.000000
MLP-159	Mf	0.999872	0.000128	0.000000
MLP-160	Mf	0.923890	0.076110	0.000000
MLP-161	Mf	0.990982	0.009018	0.000000
MLP-162	Mf	0.985346	0.014654	0.000000
MLP-164	Mf	0.999777	0.000223	0.000000
MLP-165	Mf	0.998101	0.001899	0.000000
MLP-169	Mf	0.999767	0.000233	0.000000
MLP-170	Mf	0.999906	0.000094	0.000000
MLP-171	Mf	0.999994	0.000006	0.000000
MLP-172	Mf	0.999906	0.000094	0.000000
MLP-174	Mf	0.999874	0.000126	0.000000
MLP-175	Mf	0.997113	0.002887	0.000000
MLP-176	Mf	0.999966	0.000034	0.000000
MLP-177	Mf	0.999974	0.000026	0.000000
MLP-178	Mf	0.999993	0.000007	0.000000
MLP-180	Mf	0.999993	0.000007	0.000000

Table B1 cont.

Actual classification		Mf	MSM	Oxb
ON19-2	Mf	16.4766	27.5129	213.1161
ON20-2	Mf	8.0785	26.0724	262.5423
ON-21	Mf	13.4005	35.6621	267.8218
ON22-2	Mf	9.0920	28.1103	229.3795
ON-23	Mf	17.9356	27.7211	238.3157
ON-24	Mf	5.9693	17.6414	226.2737
ON-25	Mf	7.7609	22.5165	228.1001
ON28-2	Mf	10.3661	15.4929	203.1630
ON-29	Mf	17.2825	20.7897	194.9643
ON30-2	Mf	37.0292	39.3494	255.1682
***ON31-2**	Mf	11.9301	8.9186	198.6778
ON-35	Mf	15.2103	45.3734	242.5904
ON36-1	Mf	9.5081	32.6323	215.3495
ON-37	Mf	17.9264	44.7594	228.8723
ON38-3	Mf	21.6116	45.9125	224.0304
ON41-2	Mf	7.8884	28.8369	225.0220
ON-42	Mf	10.7997	36.8201	229.1663
ON-43	Mf	9.1429	35.4931	252.8095
ON44-2	Mf	11.7745	25.9447	231.7020
ON-45	Mf	12.7642	24.2560	215.9645
OXB-42	Mf	9.6839	25.8552	226.1715
OXB-43	Mf	7.0263	21.4794	219.6800
OXB-44	Mf	15.0319	15.6950	170.3089
OXB-45	Mf	12.8533	25.9096	194.0488
OXB-50	Mf	9.4815	29.6646	229.4329
OXB-55	Mf	8.1081	26.6542	223.3679
OXB-56	Mf	9.7629	28.6021	229.5047
OXB-57	Mf	14.5837	23.0772	193.7560
OXB-58	Mf	22.9462	32.3561	187.9681
OXB-59	Mf	28.2341	31.4065	182.8541
SOM-100	Mf	10.2604	31.7156	214.4702
***SOM-40**	Mf	13.0626	9.3528	209.7775
SOM-82	Mf	8.7979	20.8863	224.4798
SOM-83	Mf	16.3020	26.2215	236.8269
SOM-84	Mf	11.4311	22.3089	215.1178
SOM-86	Mf	28.9926	42.1306	307.5918
SOM-87	Mf	7.3572	16.7987	209.0151
SOM-91	Mf	11.5558	34.0171	219.9083
SOM-92	Mf	29.5160	40.5451	280.9456
SOM-94	Mf	22.2857	40.0248	240.6190
SOM-95	Mf	6.6185	31.8190	255.5151
SOM-96	Mf	8.3363	28.9652	251.2900
SOM-97	Mf	11.5514	32.5276	239.9841

Table B2 cont.

Actual classification		Mf	MSM	Oxb
ON19-2	Mf	0.996003	0.003997	0.000000
ON20-2	Mf	0.999876	0.000124	0.000000
ON-21	Mf	0.999985	0.000015	0.000000
ON22-2	Mf	0.999926	0.000074	0.000000
ON-23	Mf	0.992555	0.007445	0.000000
ON-24	Mf	0.997088	0.002912	0.000000
ON-25	Mf	0.999375	0.000625	0.000000
ON28-2	Mf	0.928467	0.071533	0.000000
ON-29	Mf	0.852405	0.147595	0.000000
ON30-2	Mf	0.761351	0.238649	0.000000
***ON31-2**	Mf	0.181571	0.818429	0.000000
ON-35	Mf	1.000000	0.000000	0.000000
ON36-1	Mf	0.999990	0.000010	0.000000
ON-37	Mf	0.999999	0.000001	0.000000
ON38-3	Mf	0.999995	0.000005	0.000000
ON41-2	Mf	0.999972	0.000028	0.000000
ON-42	Mf	0.999998	0.000002	0.000000
ON-43	Mf	0.999998	0.000002	0.000000
ON44-2	Mf	0.999163	0.000837	0.000000
ON-45	Mf	0.996814	0.003186	0.000000
OXB-42	Mf	0.999692	0.000308	0.000000
OXB-43	Mf	0.999274	0.000726	0.000000
OXB-44	Mf	0.582140	0.417860	0.000000
OXB-45	Mf	0.998540	0.001460	0.000000
OXB-50	Mf	0.999959	0.000041	0.000000
OXB-55	Mf	0.999906	0.000094	0.000000
OXB-56	Mf	0.999919	0.000081	0.000000
OXB-57	Mf	0.985892	0.014108	0.000000
OXB-58	Mf	0.991031	0.008969	0.000000
OXB-59	Mf	0.830081	0.169919	0.000000
SOM-100	Mf	0.999978	0.000022	0.000000
***SOM-40**	Mf	0.135298	0.864702	0.000000
SOM-82	Mf	0.997634	0.002366	0.000000
SOM-83	Mf	0.993034	0.006966	0.000000
SOM-84	Mf	0.995675	0.004325	0.000000
SOM-86	Mf	0.998599	0.001401	0.000000
SOM-87	Mf	0.991170	0.008830	0.000000
SOM-91	Mf	0.999987	0.000013	0.000000
SOM-92	Mf	0.995988	0.004012	0.000000
SOM-94	Mf	0.999859	0.000141	0.000000
SOM-95	Mf	0.999997	0.000003	0.000000
SOM-96	Mf	0.999967	0.000033	0.000000
SOM-97	Mf	0.999972	0.000028	0.000000

Table B1 cont.

Actual classification		Mf	MSM	Oxb
SOM-98	Mf	6.2029	27.6946	226.0445
SOM-99	Mf	7.0504	22.5419	222.1539
SP-28	Mf	4.8963	13.5496	208.0109
SP-29	Mf	8.0811	12.4635	211.6442
SP-30	Mf	11.9885	15.7501	187.9397
SP-31	Mf	7.0234	19.5577	240.4589
SP-38	Mf	16.8976	40.2618	230.6130
SP-39	Mf	17.0842	43.0869	260.9568
SP-40	Mf	6.6147	30.9693	226.0966
SP-41	Mf	65.6176	93.9149	273.3515
SP-42	Mf	19.6941	43.6452	239.6564
SP-43	Mf	205.7887	256.7515	444.3597
SP-44B	Mf	79.8643	123.0740	309.2781
BMC-02	Mf	26.7580	44.7600	253.3015
BMC-04	Mf	28.5138	42.6193	279.9334
BMC-05	Mf	14.2937	23.0994	240.8898
BMC-06	Mf	6.5598	22.3977	220.7527
BMC-07	Mf	18.4782	42.4836	256.8152
BUS-22	Mf	10.5230	21.4280	197.5129
M10	Mf	25.7544	33.1514	240.7805
M11	Mf	19.5079	33.9851	241.6421
M12	Mf	13.4311	25.1148	238.1940
M13	Mf	16.4345	25.8228	238.1841
M130	Mf	19.8755	29.4042	260.5847
M131	Mf	15.9692	18.9711	218.0786
M132	Mf	25.9853	42.0117	262.3639
M133	Mf	8.6515	21.4317	225.0157
M134	Mf	7.1119	17.0157	205.3069
M135	Mf	9.3496	23.2230	234.6460
M14	Mf	19.5348	30.9668	247.1687
M15	Mf	19.8507	31.6657	240.4789
M16	Mf	22.5802	42.4735	284.9135
M17	Mf	13.8297	30.1701	258.3044
M18	Mf	14.1943	29.5065	233.9983
M19	Mf	26.8432	55.9933	286.1500
M20	Mf	10.0550	29.1826	262.4646
M61	Mf	54.7726	88.5653	332.4251
M62	Mf	18.5365	38.0168	260.4534
M63	Mf	66.0883	75.3431	309.5126
M64	Mf	12.7184	28.4228	258.1060
M65	Mf	20.6628	33.6341	263.4937
M66	Mf	19.7843	35.9156	257.1171
M67	Mf	22.7942	28.4797	241.7911

Table B2 cont.

Actual classification		Mf	MSM	Oxb
SOM-98	Mf	0.999978	0.000022	0.000000
SOM-99	Mf	0.999568	0.000432	0.000000
SP-28	Mf	0.986960	0.013040	0.000000
SP-29	Mf	0.899458	0.100542	0.000000
SP-30	Mf	0.867700	0.132300	0.000000
SP-31	Mf	0.998106	0.001894	0.000000
SP-38	Mf	0.999992	0.000008	0.000000
SP-39	Mf	0.999998	0.000002	0.000000
SP-40	Mf	0.999995	0.000005	0.000000
SP-41	Mf	0.999999	0.000001	0.000000
SP-42	Mf	0.999994	0.000006	0.000000
SP-43	Mf	1.000000	0.000000	0.000000
SP-44B	Mf	1.000000	0.000000	0.000000
BMC-02	Mf	0.999877	0.000123	0.000000
BMC-04	Mf	0.999136	0.000864	0.000000
BMC-05	Mf	0.987906	0.012094	0.000000
BMC-06	Mf	0.999636	0.000364	0.000000
BMC-07	Mf	0.999994	0.000006	0.000000
BUS-22	Mf	0.995733	0.004267	0.000000
M10	Mf	0.975838	0.024162	0.000000
M11	Mf	0.999282	0.000718	0.000000
M12	Mf	0.997105	0.002895	0.000000
M13	Mf	0.990934	0.009066	0.000000
M130	Mf	0.991544	0.008456	0.000000
M131	Mf	0.817714	0.182286	0.000000
M132	Mf	0.999669	0.000331	0.000000
M133	Mf	0.998325	0.001675	0.000000
M134	Mf	0.992980	0.007020	0.000000
M135	Mf	0.999029	0.000971	0.000000
M14	Mf	0.996718	0.003282	0.000000
M15	Mf	0.997288	0.002712	0.000000
M16	Mf	0.999952	0.000048	0.000000
M17	Mf	0.999717	0.000283	0.000000
M18	Mf	0.999527	0.000473	0.000000
M19	Mf	1.000000	0.000000	0.000000
M20	Mf	0.999930	0.000070	0.000000
M61	Mf	1.000000	0.000000	0.000000
M62	Mf	0.999941	0.000059	0.000000
M63	Mf	0.990315	0.009685	0.000000
M64	Mf	0.999611	0.000389	0.000000
M65	Mf	0.998477	0.001523	0.000000
M66	Mf	0.999686	0.000314	0.000000
M67	Mf	0.944943	0.055057	0.000000

Table B1 cont.

Actual classification		Mf	MSM	Oxb
M68	Mf	51.5683	59.9379	208.0878
M69	Mf	12.7159	20.1474	232.9094
MLP-01	Mf	14.3363	40.7775	258.8308
MLP-02	Mf	35.9440	44.7294	265.3087
MLP-03	Mf	17.8561	21.2670	204.8071
MLP-04	Mf	26.6728	36.3922	250.7282
MLP-05	Mf	8.7736	22.4358	203.7514
MLP-166	Mf	21.2283	30.9591	216.3765
MLP-167	Mf	11.7605	21.3543	231.6805
MLP-168	Mf	5.4807	18.9206	219.0985
ON-39	Mf	35.1575	63.8662	233.7547
ON40-2	Mf	23.5613	43.5944	257.8704
ON-47	Mf	25.6596	40.9025	249.6169
OXB-46	Mf	18.0272	33.4038	205.6906
OXB-47	Mf	20.2617	31.7327	204.3879
OXB-48	Mf	6.4768	21.3247	204.0563
OXB-49	Mf	12.5141	33.9813	217.0064
OXB-52	Mf	11.0818	24.7498	185.2046
OXB-54	Mf	9.4071	32.4693	200.5162
SP-32	Mf	6.9692	12.6400	212.8370
SP-33	Mf	11.5593	20.7846	226.0102
SP-34	Mf	13.9711	31.0355	243.8985
SP-35	Mf	20.0229	28.4357	230.7163
SP-36	Mf	19.5654	40.1659	233.0742
SP-37	Mf	46.5893	58.2669	242.7373
***BMC13-1**	MSM	16.9939	19.5229	207.5856
***BMC-14**	MSM	8.6635	9.3232	207.0174
BMC15-3	MSM	18.0324	6.9725	203.4970
BMC-16	MSM	23.6853	13.1231	208.3853
BMC-17	MSM	28.3185	8.4611	179.2417
BMC-18	MSM	21.0634	3.5742	158.2189
BUS-29	MSM	17.2342	5.7962	203.7557
BUS-30	MSM	14.1143	5.9088	216.4085
BUS-31	MSM	32.4357	21.9192	240.4901
BUS-32	MSM	16.3794	6.1345	213.3958
BUS-33	MSM	24.1846	4.7551	195.5557
MLP-146	MSM	33.7199	7.3675	184.0343
MLP-147	MSM	36.1449	11.8647	191.3122
MLP-148	MSM	19.2363	4.9618	214.1438
MLP-149	MSM	20.4341	11.7575	248.2926
MLP-150	MSM	23.8735	8.6132	217.7709
MLP-151	MSM	26.2503	10.1823	229.4544
MLP-152	MSM	21.1582	8.1857	217.3719

Table B2 cont.

Actual classification		Mf	MSM	Oxb
M68	Mf	0.985003	0.014997	0.000000
M69	Mf	0.976242	0.023758	0.000000
MLP-01	Mf	0.999998	0.000002	0.000000
MLP-02	Mf	0.987784	0.012216	0.000000
MLP-03	Mf	0.846250	0.153750	0.000000
MLP-04	Mf	0.992307	0.007693	0.000000
MLP-05	Mf	0.998921	0.001079	0.000000
MLP-166	Mf	0.992350	0.007650	0.000000
MLP-167	Mf	0.991812	0.008188	0.000000
MLP-168	Mf	0.998795	0.001205	0.000000
ON-39	Mf	0.999999	0.000001	0.000000
ON40-2	Mf	0.999955	0.000045	0.000000
ON-47	Mf	0.999510	0.000490	0.000000
OXB-46	Mf	0.999542	0.000458	0.000000
OXB-47	Mf	0.996781	0.003219	0.000000
OXB-48	Mf	0.999404	0.000596	0.000000
OXB-49	Mf	0.999978	0.000022	0.000000
OXB-52	Mf	0.998925	0.001075	0.000000
OXB-54	Mf	0.999990	0.000010	0.000000
SP-32	Mf	0.944560	0.055440	0.000000
SP-33	Mf	0.990172	0.009828	0.000000
SP-34	Mf	0.999803	0.000197	0.000000
SP-35	Mf	0.985319	0.014681	0.000000
SP-36	Mf	0.999966	0.000034	0.000000
SP-37	Mf	0.997096	0.002904	0.000000
***BMC13-1**	MSM	0.779794	0.220206	0.000000
***BMC-14**	MSM	0.581717	0.418283	0.000000
BMC15-3	MSM	0.003951	0.996049	0.000000
BMC-16	MSM	0.005061	0.994939	0.000000
BMC-17	MSM	0.000049	0.999951	0.000000
BMC-18	MSM	0.000159	0.999841	0.000000
BUS-29	MSM	0.003272	0.996728	0.000000
BUS-30	MSM	0.016258	0.983742	0.000000
BUS-31	MSM	0.005178	0.994822	0.000000
BUS-32	MSM	0.005926	0.994074	0.000000
BUS-33	MSM	0.000060	0.999940	0.000000
MLP-146	MSM	0.000002	0.999998	0.000000
MLP-147	MSM	0.000005	0.999995	0.000000
MLP-148	MSM	0.000794	0.999206	0.000000
MLP-149	MSM	0.012890	0.987110	0.000000
MLP-150	MSM	0.000485	0.999515	0.000000
MLP-151	MSM	0.000324	0.999676	0.000000
MLP-152	MSM	0.001522	0.998478	0.000000

Table B1 cont.

Actual classification		Mf	MSM	Oxb
MLP-153	MSM	23.2616	9.4276	221.8252
MLP-154	MSM	11.9717	11.4758	218.2903
***MLP-15A**	MSM	42.0027	50.0950	262.4917
MLP-15B	MSM	86.8844	55.8105	271.1201
MLP-16	MSM	151.8006	108.0554	296.9484
MLP-17	MSM	22.2772	5.4184	189.5781
MLP-18	MSM	21.3789	9.2207	218.9469
MLP-19	MSM	22.9822	14.0970	201.3884
ON-04	MSM	26.7563	8.3074	170.2405
ON33-2	MSM	27.1316	15.8924	163.9287
ON34-3	MSM	45.5194	15.0404	192.5328
OXB-37	MSM	37.7536	9.2742	155.5610
OXB-38	MSM	20.7796	15.8180	213.4337
OXB-39	MSM	39.5166	14.9419	200.3845
OXB-40	MSM	31.2862	17.0336	198.4174
OXB-41	MSM	58.2636	30.5978	187.1655
SOM-33	MSM	31.4569	22.7963	249.7214
SOM-34	MSM	24.2322	16.4673	249.8015
SOM-35	MSM	21.4130	10.1030	226.7772
SOM-36	MSM	34.9858	29.0302	259.2527
SOM-37	MSM	20.8647	7.9052	219.6771
SOM-38A	MSM	34.6476	23.9818	220.2715
SOM-39	MSM	40.3403	28.8285	286.0437
SP-21	MSM	27.0364	6.2900	187.6899
SP23-2	MSM	37.2959	13.4111	183.1280
SP-24	MSM	41.9185	14.7191	175.6545
SP-25	MSM	57.8379	34.8380	205.8552
SP-26	MSM	31.6860	15.9873	208.7348
SP-27	MSM	23.9520	20.1781	242.3920
BMC19-2	MSM	21.3288	8.4308	157.5064
BMC-20	MSM	24.6149	16.5506	151.2081
BMC25-2	MSM	24.6534	14.9197	157.8033
BMC-28	MSM	28.1364	12.3872	159.7772
BMC-29	MSM	23.7812	10.0093	140.1364
BMC32-2	MSM	28.3846	20.8325	120.3413
BUS-34	MSM	19.5601	12.1131	199.9200
BUS-35	MSM	14.8919	6.1344	192.0309
BUS-36	MSM	18.0704	13.2715	177.7194
BUS-37	MSM	16.0259	8.3049	177.7661
BUS-38	MSM	20.3729	10.6646	172.2872
BUS-39	MSM	29.0933	18.1884	192.2349
BUS-40	MSM	12.1979	5.9601	182.4938
MLM-01	MSM	19.6163	4.8845	146.9770

Table B2 cont.

Actual classification		Mf	MSM	Oxb
MLP-153	MSM	0.000990	0.999010	0.000000
MLP-154	MSM	0.438322	0.561678	0.000000
***MLP-15A**	MSM	0.982810	0.017190	0.000000
MLP-15B	MSM	0.000000	1.000000	0.000000
MLP-16	MSM	0.000000	1.000000	0.000000
MLP-17	MSM	0.000218	0.999782	0.000000
MLP-18	MSM	0.002285	0.997715	0.000000
MLP-19	MSM	0.011628	0.988372	0.000000
ON-04	MSM	0.000099	0.999901	0.000000
ON33-2	MSM	0.003613	0.996387	0.000000
ON34-3	MSM	0.000000	1.000000	0.000000
OXB-37	MSM	0.000001	0.999999	0.000000
OXB-38	MSM	0.077216	0.922784	0.000000
OXB-39	MSM	0.000005	0.999995	0.000000
OXB-40	MSM	0.000803	0.999197	0.000000
OXB-41	MSM	0.000001	0.999999	0.000000
SOM-33	MSM	0.012993	0.987007	0.000000
SOM-34	MSM	0.020184	0.979816	0.000000
SOM-35	MSM	0.003488	0.996512	0.000000
SOM-36	MSM	0.048438	0.951562	0.000000
SOM-37	MSM	0.001532	0.998468	0.000000
SOM-38A	MSM	0.004807	0.995193	0.000000
SOM-39	MSM	0.003154	0.996846	0.000000
SP-21	MSM	0.000031	0.999969	0.000000
SP23-2	MSM	0.000007	0.999993	0.000000
SP-24	MSM	0.000001	0.999999	0.000000
SP-25	MSM	0.000010	0.999990	0.000000
SP-26	MSM	0.000390	0.999610	0.000000
SP-27	MSM	0.131594	0.868406	0.000000
BMC19-2	MSM	0.001580	0.998420	0.000000
BMC-20	MSM	0.017427	0.982573	0.000000
BMC25-2	MSM	0.007639	0.992361	0.000000
BMC-28	MSM	0.000380	0.999620	0.000000
BMC-29	MSM	0.001021	0.998979	0.000000
BMC32-2	MSM	0.022399	0.977601	0.000000
BUS-34	MSM	0.023580	0.976420	0.000000
BUS-35	MSM	0.012386	0.987614	0.000000
BUS-36	MSM	0.083215	0.916785	0.000000
BUS-37	MSM	0.020623	0.979377	0.000000
BUS-38	MSM	0.007735	0.992265	0.000000
BUS-39	MSM	0.004268	0.995732	0.000000
BUS-40	MSM	0.042335	0.957665	0.000000
MLM-01	MSM	0.000632	0.999368	0.000000

Table B1 cont.

Actual classification		Mf	MSM	Oxb
MLM-02	MSM	32.8505	13.3959	154.0602
MLM-03	MSM	21.9003	7.8095	169.0998
MLM-04	MSM	24.6001	12.3892	174.4422
MLM-05	MSM	18.6724	5.3630	145.9629
MLM-06	MSM	34.0469	14.1635	144.7703
MLM-07	MSM	43.9046	26.1634	155.5780
MLM-08	MSM	18.3278	5.1208	172.1169
MLM-09	MSM	17.5624	6.3007	143.7005
MLM-10	MSM	18.3695	9.3027	160.4941
MLM-11	MSM	30.1112	12.7733	166.0157
MLM-12	MSM	22.3070	8.8582	174.5704
MLM-13	MSM	25.1948	9.5002	178.8559
MLM-14	MSM	25.2174	9.1498	168.9625
MLM-15	MSM	36.0966	13.9417	136.0451
MLM-16	MSM	34.7096	11.8612	181.4882
MLM-17	MSM	49.8592	30.0874	179.5301
MLP-124	MSM	58.9543	24.1727	143.7394
MLP-125	MSM	45.2380	16.1351	156.3560
MLP-126	MSM	47.1625	18.8016	136.7025
MLP-127	MSM	34.5343	26.1684	189.2657
MLP-128	MSM	10.2013	7.3557	168.4596
MLP-129	MSM	22.1196	20.9548	197.8371
MLP-130	MSM	53.1099	36.1543	198.9666
MLP-131	MSM	26.5985	17.2941	190.5088
MLP-132	MSM	28.4555	12.5052	183.5178
MLP-133	MSM	40.6441	25.9905	154.3044
MLP-134	MSM	39.0098	23.4789	206.6172
MLP-136	MSM	19.5293	7.1654	187.0599
MLP-137	MSM	23.9853	8.9221	185.3635
MLP-138	MSM	16.9417	7.9376	207.7971
MLP-139	MSM	16.0945	9.5456	181.0127
MLP-140	MSM	26.7377	11.2229	161.4721
MLP-141	MSM	21.3911	9.7216	169.8749
MLP-142	MSM	16.1044	4.7294	187.0197
MLP-143	MSM	18.9444	5.5994	189.0165
MLP-144	MSM	18.8487	6.6083	200.5176
MLP-145	MSM	21.5017	5.5879	171.1974
MLP-20	MSM	23.9777	12.3691	191.5056
MLP-21	MSM	407.9956	406.2668	589.8344
MLP-22	MSM	26.4349	10.0484	197.8016
MLP-23	MSM	27.7872	10.6058	169.9401
MLP-24	MSM	37.4213	15.1532	183.9343
MLP-25	MSM	18.7442	10.4823	189.4444

Table B2 cont.

Actual classification		Mf	MSM	Oxb
MLM-02	MSM	0.000060	0.999940	0.000000
MLM-03	MSM	0.000871	0.999129	0.000000
MLM-04	MSM	0.002226	0.997774	0.000000
MLM-05	MSM	0.001286	0.998714	0.000000
MLM-06	MSM	0.000048	0.999952	0.000000
MLM-07	MSM	0.000140	0.999860	0.000000
MLM-08	MSM	0.001354	0.998646	0.000000
MLM-09	MSM	0.003573	0.996427	0.000000
MLM-10	MSM	0.010629	0.989371	0.000000
MLM-11	MSM	0.000172	0.999828	0.000000
MLM-12	MSM	0.001200	0.998800	0.000000
MLM-13	MSM	0.000391	0.999609	0.000000
MLM-14	MSM	0.000324	0.999676	0.000000
MLM-15	MSM	0.000015	0.999985	0.000000
MLM-16	MSM	0.000011	0.999989	0.000000
MLM-17	MSM	0.000051	0.999949	0.000000
MLP-124	MSM	0.000000	1.000000	0.000000
MLP-125	MSM	0.000000	1.000000	0.000000
MLP-126	MSM	0.000001	0.999999	0.000000
MLP-127	MSM	0.015025	0.984975	0.000000
MLP-128	MSM	0.194226	0.805774	0.000000
MLP-129	MSM	0.358373	0.641627	0.000000
MLP-130	MSM	0.000208	0.999792	0.000000
MLP-131	MSM	0.009450	0.990550	0.000000
MLP-132	MSM	0.000344	0.999656	0.000000
MLP-133	MSM	0.000657	0.999343	0.000000
MLP-134	MSM	0.000424	0.999576	0.000000
MLP-136	MSM	0.002062	0.997938	0.000000
MLP-137	MSM	0.000536	0.999464	0.000000
MLP-138	MSM	0.010965	0.989035	0.000000
MLP-139	MSM	0.036459	0.963541	0.000000
MLP-140	MSM	0.000427	0.999573	0.000000
MLP-141	MSM	0.002916	0.997084	0.000000
MLP-142	MSM	0.003377	0.996623	0.000000
MLP-143	MSM	0.001264	0.998736	0.000000
MLP-144	MSM	0.002193	0.997807	0.000000
MLP-145	MSM	0.000350	0.999650	0.000000
MLP-20	MSM	0.003006	0.996994	0.000000
MLP-21	MSM	0.296424	0.703576	0.000000
MLP-22	MSM	0.000276	0.999724	0.000000
MLP-23	MSM	0.000186	0.999814	0.000000
MLP-24	MSM	0.000015	0.999985	0.000000
MLP-25	MSM	0.015814	0.984186	0.000000

Table B1 cont.

Actual classification		Mf	MSM	Oxb
MLP-26	MSM	20.1428	2.3348	157.2919
MLP-27	MSM	17.9337	5.4066	189.2882
MLP-28	MSM	17.9894	8.3583	173.9604
MLP-30	MSM	20.3800	6.2831	182.2869
MLP-31	MSM	27.6030	10.7343	193.0569
MLP-32	MSM	42.4607	12.9290	150.7438
MLP-33	MSM	15.0314	13.0752	184.2249
***MLP-34**	MSM	11.6739	11.9014	182.8241
MLP-35	MSM	40.6023	21.0588	158.7999
MLP-36	MSM	56.6401	23.6456	170.8289
MLP-37	MSM	73.1510	43.2901	205.0124
ON-05	MSM	21.5563	8.3145	155.8741
ON-07	MSM	25.4779	6.8589	167.5796
ON-10-2	MSM	17.6506	13.8228	199.2171
ON-11	MSM	24.2460	16.8886	173.0878
ON-16	MSM	27.0720	7.1641	148.3585
ON-17	MSM	22.4155	10.0600	184.0068
ON-18	MSM	29.1752	10.3759	197.4332
OXB-14	MSM	17.8969	9.4490	158.9721
OXB-15	MSM	25.9539	21.1811	158.9146
OXB-16	MSM	18.6451	11.0221	146.7484
OXB-18	MSM	31.9392	13.5556	150.7686
OXB-19	MSM	30.8839	7.5822	128.5446
OXB-20	MSM	40.1337	17.1655	164.9121
OXB-21	MSM	32.2516	10.4347	160.1438
OXB-26	MSM	31.4277	13.6934	170.9183
OXB-27	MSM	38.1790	9.6752	139.4366
OXB-28	MSM	16.1189	10.7150	173.1117
OXB-30	MSM	29.7482	14.0443	228.9172
OXB-31	MSM	20.3021	11.2049	169.2558
OXB-32	MSM	29.3628	20.9537	193.8487
OXB-33	MSM	21.8837	21.0254	206.3609
OXB-34	MSM	30.8154	8.2812	181.3130
OXB-35	MSM	55.6147	37.3082	214.7701
SOM-19	MSM	25.6042	12.9428	227.5550
SOM-20	MSM	36.9509	17.4486	202.3193
SOM-21	MSM	21.4917	5.8495	182.3492
SOM-22	MSM	24.9973	15.8963	227.2099
SOM-23	MSM	20.5229	9.9756	226.2632
SOM-25	MSM	61.6453	61.2556	237.9766
SOM-26	MSM	24.9421	8.2338	172.0195
SOM-27	MSM	18.5343	7.8582	191.7771
SOM-28	MSM	18.5093	3.8545	173.3268

Table B2 cont.

Actual classification		Mf	MSM	Oxb
MLP-26	MSM	0.000136	0.999864	0.000000
MLP-27	MSM	0.001901	0.998099	0.000000
MLP-28	MSM	0.008038	0.991962	0.000000
MLP-30	MSM	0.000868	0.999132	0.000000
MLP-31	MSM	0.000217	0.999783	0.000000
MLP-32	MSM	0.000000	1.000000	0.000000
MLP-33	MSM	0.273265	0.726735	0.000000
***MLP-34**	MSM	0.528403	0.471597	0.000000
MLP-35	MSM	0.000057	0.999943	0.000000
MLP-36	MSM	0.000000	1.000000	0.000000
MLP-37	MSM	0.000000	1.000000	0.000000
ON-05	MSM	0.001330	0.998670	0.000000
ON-07	MSM	0.000091	0.999909	0.000000
ON-10-2	MSM	0.128547	0.871453	0.000000
ON-11	MSM	0.024633	0.975367	0.000000
ON-16	MSM	0.000048	0.999952	0.000000
ON-17	MSM	0.002071	0.997929	0.000000
ON-18	MSM	0.000083	0.999917	0.000000
OXB-14	MSM	0.014429	0.985571	0.000000
OXB-15	MSM	0.084219	0.915781	0.000000
OXB-16	MSM	0.021637	0.978363	0.000000
OXB-18	MSM	0.000102	0.999898	0.000000
OXB-19	MSM	0.000009	0.999991	0.000000
OXB-20	MSM	0.000010	0.999990	0.000000
OXB-21	MSM	0.000018	0.999982	0.000000
OXB-26	MSM	0.000141	0.999859	0.000000
OXB-27	MSM	0.000001	0.999999	0.000000
OXB-28	MSM	0.062860	0.937140	0.000000
OXB-30	MSM	0.000389	0.999611	0.000000
OXB-31	MSM	0.010471	0.989529	0.000000
OXB-32	MSM	0.014708	0.985292	0.000000
OXB-33	MSM	0.394332	0.605668	0.000000
OXB-34	MSM	0.000013	0.999987	0.000000
OXB-35	MSM	0.000106	0.999894	0.000000
SOM-19	MSM	0.001778	0.998222	0.000000
SOM-20	MSM	0.000058	0.999942	0.000000
SOM-21	MSM	0.000401	0.999599	0.000000
SOM-22	MSM	0.010451	0.989549	0.000000
SOM-23	MSM	0.005099	0.994901	0.000000
SOM-25	MSM	0.451441	0.548559	0.000000
SOM-26	MSM	0.000235	0.999765	0.000000
SOM-27	MSM	0.004782	0.995218	0.000000
SOM-28	MSM	0.000657	0.999343	0.000000

Table B1 cont.

Actual classification		Mf	MSM	Oxb
SOM-29	MSM	16.1397	5.6278	171.8540
SOM-30	MSM	22.5570	13.1594	213.6589
SOM-31	MSM	18.0664	8.2870	199.0998
SOM-32	MSM	32.4593	26.9672	201.1218
SP10-2	MSM	34.3073	13.5572	138.5681
SP11-2	MSM	25.0112	17.0573	170.6424
SP-12	MSM	33.6232	18.8039	192.7032
SP13-3	MSM	24.4456	13.0959	199.9976
SP14-3	MSM	57.5248	40.1773	161.6968
SP16-1	MSM	15.0474	9.9558	186.8914
SP-17	MSM	19.7524	9.6538	184.6712
SP18-2	MSM	11.0810	8.7980	194.6896
SP20-2	MSM	13.6968	6.9313	191.7058
SP-22	MSM	19.6008	5.4758	186.2631
BMC-35	MSM	21.5342	5.8467	168.4679
BMC-36	MSM	10.9088	6.3286	197.7099
BMC-37	MSM	40.5902	20.0331	222.7545
MLP-111	MSM	32.0809	10.1953	150.7508
MLP-112	MSM	32.1908	8.5077	154.8043
MLP-113	MSM	26.0218	6.0582	171.0214
MLP-114	MSM	40.5576	9.9243	148.4798
MLP-115	MSM	24.4818	6.8250	173.1237
MLP-116	MSM	17.0706	4.3615	183.9742
MLP-117	MSM	18.9138	6.8801	192.1322
MLP-118	MSM	27.0958	14.9250	207.6308
MLP-119	MSM	29.0523	14.6072	199.0436
MLP-120	MSM	30.5575	18.6861	189.2333
MLP-121	MSM	41.8182	35.3014	197.1527
MLP-122	MSM	25.0294	10.6401	219.6959
MLP-123	MSM	15.3364	9.0345	228.8708
MLP-38	MSM	15.2273	8.8766	206.5817
MLP-39	MSM	15.0145	9.5852	168.5811
MLP-40	MSM	39.0394	29.2988	200.1070
MLP-41	MSM	13.9628	5.2209	170.2885
MLP-42	MSM	24.4478	12.0744	218.9016
MLP-43	MSM	30.9209	11.1632	138.3730
MLP-44	MSM	30.8331	8.9490	168.9773
MLP-45	MSM	28.3490	10.7555	166.0431
MLP-46	MSM	45.2478	21.3004	159.9890
MLP-47	MSM	26.3360	6.5059	140.0704
MLP-48	MSM	29.3963	12.0084	142.4583
MLP-50	MSM	26.9879	10.2719	132.9909
OXB-10	MSM	101.7099	86.2880	221.4751

Table B2 cont.

Actual classification		Mf	MSM	Oxb
SOM-29	MSM	0.005189	0.994811	0.000000
SOM-30	MSM	0.009024	0.990976	0.000000
SOM-31	MSM	0.007468	0.992532	0.000000
SOM-32	MSM	0.060311	0.939689	0.000000
SP10-2	MSM	0.000031	0.999969	0.000000
SP11-2	MSM	0.018398	0.981602	0.000000
SP-12	MSM	0.000605	0.999395	0.000000
SP13-3	MSM	0.003419	0.996581	0.000000
SP14-3	MSM	0.000171	0.999829	0.000000
SP16-1	MSM	0.072707	0.927293	0.000000
SP-17	MSM	0.006373	0.993627	0.000000
SP18-2	MSM	0.242041	0.757959	0.000000
SP20-2	MSM	0.032839	0.967161	0.000000
SP-22	MSM	0.000856	0.999144	0.000000
BMC-35	MSM	0.000392	0.999608	0.000000
BMC-36	MSM	0.091949	0.908051	0.000000
BMC-37	MSM	0.000034	0.999966	0.000000
MLP-111	MSM	0.000018	0.999982	0.000000
MLP-112	MSM	0.000007	0.999993	0.000000
MLP-113	MSM	0.000046	0.999954	0.000000
MLP-114	MSM	0.000000	1.000000	0.000000
MLP-115	MSM	0.000146	0.999854	0.000000
MLP-116	MSM	0.001736	0.998264	0.000000
MLP-117	MSM	0.002431	0.997569	0.000000
MLP-118	MSM	0.002271	0.997729	0.000000
MLP-119	MSM	0.000729	0.999271	0.000000
MLP-120	MSM	0.002636	0.997364	0.000000
MLP-121	MSM	0.037027	0.962973	0.000000
MLP-122	MSM	0.000750	0.999250	0.000000
MLP-123	MSM	0.041053	0.958947	0.000000
MLP-38	MSM	0.040104	0.959896	0.000000
MLP-39	MSM	0.062116	0.937884	0.000000
MLP-40	MSM	0.007612	0.992388	0.000000
MLP-41	MSM	0.012481	0.987519	0.000000
MLP-42	MSM	0.002052	0.997948	0.000000
MLP-43	MSM	0.000051	0.999949	0.000000
MLP-44	MSM	0.000018	0.999982	0.000000
MLP-45	MSM	0.000151	0.999849	0.000000
MLP-46	MSM	0.000006	0.999994	0.000000
MLP-47	MSM	0.000049	0.999951	0.000000
MLP-48	MSM	0.000168	0.999832	0.000000
MLP-50	MSM	0.000234	0.999766	0.000000
OXB-10	MSM	0.000448	0.999552	0.000000

Table B1 cont.

Actual classification		Mf	MSM	Oxb
OXB-11	MSM	24.3013	11.7125	161.0555
OXB-12	MSM	18.1336	4.6800	154.7453
OXB-13	MSM	25.9212	8.1836	134.7590
SOM-01	MSM	25.3901	6.4733	176.4758
SOM-02	MSM	39.4192	14.2040	176.1100
SOM-03	MSM	14.8974	5.3361	159.0987
SOM-04	MSM	28.8701	15.6426	174.3774
SOM-05	MSM	25.8812	12.6525	172.6668
SOM-06	MSM	15.4717	10.3609	213.8390
SOM-07	MSM	30.1467	9.0736	140.9096
SOM-08	MSM	16.5789	3.6591	159.6820
SOM-09	MSM	26.2091	11.8674	131.8940
SOM-10	MSM	24.7722	10.1656	152.9940
SOM-11	MSM	38.0437	9.9728	157.0526
SOM-12	MSM	21.6176	11.1613	205.2714
SOM-13	MSM	25.7502	9.8552	193.6657
SOM-14	MSM	31.3467	18.1369	145.7702
SOM-16	MSM	27.7905	15.0272	215.7397
SOM-18	MSM	31.2616	15.1543	206.0540
SP-01	MSM	20.0237	7.6023	163.4674
SP-02	MSM	37.0698	13.3055	135.7770
SP-03	MSM	52.3958	18.6997	156.2513
SP-04	MSM	24.0709	10.8174	191.6396
SP-05	MSM	33.3702	10.3507	157.2203
SP06-1	MSM	17.4381	9.4132	207.3508
SP06-2	MSM	23.6276	7.7576	172.8348
SP07-2	MSM	24.8290	9.9447	198.9795
SP-08	MSM	26.6250	14.0679	188.6956
MLP-60	MSM	39.4359	15.2642	152.8182
MLP-61	MSM	46.0046	20.6976	143.7318
MLP-62	MSM	74.3618	51.1442	182.5656
MLP-63	MSM	201.1636	194.9738	417.8760
MLP-64	MSM	72.4080	40.8657	139.2852
MLP-65	MSM	36.7493	18.0369	121.4429
OXB-01	MSM	63.2786	34.7703	99.0372
OXB-02	MSM	79.9549	46.8116	90.5858
OXB-03	MSM	52.6422	20.3740	106.9394
OXB-04	MSM	50.8107	22.8115	190.6174
OXB-05	MSM	55.4660	25.8416	128.9499
OXB-06	MSM	35.4241	13.6809	166.3856
OXB-07	MSM	44.3926	16.7598	151.5595
OXB-08	MSM	45.5955	17.2519	157.6889
OXB-09	MSM	90.0315	76.4544	256.2139

Table B2 cont.

Actual classification		Mf	MSM	Oxb
OXB-11	MSM	0.001843	0.998157	0.000000
OXB-12	MSM	0.001197	0.998803	0.000000
OXB-13	MSM	0.000141	0.999859	0.000000
SOM-01	MSM	0.000078	0.999922	0.000000
SOM-02	MSM	0.000003	0.999997	0.000000
SOM-03	MSM	0.008321	0.991679	0.000000
SOM-04	MSM	0.001340	0.998660	0.000000
SOM-05	MSM	0.001339	0.998661	0.000000
SOM-06	MSM	0.072065	0.927935	0.000000
SOM-07	MSM	0.000027	0.999973	0.000000
SOM-08	MSM	0.001563	0.998437	0.000000
SOM-09	MSM	0.000768	0.999232	0.000000
SOM-10	MSM	0.000673	0.999327	0.000000
SOM-11	MSM	0.000001	0.999999	0.000000
SOM-12	MSM	0.005335	0.994665	0.000000
SOM-13	MSM	0.000353	0.999647	0.000000
SOM-14	MSM	0.001352	0.998648	0.000000
SOM-16	MSM	0.001690	0.998310	0.000000
SOM-18	MSM	0.000318	0.999682	0.000000
SP-01	MSM	0.002004	0.997996	0.000000
SP-02	MSM	0.000007	0.999993	0.000000
SP-03	MSM	0.000000	1.000000	0.000000
SP-04	MSM	0.001323	0.998677	0.000000
SP-05	MSM	0.000010	0.999990	0.000000
SP06-1	MSM	0.017768	0.982232	0.000000
SP06-2	MSM	0.000358	0.999642	0.000000
SP07-2	MSM	0.000586	0.999414	0.000000
SP-08	MSM	0.001873	0.998127	0.000000
MLP-60	MSM	0.000006	0.999994	0.000000
MLP-61	MSM	0.000003	0.999997	0.000000
MLP-62	MSM	0.000009	0.999991	0.000000
MLP-63	MSM	0.043316	0.956684	0.000000
MLP-64	MSM	0.000000	1.000000	0.000000
MLP-65	MSM	0.000086	0.999914	0.000000
OXB-01	MSM	0.000001	0.999999	0.000000
OXB-02	MSM	0.000000	1.000000	0.000000
OXB-03	MSM	0.000000	1.000000	0.000000
OXB-04	MSM	0.000001	0.999999	0.000000
OXB-05	MSM	0.000000	1.000000	0.000000
OXB-06	MSM	0.000019	0.999981	0.000000
OXB-07	MSM	0.000001	0.999999	0.000000
OXB-08	MSM	0.000001	0.999999	0.000000
OXB-09	MSM	0.001125	0.998875	0.000000

Table B1 cont.

Actual classification		Mf	MSM	Oxb
OXB-14A	Oxb	204.4113	155.6456	4.6029
OXB-22	Oxb	199.4026	152.8917	1.9617
OXB-23	Oxb	243.1798	191.4391	6.5396
OXB-24	Oxb	235.9590	185.5131	1.9017

Table B2 cont.

Actual classification		Mf	MSM	Oxb
OXB-14A	Oxb	0.000000	0.000000	1.000000
OXB-22	Oxb	0.000000	0.000000	1.000000
OXB-23	Oxb	0.000000	0.000000	1.000000
OXB-24	Oxb	0.000000	0.000000	1.000000

Incorrect classifications are marked (*) and abbreviations follow Table A.

Table C1. Classification function scores for dyke population (Model 2)

	Mf	MSM	Oxbow
VM-01	25513.47	25533.39	25484.40
VM-02	25681.64	25704.59	25664.41
VM-03	25794.02	25816.47	25782.87
VM-04	26177.43	26186.28	26098.60
VM-05	26389.02	26388.89	26320.70
VM-06	25893.44	25912.98	25871.57
VM-07	25852.72	25869.75	25824.04
VM-08	25924.91	25939.65	25882.29
VM-09	25870.37	25889.64	25845.91
VM-10	25835.26	25855.40	25813.02
VM-11	25826.72	25848.69	25818.79
VM-12	25676.45	25703.93	25778.61
VM-13	25639.42	25667.16	25738.22
VM-14	26088.42	26100.69	26014.70
VM-15	26063.10	26076.84	25998.99
VM-16	26093.83	26104.25	26020.45
VM-17	25642.54	25670.05	25754.33
VM-18	26246.07	26240.99	26157.31
VM-19	26217.05	26229.53	26148.34
VM-20	25813.71	25833.11	25789.05
VM-21	26070.52	26078.43	25997.44
VM-22	25703.62	25732.11	25813.89
VM-23	25865.97	25888.87	25858.44
VM-24	25789.71	25808.32	25763.58
VM-25	26104.50	26121.07	26059.09
VM-26	25927.10	25945.96	25898.02
VM-27	25876.65	25894.66	25848.73
VM-28	25973.87	25991.86	25944.51
VM-29	24567.26	24569.81	24495.10
VM-30	26415.07	26411.46	26318.25
VM-31	26155.96	26167.76	26085.19
VM-32			
VM-33	26047.17	26057.18	25972.99
VM-34	25643.26	25654.10	25594.85
VM-35			

Table C2. Discriminant function scores for dyke population (Model 2)

	1	2	3
VM-01	MSM	Mf	Oxb
VM-02	MSM	Mf	Oxb
VM-03	MSM	Mf	Oxb
VM-04	MSM	Mf	Oxb
VM-05	Mf	MSM	Oxb
VM-06	MSM	Mf	Oxb
VM-07	MSM	Mf	Oxb
VM-08	MSM	Mf	Oxb
VM-09	MSM	Mf	Oxb
VM-10	MSM	Mf	Oxb
VM-11	MSM	Mf	Oxb
VM-12	Oxb	MSM	Mf
VM-13	Oxb	MSM	Mf
VM-14	MSM	Mf	Oxb
VM-15	MSM	Mf	Oxb
VM-16	MSM	Mf	Oxb
VM-17	Oxb	MSM	Mf
VM-18	Mf	MSM	Oxb
VM-19	MSM	Mf	Oxb
VM-20	MSM	Mf	Oxb
VM-21	MSM	Mf	Oxb
VM-22	Oxb	MSM	Mf
VM-23	MSM	Mf	Oxb
VM-24	MSM	Mf	Oxb
VM-25	MSM	Mf	Oxb
VM-26	MSM	Mf	Oxb
VM-27	MSM	Mf	Oxb
VM-28	MSM	Mf	Oxb
VM-29	MSM	Mf	Oxb
VM-30	Mf	MSM	Oxb
VM-31	MSM	Mf	Oxb
VM-32			
VM-33	MSM	Mf	Oxb
VM-34	MSM	Mf	Oxb
VM-35			

Table C3. Classification of dykes determined from classification function scores (Model 2)

	Root 1	Root 2
VM-01	5.32	-0.46
VM-02	6.18	-0.72
VM-03	6.18	-1.32
VM-04	2.07	1.02
VM-05	0.33	-1.87
VM-06	5.37	-1.12
VM-07	4.71	-1.15
VM-08	3.97	-0.55
VM-09	5.27	-0.98
VM-10	5.49	-0.96
VM-11	6.14	-1.69
VM-12	9.26	-9.27
VM-13	9.26	-8.94
VM-14	2.89	1.38
VM-15	3.38	0.95
VM-16	2.50	0.94
VM-17	9.44	-10.04
VM-18	-1.09	-1.36
VM-19	3.03	1.03
VM-20	5.29	-0.93
VM-21	1.97	0.34
VM-22	9.62	-9.70
VM-23	6.34	-1.51
VM-24	5.09	-0.99
VM-25	4.32	0.09
VM-26	5.10	-0.70
VM-27	4.94	-0.98
VM-28	4.91	-0.87
VM-29	0.84	-0.95
VM-30	-0.91	-0.37
VM-31	2.85	1.04
VM-32		
VM-33	2.40	0.91
VM-34	3.04	-0.97
VM-35		

Table C1 cont.

	Mf	MSM	Oxbow
VM-36	26456.34	26452.90	26378.30
VM-37	25523.30	25512.79	25471.06
VM-38	26368.65	26362.18	26273.89
VM-39	26232.30	26226.83	26142.74
VM-40	25703.95	25727.31	25786.29
VM-41	25663.99	25696.50	25814.57
VM-42	26545.43	26569.68	26487.26
VM-43	25818.30	25837.93	25796.05
VM-44	25711.94	25731.59	25686.26
VM-45	25838.38	25858.33	25812.85
VM-46	25855.97	25867.36	25808.35
VM-47	25993.50	26011.78	25963.17
VM-48	26311.95	26304.79	26218.93
VM-49	26404.11	26398.04	26313.91
VM-50	26030.62	26039.77	25958.00
VM-51	26088.71	26098.50	26012.81
VM-52	26577.33	26579.66	26489.19
VM-53	25843.69	25863.73	25820.60
VM-54	25535.76	25555.22	25521.55
VM-55	25988.45	26006.73	25953.10
VM-56	26572.67	26592.61	26517.40
VM-59	25789.01	25808.38	25759.86
VM-60	25817.81	25837.18	25794.75
VM-61	26390.41	26382.55	26289.44
VM-62	25836.38	25858.01	25816.29
VM-63	25815.67	25832.10	25767.03
VM-64	25963.74	25985.70	25939.60
VM-65	25912.41	25929.89	25878.34
VM-66	25823.34	25842.50	25798.83
VM-67	26984.04	26988.36	26897.21
VM-68	25849.58	25866.78	25817.28
VM-69	25658.72	25682.40	25749.58
VM-71	26321.46	26318.04	26217.58
VM-74	26275.37	26274.28	26181.67
VM-75	26024.30	26033.29	25954.58
VM-76	26007.28	26025.46	25976.09
VM-77	25827.17	25845.60	25802.70
VM-78	26538.64	26535.00	26445.69
VM-79	25998.74	26014.69	25971.65
VM-80	26066.13	26088.69	26047.03
VM-81	26425.47	26426.33	26331.96
VM-82	25777.79	25796.32	25749.92
VM-83	25816.60	25815.72	25728.54

Table C2 cont.

	1	2	3
VM-36	Mf	MSM	Oxb
VM-37	Mf	MSM	Oxb
VM-38	Mf	MSM	Oxb
VM-39	Mf	MSM	Oxb
VM-40	Oxb	MSM	Mf
VM-41	Oxb	MSM	Mf
VM-42	MSM	Mf	Oxb
VM-43	MSM	Mf	Oxb
VM-44	MSM	Mf	Oxb
VM-45	MSM	Mf	Oxb
VM-46	MSM	Mf	Oxb
VM-47	MSM	Mf	Oxb
VM-48	Mf	MSM	Oxb
VM-49	Mf	MSM	Oxb
VM-50	MSM	Mf	Oxb
VM-51	MSM	Mf	Oxb
VM-52	MSM	Mf	Oxb
VM-53	MSM	Mf	Oxb
VM-54	MSM	Mf	Oxb
VM-55	MSM	Mf	Oxb
VM-56	MSM	Mf	Oxb
VM-59	MSM	Mf	Oxb
VM-60	MSM	Mf	Oxb
VM-61	Mf	MSM	Oxb
VM-62	MSM	Mf	Oxb
VM-63	MSM	Mf	Oxb
VM-64	MSM	Mf	Oxb
VM-65	MSM	Mf	Oxb
VM-66	MSM	Mf	Oxb
VM-67	MSM	Mf	Oxb
VM-68	MSM	Mf	Oxb
VM-69	Oxb	MSM	Mf
VM-71	Mf	MSM	Oxb
VM-74	Mf	MSM	Oxb
VM-75	MSM	Mf	Oxb
VM-76	MSM	Mf	Oxb
VM-77	MSM	Mf	Oxb
VM-78	Mf	MSM	Oxb
VM-79	MSM	Mf	Oxb
VM-80	MSM	Mf	Oxb
VM-81	MSM	Mf	Oxb
VM-82	MSM	Mf	Oxb
VM-83	Mf	MSM	Oxb

Table C3 cont.

	Root 1	Root 2
VM-36	-0.55	-1.85
VM-37	-1.61	-5.53
VM-38	-1.49	-1.19
VM-39	-1.19	-1.38
VM-40	8.03	-8.62
VM-41	11.19	-12.02
VM-42	5.74	2.86
VM-43	5.38	-1.07
VM-44	5.32	-0.79
VM-45	5.39	-0.74
VM-46	3.17	-0.91
VM-47	4.95	-0.73
VM-48	-1.61	-1.49
VM-49	-1.32	-1.47
VM-50	2.25	0.59
VM-51	2.33	0.99
VM-52	0.51	0.28
VM-53	5.46	-0.91
VM-54	5.49	-1.76
VM-55	4.86	-0.33
VM-56	4.87	1.65
VM-59	5.21	-0.58
VM-60	5.31	-1.07
VM-61	-1.90	-1.01
VM-62	5.85	-0.79
VM-63	4.23	0.32
VM-64	5.85	-0.39
VM-65	4.71	-0.61
VM-66	5.24	-1.00
VM-67	0.96	0.63
VM-68	4.68	-0.82
VM-69	8.25	-9.23
VM-71	-1.00	0.24
VM-74	-0.32	-0.05
VM-75	2.26	0.32
VM-76	4.92	-0.68
VM-77	5.09	-1.17
VM-78	-0.85	-0.69
VM-79	4.51	-1.52
VM-80	6.06	-0.66
VM-81	0.10	0.38
VM-82	5.05	-0.87
VM-83	-0.18	-0.46

Table C1 cont.					Table C2 cont.					Table C3 cont.		
	Mf	**MSM**	**Oxbow**			**1**	**2**	**3**			**Root 1**	**Root 2**
VM-84	25607.39	25629.82	256s88.86		**VM-84**	Oxb	MSM	Mf		**VM-84**	7.81	-8.76
VM-85	25906.19	25925.74	25879.84		**VM-85**	MSM	Mf	Oxb		**VM-85**	5.29	-0.76
VM-86	25738.17	25755.58	25718.40		**VM-86**	MSM	Mf	Oxb		**VM-86**	4.95	-1.78
VM-87	26098.05	26114.80	26062.68		**VM-87**	MSM	Mf	Oxb		**VM-87**	4.53	-0.67
VM-88	26111.64	26119.15	26038.51		**VM-88**	MSM	Mf	Oxb		**VM-88**	1.89	0.25
VM-89	26294.28	26293.01	26200.85		**VM-89**	Mf	MSM	Oxb		**VM-89**	-0.35	-0.12
VM-90	26287.68	26281.95	26201.10		**VM-90**	Mf	MSM	Oxb		**VM-90**	-1.19	-1.68
VM-91	25783.37	25791.91	25746.14		**VM-91**	MSM	Mf	Oxb		**VM-91**	2.74	-2.39
VM-92	26265.68	26265.64	26192.61		**VM-92**	Mf	MSM	Oxb		**VM-92**	0.27	-1.47
VM-93	25771.13	25790.00	25745.54		**VM-93**	MSM	Mf	Oxb		**VM-93**	5.16	-0.98
KMK100	26431.21	26403.48	26328.65		**KMK100**	Mf	MSM	Oxb		**KMK100**	-6.18	-5.41
KMK101	25967.51	25977.16	25901.05		**KMK101**	MSM	Mf	Oxb		**KMK101**	2.46	0.20
GRT102	25715.85	25734.07	25689.84		**GRT102**	MSM	Mf	Oxb		**GRT102**	5.01	-1.09
AGG	26722.20	26716.35	26622.48		**AGG**	Mf	MSM	Oxb		**AGG**	-1.45	-0.65

CLASSIFICATION FUNCTIONS:

Mf = 3.6Zr + 1704.2TiO_2 + 1792.5P_2O_5 + 0.7Cr + 121.4FeO* - 5.1Y + 0.7Cu + 611.3SiO_2 + 3.1V + 735.1Al_2O_3 + 5.9Nb + 651.8MgO + 233Na_2O - 168.3K_2O - 1.4Sr - 2.6Ni + 4.6La + 1.9Rb -26280.3 **(2)**

MSM = 4.3Zr + 1665TiO_2 + 1667P_2O_5 + 0.6Cr + 122.6FeO* - 5.8Y + 0.7Cu + 607.5SiO_2 + 3.2V + 731Al_2O_3 + 5.5Nb + 648.3MgO + 229.6Na_2O - 164K_2O - 1.4Sr - 2.5Ni + 4.6La + 1.8Rb – 25980.8 **(3)**

Oxb = 4.5Zr + 1866.7TiO_2 + 810P_2O_5 + 0.6Cr + 122.3FeO* - 9.4Y + 1Cu + 599.3SiO_2 + 3.3V + 720.3Al_2O_3 + 6.6Nb + 642.6MgO + 229.5Na_2O - 165K_2O - 1.3Sr - 2.5Ni + 4.1La + 2.1Rb -25486.7 **(4)**

DISCRIMINANT FUNCTIONS:

root 1 = 0.01470Zr - 5.5411 TiO_2 - 44.1494P_2O_5 - 0.0116Cr + 0.2604FeO* - 0.2163Y + 0.0101Cu - 0.0374SiO_2 + 0.0169V - 1.14Al_2O_3 - 0.0846Nb - 0.9146MgO - 0.7954Na_2O + 0.9741K_2O + 0.002Sr + 0.0076Ni - 0.0012La - 0.0067Rb + 79.7665 **(5)**

root 2 = 0.0753Zr - 21.9822TiO_2 + 50.4097P_2O_5 - 0.0027Cr + 0.1866FeO* + 0.1917Y - 0.0184Cu + 0.0909SiO_2 - 0.0002V + 0.2546Al_2O_3 - 0.1555Nb - 0.0616MgO - 0.5Na_2O + 0.7103K_2O - 0.008Sr - 0.0021Ni + 0.0465La - 0.0291Rb - 2.8458 **(6)**

Table D: CLASSIFICATION OF LAVAS (Model 3)

Misclassified lavas are marked (*) and highlighted

Abbreviations: Mf (Mafika Lisiu), MS (Maloti and Senqu), Mo (Mothae)

	Observed Classification	1	2	3			Observed Classification	1	2	3			Observed Classification	1	2	3
BMC-10	Mf	Mf	MS	Mo		**M23**	Mf	Mf	MS	Mo		**M76**	Mf	Mf	MS	Mo
BMC-11	Mf	Mf	MS	Mo		**M24**	Mf	Mf	MS	Mo		**M77**	Mf	Mf	MS	Mo
BMC-12	Mf	Mf	MS	Mo		**M25**	Mf	Mf	MS	Mo		**M78**	Mf	Mf	MS	Mo
BUS-10	Mf	Mf	MS	Mo		**M26**	Mf	Mf	MS	Mo		**M8**	Mf	Mf	MS	Mo
BUS-11	Mf	Mf	MS	Mo		**M27**	Mf	Mf	MS	Mo		**M80**	Mf	Mf	MS	Mo
BUS-13	Mf	Mf	MS	Mo		**M28**	Mf	Mf	MS	Mo		**M81**	Mf	Mf	MS	Mo
BUS-14	Mf	Mf	MS	Mo		**M29**	Mf	Mf	MS	Mo		**M82**	Mf	Mf	MS	Mo
BUS-15	Mf	Mf	MS	Mo		**M3**	Mf	Mf	MS	Mo		**M83**	Mf	Mf	MS	Mo
BUS-16	Mf	Mf	MS	Mo		**M30**	Mf	Mf	MS	Mo		**M84**	Mf	Mf	MS	Mo
BUS-17	Mf	Mf	MS	Mo		**M31**	Mf	Mf	MS	Mo		**M85**	Mf	Mf	MS	Mo
BUS-19	Mf	Mf	MS	Mo		**M32**	Mf	Mf	MS	Mo		**M86**	Mf	Mf	MS	Mo
BUS-20	Mf	Mf	MS	Mo		**M33**	Mf	Mf	MS	Mo		**M87**	Mf	Mf	MS	Mo
BUS-21	Mf	Mf	MS	Mo		**M34**	Mf	Mf	MS	Mo		**M88**	Mf	Mf	MS	Mo
BUS-24	Mf	Mf	MS	Mo		**M35**	Mf	Mf	MS	Mo		**M89**	Mf	Mf	MS	Mo
BUS-25	Mf	Mf	MS	Mo		**M36**	Mf	Mf	MS	Mo		**M9**	Mf	Mf	MS	Mo
BUS-26	Mf	Mf	MS	Mo		**M37**	Mf	Mf	MS	Mo		**M91**	Mf	Mf	MS	Mo
BUS-27	Mf	Mf	MS	Mo		**M38**	Mf	Mf	MS	Mo		**M92**	Mf	Mf	MS	Mo
BUS-28	Mf	Mf	MS	Mo		**M39**	Mf	Mf	MS	Mo		**M93**	Mf	Mf	MS	Mo
M1	Mf	Mf	MS	Mo		**M4**	Mf	Mf	MS	Mo		**M94**	Mf	Mf	MS	Mo
M100	Mf	Mf	MS	Mo		**M40**	Mf	Mf	MS	Mo		**M95**	Mf	Mf	MS	Mo

Table D cont.

	Observed Classification	1	2	3			Observed Classification	1	2	3			Observed Classification	1	2	3
***M101**	Mf	MS	Mo	Mf		**M41**	Mf	Mf	MS	Mo		**M96**	Mf	Mf	MS	Mo
***M102**	Mf	MS	Mf	Mo		**M42**	Mf	Mf	MS	Mo		**M97**	Mf	Mf	MS	Mo
M103	Mf	Mf	MS	Mo		**M45**	Mf	Mf	MS	Mo		**M98**	Mf	Mf	MS	Mo
M104	Mf	Mf	MS	Mo		**M46**	Mf	Mf	MS	Mo		**M99**	Mf	Mf	MS	Mo
M128	Mf	Mf	MS	Mo		**M47**	Mf	Mf	MS	Mo		**MLP-07**	Mf	Mf	MS	Mo
M129	Mf	Mf	MS	Mo		**M48**	Mf	Mf	MS	Mo		**MLP-08**	Mf	Mf	MS	Mo
M136	Mf	Mf	MS	Mo		**M5**	Mf	Mf	MS	Mo		**MLP-09**	Mf	Mf	MS	Mo
M137	Mf	Mf	MS	Mo		**M59**	Mf	Mf	MS	Mo		**MLP-11**	Mf	Mf	MS	Mo
M138	Mf	Mf	MS	Mo		**M6**	Mf	Mf	MS	Mo		**MLP-12**	Mf	Mf	MS	Mo
M139	Mf	Mf	MS	Mo		**M60**	Mf	Mf	MS	Mo		**MLP-13**	Mf	Mf	MS	Mo
M140	Mf	Mf	MS	Mo		**M7**	Mf	Mf	MS	Mo		**MLP-14**	Mf	Mf	MS	Mo
M141	Mf	Mf	MS	Mo		**M70**	Mf	Mf	MS	Mo		**MLP-155**	Mf	Mf	MS	Mo
M142	Mf	Mf	MS	Mo		**M71**	Mf	Mf	MS	Mo		**MLP-156**	Mf	Mf	MS	Mo
M143	Mf	Mf	MS	Mo		**M72**	Mf	Mf	MS	Mo		**MLP-157**	Mf	Mf	MS	Mo
M2	Mf	Mf	MS	Mo		**M73**	Mf	Mf	MS	Mo		**MLP-158**	Mf	Mf	MS	Mo
M21	Mf	Mf	MS	Mo		**M74**	Mf	Mf	MS	Mo		**MLP-159**	Mf	Mf	MS	Mo
M22	Mf	Mf	MS	Mo		**M75**	Mf	Mf	MS	Mo		**MLP-160**	Mf	Mf	MS	Mo
MLP-161	Mf	Mf	MS	Mo		**OXB-57**	Mf	Mf	MS	Mo		**M132**	Mf	Mf	MS	Mo
MLP-162	Mf	Mf	MS	Mo		**OXB-58**	Mf	Mf	MS	Mo		**M133**	Mf	Mf	MS	Mo
MLP-164	Mf	Mf	MS	Mo		**OXB-59**	Mf	Mf	MS	Mo		**M134**	Mf	Mf	MS	Mo
MLP-165	Mf	Mf	MS	Mo		**SOM-100**	Mf	Mf	MS	Mo		**M135**	Mf	Mf	MS	Mo
MLP-169	Mf	Mf	MS	Mo		***SOM-40**	Mf	MS	Mf	Mo		**M14**	Mf	Mf	MS	Mo
MLP-170	Mf	Mf	MS	Mo		**SOM-82**	Mf	Mf	MS	Mo		**M15**	Mf	Mf	MS	Mo
MLP-171	Mf	Mf	MS	Mo		**SOM-83**	Mf	Mf	MS	Mo		**M16**	Mf	Mf	MS	Mo

Table D cont.

	Observed Classification	1	2	3			Observed Classification	1	2	3			Observed Classification	1	2	3
MLP-172	Mf	Mf	MS	Mo		**SOM-84**	Mf	Mf	MS	Mo		**M17**	Mf	Mf	MS	Mo
MLP-174	Mf	Mf	MS	Mo		**SOM-86**	Mf	Mf	MS	Mo		**M18**	Mf	Mf	MS	Mo
MLP-175	Mf	Mf	MS	Mo		**SOM-87**	Mf	Mf	MS	Mo		**M19**	Mf	Mf	MS	Mo
MLP-176	Mf	Mf	MS	Mo		**SOM-91**	Mf	Mf	MS	Mo		**M20**	Mf	Mf	MS	Mo
MLP-177	Mf	Mf	MS	Mo		**SOM-92**	Mf	Mf	MS	Mo		**M61**	Mf	Mf	MS	Mo
MLP-178	Mf	Mf	MS	Mo		**SOM-94**	Mf	Mf	MS	Mo		**M62**	Mf	Mf	MS	Mo
MLP-180	Mf	Mf	MS	Mo		**SOM-95**	Mf	Mf	MS	Mo		**M63**	Mf	Mf	MS	Mo
ON19-2	Mf	Mf	MS	Mo		**SOM-96**	Mf	Mf	MS	Mo		**M64**	Mf	Mf	MS	Mo
ON20-2	Mf	Mf	MS	Mo		**SOM-97**	Mf	Mf	MS	Mo		**M65**	Mf	Mf	MS	Mo
ON-21	Mf	Mf	MS	Mo		**SOM-98**	Mf	Mf	MS	Mo		**M66**	Mf	Mf	MS	Mo
ON22-2	Mf	Mf	MS	Mo		**SOM-99**	Mf	Mf	MS	Mo		**M67**	Mf	Mf	MS	Mo
ON-23	Mf	Mf	MS	Mo		**SP-28**	Mf	Mf	MS	Mo		**M68**	Mf	Mf	MS	Mo
ON-24	Mf	Mf	MS	Mo		**SP-29**	Mf	Mf	MS	Mo		**M69**	Mf	Mf	MS	Mo
ON-25	Mf	Mf	MS	Mo		**SP-30**	Mf	Mf	MS	Mo		**MLP-01**	Mf	Mf	MS	Mo
ON28-2	Mf	Mf	MS	Mo		**SP-31**	Mf	Mf	MS	Mo		**MLP-02**	Mf	Mf	MS	Mo
ON-29	Mf	Mf	MS	Mo		**SP-38**	Mf	Mf	MS	Mo		**MLP-03**	Mf	Mf	MS	Mo
ON30-2	Mf	Mf	MS	Mo		**SP-39**	Mf	Mf	MS	Mo		**MLP-04**	Mf	Mf	MS	Mo
***ON31-2**	Mf	MS	Mf	Mo		**SP-40**	Mf	Mf	MS	Mo		**MLP-05**	Mf	Mf	MS	Mo
ON-35	Mf	Mf	MS	Mo		**SP-41**	Mf	Mf	MS	Mo		**MLP-166**	Mf	Mf	MS	Mo
ON36-1	Mf	Mf	MS	Mo		**SP-42**	Mf	Mf	MS	Mo		**MLP-167**	Mf	Mf	MS	Mo
ON-37	Mf	Mf	MS	Mo		**SP-43**	Mf	Mf	MS	Mo		**MLP-168**	Mf	Mf	MS	Mo
ON38-3	Mf	Mf	MS	Mo		**SP-44B**	Mf	Mf	MS	Mo		**ON-39**	Mf	Mf	MS	Mo
ON41-2	Mf	Mf	MS	Mo		**BMC-02**	Mf	Mf	MS	Mo		**ON40-2**	Mf	Mf	MS	Mo
ON-42	Mf	Mf	MS	Mo		**BMC-04**	Mf	Mf	MS	Mo		**ON-47**	Mf	Mf	MS	Mo

Table D cont.

	Observed Classification	1	2	3			Observed Classification	1	2	3			Observed Classification	1	2	3
ON-43	Mf	Mf	MS	Mo		**BMC-05**	Mf	Mf	MS	Mo		**OXB-46**	Mf	Mf	MS	Mo
ON44-2	Mf	Mf	MS	Mo		**BMC-06**	Mf	Mf	MS	Mo		**OXB-47**	Mf	Mf	MS	Mo
ON-45	Mf	Mf	MS	Mo		**BMC-07**	Mf	Mf	MS	Mo		**OXB-48**	Mf	Mf	MS	Mo
OXB-42	Mf	Mf	MS	Mo		**BUS-22**	Mf	Mf	MS	Mo		**OXB-49**	Mf	Mf	MS	Mo
OXB-43	Mf	Mf	MS	Mo		**M10**	Mf	Mf	MS	Mo		**OXB-52**	Mf	Mf	MS	Mo
OXB-44	Mf	Mf	MS	Mo		**M11**	Mf	Mf	MS	Mo		**OXB-54**	Mf	Mf	MS	Mo
OXB-45	Mf	Mf	MS	Mo		**M12**	Mf	Mf	MS	Mo		**SP-32**	Mf	Mf	MS	Mo
OXB-50	Mf	Mf	MS	Mo		**M13**	Mf	Mf	MS	Mo		**SP-33**	Mf	Mf	MS	Mo
OXB-55	Mf	Mf	MS	Mo		**M130**	Mf	Mf	MS	Mo		**SP-34**	Mf	Mf	MS	Mo
OXB-56	Mf	Mf	MS	Mo		**M131**	Mf	Mf	MS	Mo		**SP-35**	Mf	Mf	MS	Mo
SP-36	Mf	Mf	MS	Mo		**SOM-38A**	MS	MS	Mf	Mo		**MLP-127**	MS	MS	Mf	Mo
SP-37	Mf	Mf	MS	Mo		**SOM-39**	MS	MS	Mf	Mo		**MLP-128**	MS	MS	Mf	Mo
***BMC13-1**	MS	Mf	MS	Mo		**SP-21**	MS	MS	Mo	Mf		**MLP-129**	MS	MS	Mf	Mo
***BMC-14**	MS	Mf	MS	Mo		**SP23-2**	MS	MS	Mo	Mf		**MLP-130**	MS	MS	Mo	Mf
BMC15-3	MS	MS	Mf	Mo		**SP-24**	MS	MS	Mo	Mf		**MLP-131**	MS	MS	Mf	Mo
BMC-16	MS	MS	Mf	Mo		**SP-25**	MS	MS	Mo	Mf		**MLP-132**	MS	MS	Mo	Mf
BMC-17	MS	MS	Mo	Mf		**SP-26**	MS	MS	Mf	Mo		**MLP-133**	MS	MS	Mo	Mf
BMC-18	MS	MS	Mf	Mo		**SP-27**	MS	MS	Mf	Mo		**MLP-134**	MS	MS	Mo	Mf
BUS-29	MS	MS	Mf	Mo		**BMC19-2**	MS	MS	Mf	Mo		**MLP-136**	MS	MS	Mf	Mo
BUS-30	MS	MS	Mf	Mo		**BMC-20**	MS	MS	Mf	Mo		**MLP-137**	MS	MS	Mf	Mo
BUS-31	MS	MS	Mf	Mo		**BMC25-2**	MS	MS	Mf	Mo		**MLP-138**	MS	MS	Mf	Mo
BUS-32	MS	MS	Mf	Mo		**BMC-28**	MS	MS	Mf	Mo		**MLP-139**	MS	MS	Mo	Mf
BUS-33	MS	MS	Mo	Mf		**BMC-29**	MS	MS	Mf	Mo		**MLP-140**	MS	MS	Mo	Mf
MLP-146	MS	MS	Mo	Mf		**BMC32-2**	MS	MS	Mo	Mf		**MLP-141**	MS	MS	Mo	Mf

Table D cont.

	Observed Classification	1	2	3			Observed Classification	1	2	3			Observed Classification	1	2	3
MLP-147	MS	MS	Mo	Mf		**BUS-34**	MS	MS	Mf	Mo		**MLP-142**	MS	MS	Mf	Mo
MLP-148	MS	MS	Mf	Mo		**BUS-35**	MS	MS	Mf	Mo		**MLP-143**	MS	MS	Mo	Mf
MLP-149	MS	MS	Mf	Mo		**BUS-36**	MS	MS	Mf	Mo		**MLP-144**	MS	MS	Mf	Mo
MLP-150	MS	MS	Mf	Mo		**BUS-37**	MS	MS	Mf	Mo		**MLP-145**	MS	MS	Mo	Mf
MLP-151	MS	MS	Mf	Mo		**BUS-38**	MS	MS	Mf	Mo		**MLP-20**	MS	MS	Mf	Mo
MLP-152	MS	MS	Mf	Mo		**BUS-39**	MS	MS	Mf	Mo		***MLP-21**	MS	Mf	MS	Mo
MLP-153	MS	MS	Mf	Mo		**BUS-40**	MS	MS	Mf	Mo		**MLP-22**	MS	MS	Mo	Mf
***MLP-154**	MS	Mf	MS	Mo		**MLM-01**	MS	MS	Mo	Mf		**MLP-23**	MS	MS	Mo	Mf
***MLP-15A**	MS	Mf	MS	Mo		**MLM-02**	MS	MS	Mo	Mf		**MLP-24**	MS	MS	Mo	Mf
MLP-15B	MS	MS	Mo	Mf		**MLM-03**	MS	MS	Mf	Mo		**MLP-25**	MS	MS	Mf	Mo
MLP-16	MS	MS	Mo	Mf		**MLM-04**	MS	MS	Mf	Mo		**MLP-26**	MS	MS	Mo	Mf
MLP-17	MS	MS	Mo	Mf		**MLM-05**	MS	MS	Mf	Mo		**MLP-27**	MS	MS	Mf	Mo
MLP-18	MS	MS	Mf	Mo		**MLM-06**	MS	MS	Mo	Mf		**MLP-28**	MS	MS	Mf	Mo
MLP-19	MS	MS	Mf	Mo		**MLM-07**	MS	MS	Mo	Mf		**MLP-30**	MS	MS	Mf	Mo
ON-04	MS	MS	Mo	Mf		**MLM-08**	MS	MS	Mf	Mo		**MLP-31**	MS	MS	Mf	Mo
ON33-2	MS	MS	Mf	Mo		**MLM-09**	MS	MS	Mo	Mf		**MLP-32**	MS	MS	Mo	Mf
ON34-3	MS	MS	Mo	Mf		**MLM-10**	MS	MS	Mf	Mo		**MLP-33**	MS	MS	Mf	Mo
OXB-37	MS	MS	Mo	Mf		**MLM-11**	MS	MS	Mo	Mf		**MLP-34**	MS	MS	Mf	Mo
OXB-38	MS	MS	Mf	Mo		**MLM-12**	MS	MS	Mf	Mo		***MLP-35**	MS	Mo	MS	Mf
OXB-39	MS	MS	Mo	Mf		**MLM-13**	MS	MS	Mf	Mo		***MLP-36**	MS	Mo	MS	Mf
OXB-40	MS	MS	Mf	Mo		**MLM-14**	MS	MS	Mf	Mo		***MLP-37**	MS	Mo	MS	Mf
OXB-41	MS	MS	Mf	Mo		**MLM-15**	MS	MS	Mo	Mf		**ON-05**	MS	MS	Mf	Mo
SOM-33	MS	MS	Mf	Mo		**MLM-16**	MS	MS	Mo	Mf		**ON-07**	MS	MS	Mo	Mf
SOM-34	MS	MS	Mf	Mo		**MLM-17**	MS	MS	Mo	Mf		**ON-10-2**	MS	MS	Mf	Mo

Table D cont.

	Observed Classification	1	2	3			Observed Classification	1	2	3			Observed Classification	1	2	3
SOM-35	MS	MS	Mf	Mo		***MLP-124**	MS	Mo	MS	Mf		**ON-11**	MS	MS	Mf	Mo
SOM-36	MS	MS	Mf	Mo		***MLP-125**	MS	Mo	MS	Mf		**ON-16**	MS	MS	Mo	Mf
SOM-37	MS	MS	Mf	Mo		***MLP-126**	MS	Mo	MS	Mf		**ON-17**	MS	MS	Mf	Mo
ON-18	MS	MS	Mo	Mf		**BMC-36**	MS	MS	Mf	Mo		***SOM-11**	MS	Mo	MS	Mf
OXB-14	MS	MS	Mf	Mo		**BMC-37**	MS	MS	Mf	Mo		**SOM-12**	MS	MS	Mf	Mo
OXB-15	MS	MS	Mo	Mf		**MLP-111**	MS	MS	Mo	Mf		**SOM-13**	MS	MS	Mf	Mo
OXB-16	MS	MS	Mf	Mo		**MLP-112**	MS	MS	Mo	Mf		**SOM-14**	MS	MS	Mo	Mf
OXB-18	MS	MS	Mf	Mo		**MLP-113**	MS	MS	Mf	Mo		**SOM-16**	MS	MS	Mf	Mo
OXB-19	MS	MS	Mo	Mf		**MLP-114**	MS	MS	Mo	Mf		**SOM-18**	MS	MS	Mf	Mo
OXB-20	MS	MS	Mo	Mf		**MLP-115**	MS	MS	Mo	Mf		**SP-01**	MS	MS	Mo	Mf
OXB-21	MS	MS	Mo	Mf		**MLP-116**	MS	MS	Mf	Mo		**SP-02**	MS	MS	Mo	Mf
OXB-26	MS	MS	Mo	Mf		**MLP-117**	MS	MS	Mf	Mo		**SP-03**	MS	MS	Mo	Mf
OXB-27	MS	MS	Mo	Mf		**MLP-118**	MS	MS	Mf	Mo		**SP-04**	MS	MS	Mf	Mo
OXB-28	MS	MS	Mf	Mo		**MLP-119**	MS	MS	Mf	Mo		**SP-05**	MS	MS	Mo	Mf
OXB-30	MS	MS	Mf	Mo		**MLP-120**	MS	MS	Mf	Mo		**SP06-1**	MS	MS	Mf	Mo
OXB-31	MS	MS	Mf	Mo		**MLP-121**	MS	MS	Mf	Mo		**SP06-2**	MS	MS	Mo	Mf
OXB-32	MS	MS	Mf	Mo		**MLP-122**	MS	MS	Mf	Mo		**SP07-2**	MS	MS	Mf	Mo
OXB-33	MS	MS	Mf	Mo		**MLP-123**	MS	MS	Mf	Mo		**SP-08**	MS	MS	Mf	Mo
OXB-34	MS	MS	Mo	Mf		**MLP-38**	MS	MS	Mf	Mo		**MLP-60**	Mo	Mo	MS	Mf
OXB-35	MS	MS	Mo	Mf		**MLP-39**	MS	MS	Mf	Mo		**MLP-61**	Mo	Mo	MS	Mf
SOM-19	MS	MS	Mf	Mo		**MLP-40**	MS	MS	Mf	Mo		**MLP-62**	Mo	Mo	MS	Mf
SOM-20	MS	MS	Mo	Mf		**MLP-41**	MS	MS	Mf	Mo		**MLP-63**	Mo	Mo	MS	Mf
SOM-21	MS	MS	Mo	Mf		**MLP-42**	MS	MS	Mf	Mo		**MLP-64**	Mo	Mo	MS	Mf
SOM-22	MS	MS	Mf	Mo		**MLP-43**	MS	MS	Mf	Mo		**MLP-65**	Mo	Mo	MS	Mf

Table D cont.

	Observed Classification	1	2	3			Observed Classification	1	2	3			Observed Classification	1	2	3
SOM-23	MS	MS	Mf	Mo		**MLP-44**	MS	MS	Mo	Mf		**OXB-01**	Mo	Mo	MS	Mf
***SOM-25**	MS	Mf	MS	Mo		**MLP-45**	MS	MS	Mf	Mo		**OXB-02**	Mo	Mo	MS	Mf
SOM-26	MS	MS	Mo	Mf		**MLP-46**	MS	MS	Mo	Mf		**OXB-03**	Mo	Mo	MS	Mf
SOM-27	MS	MS	Mf	Mo		**MLP-47**	MS	MS	Mo	Mf		**OXB-04**	Mo	Mo	MS	Mf
SOM-28	MS	MS	Mf	Mo		**MLP-48**	MS	MS	Mo	Mf		**OXB-05**	Mo	Mo	MS	Mf
SOM-29	MS	MS	Mf	Mo		**MLP-50**	MS	MS	Mo	Mf		**OXB-06**	Mo	Mo	MS	Mf
SOM-30	MS	MS	Mf	Mo		**OXB-10**	MS	MS	Mf	Mo		**OXB-07**	Mo	Mo	MS	Mf
SOM-31	MS	MS	Mf	Mo		**OXB-11**	MS	MS	Mf	Mo		**OXB-08**	Mo	Mo	MS	Mf
SOM-32	MS	MS	Mf	Mo		**OXB-12**	MS	MS	Mf	Mo		***OXB-09**	Mo	MS	Mf	Mo
SP10-2	MS	MS	Mo	Mf		**OXB-13**	MS	MS	Mo	Mf						
SP11-2	MS	MS	Mo	Mf		**SOM-01**	MS	MS	Mo	Mf						
SP-12	MS	MS	Mf	Mo		**SOM-02**	MS	MS	Mo	Mf						
SP13-3	MS	MS	Mf	Mo		**SOM-03**	MS	MS	Mf	Mo						
SP14-3	MS	MS	Mo	Mf		**SOM-04**	MS	MS	Mf	Mo						
SP16-1	MS	MS	Mf	Mo		**SOM-05**	MS	MS	Mf	Mo						
SP-17	MS	MS	Mf	Mo		**SOM-06**	MS	MS	Mf	Mo						
SP18-2	MS	MS	Mf	Mo		**SOM-07**	MS	MS	Mo	Mf						
SP20-2	MS	MS	Mf	Mo		**SOM-08**	MS	MS	Mo	Mf						
SP-22	MS	MS	Mf	Mo		**SOM-09**	MS	MS	Mo	Mf						
BMC-35	MS	MS	Mf	Mo		***SOM-10**	MS	Mo	MS	Mf						

Table E1- Squared Mahalanobis Distances from Group Centroids for each lava (Model 3)						Table E2- Posterior Probabilities for each lava (Model 3)				
	Observed Classification	Mf	MS	Mo			Observed Classification	Mf	MS	Mo
BMC-10	Mf	46.5639	50.2960	70.5404		**BMC-10**	Mf	0.866000	0.133995	0.000005
BMC-11	Mf	22.7428	22.9872	39.9884		**BMC-11**	Mf	0.530456	0.469449	0.000095
BMC-12	Mf	9.6736	24.3430	55.5631		**BMC-12**	Mf	0.999348	0.000652	0.000000
BUS-10	Mf	22.3418	33.8609	55.5723		**BUS-10**	Mf	0.996857	0.003143	0.000000
BUS-11	Mf	15.2634	24.1419	43.0446		**BUS-11**	Mf	0.988332	0.011667	0.000001
BUS-13	Mf	19.0955	29.0206	40.4624		**BUS-13**	Mf	0.993031	0.006946	0.000023
BUS-14	Mf	9.2945	17.2743	47.7719		**BUS-14**	Mf	0.981835	0.018165	0.000000
BUS-15	Mf	7.4511	25.6605	58.7374		**BUS-15**	Mf	0.999889	0.000111	0.000000
BUS-16	Mf	11.8064	35.3135	54.9404		**BUS-16**	Mf	0.999992	0.000008	0.000000
BUS-17	Mf	11.8531	31.6124	48.8501		**BUS-17**	Mf	0.999949	0.000051	0.000000
BUS-19	Mf	7.3385	28.9186	60.2659		**BUS-19**	Mf	0.999979	0.000021	0.000000
BUS-20	Mf	3.4093	17.5984	48.7890		**BUS-20**	Mf	0.999171	0.000829	0.000000
BUS-21	Mf	3.9955	22.5248	53.5543		**BUS-21**	Mf	0.999905	0.000095	0.000000
BUS-24	Mf	4.8015	19.1335	43.5112		**BUS-24**	Mf	0.999228	0.000772	0.000000
BUS-25	Mf	7.5287	12.1952	35.4480		**BUS-25**	Mf	0.911596	0.088403	0.000001
BUS-26	Mf	8.4835	24.5132	57.3605		**BUS-26**	Mf	0.999670	0.000330	0.000000
BUS-27	Mf	6.2591	14.4723	45.9736		**BUS-27**	Mf	0.983803	0.016197	0.000000
BUS-28	Mf	6.8639	17.2664	43.2702		**BUS-28**	Mf	0.994520	0.005480	0.000000
M1	Mf	11.7872	23.5797	56.5764		**M1**	Mf	0.997258	0.002742	0.000000
M100	Mf	1.7859	18.2570	51.5697		**M100**	Mf	0.999735	0.000265	0.000000
***M101**	Mf	28.4805	23.2156	27.9898		***M101**	Mf	0.061781	0.859259	0.078960
***M102**	Mf	19.9288	7.8944	34.0933		***M102**	Mf	0.002431	0.997567	0.000002
M103	Mf	17.5026	35.3761	73.8345		**M103**	Mf	0.999869	0.000131	0.000000
M104	Mf	9.4892	26.0702	59.1468		**M104**	Mf	0.999749	0.000251	0.000000
M128	Mf	0.5943	17.3189	49.2969		**M128**	Mf	0.999767	0.000233	0.000000
M129	Mf	9.3216	9.7294	24.7356		**M129**	Mf	0.550658	0.449095	0.000248
M136	Mf	12.1696	30.4443	62.2933		**M136**	Mf	0.999892	0.000108	0.000000
M137	Mf	7.3539	25.0114	61.1940		**M137**	Mf	0.999854	0.000146	0.000000
M138	Mf	3.9519	23.7910	59.9474		**M138**	Mf	0.999951	0.000049	0.000000
M139	Mf	9.4161	28.4994	63.9101		**M139**	Mf	0.999928	0.000072	0.000000
M140	Mf	15.1488	35.1762	79.4794		**M140**	Mf	0.999955	0.000045	0.000000
M141	Mf	7.1220	25.1809	60.3080		**M141**	Mf	0.999880	0.000120	0.000000
M142	Mf	4.8615	21.3975	54.9129		**M142**	Mf	0.999743	0.000257	0.000000
M143	Mf	9.2389	31.9525	73.7609		**M143**	Mf	0.999988	0.000012	0.000000
M2	Mf	7.9337	18.2783	52.6784		**M2**	Mf	0.994360	0.005640	0.000000
M21	Mf	6.1902	21.9692	48.2567		**M21**	Mf	0.999625	0.000375	0.000000
M22	Mf	8.3315	21.4770	51.7496		**M22**	Mf	0.998604	0.001396	0.000000
M23	Mf	5.5034	16.5527	43.2114		**M23**	Mf	0.996028	0.003971	0.000000
M24	Mf	5.4061	17.6474	48.8304		**M24**	Mf	0.997808	0.002192	0.000000

Table E1 cont.

	Observed Classification	Mf	MS	Mo
M25	Mf	8.1495	24.0833	56.5028
M26	Mf	6.9414	15.2807	45.9994
M27	Mf	7.1620	17.7134	45.8846
M28	Mf	4.5983	13.4529	40.5473
M29	Mf	5.5234	16.5675	49.5095
M3	Mf	5.5914	16.8527	50.7593
M30	Mf	4.2294	16.4738	49.0816
M31	Mf	8.9123	16.2085	42.9098
M32	Mf	6.3691	21.2433	52.2947
M33	Mf	7.2692	29.5921	65.0685
M34	Mf	9.1472	33.6168	69.6809
M35	Mf	12.7390	44.9104	88.7579
M36	Mf	70.0830	89.3093	111.3330
M37	Mf	6.0859	22.1038	40.2492
M38	Mf	21.7086	30.9268	58.4740
M39	Mf	12.9905	24.2459	56.9120
M4	Mf	7.2621	16.6176	44.0366
M40	Mf	6.0471	24.4286	66.4739
M41	Mf	8.8907	22.8462	49.7733
M42	Mf	9.6292	23.8185	59.8699
M45	Mf	16.6897	32.7297	63.7323
M46	Mf	9.8830	26.8238	56.6370
M47	Mf	14.7426	31.2440	64.7846
M48	Mf	8.9194	26.0223	62.5175
M5	Mf	4.7849	11.5837	42.7783
M59	Mf	5.3331	16.4125	46.7268
M6	Mf	3.9120	18.0795	52.4977
M60	Mf	2.7029	13.2844	42.1798
M7	Mf	130.9104	139.1941	169.3904
M70	Mf	6.3121	23.6842	55.6914
M71	Mf	2.7669	16.4034	49.3672
M72	Mf	5.5961	19.6132	54.1190
M73	Mf	4.9650	22.7071	56.2538
M74	Mf	7.5648	24.4823	59.8158
M75	Mf	9.5871	19.3963	55.8163
M76	Mf	8.9716	19.0161	47.5948
M77	Mf	6.5541	22.4541	58.0428
M78	Mf	4.4251	21.7134	58.9662
M8	Mf	13.4855	37.0802	85.4062
M80	Mf	6.9293	20.5964	53.6019
M81	Mf	8.1708	22.8993	57.8442
M82	Mf	5.8250	23.1869	51.6575

Table E2 cont.

	Observed Classification	Mf	MS	Mo
M25	Mf	0.999653	0.000347	0.000000
M26	Mf	0.984778	0.015222	0.000000
M27	Mf	0.994912	0.005088	0.000000
M28	Mf	0.988194	0.011806	0.000000
M29	Mf	0.996018	0.003982	0.000000
M3	Mf	0.996427	0.003573	0.000000
M30	Mf	0.997811	0.002189	0.000000
M31	Mf	0.974620	0.025380	0.000000
M32	Mf	0.999411	0.000589	0.000000
M33	Mf	0.999986	0.000014	0.000000
M34	Mf	0.999995	0.000005	0.000000
M35	Mf	1.000000	0.000000	0.000000
M36	Mf	0.999933	0.000067	0.000000
M37	Mf	0.999668	0.000332	0.000000
M38	Mf	0.990137	0.009863	0.000000
M39	Mf	0.996416	0.003584	0.000000
M4	Mf	0.990786	0.009214	0.000000
M40	Mf	0.999898	0.000102	0.000000
M41	Mf	0.999068	0.000932	0.000000
M42	Mf	0.999171	0.000829	0.000000
M45	Mf	0.999671	0.000329	0.000000
M46	Mf	0.999790	0.000210	0.000000
M47	Mf	0.999739	0.000261	0.000000
M48	Mf	0.999807	0.000193	0.000000
M5	Mf	0.967687	0.032313	0.000000
M59	Mf	0.996088	0.003912	0.000000
M6	Mf	0.999162	0.000838	0.000000
M60	Mf	0.994987	0.005013	0.000000
M7	Mf	0.984355	0.015645	0.000000
M70	Mf	0.999831	0.000169	0.000000
M71	Mf	0.998908	0.001092	0.000000
M72	Mf	0.999097	0.000903	0.000000
M73	Mf	0.999860	0.000140	0.000000
M74	Mf	0.999788	0.000212	0.000000
M75	Mf	0.992642	0.007358	0.000000
M76	Mf	0.993453	0.006547	0.000000
M77	Mf	0.999647	0.000353	0.000000
M78	Mf	0.999824	0.000176	0.000000
M8	Mf	0.999992	0.000008	0.000000
M80	Mf	0.998924	0.001076	0.000000
M81	Mf	0.999367	0.000633	0.000000
M82	Mf	0.999830	0.000170	0.000000

Table E1 cont.

	Observed Classification	Mf	MS	Mo
M83	Mf	9.4919	37.6706	68.2241
M84	Mf	8.9915	36.6319	75.7406
M85	Mf	7.9093	24.4427	46.1648
M86	Mf	4.5596	25.4991	55.9162
M87	Mf	12.6586	25.0745	49.2764
M88	Mf	3.6117	23.6056	65.6945
M89	Mf	6.7982	27.9525	64.2996
M9	Mf	6.2050	21.3375	48.3143
M91	Mf	6.8470	21.6152	53.5750
M92	Mf	14.3311	30.4932	71.4893
M93	Mf	4.9452	16.7682	47.7774
M94	Mf	5.8195	28.3982	65.9652
M95	Mf	8.7034	27.2462	61.9555
M96	Mf	7.9769	30.0061	64.6957
M97	Mf	8.8260	40.8446	79.3147
M98	Mf	5.1635	25.9190	57.5396
M99	Mf	3.8800	25.8523	62.0967
MLP-07	Mf	6.4061	17.9572	44.8574
MLP-08	Mf	6.2190	18.7534	45.6500
MLP-09	Mf	6.2279	13.9175	37.5269
MLP-11	Mf	9.5334	14.1871	37.9221
MLP-12	Mf	52.7669	58.3944	85.1562
MLP-13	Mf	51.1542	58.1477	85.6740
MLP-14	Mf	8.5335	19.6878	53.8421
MLP-155	Mf	12.5546	22.4422	50.7073
MLP-156	Mf	8.9328	20.6154	57.9899
MLP-157	Mf	8.1852	20.0890	56.8121
MLP-158	Mf	6.4607	29.1291	67.1069
MLP-159	Mf	4.5685	23.9994	59.7409
MLP-160	Mf	4.9180	12.3612	43.3644
MLP-161	Mf	6.2364	16.8288	44.3456
MLP-162	Mf	8.8750	18.4202	45.4658
MLP-164	Mf	10.3628	25.7409	45.1174
MLP-165	Mf	2.7933	15.9023	46.0997
MLP-169	Mf	1.7840	21.0718	53.0249
MLP-170	Mf	15.4250	32.5614	68.4582
MLP-171	Mf	6.8299	30.6099	60.0293
MLP-172	Mf	5.4950	23.0636	51.4914
MLP-174	Mf	12.4230	29.7346	65.6331
MLP-175	Mf	3.7677	17.6133	46.2131
MLP-176	Mf	10.5571	29.8588	61.3154
MLP-177	Mf	34.5789	50.0604	61.4989

Table E2 cont.

	Observed Classification	Mf	MS	Mo
M83	Mf	0.999999	0.000001	0.000000
M84	Mf	0.999999	0.000001	0.000000
M85	Mf	0.999743	0.000257	0.000000
M86	Mf	0.999972	0.000028	0.000000
M87	Mf	0.997991	0.002009	0.000000
M88	Mf	0.999954	0.000046	0.000000
M89	Mf	0.999975	0.000025	0.000000
M9	Mf	0.999483	0.000517	0.000000
M91	Mf	0.999379	0.000621	0.000000
M92	Mf	0.999691	0.000309	0.000000
M93	Mf	0.997299	0.002701	0.000000
M94	Mf	0.999987	0.000013	0.000000
M95	Mf	0.999906	0.000094	0.000000
M96	Mf	0.999984	0.000016	0.000000
M97	Mf	1.000000	0.000000	0.000000
M98	Mf	0.999969	0.000031	0.000000
M99	Mf	0.999983	0.000017	0.000000
MLP-07	Mf	0.996907	0.003093	0.000000
MLP-08	Mf	0.998106	0.001894	0.000000
MLP-09	Mf	0.979057	0.020943	0.000000
MLP-11	Mf	0.911075	0.088925	0.000001
MLP-12	Mf	0.943416	0.056584	0.000000
MLP-13	Mf	0.970595	0.029405	0.000000
MLP-14	Mf	0.996231	0.003769	0.000000
MLP-155	Mf	0.992923	0.007077	0.000000
MLP-156	Mf	0.997103	0.002897	0.000000
MLP-157	Mf	0.997406	0.002594	0.000000
MLP-158	Mf	0.999988	0.000012	0.000000
MLP-159	Mf	0.999940	0.000060	0.000000
MLP-160	Mf	0.976375	0.023625	0.000000
MLP-161	Mf	0.995014	0.004986	0.000000
MLP-162	Mf	0.991613	0.008387	0.000000
MLP-164	Mf	0.999542	0.000458	0.000000
MLP-165	Mf	0.998578	0.001422	0.000000
MLP-169	Mf	0.999935	0.000065	0.000000
MLP-170	Mf	0.999810	0.000190	0.000000
MLP-171	Mf	0.999993	0.000007	0.000000
MLP-172	Mf	0.999847	0.000153	0.000000
MLP-174	Mf	0.999826	0.000174	0.000000
MLP-175	Mf	0.999016	0.000984	0.000000
MLP-176	Mf	0.999936	0.000064	0.000000
MLP-177	Mf	0.999564	0.000435	0.000001

Table E1 cont.

	Observed Classification	Mf	MS	Mo
MLP-178	Mf	13.4038	34.6407	69.9034
MLP-180	Mf	11.6280	33.0962	65.2152
ON19-2	Mf	5.6513	19.1241	47.0303
ON20-2	Mf	6.8279	26.3827	67.4981
ON-21	Mf	11.6553	35.8801	81.5109
ON22-2	Mf	9.2148	29.1404	73.6633
ON-23	Mf	5.4980	15.7962	54.5732
ON-24	Mf	5.2319	17.1310	47.6307
ON-25	Mf	4.0710	20.5359	52.7479
ON28-2	Mf	7.5346	14.4339	46.6854
ON-29	Mf	14.1557	15.3190	38.8308
ON30-2	Mf	38.0076	43.6823	104.1577
***ON31-2**	Mf	10.1323	7.9025	26.0204
ON-35	Mf	14.0217	44.6204	80.7790
ON36-1	Mf	8.8838	31.5251	66.1802
ON-37	Mf	16.8698	43.3617	85.7219
ON38-3	Mf	15.2036	41.1283	82.7935
ON41-2	Mf	6.8706	26.9948	59.3538
ON-42	Mf	9.1500	36.5961	74.9381
ON-43	Mf	8.2219	34.8353	65.2689
ON44-2	Mf	5.7373	21.8714	52.4529
ON-45	Mf	9.8222	23.2009	60.8239
OXB-42	Mf	8.3458	24.6776	64.3520
OXB-43	Mf	5.7859	20.0487	51.1932
OXB-44	Mf	13.8830	14.3435	41.6296
OXB-45	Mf	10.8792	22.3967	52.7937
OXB-50	Mf	7.6399	26.9288	65.4643
OXB-55	Mf	5.6920	26.1026	63.4443
OXB-56	Mf	6.9785	26.4137	62.8091
OXB-57	Mf	11.2473	20.9057	47.6139
OXB-58	Mf	19.9568	31.3646	67.2191
OXB-59	Mf	21.4287	24.2821	53.0091
SOM-100	Mf	7.6699	27.8331	60.5457
***SOM-40**	Mf	12.8227	8.9373	31.1742
SOM-82	Mf	8.1982	19.3927	41.2380
SOM-83	Mf	6.7259	19.0255	54.7698
SOM-84	Mf	10.2545	22.0082	51.2309
SOM-86	Mf	22.3259	36.4423	61.7456
SOM-87	Mf	6.1747	16.4684	52.4748
SOM-91	Mf	9.7182	32.2812	62.2261
SOM-92	Mf	14.0809	22.4679	58.5026
SOM-94	Mf	17.8719	33.8759	60.8671

Table E2 cont.

	Observed Classification	Mf	MS	Mo
MLP-178	Mf	0.999976	0.000024	0.000000
MLP-180	Mf	0.999978	0.000022	0.000000
ON19-2	Mf	0.998815	0.001185	0.000000
ON20-2	Mf	0.999943	0.000057	0.000000
ON-21	Mf	0.999995	0.000005	0.000000
ON22-2	Mf	0.999953	0.000047	0.000000
ON-23	Mf	0.994229	0.005771	0.000000
ON-24	Mf	0.997400	0.002600	0.000000
ON-25	Mf	0.999734	0.000266	0.000000
ON28-2	Mf	0.969220	0.030780	0.000000
ON-29	Mf	0.641442	0.358555	0.000003
ON30-2	Mf	0.944661	0.055339	0.000000
***ON31-2**	Mf	0.246930	0.752982	0.000088
ON-35	Mf	1.000000	0.000000	0.000000
ON36-1	Mf	0.999988	0.000012	0.000000
ON-37	Mf	0.999998	0.000002	0.000000
ON38-3	Mf	0.999998	0.000002	0.000000
ON41-2	Mf	0.999957	0.000043	0.000000
ON-42	Mf	0.999999	0.000001	0.000000
ON-43	Mf	0.999998	0.000002	0.000000
ON44-2	Mf	0.999686	0.000314	0.000000
ON-45	Mf	0.998757	0.001243	0.000000
OXB-42	Mf	0.999716	0.000284	0.000000
OXB-43	Mf	0.999201	0.000799	0.000000
OXB-44	Mf	0.557303	0.442696	0.000001
OXB-45	Mf	0.996855	0.003145	0.000000
OXB-50	Mf	0.999935	0.000065	0.000000
OXB-55	Mf	0.999963	0.000037	0.000000
OXB-56	Mf	0.999940	0.000060	0.000000
OXB-57	Mf	0.992070	0.007930	0.000000
OXB-58	Mf	0.996678	0.003322	0.000000
OXB-59	Mf	0.806388	0.193612	0.000000
SOM-100	Mf	0.999958	0.000042	0.000000
***SOM-40**	Mf	0.125354	0.874633	0.000013
SOM-82	Mf	0.996306	0.003694	0.000000
SOM-83	Mf	0.997871	0.002129	0.000000
SOM-84	Mf	0.997204	0.002796	0.000000
SOM-86	Mf	0.999140	0.000860	0.000000
SOM-87	Mf	0.994216	0.005784	0.000000
SOM-91	Mf	0.999987	0.000013	0.000000
SOM-92	Mf	0.985131	0.014869	0.000000
SOM-94	Mf	0.999665	0.000335	0.000000

Table E1 cont.

	Observed Classification	Mf	MS	Mo
SOM-95	Mf	5.9809	31.4096	74.5921
SOM-96	Mf	5.9407	27.6648	61.1683
SOM-97	Mf	8.9676	29.8492	60.4318
SOM-98	Mf	5.3767	26.6070	62.4955
SOM-99	Mf	6.6072	21.1668	51.1480
SP-28	Mf	4.2900	12.3983	41.9773
SP-29	Mf	3.5924	10.1089	37.7094
SP-30	Mf	9.7902	12.7171	29.2739
SP-31	Mf	4.9212	16.4586	54.0815
SP-38	Mf	15.9227	38.7842	68.5393
SP-39	Mf	12.3789	37.2657	76.7092
SP-40	Mf	5.4262	28.7319	57.8244
SP-41	Mf	62.2777	87.2169	108.5482
SP-42	Mf	17.3240	42.3674	69.4832
SP-43	Mf	197.1263	246.6727	255.5232
SP-44B	Mf	77.8966	121.8642	165.9779
BMC-02	Mf	18.4833	34.4805	71.8077
BMC-04	Mf	28.0888	40.4508	59.1841
BMC-05	Mf	13.8239	20.9086	37.5241
BMC-06	Mf	3.1055	17.3516	47.6122
BMC-07	Mf	14.9960	37.2538	71.6082
BUS-22	Mf	5.5966	14.3708	44.0968
M10	Mf	16.6080	20.9839	52.8175
M11	Mf	16.5777	29.7229	59.0378
M12	Mf	8.9473	18.2553	47.8954
M13	Mf	12.3948	21.5566	54.0125
M130	Mf	10.4140	20.4868	61.6000
M131	Mf	8.9141	11.9755	45.2781
M132	Mf	20.6897	37.6816	79.1336
M133	Mf	7.7693	19.5429	47.4150
M134	Mf	6.0432	15.4190	50.0446
M135	Mf	4.8443	17.6304	46.5217
M14	Mf	15.5231	24.9615	53.1362
M15	Mf	14.6924	24.6771	50.8829
M16	Mf	18.3871	36.7814	66.0835
M17	Mf	10.7500	25.7398	59.2858
M18	Mf	12.5471	26.2687	48.0125
M19	Mf	26.5746	55.5676	96.7764
M20	Mf	9.2883	27.4142	54.8761
M61	Mf	53.4096	85.9367	113.5066
M62	Mf	12.3353	28.2132	57.6110
M63	Mf	65.1709	73.0418	98.4813

Table E2 cont.

	Observed Classification	Mf	MS	Mo
SOM-95	Mf	0.999997	0.000003	0.000000
SOM-96	Mf	0.999981	0.000019	0.000000
SOM-97	Mf	0.999971	0.000029	0.000000
SOM-98	Mf	0.999975	0.000025	0.000000
SOM-99	Mf	0.999311	0.000689	0.000000
SP-28	Mf	0.982946	0.017054	0.000000
SP-29	Mf	0.962970	0.037030	0.000000
SP-30	Mf	0.812024	0.187928	0.000048
SP-31	Mf	0.996886	0.003114	0.000000
SP-38	Mf	0.999989	0.000011	0.000000
SP-39	Mf	0.999996	0.000004	0.000000
SP-40	Mf	0.999991	0.000009	0.000000
SP-41	Mf	0.999996	0.000004	0.000000
SP-42	Mf	0.999996	0.000004	0.000000
SP-43	Mf	1.000000	0.000000	0.000000
SP-44B	Mf	1.000000	0.000000	0.000000
BMC-02	Mf	0.999664	0.000336	0.000000
BMC-04	Mf	0.997936	0.002064	0.000000
BMC-05	Mf	0.971863	0.028130	0.000007
BMC-06	Mf	0.999194	0.000806	0.000000
BMC-07	Mf	0.999985	0.000015	0.000000
BUS-22	Mf	0.987716	0.012284	0.000000
M10	Mf	0.899164	0.100836	0.000000
M11	Mf	0.998604	0.001396	0.000000
M12	Mf	0.990567	0.009433	0.000000
M13	Mf	0.989858	0.010142	0.000000
M130	Mf	0.993545	0.006455	0.000000
M131	Mf	0.822106	0.177894	0.000000
M132	Mf	0.999796	0.000204	0.000000
M133	Mf	0.997232	0.002768	0.000000
M134	Mf	0.990878	0.009122	0.000000
M135	Mf	0.998330	0.001670	0.000000
M14	Mf	0.991157	0.008843	0.000000
M15	Mf	0.993256	0.006744	0.000000
M16	Mf	0.999899	0.000101	0.000000
M17	Mf	0.999444	0.000556	0.000000
M18	Mf	0.998953	0.001047	0.000000
M19	Mf	0.999999	0.000001	0.000000
M20	Mf	0.999884	0.000116	0.000000
M61	Mf	1.000000	0.000000	0.000000
M62	Mf	0.999644	0.000356	0.000000
M63	Mf	0.980837	0.019163	0.000000

Table E1 cont.

	Observed Classification	Mf	MS	Mo
M64	Mf	9.4061	24.0322	59.3442
M65	Mf	13.5308	24.0512	56.0769
M66	Mf	14.7993	30.7212	64.4048
M67	Mf	18.0761	21.6584	56.4979
M68	Mf	4.0183	14.2667	44.4136
M69	Mf	8.5676	13.4001	41.6036
MLP-01	Mf	10.2784	35.8435	70.5332
MLP-02	Mf	32.5631	41.0376	71.0235
MLP-03	Mf	16.0549	18.3384	49.2575
MLP-04	Mf	19.8597	28.4553	57.3373
MLP-05	Mf	4.4252	15.4190	45.2629
MLP-166	Mf	12.2814	21.9816	50.2846
MLP-167	Mf	10.4287	18.5354	46.2288
MLP-168	Mf	3.5851	16.3506	43.3890
ON-39	Mf	34.2090	60.0569	77.4352
ON40-2	Mf	18.2264	36.8160	73.2153
ON-47	Mf	10.5373	22.3937	50.3762
OXB-46	Mf	14.5517	29.1771	58.5037
OXB-47	Mf	9.5998	17.5455	43.9961
OXB-48	Mf	6.2732	20.4674	48.8120
OXB-49	Mf	8.2333	27.3564	58.0125
OXB-52	Mf	7.2079	19.0594	56.8464
OXB-54	Mf	6.2852	26.8086	55.7365
SP-32	Mf	5.5405	9.9084	37.4988
SP-33	Mf	8.7745	16.2485	46.1899
SP-34	Mf	8.6932	23.2729	53.9734
SP-35	Mf	14.7868	19.6021	42.5516
SP-36	Mf	12.9844	29.4109	46.7735
SP-37	Mf	41.1667	50.9359	79.1104
***BMC13-1**	MS	15.1925	18.0623	54.7237
***BMC-14**	MS	7.3432	7.7102	37.4916
BMC15-3	MS	15.1108	3.6036	34.2647
BMC-16	MS	16.6133	4.3950	31.9910
BMC-17	MS	25.9285	6.4954	25.0213
BMC-18	MS	20.1086	1.7073	21.1855
BUS-29	MS	16.5579	3.8351	28.0660
BUS-30	MS	13.0397	4.7805	32.0059
BUS-31	MS	30.2820	19.2234	43.2127
BUS-32	MS	15.3408	5.4603	32.6224
BUS-33	MS	23.5463	2.3020	17.9607
MLP-146	MS	34.1085	7.2839	18.1032
MLP-147	MS	33.7165	7.3106	17.7153

Table E2 cont.

	Observed Classification	Mf	MS	Mo
M64	Mf	0.999334	0.000666	0.000000
M65	Mf	0.994832	0.005168	0.000000
M66	Mf	0.999651	0.000349	0.000000
M67	Mf	0.857071	0.142929	0.000000
M68	Mf	0.994084	0.005916	0.000000
M69	Mf	0.918059	0.081941	0.000000
MLP-01	Mf	0.999997	0.000003	0.000000
MLP-02	Mf	0.985759	0.014241	0.000000
MLP-03	Mf	0.758009	0.241991	0.000000
MLP-04	Mf	0.986584	0.013416	0.000000
MLP-05	Mf	0.995917	0.004083	0.000000
MLP-166	Mf	0.992233	0.007767	0.000000
MLP-167	Mf	0.982933	0.017067	0.000000
MLP-168	Mf	0.998312	0.001688	0.000000
ON-39	Mf	0.999998	0.000002	0.000000
ON40-2	Mf	0.999908	0.000092	0.000000
ON-47	Mf	0.997344	0.002656	0.000000
OXB-46	Mf	0.999333	0.000667	0.000000
OXB-47	Mf	0.981528	0.018472	0.000000
OXB-48	Mf	0.999173	0.000827	0.000000
OXB-49	Mf	0.999930	0.000070	0.000000
OXB-52	Mf	0.997337	0.002663	0.000000
OXB-54	Mf	0.999965	0.000035	0.000000
SP-32	Mf	0.898796	0.101204	0.000000
SP-33	Mf	0.976729	0.023271	0.000000
SP-34	Mf	0.999318	0.000682	0.000000
SP-35	Mf	0.917407	0.082592	0.000001
SP-36	Mf	0.999729	0.000271	0.000000
SP-37	Mf	0.992495	0.007505	0.000000
***BMC13-1**	MS	0.807665	0.192335	0.000000
***BMC-14**	MS	0.545757	0.454243	0.000000
BMC15-3	MS	0.003161	0.996838	0.000000
BMC-16	MS	0.002218	0.997781	0.000001
BMC-17	MS	0.000060	0.999845	0.000095
BMC-18	MS	0.000101	0.999840	0.000059
BUS-29	MS	0.001724	0.998271	0.000005
BUS-30	MS	0.015835	0.984164	0.000001
BUS-31	MS	0.003953	0.996041	0.000006
BUS-32	MS	0.007102	0.992897	0.000001
BUS-33	MS	0.000024	0.999578	0.000398
MLP-146	MS	0.000001	0.995545	0.004453
MLP-147	MS	0.000002	0.994525	0.005473

Table E1 cont.

	Observed Classification	Mf	MS	Mo
MLP-148	MS	18.6982	4.2171	29.9738
MLP-149	MS	19.4280	11.3695	36.0978
MLP-150	MS	22.4547	7.9981	34.8808
MLP-151	MS	25.1303	9.2547	32.9327
MLP-152	MS	20.3351	7.3545	30.9725
MLP-153	MS	21.8099	8.5370	34.3413
***MLP-154**	MS	7.0426	9.6705	45.8044
***MLP-15A**	MS	28.1195	34.1135	56.8054
MLP-15B	MS	61.3223	32.4628	59.3160
MLP-16	MS	149.6695	105.5361	141.8521
MLP-17	MS	22.9330	4.9107	20.2780
MLP-18	MS	18.7683	6.7180	30.1553
MLP-19	MS	18.4984	7.3543	35.9114
ON-04	MS	28.4771	7.0130	14.9282
ON33-2	MS	25.6816	13.3406	28.6934
ON34-3	MS	42.7991	11.8771	28.7110
OXB-37	MS	37.3483	8.9360	21.7582
OXB-38	MS	19.6002	13.8586	43.8342
OXB-39	MS	36.1783	12.8443	33.1485
OXB-40	MS	29.5427	14.7055	41.6840
OXB-41	MS	55.1580	29.1587	65.1695
SOM-33	MS	18.9259	7.7211	33.4281
SOM-34	MS	23.0620	15.9052	46.4945
SOM-35	MS	16.7020	7.5087	33.9868
SOM-36	MS	28.6012	22.5503	48.1736
SOM-37	MS	17.6286	6.0427	32.6305
SOM-38A	MS	29.8497	18.6060	52.2910
SOM-39	MS	25.5117	12.5184	32.3850
SP-21	MS	24.3166	3.8854	22.0758
SP23-2	MS	35.1845	10.6242	35.0698
SP-24	MS	40.6770	12.3806	29.0432
SP-25	MS	36.0798	9.4429	20.7452
SP-26	MS	28.7257	11.9836	40.2433
SP-27	MS	20.7816	18.9174	54.4206
BMC19-2	MS	21.7723	7.2812	23.1756
BMC-20	MS	19.9653	10.6331	25.6025
BMC25-2	MS	18.2436	10.5126	38.8493
BMC-28	MS	26.9293	9.0186	27.2800
BMC-29	MS	21.1558	6.6806	32.1196
BMC32-2	MS	28.5068	19.1944	24.6163
BUS-34	MS	14.8855	7.1905	35.8514
BUS-35	MS	15.0306	5.0574	26.0282

Table E2 cont.

	Observed Classification	Mf	MS	Mo
MLP-148	MS	0.000716	0.999281	0.000003
MLP-149	MS	0.017477	0.982519	0.000004
MLP-150	MS	0.000725	0.999273	0.000001
MLP-151	MS	0.000357	0.999636	0.000007
MLP-152	MS	0.001516	0.998477	0.000007
MLP-153	MS	0.001310	0.998688	0.000002
***MLP-154**	MS	0.788173	0.211827	0.000000
***MLP-15A**	MS	0.952439	0.047560	0.000001
MLP-15B	MS	0.000001	0.999998	0.000001
MLP-16	MS	0.000000	1.000000	0.000000
MLP-17	MS	0.000122	0.999418	0.000460
MLP-18	MS	0.002411	0.997581	0.000008
MLP-19	MS	0.003788	0.996211	0.000001
ON-04	MS	0.000021	0.981229	0.018750
ON33-2	MS	0.002085	0.997453	0.000462
ON34-3	MS	0.000000	0.999779	0.000221
OXB-37	MS	0.000001	0.998359	0.001641
OXB-38	MS	0.053615	0.946385	0.000000
OXB-39	MS	0.000009	0.999952	0.000039
OXB-40	MS	0.000600	0.999399	0.000001
OXB-41	MS	0.000002	0.999998	0.000000
SOM-33	MS	0.003675	0.996322	0.000003
SOM-34	MS	0.027162	0.972838	0.000000
SOM-35	MS	0.009985	0.990013	0.000002
SOM-36	MS	0.046288	0.953709	0.000003
SOM-37	MS	0.003040	0.996959	0.000002
SOM-38A	MS	0.003605	0.996395	0.000000
SOM-39	MS	0.001506	0.998445	0.000048
SP-21	MS	0.000037	0.999851	0.000112
SP23-2	MS	0.000005	0.999990	0.000005
SP-24	MS	0.000001	0.999758	0.000241
SP-25	MS	0.000002	0.996497	0.003501
SP-26	MS	0.000231	0.999768	0.000001
SP-27	MS	0.282495	0.717505	0.000000
BMC19-2	MS	0.000713	0.998934	0.000353
BMC-20	MS	0.009316	0.990128	0.000556
BMC25-2	MS	0.020522	0.979477	0.000001
BMC-28	MS	0.000129	0.999763	0.000108
BMC-29	MS	0.000719	0.999279	0.000003
BMC32-2	MS	0.008832	0.929389	0.061779
BUS-34	MS	0.020887	0.979112	0.000001
BUS-35	MS	0.006782	0.993190	0.000028

Table E1 cont.

	Observed Classification	Mf	MS	Mo
BUS-36	MS	15.7675	10.6940	34.4658
BUS-37	MS	16.1882	7.7291	19.6315
BUS-38	MS	20.0143	9.0983	28.1291
BUS-39	MS	23.0748	10.1150	24.2057
BUS-40	MS	11.5588	5.2012	27.9830
MLM-01	MS	19.3212	3.2902	16.4960
MLM-02	MS	30.1832	10.1888	22.8167
MLM-03	MS	20.1992	6.8308	27.9885
MLM-04	MS	21.9076	8.1558	37.5120
MLM-05	MS	17.8438	3.5572	18.2255
MLM-06	MS	27.9185	6.0573	21.7426
MLM-07	MS	25.9449	3.8276	9.9605
MLM-08	MS	14.4296	2.7715	21.3717
MLM-09	MS	18.5390	5.4860	17.5183
MLM-10	MS	13.8700	6.7855	29.8463
MLM-11	MS	27.5671	9.1163	21.3581
MLM-12	MS	21.2398	7.9258	35.5050
MLM-13	MS	23.9391	7.7836	26.1150
MLM-14	MS	24.4559	8.3020	29.6329
MLM-15	MS	34.6704	11.7379	29.9566
MLM-16	MS	34.1754	11.0764	32.0094
MLM-17	MS	42.5296	23.7940	36.6783
***MLP-124**	MS	52.1184	17.1040	13.2587
***MLP-125**	MS	44.8707	14.8275	13.6839
***MLP-126**	MS	39.0061	11.6977	8.8354
MLP-127	MS	26.3508	20.9683	46.8945
MLP-128	MS	8.5799	5.9750	24.6021
MLP-129	MS	13.4731	12.2598	27.6084
MLP-130	MS	39.8551	21.4505	27.3351
MLP-131	MS	22.9487	14.1383	26.1446
MLP-132	MS	27.3669	11.0456	24.2741
MLP-133	MS	25.7767	11.0911	14.2660
MLP-134	MS	38.7168	22.7762	30.6064
MLP-136	MS	18.6464	6.2354	22.7651
MLP-137	MS	22.0281	6.5068	26.0479
MLP-138	MS	14.2872	5.1768	20.6607
MLP-139	MS	16.7971	7.1591	14.2437
MLP-140	MS	27.5556	10.3253	18.0911
MLP-141	MS	22.8042	10.1608	14.6402
MLP-142	MS	15.6507	4.4323	19.6291
MLP-143	MS	19.6849	4.9707	13.8082
MLP-144	MS	17.8296	5.2203	22.1317

Table E2 cont.

	Observed Classification	Mf	MS	Mo
BUS-36	MS	0.073321	0.926672	0.000006
BUS-37	MS	0.014313	0.983128	0.002559
BUS-38	MS	0.004244	0.995683	0.000073
BUS-39	MS	0.001530	0.997600	0.000869
BUS-40	MS	0.039970	0.960019	0.000011
MLM-01	MS	0.000330	0.998316	0.001354
MLM-02	MS	0.000045	0.998147	0.001807
MLM-03	MS	0.001249	0.998726	0.000025
MLM-04	MS	0.001031	0.998968	0.000000
MLM-05	MS	0.000789	0.998559	0.000652
MLM-06	MS	0.000018	0.999590	0.000392
MLM-07	MS	0.000015	0.955474	0.044510
MLM-08	MS	0.002932	0.996977	0.000091
MLM-09	MS	0.001458	0.996112	0.002430
MLM-10	MS	0.028134	0.971856	0.000010
MLM-11	MS	0.000098	0.997710	0.002191
MLM-12	MS	0.001283	0.998716	0.000001
MLM-13	MS	0.000310	0.999585	0.000105
MLM-14	MS	0.000311	0.999666	0.000023
MLM-15	MS	0.000010	0.999879	0.000111
MLM-16	MS	0.000010	0.999962	0.000028
MLM-17	MS	0.000085	0.998324	0.001590
***MLP-124**	MS	0.000000	0.127566	0.872434
***MLP-125**	MS	0.000000	0.360823	0.639177
***MLP-126**	MS	0.000000	0.192924	0.807076
MLP-127	MS	0.063492	0.936505	0.000002
MLP-128	MS	0.213731	0.786198	0.000071
MLP-129	MS	0.352727	0.646972	0.000301
MLP-130	MS	0.000096	0.949807	0.050097
MLP-131	MS	0.012037	0.985528	0.002435
MLP-132	MS	0.000285	0.998376	0.001339
MLP-133	MS	0.000537	0.829810	0.169653
MLP-134	MS	0.000339	0.980119	0.019542
MLP-136	MS	0.002014	0.997730	0.000257
MLP-137	MS	0.000426	0.999517	0.000057
MLP-138	MS	0.010398	0.989172	0.000430
MLP-139	MS	0.007786	0.964301	0.027913
MLP-140	MS	0.000178	0.979651	0.020171
MLP-141	MS	0.001621	0.902294	0.096085
MLP-142	MS	0.003649	0.995852	0.000499
MLP-143	MS	0.000630	0.987471	0.011899
MLP-144	MS	0.001824	0.997964	0.000212

Table E1 cont.

	Observed Classification	Mf	MS	Mo
MLP-145	MS	22.1286	5.6030	17.8006
MLP-20	MS	17.4197	4.0312	18.4260
***MLP-21**	MS	400.0471	401.4960	439.4018
MLP-22	MS	22.2625	5.4928	19.2500
MLP-23	MS	27.4176	8.7462	12.5128
MLP-24	MS	33.1896	10.1400	11.0285
MLP-25	MS	14.7885	8.0388	35.3389
MLP-26	MS	20.1316	2.1565	17.6993
MLP-27	MS	17.3346	4.5726	24.6821
MLP-28	MS	12.3424	3.4802	22.6839
MLP-30	MS	18.9182	5.4607	33.5434
MLP-31	MS	25.6392	9.4864	39.9205
MLP-32	MS	40.7394	10.9230	14.1956
MLP-33	MS	14.4226	11.0981	24.6030
MLP-34	MS	11.3596	11.2371	24.5449
***MLP-35**	MS	47.1823	22.9553	13.0425
***MLP-36**	MS	53.8785	19.8559	14.2914
***MLP-37**	MS	63.8470	31.4698	25.6030
ON-05	MS	18.5431	5.4821	19.0504
ON-07	MS	27.4420	6.7958	10.8532
ON-10-2	MS	15.6481	11.2458	33.7486
ON-11	MS	11.8531	5.8516	34.2429
ON-16	MS	27.6003	7.0291	20.1963
ON-17	MS	21.3632	7.5309	28.2814
ON-18	MS	26.0473	7.7303	24.0144
OXB-14	MS	17.4852	7.6328	21.3203
OXB-15	MS	21.6347	13.1671	19.5883
OXB-16	MS	17.5772	9.9415	22.4852
OXB-18	MS	29.0308	9.3592	33.1062
OXB-19	MS	32.5332	8.1214	16.0747
OXB-20	MS	35.1042	11.1281	14.4213
OXB-21	MS	30.3192	8.0184	17.5205
OXB-26	MS	30.6445	10.5392	20.5501
OXB-27	MS	37.5716	8.7037	23.5796
OXB-28	MS	14.9049	8.9619	38.1649
OXB-30	MS	26.1333	11.9935	36.1885
OXB-31	MS	14.4901	5.9854	25.5355
OXB-32	MS	27.9651	17.2006	33.2859
OXB-33	MS	15.9583	14.6898	35.0416
OXB-34	MS	32.1966	8.2512	8.7601
OXB-35	MS	24.1358	3.5587	22.5860
SOM-19	MS	20.6368	9.2555	27.3252

Table E2 cont.

	Observed Classification	Mf	MS	Mo
MLP-145	MS	0.000257	0.997503	0.002240
MLP-20	MS	0.001236	0.998017	0.000747
***MLP-21**	MS	0.673586	0.326414	0.000000
MLP-22	MS	0.000228	0.998744	0.001028
MLP-23	MS	0.000077	0.867929	0.131995
MLP-24	MS	0.000006	0.609265	0.390729
MLP-25	MS	0.033091	0.966908	0.000001
MLP-26	MS	0.000125	0.999454	0.000421
MLP-27	MS	0.001691	0.998267	0.000043
MLP-28	MS	0.011761	0.988172	0.000067
MLP-30	MS	0.001195	0.998805	0.000001
MLP-31	MS	0.000311	0.999689	0.000000
MLP-32	MS	0.000000	0.837027	0.162972
MLP-33	MS	0.159303	0.839717	0.000981
MLP-34	MS	0.484371	0.514965	0.000664
***MLP-35**	MS	0.000000	0.006989	0.993011
***MLP-36**	MS	0.000000	0.058291	0.941709
***MLP-37**	MS	0.000000	0.050526	0.949474
ON-05	MS	0.001454	0.997417	0.001129
ON-07	MS	0.000029	0.883751	0.116220
ON-10-2	MS	0.099646	0.900342	0.000012
ON-11	MS	0.047391	0.952608	0.000001
ON-16	MS	0.000034	0.998585	0.001381
ON-17	MS	0.000991	0.998978	0.000031
ON-18	MS	0.000105	0.999604	0.000291
OXB-14	MS	0.007194	0.991748	0.001057
OXB-15	MS	0.013744	0.948019	0.038237
OXB-16	MS	0.021463	0.976692	0.001845
OXB-18	MS	0.000054	0.999940	0.000007
OXB-19	MS	0.000005	0.981592	0.018403
OXB-20	MS	0.000005	0.838429	0.161566
OXB-21	MS	0.000014	0.991417	0.008569
OXB-26	MS	0.000043	0.993301	0.006656
OXB-27	MS	0.000001	0.999411	0.000588
OXB-28	MS	0.048730	0.951270	0.000000
OXB-30	MS	0.000850	0.999145	0.000006
OXB-31	MS	0.014030	0.985914	0.000056
OXB-32	MS	0.004575	0.995105	0.000320
OXB-33	MS	0.346538	0.653437	0.000025
OXB-34	MS	0.000004	0.563265	0.436731
OXB-35	MS	0.000034	0.999892	0.000074
SOM-19	MS	0.003366	0.996516	0.000119

Table E1 cont.

	Observed Classification	Mf	MS	Mo
SOM-20	MS	34.4590	14.7807	28.1569
SOM-21	MS	20.2061	4.8566	20.1645
SOM-22	MS	23.9454	14.3902	31.7663
SOM-23	MS	19.7047	9.2801	27.5691
***SOM-25**	MS	12.0621	12.8257	35.2423
SOM-26	MS	25.0951	7.4976	11.6976
SOM-27	MS	17.8669	7.1086	27.1924
SOM-28	MS	17.0977	2.7166	18.4020
SOM-29	MS	15.3163	4.3093	20.7599
SOM-30	MS	19.6171	11.1178	29.8178
SOM-31	MS	15.3480	5.1070	27.3189
SOM-32	MS	27.0194	19.1396	28.6210
SP10-2	MS	34.5195	12.8922	13.4446
SP11-2	MS	27.1839	16.1481	16.9939
SP-12	MS	28.8119	14.5156	30.7570
SP13-3	MS	16.9132	3.2366	25.1070
SP14-3	MS	23.4463	8.7817	20.5421
SP16-1	MS	12.6335	8.4263	43.0129
SP-17	MS	15.2585	7.1415	36.7311
SP18-2	MS	10.2409	7.9923	36.2314
SP20-2	MS	12.2577	3.6864	25.0653
SP-22	MS	17.3666	2.8764	18.1832
BMC-35	MS	19.7070	3.6688	20.3528
BMC-36	MS	8.6726	4.6884	25.7780
BMC-37	MS	30.9916	12.0618	35.7402
MLP-111	MS	30.0148	6.0737	19.4445
MLP-112	MS	24.8211	2.5811	17.7464
MLP-113	MS	21.6123	2.8430	23.5735
MLP-114	MS	41.4515	8.8955	19.6530
MLP-115	MS	24.5400	6.1391	19.3625
MLP-116	MS	16.8935	3.4047	27.0850
MLP-117	MS	15.6789	4.8549	26.3623
MLP-118	MS	21.5494	11.0186	42.2212
MLP-119	MS	19.6763	8.2342	35.6401
MLP-120	MS	14.7795	2.9020	20.1845
MLP-121	MS	36.9944	31.0490	50.2626
MLP-122	MS	21.0038	6.8623	25.8024
MLP-123	MS	10.2312	6.1968	34.7932
MLP-38	MS	13.7065	7.4695	32.6880
MLP-39	MS	14.8890	8.9867	23.9172
MLP-40	MS	17.2572	10.2731	38.4104
MLP-41	MS	11.6815	4.1813	28.2319

Table E2 cont.

	Observed Classification	Mf	MS	Mo
SOM-20	MS	0.000053	0.998703	0.001244
SOM-21	MS	0.000464	0.999062	0.000474
SOM-22	MS	0.008344	0.991488	0.000167
SOM-23	MS	0.005419	0.994475	0.000106
***SOM-25**	MS	0.594304	0.405690	0.000006
SOM-26	MS	0.000134	0.890781	0.109085
SOM-27	MS	0.004590	0.995366	0.000043
SOM-28	MS	0.000753	0.998855	0.000392
SOM-29	MS	0.004055	0.995679	0.000267
SOM-30	MS	0.014068	0.985846	0.000086
SOM-31	MS	0.005937	0.994048	0.000015
SOM-32	MS	0.018917	0.972590	0.008493
SP10-2	MS	0.000011	0.568612	0.431376
SP11-2	MS	0.002419	0.602710	0.394871
SP-12	MS	0.000785	0.998918	0.000297
SP13-3	MS	0.001071	0.998911	0.000018
SP14-3	MS	0.000652	0.996563	0.002785
SP16-1	MS	0.108749	0.891251	0.000000
SP-17	MS	0.016982	0.983018	0.000000
SP18-2	MS	0.245217	0.754783	0.000001
SP20-2	MS	0.013578	0.986400	0.000022
SP-22	MS	0.000713	0.998813	0.000474
BMC-35	MS	0.000329	0.999433	0.000238
BMC-36	MS	0.120035	0.879942	0.000023
BMC-37	MS	0.000078	0.999915	0.000007
MLP-111	MS	0.000006	0.998746	0.001247
MLP-112	MS	0.000015	0.999476	0.000509
MLP-113	MS	0.000084	0.999885	0.000032
MLP-114	MS	0.000000	0.995408	0.004592
MLP-115	MS	0.000101	0.998557	0.001343
MLP-116	MS	0.001176	0.998817	0.000007
MLP-117	MS	0.004443	0.995536	0.000021
MLP-118	MS	0.005141	0.994859	0.000000
MLP-119	MS	0.003266	0.996733	0.000001
MLP-120	MS	0.002628	0.997196	0.000176
MLP-121	MS	0.048672	0.951264	0.000064
MLP-122	MS	0.000849	0.999074	0.000077
MLP-123	MS	0.117408	0.882591	0.000001
MLP-38	MS	0.042350	0.957646	0.000003
MLP-39	MS	0.049656	0.949800	0.000544
MLP-40	MS	0.029539	0.970460	0.000001
MLP-41	MS	0.022976	0.977018	0.000006

Table E1 cont.

	Observed Classification	Mf	MS	Mo
MLP-42	MS	17.1856	5.3427	29.7191
MLP-43	MS	30.3088	10.1628	32.7058
MLP-44	MS	28.6285	6.4476	27.9209
MLP-45	MS	24.5509	6.4315	28.9241
MLP-46	MS	44.0959	18.9286	36.7887
MLP-47	MS	26.4556	6.1107	23.2264
MLP-48	MS	29.2563	9.0794	21.2815
MLP-50	MS	26.7250	8.4103	24.1242
OXB-10	MS	25.2063	12.9918	37.8403
OXB-11	MS	22.6270	8.5032	26.3017
OXB-12	MS	16.9584	3.8202	27.7843
OXB-13	MS	24.4948	6.7913	18.7682
SOM-01	MS	25.9766	4.8163	17.2094
SOM-02	MS	32.8935	8.8240	19.2394
SOM-03	MS	12.1027	3.4201	23.3930
SOM-04	MS	25.8496	12.4358	29.2124
SOM-05	MS	20.9860	8.9784	28.1429
SOM-06	MS	10.5026	6.5843	30.7403
SOM-07	MS	29.2681	7.6022	13.0619
SOM-08	MS	15.9951	3.1732	14.1249
SOM-09	MS	26.7430	11.0563	21.0476
***SOM-10**	MS	29.7334	13.3404	7.5663
***SOM-11**	MS	44.0560	13.8929	3.4951
SOM-12	MS	18.0817	8.6135	22.9313
SOM-13	MS	21.3936	4.8155	27.0817
SOM-14	MS	24.4773	9.6902	24.4728
SOM-16	MS	27.2137	13.3679	34.3397
SOM-18	MS	22.2764	8.1067	38.2994
SP-01	MS	22.9844	7.0415	10.2219
SP-02	MS	34.7958	9.6131	17.3635
SP-03	MS	53.2462	17.1117	19.2703
SP-04	MS	21.8553	9.0556	21.9134
SP-05	MS	33.0281	8.9642	29.9281
SP06-1	MS	14.6600	5.5817	21.5662
SP06-2	MS	23.9633	7.5281	18.2265
SP07-2	MS	19.3474	5.0823	29.2315
SP-08	MS	22.3053	10.9900	35.3134
MLP-60	Mo	39.3141	14.9653	5.9260
MLP-61	Mo	43.4830	14.5775	9.5192
MLP-62	Mo	81.6259	50.6217	16.2200
MLP-63	Mo	215.0956	198.8726	152.4742
MLP-64	Mo	89.3652	52.1498	19.7884

Table E2 cont.

	Observed Classification	Mf	MS	Mo
MLP-42	MS	0.002674	0.997321	0.000005
MLP-43	MS	0.000042	0.999945	0.000013
MLP-44	MS	0.000015	0.999963	0.000022
MLP-45	MS	0.000116	0.999871	0.000013
MLP-46	MS	0.000003	0.999864	0.000132
MLP-47	MS	0.000038	0.999770	0.000192
MLP-48	MS	0.000041	0.997723	0.002235
MLP-50	MS	0.000105	0.999508	0.000387
OXB-10	MS	0.002222	0.997774	0.000004
OXB-11	MS	0.000856	0.999007	0.000136
OXB-12	MS	0.001401	0.998593	0.000006
OXB-13	MS	0.000143	0.997356	0.002501
SOM-01	MS	0.000025	0.997942	0.002032
SOM-02	MS	0.000006	0.994550	0.005444
SOM-03	MS	0.012852	0.987103	0.000045
SOM-04	MS	0.001221	0.998552	0.000227
SOM-05	MS	0.002463	0.997468	0.000069
SOM-06	MS	0.123557	0.876438	0.000005
SOM-07	MS	0.000019	0.938747	0.061234
SOM-08	MS	0.001634	0.994204	0.004162
SOM-09	MS	0.000390	0.992891	0.006719
***SOM-10**	MS	0.000015	0.052798	0.947187
***SOM-11**	MS	0.000000	0.005492	0.994508
SOM-12	MS	0.008707	0.990522	0.000771
SOM-13	MS	0.000251	0.999734	0.000015
SOM-14	MS	0.000614	0.998770	0.000616
SOM-16	MS	0.000984	0.998988	0.000028
SOM-18	MS	0.000837	0.999163	0.000000
SP-01	MS	0.000287	0.830401	0.169312
SP-02	MS	0.000003	0.979669	0.020328
SP-03	MS	0.000000	0.746359	0.253641
SP-04	MS	0.001656	0.996735	0.001609
SP-05	MS	0.000006	0.999966	0.000028
SP06-1	MS	0.010566	0.989100	0.000334
SP06-2	MS	0.000269	0.995003	0.004728
SP07-2	MS	0.000798	0.999196	0.000006
SP-08	MS	0.003479	0.996516	0.000005
MLP-60	Mo	0.000000	0.010775	0.989225
MLP-61	Mo	0.000000	0.073840	0.926160
MLP-62	Mo	0.000000	0.000000	1.000000
MLP-63	Mo	0.000000	0.000000	1.000000
MLP-64	Mo	0.000000	0.000000	1.000000

Table E1 cont.

	Observed Classification	Mf	MS	Mo
MLP-65	Mo	48.2358	25.6826	4.7016
OXB-01	Mo	69.9244	39.9354	14.4832
OXB-02	Mo	102.1881	64.1093	23.0338
OXB-03	Mo	59.5449	25.2877	10.9320
OXB-04	Mo	50.2060	22.1390	10.4974
OXB-05	Mo	57.3093	23.7197	15.0680
OXB-06	Mo	42.8030	18.7120	4.3332
OXB-07	Mo	53.2891	22.9071	7.9146
OXB-08	Mo	37.8874	10.0313	9.1152
***OXB-09**	Mo	87.2588	73.1616	88.3941

Table E2 cont.

	Observed Classification	Mf	MS	Mo
MLP-65	Mo	0.000000	0.000028	0.999972
OXB-01	Mo	0.000000	0.000003	0.999997
OXB-02	Mo	0.000000	0.000000	1.000000
OXB-03	Mo	0.000000	0.000763	0.999237
OXB-04	Mo	0.000000	0.002957	0.997043
OXB-05	Mo	0.000000	0.013050	0.986950
OXB-06	Mo	0.000000	0.000754	0.999246
OXB-07	Mo	0.000000	0.000555	0.999445
OXB-08	Mo	0.000000	0.387440	0.612560
***OXB-09**	Mo	0.000867	0.998641	0.000492

Incorrect classifications are marked (*) and abbreviations follow Table A.

Table F1. Classification function scores for dyke population (Model 3)

	Mf	MS	Mothae
VM-01	24818.07	24838.05	24836.06
VM-02	24946.38	24969.34	24980.74
VM-03	25053.31	25075.82	25085.59
VM-04	25488.76	25497.25	25486.65
VM-05	25711.63	25710.65	25698.89
VM-06	25167.85	25187.08	25191.13
VM-07	25139.68	25156.79	25156.96
VM-08	25171.66	25185.21	25182.43
VM-09	25138.65	25158.30	25162.55
VM-10	25102.19	25121.94	25127.19
VM-11	25135.59	25158.50	25170.48
VM-14	25381.67	25392.79	25384.82
VM-15	25357.08	25369.91	25366.11
VM-16	25384.98	25394.35	25386.59
VM-18	25566.28	25561.49	25547.92
VM-19	25527.20	25538.40	25528.20
VM-20	25105.92	25125.83	25131.03
VM-21	25385.36	25392.41	25380.03
VM-23	25123.45	25146.59	25157.42
VM-24	25073.28	25091.89	25095.11
VM-25	25271.58	25287.86	25288.29
VM-26	25242.08	25260.30	25260.57
VM-27	25308.75	25325.72	25325.98
VM-28	25257.87	25276.27	25277.76
VM-29	23989.64	23987.66	23975.63
VM-30	25714.76	25710.27	25698.17
VM-31	25441.39	25451.87	25444.54
VM-32	25241.52	25254.06	25249.99
VM-33	25358.14	25368.22	25361.77
VM-34	24922.42	24934.06	24928.31
VM-35	25594.47	25588.96	25576.50
VM-36	25749.58	25745.39	25730.28
VM-37	24951.39	24942.44	24947.56
VM-38	25672.94	25666.18	25653.46
VM-39	25552.18	25546.70	25533.70

Table F2. Discriminant function scores for dyke population (Model 3)

	Root 1	Root 2
VM-01	-5.15	-0.4733
VM-02	-6.31	2.5597
VM-03	-6.14	2.2033
VM-04	-2.07	-0.9853
VM-05	0.28	0.1334
VM-06	-5.16	1.2085
VM-07	-4.52	0.5169
VM-08	-3.55	0.2868
VM-09	-5.27	1.1959
VM-10	-5.33	1.4426
VM-11	-6.31	2.7165
VM-14	-2.79	-0.6963
VM-15	-3.34	0.1306
VM-16	-2.37	-0.3781
VM-18	1.27	0.2321
VM-19	-2.74	-1.2893
VM-20	-5.36	1.4045
VM-21	-1.66	-1.2331
VM-23	-6.33	2.3849
VM-24	-4.98	1.0849
VM-25	-4.32	0.7094
VM-26	-4.79	0.3774
VM-27	-4.49	0.5605
VM-28	-4.88	0.6650
VM-29	0.54	0.2110
VM-30	1.15	0.5730
VM-31	-2.66	-0.4340
VM-32	-3.27	0.1053
VM-33	-2.59	-0.1438
VM-34	-2.99	-0.1968
VM-35	1.42	0.6336
VM-36	1.17	-0.2573
VM-37	1.69	5.7134
VM-38	1.73	0.7493
VM-39	1.43	0.4872

Table F3. Classification of dykes determined from classification function scores (Model 3)

	Previous Classification	1	2	3
VM-01	MSM	**MS**	Mo	Mf
VM-02	MSM	**Mo**	MS	Mf
VM-03	MSM	**Mo**	MS	Mf
VM-04	MSM	**MS**	Mf	Mo
VM-05	Mf	**Mf**	MS	Mo
VM-06	MSM	**Mo**	MS	Mf
VM-07	MSM	**Mo**	MS	Mf
VM-08	MSM	**MS**	Mo	Mf
VM-09	MSM	**Mo**	MS	Mf
VM-10	MSM	**Mo**	MS	Mf
VM-11	MSM	**Mo**	MS	Mf
VM-14	MSM	**MS**	Mo	Mf
VM-15	MSM	**MS**	Mo	Mf
VM-16	MSM	**MS**	Mo	Mf
VM-18	Mf	**Mf**	MS	Mo
VM-19	MSM	**MS**	Mf	Mo
VM-20	MSM	**Mo**	Mo	Mf
VM-21	MSM	**MS**	Mf	Mo
VM-23	MSM	**Mo**	MS	Mf
VM-24	MSM	**Mo**	MS	Mf
VM-25	MSM	**Mo**	MS	Mf
VM-26	MSM	**Mo**	MS	Mf
VM-27	MSM	**Mo**	MS	Mf
VM-28	MSM	**Mo**	MS	Mf
VM-29	MSM	**Mf**	MS	Mo
VM-30	Mf	**Mf**	MS	Mo
VM-31	MSM	**MS**	Mo	Mf
VM-32		**MS**	Mo	Mf
VM-33	MSM	**MS**	Mo	Mf
VM-34	MSM	**MS**	Mo	Mf
VM-35		**Mf**	MS	Mo
VM-36	Mf	**Mf**	MS	Mo
VM-37	Mf	**Mf**	Mo	MS
VM-38	Mf	**Mf**	MS	Mo
VM-39	Mf	**Mf**	MS	Mo

Table F1 cont.					Table F2 cont.				Table F3 cont.				
	Mf	**MS**	**Mothae**			**Root 1**	**Root 2**			**Previous Classification**	**1**	**2**	**3**
VM-42	25839.29	25862.15	25850.37		**VM-42**	-5.54	-3.4458		**VM-42**	MSM	**MS**	Mo	Mf
VM-43	25081.45	25100.46	25104.58		**VM-43**	-5.11	1.2625		**VM-43**	MSM	**Mo**	MS	Mf
VM-44	24959.90	24978.66	24983.87		**VM-44**	-5.08	1.5804		**VM-44**	MSM	**Mo**	MS	Mf
VM-45	25114.05	25133.93	25139.18		**VM-45**	-5.36	1.4224		**VM-45**	MSM	**Mo**	MS	Mf
VM-46	25123.92	25134.81	25127.13		**VM-46**	-2.75	-0.5896		**VM-46**	MSM	**MS**	Mo	Mf
VM-47	25239.37	25257.08	25248.98		**VM-47**	-4.40	-1.7169		**VM-47**	MSM	**MS**	Mo	Mf
VM-48	25628.25	25621.10	25608.96		**VM-48**	1.80	0.9604		**VM-48**	Mf	**Mf**	MS	Mo
VM-49	25709.34	25703.62	25691.50		**VM-49**	1.46	0.7522		**VM-49**	Mf	**Mf**	MS	Mo
VM-50	25312.32	25321.12	25314.65		**VM-50**	-2.27	0.0420		**VM-50**	MSM	**MS**	Mo	Mf
VM-51	25383.63	25392.53	25382.34		**VM-51**	-2.18	-0.9401		**VM-51**	MSM	**MS**	Mf	Mo
VM-52	25826.17	25827.20	25818.70		**VM-52**	-0.31	0.6769		**VM-52**	MSM	**MS**	Mf	Mo
VM-53	25132.02	25152.04	25157.17		**VM-53**	-5.39	1.3718		**VM-53**	MSM	**Mo**	MS	Mf
VM-54	24882.51	24902.43	24900.79		**VM-54**	-5.15	-0.3728		**VM-54**	MSM	**MS**	Mo	Mf
VM-55	25277.37	25295.09	25298.01		**VM-55**	-4.76	1.1412		**VM-55**	MSM	**Mo**	MS	Mf
VM-56	25898.15	25917.60	25904.94		**VM-56**	-4.68	-3.1648		**VM-56**	MSM	**MS**	Mo	Mf
VM-59	25086.25	25105.01	25107.54		**VM-59**	-5.00	0.8846		**VM-59**	MSM	**Mo**	MS	Mf
VM-60	25172.44	25190.50	25193.07		**VM-60**	-4.83	1.0015		**VM-60**	MSM	**Mo**	MS	Mf
VM-61	25684.48	25676.59	25664.43		**VM-61**	1.99	1.0684		**VM-61**	Mf	**Mf**	MS	Mo
VM-62	25097.73	25119.32	25127.92		**VM-62**	-5.88	2.0348		**VM-62**	MSM	**Mo**	MS	Mf
VM-63	25104.60	25120.64	25119.04		**VM-63**	-4.20	0.2189		**VM-63**	MSM	**MS**	Mo	Mf
VM-64	25222.01	25243.75	25250.65		**VM-64**	-5.86	1.5736		**VM-64**	MSM	**Mo**	MS	Mf
VM-65	25196.35	25213.69	25213.86		**VM-65**	-4.57	0.4860		**VM-65**	MSM	**Mo**	MS	Mf
VM-66	25113.13	25131.51	25134.68		**VM-66**	-4.92	1.1088		**VM-66**	MSM	**Mo**	MS	Mf
VM-67	26378.69	26382.30	26367.08		**VM-67**	-0.73	-1.4566		**VM-67**	MSM	**MS**	Mf	Mo
VM-68	25127.04	25144.13	25148.10		**VM-68**	-4.64	1.5089		**VM-68**	MSM	**Mo**	MS	Mf
VM-71	25611.28	25606.66	25592.88		**VM-71**	1.24	0.1551		**VM-71**	Mf	**Mf**	MS	Mo
VM-74	25589.05	25587.14	25574.27		**VM-74**	0.55	-0.0168		**VM-74**	Mf	**Mf**	MS	Mo
VM-75	25328.47	25336.71	25326.47		**VM-75**	-2.02	-0.8548		**VM-75**	MSM	**MS**	Mo	Mf
VM-76	25264.57	25282.95	25283.56		**VM-76**	-4.84	0.4405		**VM-76**	MSM	**Mo**	MS	Mf
VM-77	25097.42	25115.84	25120.24		**VM-77**	-4.97	1.4217		**VM-77**	MSM	**Mo**	MS	Mf
VM-78	25850.97	25845.42	25830.66		**VM-78**	1.50	0.0386		**VM-78**	Mf	**Mf**	MS	Mo
VM-79	25323.02	25338.18	25337.76		**VM-79**	-4.02	0.6564		**VM-79**	MSM	**MS**	Mo	Mf
VM-80	25278.80	25300.60	25311.57		**VM-80**	-6.01	2.6215		**VM-80**	MSM	**Mo**	MS	Mf
VM-81	25742.80	25742.51	25728.96		**VM-81**	0.17	-0.4352		**VM-81**	MSM	**Mf**	MS	Mo
VM-82	25065.75	25084.33	25082.12		**VM-82**	-4.80	-0.3189		**VM-82**	MSM	**MS**	Mo	Mf
VM-83	25119.53	25118.59	25109.65		**VM-83**	0.18	0.8604		**VM-83**	Mf	**Mf**	MS	Mo
VM-85	25187.38	25206.85	25207.97		**VM-85**	-5.13	0.4117		**VM-85**	MSM	**Mo**	MS	Mf
VM-86	25107.32	25124.75	25119.60		**VM-86**	-4.43	-0.9093		**VM-86**	MSM	**MS**	Mo	Mf
VM-87	25366.19	25382.53	25377.53		**VM-87**	-4.16	-0.7087		**VM-87**	MSM	**Mo**	MS	Mf
VM-88	25396.40	25403.14	25393.41		**VM-88**	-1.67	-0.4960		**VM-88**	MSM	**MS**	Mf	Mo
VM-89	25606.52	25604.18	25591.02		**VM-89**	0.66	-0.0266		**VM-89**	Mf	**Mf**	MS	Mo
VM-90	25618.74	25613.56	25601.70		**VM-90**	1.31	0.7383		**VM-90**	Mf	**Mf**	MS	Mo

Table F1 cont.					Table F2 cont.				Table F3 cont.				
	Mf	MS	Mothae			Root 1	Root 2			Previous Classification	1	2	3
VM-91	25087.10	25096.68	25092.19		**VM-91**	-2.53	0.4384		**VM-91**	MSM	**MS**	Mo	Mf
VM-92	25692.55	25690.20	25678.21		**VM-92**	0.63	0.2812		**VM-92**	Mf	**Mf**	MS	Mo
VM-93	25061.22	25079.78	25075.13		**VM-93**	-4.72	-0.9530		**VM-93**	MSM	**MS**	Mo	Mf
KMK100	25839.98	25810.42	25803.90		**KMK100**	7.10	5.7836		**KMK100**	Mf	**Mf**	MS	Mo
KMK101	25247.27	25255.87	25244.92		**KMK101**	-2.08	-1.0941		**KMK101**	MSM	**Mf**	MS	Mo
GRT102	24991.35	25009.61	25011.67		**GRT102**	-4.86	0.8391		**GRT102**	MSM	**Mo**	MS	Mf
AGG	25973.32	25964.92	25957.23		**AGG**	1.97	2.3011		**AGG**	Mf	**Mf**	MS	Mo

NOTE: Table F3 differs from Table C3 in that the dyke classifications of Model 2 are compared with those of Model 3 and the misclassifications between the two Models are highlighted.

CLASSIFICATION FUNCTIONS:

$$\mathbf{Mf = 4.4Zr + 1964.8P_2O_5 + 0.7Cr + 111.8FeO^* + 1568.8TiO_2 + 593.5SiO_2 + 708.4Al_2O_3 + 3.6V - 4.7Y + 214.8Na_2O + 636.6MgO - 2.4Ni - 145.5K_2O - 25589.2} \quad \mathbf{(7)}$$

$$\mathbf{MS = 5Zr + 1799.3P_2O_5 + 0.6Cr + 113.2FeO^* + 1537.9TiO_2 + 589.7SiO_2 + 703.7Al_2O_3 + 3.6V - 5.2Y + 211.1Na_2O + 632.8MgO - 2.4Ni - 142.4K_2O – 25283} \quad \mathbf{(8)}$$

$$\mathbf{Mo = 4.9Zr + 1722.8P_2O_5 + 0.6Cr + 114.2FeO^* + 1575.9TiO_2 + 588.9SiO_2 + 698.7Al_2O_3 + 3.6V - 4.6Y + 206.7Na_2O + 629.9MgO - 2.3Ni + 140.3K_2O - 25186.7} \quad \mathbf{(9)}$$

DISCRIMINANT FUNCTIONS:

$$\mathbf{root\ 1 = - 0.1359Zr + 42.9110P_2O_5 + 0.0121Cr - 0.3702FeO^* + 6.3456TiO_2 + 0.9593SiO_2 + 1.2880Al_2O_3 - 0.0136V + 0.0921Y + 1.0539Na_2O + 1.0249MgO - 0.0093Ni - 0.8284K_2O - 78.2540} \quad \mathbf{(10)}$$

$$\mathbf{root\ 2 = - 0.0933Zr + 4.9645P_2O_5 + 0.0059Cr + 0.0646FeO^* + 14.5073TiO_2 + 0.3594SiO_2 - 0.6124Al_2O_3 - 0.0177V + 0.2288Y - 0.5742Na_2O - 0.1730MgO + 0.0048Ni + 0.772K_2O - 17.8669} \quad \mathbf{(11)}$$

REFERENCES

Ahrens, L.H. (1965). Distribution of the Elements in Our Planet. McGraw-Hill, Inc., 110pp.

Anon. (2001). ENPAT/TOURPAT: Environmental Potential Atlas. DFR Version 1. The Department of Environment Affairs, Pretoria.

Bangert, B., Stollhofen, H., Lorenz, V., and Armstrong, R. (1999). The geochronology and significance of ash-fall tuffs in the glaciogenic Carboniferous-Permican Dwyka Group of Namibia and South Africa. Journal of African Earth Sciences, 29, 33-49.

Bordy, E.M., Hancox, P.J., and Rubidge, B.S. (2004a). Fluvial style variations in the Late Triassic-Early Jurassic Elliot Formation, main Karoo Basin, South Africa. Journal of African Earth Sciences, 38, 383-400.

Bordy, E.M., Hancox, P.J., and Rubidge, B.S. (2004b). Provenance study of the Late Triassic-Early Jurassic Elliot Formation, main Karoo Basin, South Africa. South African Journal of Geology, 104, 587-602.

Bowen, T.B., Marsh, J.S., Bowen, M.P., and Eales, H.V. (1986). Volcanic rocks of the Witwatersrand Triad, South Africa. I: Description, classification and geochemical stratigraphy. Precambrian Research, 31, 297-324.

Campbell, I.H., and Griffiths, R.W. (1990). Implications of mantle plume structure for the evolution of flood basalts. Earth and Planetary Science Letters, 99, 79-93.

Catanuneau, O., Hancox, P.J. and Rubidge, B.S. (1998). Reciprocal flexural behaviour and contrasting stratigraphies: a new basin development model for the Karoo retroarc foreland system, South Africa. Basin Research, 10, 417-439.

Chevallier, L., and Woodford, A. (1999). Morpho-tectonics and mechanism of emplacement of the dolerite rings and sills of the western Karoo, South Africa. South African Journal of Geology, 102, 43-54.

Coffin, M.F., and Edholm, O. (1992). Volcanism and continental break-up: a global compilation of large igneous provinces, 17-30. In: Storey, B.C., Alabaster, T., Eds. Magmatism and the causes of continental break-up, Geological Society Special Publication, 393pp.

Courtillot, V.E., and Renne, P.R. (2003). On the ages of flood basalt events. Comptes Rendus Geoscience, 335, 113-140.

Courtillot, V., Jaupart, C., Manighetti, I., Tapponnier, P., and Besse, J. (1999). On causal links between flood basalts and continental breakup. Earth and Planetary Science Letters, 166, 177-195.

Cox, K.G., Macdonald, R., and Hornung, G. (1967). Geochemical and petrographic provinces in the Karroo basalts of Southern Africa. The American Mineralogist, 52, 1451-1474.

Cox, K.G., and Hornung, G. (1966). The petrology of the Karroo basalts of Basutoland. The American Mineralogist, 51, 1414-1432.

Dalziel, I.W.D., Lawver, L.A., and Murphy, J.B. (2000). Plumes, orogenesis, and supercontinental fragmentation. Earth and Planetary Science Letters, 178, 1-11.

Du Toit, A.L. (1920). The Karroo dolerites of South Africa: a study of hypabyssal injection. Transactions of the Geological Society of South Africa, 23, 1-42.

Duncan, A.R., Erlank, A.J., and Betton, P.J. (1984a). Appendix 1 analytical techniques and database descriptions, Special Publication of the Geological Society of South Africa, 13, 389-395.

Duncan, A.R., Erlank, A.J., and Marsh, J.S. (1984b). Regional Geochemistry of the Karoo Igneous Province, Special Publication of the Geological Society of South Africa, 13, 355-388.

Duncan, R.A., Hooper, P.R., Řeháček, J., Marsh, J.S., and Duncan, A.R. (1997). The timing and duration of the Karoo igneous event, southern Gondwana. Journal of Geophysical Research, 102, 18,127-18,138.

Duncan, R.A., and Richards, M.A. (1991). Hotspots, mantle plumes, flood basalts, and true polar wander. Reviews of Geophysics, 29, 31-50.

Eales, H.V., Marsh, J.S., and Cox, K.G. (1984). The Karoo Igneous Province: and introduction, Special Publication of the Geological Society of South Africa, 13, 1-26.

Elburg, M., and Goldberg, A. (2000). Age and geochemistry of Karoo dolerite dykes from northeast Botswana. Journal of African Earth Sciences, 31, 539-544.

Elliot, D.H., and Fleming, T.H. (2004). Occurrence and dispersal of magmas in the Jurassic Ferrar Large Igneous Province, Antarctica. Gondwana Research, 7, 223-237.

Elliot, D.H., and Fleming, T.H. (2000). Weddell triple junction: the principal focus of Ferrar and Karoo magmatism during initial breakup of Gondwana. Geology, 28, 539-542.

Elliot, D.H., Fleming, T.H., Kyle, P.R., and Foland, K.A. (1999). Long distance transport of magmas in the Jurassic Ferrar Large Igneous Province, Antarctica. Earth and Planetary Science Letters, 167, 67-104.

Encarnacion, J., Fleming, T.H., Elliot, D.H., and Eales, H.V. (1996). Synchronous emplacement of Ferrar and Karoo dolerites and the early breakup of Gondwana. Geology, 24, 535–538.

Ernst, R.E., Buchan, K.L., and Campbell, I.H. (2005). Frontiers in Large Igneous Province research. Lithos, 79, 271-297.

Ernst, R.E., and Buchan, K.L. (1999). Layered mafic intrusions: a model for their feeder systems and relationship with giant dyke swarms and mantle plume centres. South African Journal of Geology, 100, 319-334.

Fitch, F.J., and Miller, J.A. (1984). Dating Karoo igneous rocks by the conventional K-Ar and $^{40}Ar/^{39}Ar$ age spectrum methods, Special Publication of the Geological Society of South Africa, 13, 247-266.

Graham, K.W.T., and Hales, A.L. (1957). Palaeomagnetic measurements on Karroo dolerites. Philosophical Magazine Supplement, 6, 149-161.

Hälbich, I.W., Fitch, F.J., and Miller, J.A. (1983). Dating the Cape orogeny. In: Söhnge, A.P.G., Hälbich, I.W. (Eds.), Geodynamics of the Cape Fold Belt. Geological Society of South Africa Special Publication, 12, 149-164.

Hancox, P.J., and Rubidge, B.S. (2001). Breakthrough in the biodiversity, biogeography, biostratigraphy, and basin analysis of the Beaufort group. Journal of African Earth Sciences, 33, 563-577.

Harris, C., Marsh, J.S., Duncan, A.R., and Erlank, A.J. (1990). The petrogenesis of the Kirwan basalts of Dronning Maud Land, Antarctica. Journal of Petrology, 31, 341-369.

Hart, G.F., and Ferrel, R.E. (no date). Probabilistic environmental recognition using discriminant function analysis. Accessed online at: http://www.geol.lsu.edu/deltaweb/FILES/MANUSCRIPTS/gsa2000.htm [26/07/2006].

Hawkesworth, C., Kelley, S., Turner, S., Le Roex, A., and Storey, B. (1999). Mantle processes during Gondwana break-up and dispersal. Journal of African Earth Sciences, 28, 239-261.

Heimann, A., Flemming, T.H., Elliot, D.H., and Foland, K.A. (1994). A short interval of Jurassic continental flood basalt volcanism in Antarctica as demonstrated by ^{40}Ar-^{39}Ar geochronology. Earth and Planetary Science Letters, 121, 19-41.

Hargraves, R.B., Rehacek, J., and Hooper, P.R. (1997). Palaeomagnetism of the Karoo igneous rocks in southern Africa. South African Journal of Geology, 100, 195-212.

Johnson, M.R., Van Vuuren, C.J., Hegenberger, W.F., Key, R., and Shoko, U. (1996). Stratigraphy of the Karoo Supergroup in southern Africa: an overview. Journal of African Earth Sciences, 23, 3-15.

Jones, D.L., Duncan, R.A., Briden, J.C., Randall, D.E., MacNiocaill, C. (2001). Age of the Batoka basalts, northern Zimbabwe, and the duration of Karoo Large Igneous Province magmatism. Geochemistry, Geophysics, Geosystems, 2, 1–15.

Jourdan, F., Féraud, G., Bertrand, H., Kampunzu, A.B., Tshoso, G., Le Gall, B., Tiercelin, J.J., and Capiez, P. (2004). The Karoo triple junction questioned: evidence from Jurassic and Proterozoic $^{40}Ar/^{39}Ar$ ages and geochemistry of the giant Okavango dyke swarm (Botswana). Earth and Planetary Science Letters, 222, 989-1006.

Kent, R.W., Storey, M., and Saunders, A.D. (1992). Large igneous provinces: sites of plume impact or plume incubation? Geology, 20, 891-894.

Le Bas, M.J., Le Maitre, R.W., Streckeisen, A., and Zanettin, B. (1986). A chemical classification of volcanic rocks based on the Total Alkali-Silica diagram. Journal of Petrology, 27, 745-750.

Le Gall, B., Tshoso, G., Jourdan, F., Feraud, G., Bertrand, H., Tiercelin, J.J., Kampunzu, A.B., Modisi, M.P., Dyment, J., and Maia, M. (2002). $^{40}Ar/^{39}Ar$ geochronology and structural data from the giant Okavango and related mafic dyke swarms, Karoo igneous province, northern Botswana. Earth and Planetary Science Letters, 202, 595-606.

Lock, B.E., Paverd, A.L., and Broderick, T.J. (1974). Stratigraphy of the Karoo volcanic rocks of the Barkly East district. Transactions of the Geological Society of South Africa, 77, 117-130.

Lombaard, B.V. (1952). Karoo dolerites and lavas. Transactions of the Geological Society of South Africa, 55, 175-198.

Mahoney, J.J., Seth, H.C., Chandrasekharam, D., and Peng, Z.X. (2000). Geochemistry of flood basalts of the Toranmal Section, Northern Deccan Traps, India: implications for regional Deccan stratigraphy. Journal of Petrology, 41, 1099-1120.

Marsh, J.S. (2001). Karoo dykes, sills and volcanics in the Eastern Cape : Field Trip A1. Fourth international dyke conference, Rhodes University, Grahamstown, 57pp.

Marsh, J.S. (1998). Geochemical stratigraphy in basalts of the Mohale Dam – Katse dam areas, Lesotho. Report on Contract LHDA 1009, Mohale Tunnel: Sampling and testing of cores. Lesotho Highlands Tunnel Partnership (Mohale) (unpubl.). Rhodes University, Grahamstown, 21 pp.

Marsh, J.S., and Mndaweni, M.J. (1998). Geochemical variations in a long Karoo dyke, Eastern Cape. South African Journal of Geology, 101, 119-122.

Marsh, J.S., Hooper, P.R., Řeháček, J., Duncan, R.A., and Duncan, A.R. (1997). Stratigraphy and age of Karoo basalts of Lesotho and implications for correlations within the Karoo Igneous Province, 247-272. In: Mahoney, J.J., Coffin, M.F., Eds. Large igneous provinces: continental, oceanic and planetary flood volcanism. Geophysical Monograph 100, American Geophysical Union, 438 pp.

Marsh, J.S., and Eales, H.V. (1984). The chemistry and petrogenesis of igneous rocks of the Karoo Central Area, Southern Africa, Special Publication of the Geological Society of South Africa, 13, 27-67.

Marsh, J.S. (1984). Geochemistry of Karoo basalts and dolerites in the North-Western Orange Free State: recognition and origin of two new Karoo basalt magma types. 20th geological congress of the Geological Society of South Africa, Potchefstroom, 91-94 (Abstract).

Mège, D., and Korme, T. (2004). Fissure eruption of flood basalts from statistical analysis of dyke fracture length. Journal of Volcanology and Geothermal Research, 131, 77-92.

Meyboom, A.F., and Wallace, R.C. (1978). Occurrence and origin of ring-shaped dolerite outcrops in the Eastern Cape Province and western Transkei. Transactions of the Geological Society of South Africa, 81, 95-99.

Mitchell, A.A., Ramluckan, V.R., Dunlevey, J.N., and Eglington, B.M. (1996). The basalt stratigraphy of the Sani Pass, Kwazulu/Natal Drakensberg. South African Journal of Geology, 99, 251-262.

Mitchell, A.A. (1980). The petrology of Karoo basalts in the Molteno-Jamestown district. MSc. thesis (unpubl.), Rhodes University, 195 pp.

Mountain, A.D. (1943). The dikes of the Transkei gaps. Transactions of the Geological Society of South Africa, 4, 55-74.

Norrish, K., and Hutton, J.T. (1969). An accurate X-ray spectrographic method for the analysis of a wide range of geological samples. Geochimica et Cosmochimica Acta, 33, 431-453.

Partridge, T.C., and Maud, R.R. (1987). Geomorphic evolution of Southern Africa since the Mesozoic. South African Journal of Geology, 90, 179-208.

Pearce, J.A., and Cann, J.R. (1973). Tectonic setting of basic rocks determined using trace element analyses. Earth and Planetary Science Letters, 19, 290-300.

Pemberton, J. (1978). The geochemistry and petrology of Karroo basalts of the Barkly East area, North Eastern Cape. BSc (Hons.) thesis (unpubl.), Rhodes University, 139pp.

Ragland, P.C., and Defant, M.J. (1983). Silica standardization: a discriminant technique applied to a volcanic arc system. Earth and Planetary Science Letters, 64, 387-395.

Rehácek, J. (1995). Chemical and Palaeomagnetic stratigraphy of basalts in northern Lesotho, Karoo Province. PhD thesis (unpubl.)., Washington State University, 299 pp.

Reidel, S.P., and Tolan, T.L. (1992). Eruption and emplacement of flood basalt: an example from the large-volume Teepee Butte Member, Columbia River Basalt Group. Geological Society of America Bulletin, 104, 1650-1671.

Richards, M.A., Duncan, R.A., and Courtillot, V.E. (1989). Flood basalts and hot-spot tracks: plume heads and tails. Science, 246, 103-107.

Riley, T.R., and Knight, K.B. (2001). Review: age and pre-break-up Gondwana magmatism. Antarctic Science, 13, 99-110.

Robey, J. van A. (1976). Aspects of the geochemistry of the dolerites and basalts of the north-eastern Cape Province, South Africa. M.Sc. thesis (unpubl.), Rhodes University, Grahamstown, 174pp.

Rogers, R.R., Curry Rogers, K., Munyikwa, D., Terry, R.C., and Singer, B.S. (2004). Sedimentology and taphonomy of the upper Karoo-equivalent Mpandi Formation in the Tuli Basin of Zimbabwe, with a new $^{40}Ar/^{39}Ar$ age for the Tuli basalts. Journal of African Earth Sciences, 40, 147-161.

Self, S., Thordarson, T., and Keszthelyi, L. (1997). Emplacement of continental flood basalt lava flows, 381-410. In: Mahoney, J.J., Coffin, M.F., Eds. Large igneous provinces: continental, oceanic and planetary flood volcanism. Geophysical Monograph 100, American Geophysical Union, 438pp.

Seth, H.C., Mahoney, J.J., and Chandrasekharam, D. (2004). Geochemical stratigraphy of Deccan flood basalts of the Bijasan Ghat section, Satpura Range, India. Journal of Asian Earth Sciences, 23, 127-139.

Smith, R.M.H., Eriksson, P.G., and Botha, W.J. (1990). A review of the stratigraphy and sedimentary environments of the Karoo-aged basins of Southern Africa. Journal of African Earth Sciences, 16,143-169.

StatSoft, Inc. (2002). *STATISTICA* for Windows [Computer program manual]. Tulsa, OK: StatSoft, Inc., 2300 East 14th Street, Tulsa, OK, 74104-4442, (918) 749-1119, fax: (918) 749-2217, e-mail: info@statsoft.com, Web: http://www.statsoft.com.

Storey, B.C., Leat, P.T., and Ferris, J.K. (2001). The location of mantle-plume centres during the initial stages of Gondwana breakup, 71-80. In: Ernst, R.E., and Buchan, K.L., Eds., Mantle Plumes: their identification through time. Boulder, Colorado, Geological Society of America Special Paper, 352, 575pp.

Storey, B.C., and Kyle, P.R. (1997). An active mantle mechanism for Gondwana breakup. South African Journal of Geology, 100, 283-290.

Storey, B.C. (1995). The role of mantle plumes in continental breakup: case histories from Gondwanaland. Nature, 377, 301-308.

Sun, S.S., and McDonough, W.F. (1989). Chemical and isotopic systematics of oceanic basalts: implications for mantle composition and processes, 313-345. In:

Saunders, A.D., and Norry, M.J., Eds., Magmatism in the Ocean Basins. Geological Society Special Publication, 42, 398pp.

Swanson, D.A., Wright, T.L., and Helz, R.T. (1975). Linear vent systems and estimated rates of magma production and eruption for the Yakima Basalt on the Columbia Plateau. American Journal of Science, 275, 877-905.

Sweeney, R.J., and Watkeys, M.K. (1990). A possible link between Mesozoic lithospheric architecture and Gondwana flood basalts. Journal of African Earth Sciences, 10, 707-716.

Turner, B.R. (1999). Tectonostratigraphical development of the Upper Karoo foreland basin: orogenic unloading versus thermally induced Gondwana rifting. Journal of African Earth Sciences, 28, 216–238.

Van Zijl, J.S.V., Graham, K.W.T., and Hales, A.L. (1962a). The palaeomagnetism of the Stormberg lavas of South Africa, I: Evidence for a genuine reversal of the Earth's field in Triassic-Jurassic times. Geophysical Journal of the Royal Astronomy Society, 7, 23-29.

Van Zijl, J.S.V., Graham, K.W.T., and Hales, A.L. (1962b). The palaeomagnetism of the Stormberg lavas of South Africa, I: Evidence for a genuine reversal of the Earth's field in Triassic-Jurassic times. Geophysical Journal of the Royal Astronomy Society, 7, 169-182.

Veevers, J.J. (2004). Gondwanaland from 650-500 Ma assembly through 320 Ma merger in Pangea to 185-100 Ma breakup: supercontinental tectonics via stratigraphy and radiometric dating. Earth Science Reviews, 68, 1-132.

Veevers, J.J., Cole, D.I., and Cowan, E.J. (1994a). Southern Africa: Karoo basin and Cape Fold Belt, 223-279. In Veevers, J.J., and Powell, C.McA., Eds., Permian-Triassic Pangean basins and foldbelts along the Panthalassan margin of Gondwanaland, Geological Society of America, Inc., Colorado, 368 pp.

Veevers, J.J., Powell, C.McA., Collinson, J.W., and López-Gamundí, O.R. (1994b). Synthesis, 355-353. In Veevers, J.J., and Powell, C.McA., Eds., Permian-Triassic Pangean basins and foldbelts along the Panthalassan margin of Gondwanaland. Geological Society of America, Inc., Colorado, 368 pp.

Walker, F., and Poldervaart, A. (1949). Karroo dolerites of the Union of South Africa. Bulletin of the Geological Society of America, 60, 591-706.

White, R.S. (1997). Mantle plume origin for the Karoo and Ventersdorp flood basalts, South Africa. South African Journal of Geology, 100, 271-282.

White, R.S. (1992). Magmatism during and after continental break-up, 1-16. In Storey, B.C., Alabaster, T., and Pankhurst, R.J. Eds., Magmatism and the causes of continental break-up. Geological Society Special Publication, 68, 393pp.

White, R., and McKenzie, D. (1989). Magmatism at rift zones: the generation of volcanic continental margins and flood basalts. Journal of Geophysical Research, 94, 7685-7729.

Wood, B.J., and Blundy, J.D. (2003). Trace element partitioning under crustal and uppermost mantle conditions: the influences of ionic radius, cation charge, pressure, and temperature, 395-424. In: Holland, H.D. and Turekian, K.K. Eds., Treatise on Geochemistry, Elsevier, Holland. Accessed online at: http://www.sciencedirect.com [01/06/2005].

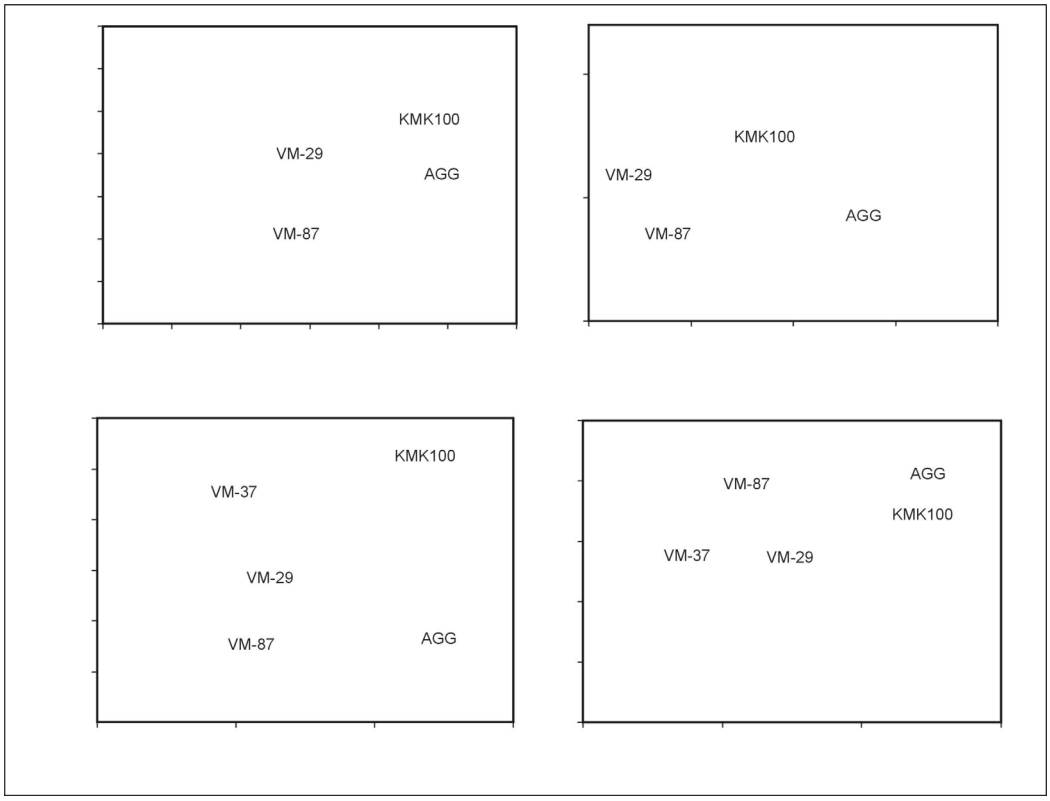
KMK100
VM-29
AGG
VM-87
KMK100
VM-29
AGG
VM-87
KMK100
VM-37
VM-29
VM-87
AGG
VM-87
AGG
KMK100
VM-37
VM-29

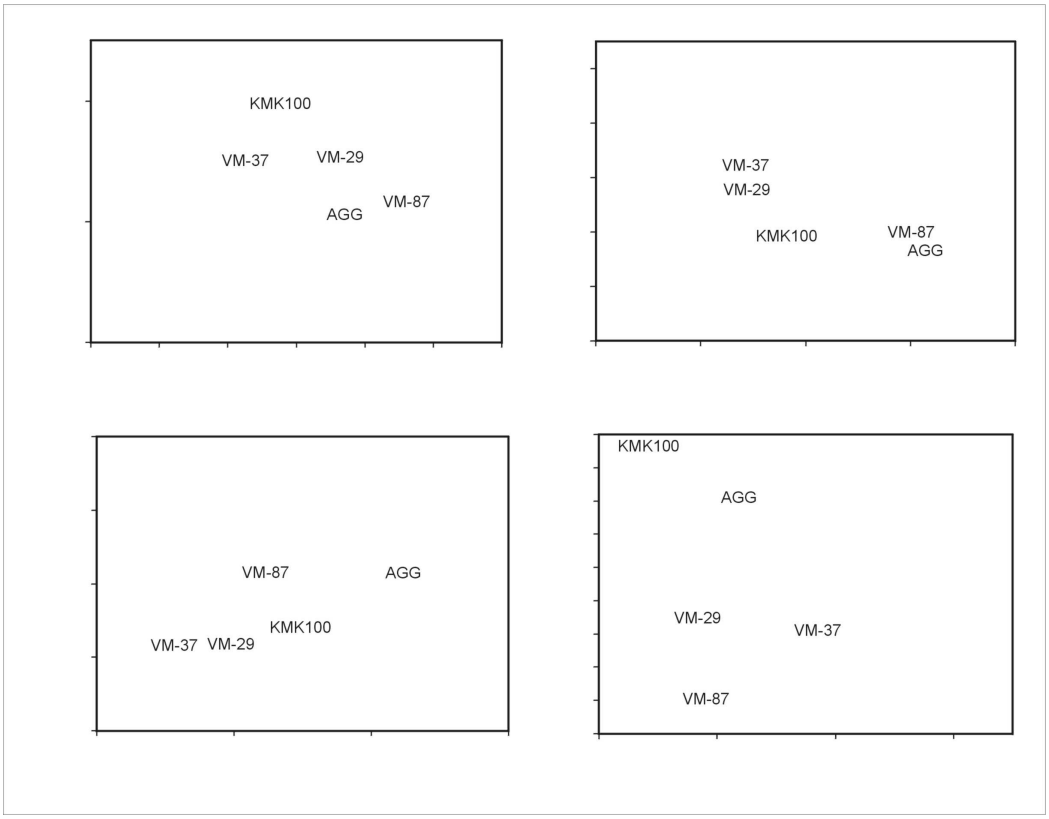
KMK100
VM-37
VM-29
VM-87
AGG
VM-37
VM-29
KMK100
VM-87
AGG
VM-87
AGG
KMK100
VM-37
VM-29
KMK100
AGG
VM-29
VM-37
VM-87

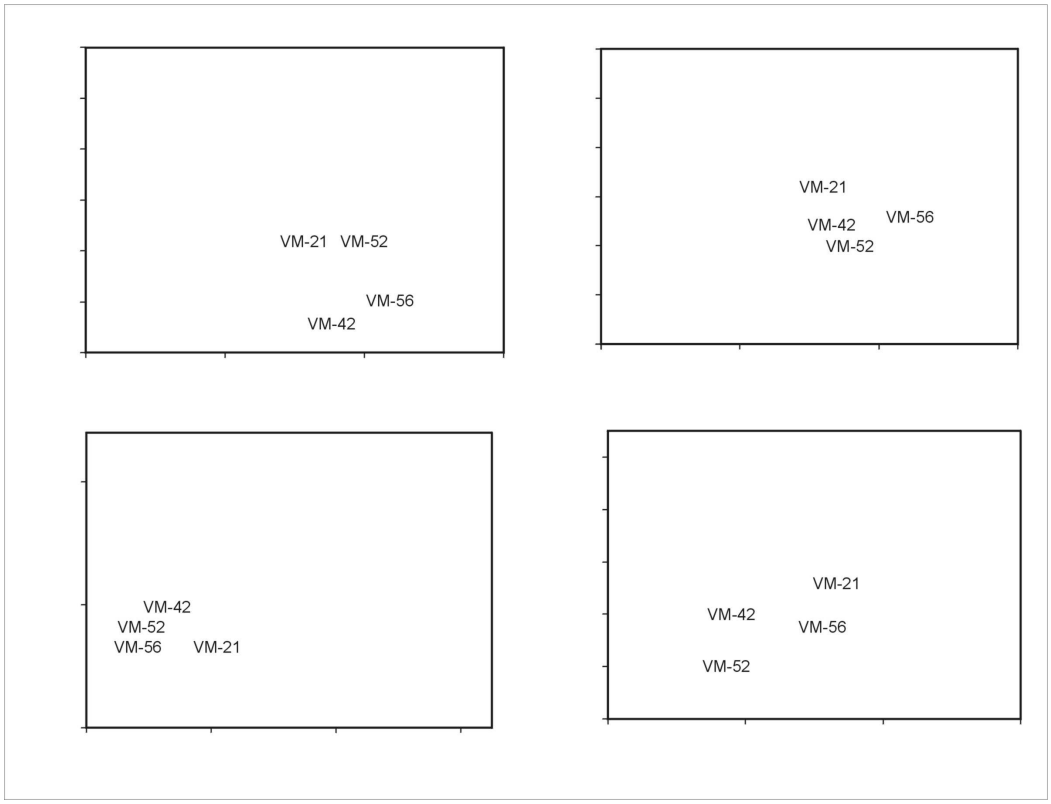
VM-21
VM-52
VM-56
VM-42
VM-21
VM-42
VM-56
VM-52
VM-42
VM-52
VM-56
VM-21
VM-21
VM-42
VM-56
VM-52